



The role of the microtubule destabilising protein stathmin in neuroblastoma metastasis

Author:

Fife, Christopher

Publication Date:

2015

DOI:

<https://doi.org/10.26190/unsworks/18514>

License:

<https://creativecommons.org/licenses/by-nc-nd/3.0/au/>

Link to license to see what you are allowed to do with this resource.

Downloaded from <http://hdl.handle.net/1959.4/55096> in <https://unsworks.unsw.edu.au> on 2024-05-01

The role of the microtubule destabilising protein stathmin in neuroblastoma metastasis

Christopher Fife

**A thesis submitted in fulfillment of the requirements for
degree of Doctor of Philosophy**



School of Women's and Children's Health

Faculty of Medicine

The University of New South Wales

Sydney, January 2015

Table of Contents

CHAPTER 1. INTRODUCTION	1
1 Introduction	2
1.1. Neuroblastoma	2
1.1.1. Clinical Presentation	2
1.1.2 Neuroblastoma Staging and Treatment Strategies	3
1.1.3. Biological Variables and Carcinoma-related Pathways	5
1.1.4. Cellular Heterogeneity in Neuroblastoma	6
1.1.5. Metastatic Disease.....	6
1.2 Cell Migration and Metastasis.....	10
1.3 Cytoskeletal Structure/Function	14
1.3.1 Microtubules	14
1.3.2 Actin	20
1.3.3 Rho GTPases as Cytoskeletal Regulators of Migration	21
1.3.4 Cofilin, cell motility and metastasis	27
1.3.5 Intermediate Filaments.....	29
1.4 Stathmin.....	30
1.4.1. Structure and Function.....	31
1.4.2 Phosphorylation	36
1.4.3 Cell Cycle Regulation	39
1.4.4. Stathmin and its Role in Metastasis	40
1.4.5 Stathmin in Neuroblastoma	41
1.5 Thesis Aims	42
CHAPTER 2. MATERIALS & METHODS	43
2. Materials & Methods.....	44
2.1. Cell Culture.....	44

2.2.	siRNA-mediated stathmin suppression.....	45
2.3.	RNA isolation and cDNA synthesis – Cell culture	46
2.4.	RNA isolation and cDNA synthesis – Animal tissues	48
2.5.	Quantitative PCR (qPCR)	49
2.6.	Protein expression analysis	49
2.7	Bromo deoxyuridine (BrdU) cell proliferation assay.....	51
2.8.	Chemotactic migration & invasion assays.....	52
2.9.	3D Tumour spheroid culture	53
2.10.	3D Tumour spheroid outgrowth into extracellular matrices	54
2.11.	Anoikis Assay.....	54
2.12.	Transendothelial migration assay.....	55
2.13.	HMEC-1 immunofluorescence staining.....	58
2.14.	Rho GTPase (Rac1, Cdc42 and RhoA) activation assays.....	59
2.15	Tubulin polymerisation assay	60
2.16.	Restoration of stathmin levels with wild-type or 4E:mutant stathmin in SK-N-BE(2)/TGL neuroblastoma cells.....	61
2.17.	Experimental metastasis neuroblastoma <i>in vivo</i> mouse model.....	62
2.18.	<i>In vivo</i> & <i>Ex vivo</i> imaging of tumour growth in mice.....	63
2.19.	Immunohistochemistry.....	64
2.20.	Delivery of InvivoFectamine®:stathmin sequence 3 siRNA <i>in vivo</i>	65
2.20.1.	Visualisation of uptake of InvivoFectamine®:STMN1 Seq.3 _{SI} siRNA.....	66
2.20.2.	Stathmin gene silencing efficacy using InvivoFectamine®:STMN1 Seq.3 _{SI} siRNA <i>in vivo</i> ...	67
2.20.3.	Effect of STMN1 Seq.3 _{SI} delivery on metastatic neuroblastoma tumour burden <i>in vivo</i>	67
2.21.	Statistical analyses.....	68
CHAPTER 3.....		69
3	Evaluation of stathmin’s role in the steps of the metastatic cascade in neuroblastoma cells....	70
3.1	Introduction.....	70

3.2	Stathmin expression in neuroblastoma cell lines.....	71
3.3	Stathmin gene silencing using siRNA in neuroblastoma cells	74
3.4	Stathmin suppression does not affect neuroblastoma cell proliferation in 2-dimensional or 3-dimensional culture	85
3.5	Stathmin mediates chemotactic-induced neuroblastoma cell migration and invasion	91
3.6	Stathmin suppression reduces 3D tumour spheroid invasion into 3D extracellular matrices 97	
3.7	Stathmin does not affect neuroblastoma cell sensitivity to anoikis.....	100
3.8	Stathmin regulates chemotactic-induced neuroblastoma cell transendothelial migration	104
3.9	Discussion.....	108
CHAPTER 4.....		113
4	Stathmin and its role in signalling in cell migration in neuroblastoma cells	114
4.1	Introduction.....	114
4.2	Stathmin regulates chemotactic-induced neuroblastoma cell transendothelial migration via ROCK signalling.....	115
4.3	Stathmin does not influence Rac1 activation	121
4.4	Stathmin does not influence Cdc42 activation.....	124
4.5	Stathmin suppression increases RhoA activation	127
4.6	Stathmin does not influence guanine nucleotide exchange factor H1 microtubule association 131	
4.7	Stathmin's influence on cell migration is independent of its tubulin-binding ability.....	135
4.8	Discussion.....	139
CHAPTER 5.....		145
5	Effect of stathmin on transendothelial migration <i>in vivo</i>	146
5.1	Introduction.....	146
5.2	Stathmin suppression reduced whole-body neuroblastoma metastatic tumour burden.....	146
5.3	Stathmin suppression does not reduce neuroblastoma metastasis to the spleen, brain or legs 152	
5.4	Stathmin suppression reduces neuroblastoma kidney metastasis	157

5.5	Stathmin suppression reduces neuroblastoma lung metastasis.....	160
5.6	Stathmin suppression reduces neuroblastoma liver metastasis	163
5.7	Discussion.....	174
CHAPTER 6.....		177
6	Therapeutic potential of targeting stathmin to reduce metastasis in neuroblastoma <i>in vivo</i>	178
6.1	Introduction.....	178
6.2	Determining the ability to deliver stathmin siRNA to metastatic neuroblastoma	179
6.3	Invivofectamine®:stathmin siRNA complexes silence stathmin expression in liver metastatic tumours	185
6.4	Therapeutic evaluation of <i>in vivo</i> stathmin suppression on neuroblastoma metastatic tumour burden in the liver of mice	188
6.5	Discussion.....	192
CHAPTER 7. CONCLUSIONS AND FUTURE PERSPECTIVES		197
CHAPTER 8. REFERENCES		207

THE UNIVERSITY OF NEW SOUTH WALES

Thesis/Dissertation Sheet

Surname or Family name: Fife

First name: Christopher

Other names: Michael

Abbreviation for degree as given in the University

calendar: PhD

School: School of Women's and Children's Health Faculty: Faculty of Medicine

Title: The role of the microtubule destabilising protein stathmin in neuroblastoma metastasis

Neuroblastoma, the most common extra-cranial solid tumour in children, accounts for 15% of paediatric cancer deaths. Survival for patients with distant metastases carries a very poor prognosis. This highlights the need to address metastatic neuroblastoma, the mechanisms of which are poorly understood. Metastasis, the movement of disease from one site to another, involves cell cytoskeletal remodelling. The overexpression of the microtubule destabilising protein, stathmin, is an important contributor of metastasis in neuroblastoma. There is limited knowledge of stathmin's role in neuroblastoma metastasis. This study evaluated stathmin's contribution in specific steps of metastasis, how stathmin exerts these effects and whether stathmin can be therapeutically targeted in metastatic neuroblastoma.

Stathmin suppression reduced cell migration and invasion, and 3D tumour spheroid invasion into 3D extracellular matrices, without influencing anoikis. Moreover, stathmin suppression reduced transendothelial migration (TEM). Additionally, to examine TEM *in vivo*, stathmin suppression reduced whole body, lung, kidney and liver metastasis. Treatment of neuroblastoma cells with ROCK inhibitors returned TEM to control levels highlighting that stathmin regulates TEM through ROCK. Stathmin suppression increased the activation of upstream RhoA. Examination of the microtubule-bound GEF-H1 was found not to be influenced by stathmin levels, highlighting that stathmin influences RhoA activation via another means. Interestingly, restoration of stathmin levels with either wild-type stathmin or 4E:mutant (defective tubulin-binding ability) stathmin returned cell migration back to controls indicating that stathmin influences migration in neuroblastoma cells independently of tubulin binding.

To target stathmin therapeutically in metastatic neuroblastoma, stathmin siRNA was delivered, using Invivofectamine™, to suppress stathmin *in vivo*. Stathmin siRNA was delivered and partially reduced (~30%) stathmin expression in tumour cells. This level of stathmin suppression did not influence metastasis.

In conclusion, this study demonstrates that stathmin regulates neuroblastoma cell migration and invasion, and TEM via RhoA activation. Furthermore, stathmin's influence on cell migration is independent of tubulin binding. Further investigation is required to determine how stathmin is regulating these phenotypes in a microtubule independent manner and how to enhance stathmin therapeutic targeting through exploitation of key metastasis-related signalling pathways.

Declaration relating to disposition of project thesis/dissertation

I hereby grant to the University of New South Wales or its agents the right to archive and to make available my thesis or dissertation in whole or in part in the University libraries in all forms of media, now or here after known, subject to the provisions of the Copyright Act 1968. I retain all property rights, such as patent rights. I also retain the right to use in future works (such as articles or books) all or part of this thesis or dissertation.

I also authorise University Microfilms to use the 350 word abstract of my thesis in Dissertation Abstracts International (this is applicable to doctoral theses only).

.....
Signature Witness Date

The University recognises that there may be exceptional circumstances requiring restrictions on copying or conditions on use. Requests for restriction for a period of up to 2 years must be made in writing. Requests for a longer period of restriction may be considered in exceptional circumstances and require the approval of the Dean of Graduate Research.

FOR OFFICE USE ONLY

Date of completion of requirements for Award:

ORIGINALITY STATEMENT

‘I hereby declare that this submission is my own work and to the best of my knowledge it contains no materials previously published or written by another person, or substantial proportions of material which have been accepted for the award of any other degree or diploma at UNSW or any other educational institution, except where due acknowledgement is made in the thesis. Any contribution made to the research by others, with whom I have worked at UNSW or elsewhere, is explicitly acknowledged in the thesis. I also declare that the intellectual content of this thesis is the product of my own work, except to the extent that assistance from others in the project’s design and conception or in style, presentation and linguistic expression is acknowledged.’

Signed

Date

COPYRIGHT STATEMENT

‘I hereby grant the University of New South Wales or its agents the right to archive and to make available my thesis or dissertation in whole or part in the University libraries in all forms of media, now or here after known, subject to the provisions of the Copyright Act 1968. I retain all proprietary rights, such as patent rights. I also retain the right to use in future works (such as articles or books) all or part of this thesis or dissertation.

I also authorize University Microfilms to use the 350 word abstract of my thesis in Dissertation Abstract International (this is applicable to doctoral theses only).

I have either used no substantial portions of copyright material in my thesis or I have obtained permission to use copyright material; where permission has not been granted I have applied/will apply for a partial restriction of the digital copy of my thesis or dissertation.’

Signed

Date

AUTHENTICITY STATEMENT

‘I certify that the Library deposit digital copy is a direct equivalent of the final officially approved version of my thesis. No emendation of content has occurred and if there are minor variations in formatting, they are the result of the conversion to digital format.’

Signed

Date

List of Figures

Figure 1.1 The metastatic cascade.....	9
Figure 1.2 The cell cytoskeleton and 4 steps of cell migration.....	13
Figure 1.3 Microtubule ‘dynamic instability’ is dictated by GTP hydrolysis.....	17
Figure 1.4 Typical protrusive structures in invasive cancer cells.....	23
Figure 1.5 Rho GTPases and their effector proteins that mediate actin cytoskeletal regulation.....	25
Figure 1.6 The T2S complex.....	33
Figure 1.7 Stathmin mediates microtubule dynamics by sequestering tubulin and/or increasing microtubule catastrophe.....	35
Figure 1.8 Signalling pathways that influence stathmin phosphorylation.....	38
Figure 3.1 Stathmin mRNA and protein expression in neuroblastoma cell lines.....	72
Figure 3.2 Stathmin siRNA sequence selection in SK-N-BE(2)/TGL neuroblastoma cells...	76
Figure 3.3 Stathmin siRNA sequence selection in SH-SY5Y neuroblastoma cells.....	78
Figure 3.4 Stathmin siRNA sequence concentration optimisation in SK-N-BE(2)/TGL neuroblastoma cells.....	81
Figure 3.5 Stathmin siRNA sequence concentration optimisation in SH-SY5Y neuroblastoma cells.....	83
Figure 3.6 Stathmin does not influence SK-N-BE(2)/TGL cell proliferation in 2D monolayer culture.....	86
Figure 3.7 Stathmin does not influence neuroblastoma 3D tumour spheroid growth.....	89
Figure 3.8 Stathmin regulates chemotactic-induced neuroblastoma cell migration.....	92
Figure 3.9 Stathmin regulates chemotactic-induced neuroblastoma cell invasion.....	94

Figure 3.10 Stathmin suppression reduces 3D tumour spheroid invasion into 3D extracellular matrices.....	98
Figure 3.11 Stathmin suppression does not alter sensitivity to anoikis.....	102
Figure 3.12 Stathmin suppression reduces neuroblastoma cell transendothelial migration..	106
Figure 4.1 Effect of ROCK inhibition on endothelial permeability.....	117
Figure 4.2 Stathmin suppression-induced reduction of cell transendothelial migration is reversed by ROCK inhibition.....	119
Figure 4.3 Stathmin suppression does not markedly influence total Rac1 or Rac1 activation levels.....	122
Figure 4.4 Stathmin suppression does not markedly influence total Cdc42 or Cdc42 activation levels.....	125
Figure 4.5 Stathmin suppression increases RhoA activation.....	129
Figure 4.6 Stathmin does not influence GEF-H1 microtubule association.....	133
Figure 4.7 Stathmin's influence on cell migration is independent of its tubulin-binding ability.....	137
Figure 5.1 shRNA-expressing SK-N-BE(2)/TGL cells express similar levels of luciferase.....	148
Figure 5.2 Stathmin suppression reduces neuroblastoma metastatic tumour burden in the whole-body of living mice by bioluminescent imaging.....	150
Figure 5.3 Neuroblastoma metastatic spread in the experimental metastasis model.....	153
Figure 5.4 Stathmin suppression does not influence neuroblastoma metastatic tumour burden in the spleen, brain or legs of mice measured by bioluminescent imaging.....	155
Figure 5.5 Stathmin suppression reduces neuroblastoma metastatic tumour burden in the kidneys of mice by bioluminescent imaging.....	158

Figure 5.6 Stathmin suppression reduces neuroblastoma metastatic tumour burden in the lungs of mice by bioluminescent imaging.....	161
Figure 5.7 Stathmin suppression reduces neuroblastoma metastatic tumour burden in the livers of mice by bioluminescent imaging.....	164
Figure 5.8 Luciferase and stathmin expression in neuroblastoma metastatic tumours in mouse liver tissue by immunohistochemistry staining.....	167
Figure 5.9 Stathmin gene suppression was maintained in metastatic neuroblastoma tumours.....	169
Figure 5.10 Stathmin suppression reduces neuroblastoma metastatic tumour burden in the liver of mice by histological quantification.....	172
Figure 6.1 Uptake of fluorescently labelled siRNA, using InvivoFectamine™, to neuroblastoma tumours inside mouse liver measured using Xenogen IVIS.....	181
Figure 6.2 Uptake of fluorescently labelled siRNA, using InvivoFectamine™, to neuroblastoma tumours inside mouse liver measured using confocal microscopy.....	183
Figure 6.3 InvivoFectamine™:stathmin-siRNA complexes silence stathmin gene expression in liver metastatic tumours.....	186
Figure 6.4 Therapeutic effect of stathmin suppression using InvivoFectamine™:stathmin siRNA complexes on neuroblastoma metastatic tumour burden in mice.....	190

List of Tables

Table 2.1 Stathmin siRNA sequences.....	46
Table 2.2 Antibody dilutions for western blots.....	51
Table 2.3 Fluorescent dextran dilution and fluorescence measurements.....	56

Abbreviations

2D	Two-Dimensional
3D	Three-Dimensional
7-AAD	7-Aminoactinomycin D
ADF	Actin Depolymerising Factor
ADP	Adenosine Diphosphate
ALK	Anaplastic Lymphoma Kinase
ATP	Adenosine Triphosphate
BLI	Bioluminescent Imaging
BrdU	Bromodeoxyuridine
BSA	Bovine Serum Albumin
cDNA	Complementary DNA
DAPI	4',6-diamidino-2-phenylindole
DMEM	Dulbecco's Modified Eagle Medium
DNA	Deoxyribonucleic Acid
dNTP	Deoxynucleotide Phosphate
DPBS	Dulbecco's Phosphate-Buffered Saline
EB	End-binding
ECM	Extracellular Matrix
EGTA	Ethylene Glycol Tetraacetic Acid
EMT	Epithelial to Mesenchymal Transition
F-actin	Filamentous Actin
FACS	Flow assisted Cell Sorting

FAK	Focal Adhesion Kinase
FCS	Fetal Calf Serum
G-actin	Globular Actin
GAP	GTPase Activating Protein
GAPDH	Glyceraldehyde 3-Phosphate Dehydrogenase
gDNA	Genomic DNA
GDP	Guanosine Diphosphate
GEF	Guanine Nucleotide Exchange Factor
GFP	Green Fluorescent Protein
Glu-MT	Glutamylated microtubule
GPCR	G Protein Coupled Receptor
GTP	Guanosine Triphosphate
GTPase	Guanosine Triphosphatase
H&E	Haematoxylin & Eosin
HMEC	Human Microvascular Endothelial Cell
HRP	Horse Radish Peroxidase
HSV-tk	Herpes Simplex Virus - Thymidine Kinase
IF	Intermediate Filament
IHC	Immunohistochemistry
INRG	International Neuroblastoma Risk Group
INSS	International Neuroblastoma Staging System
KIS	Kinase Interacting with Stathmin
LIMK	LIM domain-containing Kinase
mA	Milliamps
MAPK	Mitogen-Activated Protein Kinase

MAP	Microtubule-Associated Protein
MIBG	Meta-Iodobenzyl-Guanidine
MLC	Myosin Light Chain
mRNA	Messenger RNA
MTOC	Microtubule Organising Center
MT	Microtubule
OCT	Optimum Cutting Temperature
PAGE	Polyacrylamide Gel Electrophoresis
PBS	Phosphate-Buffered Saline
PBS-T	0.05% Tween-20/Phosphate-Buffered Saline
PDGF	Platelet Derived Growth Factor
PI	Propidium Iodide
qPCR	Quantitative Polymerase Chain Reaction
RIPA	Radio-Immunoprecipitation Assay
RNA	Ribonucleic Acid
RNAi	Ribonucleic Acid Interference
ROCK	Rho-associated coiled-coil forming Protein Kinase
ROI	Region Of Interest
RT	Room Temperature
RTK	Receptor Tyrosine Kinase
SCID	Severe Combined Immunodeficiency
SDS	Sodium Dodecyl Sulphate
SEM	Standard Error of Mean
Ser	Serine
shRNA	Short-Hairpin Ribonucleic Acid

siRNA	Short-Interfering Nucleic Acid
SMP	Skim Milk Powder
T2S	1 stathmin molecule: 2 tubulin heterodimers
TBS	Tris-Buffered Saline
TBS-T	0.5% Tween-20/Tris-Buffered Saline
TEM	Transendothelial Migration
TGL	Thymidine Kinase/GFP/Luciferase
TNF- α	Tumour Necrosis Factor Alpha
WASP	Wiskott-Aldrich Syndrome Protein
WAVE	WASP and Verprolin homologus protein
WT	Wild-type
β 2M	Beta-2-Microglobulin

Publications arising from this thesis

1. Fife, C. M., McCarroll, J. M., Kavallaris, M. (2014). “Movers and shakers: cell cytoskeleton in cancer metastasis.” *British Journal of Pharmacology* **171**(24): 5507-5523. **Note:** Sections of this review article have been used in Chapter 1 (Introduction) of this thesis. I have received permission to re-use sections of the article in this thesis. License between Christopher Fife and John Wiley and Sons. License number: 3513300188278
2. Fife, C. M., Sagnella, S. M., Byrne, F. L., Ng, D., Davis, T. P., McCarroll, J. M., Kavallaris, M. “Stathmin suppression alters transendothelial migration and RhoA signalling in neuroblastoma cells” *Manuscript in preparation*.

Abstracts

C Fife, F Byrne, S Sagnella, T Davis, J McCarroll, M Kavallaris. Stathmin regulates cell migration, invasion and transendothelial migration via RhoA activation in neuroblastoma. American Association for Cancer Research (AACR) Annual Meeting 2014, San Diego, CA, USA 2014. *Poster presentation*.

C Fife*, F Byrne, S Sagnella, T Davis, J McCarroll, M Kavallaris. Stathmin suppression alters ROCK signalling and reduces cell migration, invasion and transendothelial migration in neuroblastoma. Australian Society of Medical Research (NSW) Scientific Meeting, Sydney, Australia 2013. *Poster presentation*.

* Received Australian Society of Medical Research (NSW) Scientific Meeting Best Student Poster Award, June 2013.

C Fife, F Byrne, S Sagnella, T Davis, J McCarroll, M Kavallaris. Understanding stathmin’s role in neuroblastoma metastasis. 25th Lorne Cancer Conference, Lorne, Australia 2013. *Poster presentation*.

Acknowledgements

First and foremost, I would like to thank my supervisor Professor Maria Kavallaris for not only allowing me to complete my PhD with her, but also for her excellent mentorship, professionalism, guidance, support and trust throughout my project. She fostered independent thinking and provided me with an environment where I could truly grow as a scientist. Her motivation, dedication and enthusiasm have made her a great role model and I believe I could not have found a better supervisor. I would also like to thank my other supervisor Professor Tom Davis and co-supervisor Dr. Joshua McCarroll. In particular Josh for proofreading parts of my thesis; your advice made thesis writing a quicker and easier experience. I would like to express my gratitude to Professor Michelle Haber and everyone else at the Children's Cancer Institute Australia.

Of special note, I would like to thank Dr. Sharon Sagnella for all of her guidance, assistance and encouragement during my PhD. Sharon not only provided invaluable assistance in the lab but she was also there through the many ups and downs during my PhD and was always glad to selflessly help me in any way. Our many discussions about running, diving and picking on each other's accents made for a nice break from the daily grind of science. Sharon has been a true friend, a great role model and an excellent mentor in so many aspects of my PhD and my life in general and I cannot imagine how I could have got through my PhD without her!

The past few years being part of the Tumour Biology & Targeting program has been very enjoyable. Thank you to all TBT members, you have been a very friendly, intelligent and supportive group who have made even the toughest days fun. I will miss you all very much. Thank you to Eddy for the energy and passion you bring to science; and also for all the great tissue culture CDs! Big thanks to Tanya for being an awesome program officer and friend throughout my PhD, our daily banter about freezer inventories, incubator cleaning, holiday plans, beer and whether we are nutcases or not has made this PhD a more pleasant and amusing experience.

Huge thanks to all the students at CCIA, in particular the past (Gorjana, Frances, Michael and Miriam) and present members (Amelia, Felicity, Joann and Walter) of TBT and also to Bex and Phil. We have all gone through the PhD rollercoaster together and you all have uniquely

provided me with vital support during my project and in particular for listening to my many rants and complaints and for picking me back up after the tough meetings with Maria. In particular, I would like to thank Amelia for the many helpful discussions, weekend work and your awesome taste in music. Even though you are too modest to accept this comment you are a genius and a true inspiration.

I would also like to thank the Animal facility staff, Anna for her invaluable assistance in the lab, and also Amanda Philp for organising the many student activities and also for providing important career guidance. Outside of CCIA, I would like to thank our collaborator Dr. Dominic Ng for his assistance with my study. I am grateful to Dr. Renee Whan and the BMIF team, and also Dr. Maria Sarris and the HMU team for their services and valuable assistance.

And last, but definitely not least, a massive thank you to my wonderful family and friends; in particular, my parents (William and Cheryl), brother (Daniel), sister (Sheree) and brother-in-law (Anthony). Your love, support and encouragement throughout my PhD has been very important to me. Many thanks also to my friends for sticking with a very busy friend like me. A huge thanks to my amazing friend Jose, you have stood by me during the good times and the bad and I cherish our friendship greatly.

From the outside a PhD seems like a solo effort but really I couldn't have achieved what I have without the love and support of so many people. Thank you.

Abstract

Neuroblastoma, the most common extra-cranial solid tumour in children, accounts for 15% of paediatric cancer deaths. Survival for patients with distant metastases carries a very poor prognosis. This highlights the need to address metastatic neuroblastoma, the mechanisms of which are poorly understood. Metastasis, the movement of disease from one site to another, involves cell cytoskeletal remodelling. The overexpression of the microtubule destabilising protein, stathmin, is an important contributor of metastasis in neuroblastoma. There is limited knowledge of stathmin's role in neuroblastoma metastasis. This study evaluated stathmin's contribution in specific steps of metastasis, how stathmin exerts these effects and whether stathmin can be therapeutically targeted in metastatic neuroblastoma.

Stathmin suppression reduced cell migration and invasion, and 3D tumour spheroid invasion into 3D extracellular matrices, without influencing anoikis. Moreover, stathmin suppression reduced transendothelial migration (TEM). Additionally, to examine TEM *in vivo*, stathmin suppression reduced whole body, lung, kidney and liver metastasis. Treatment of neuroblastoma cells with ROCK inhibitors returned TEM to control levels highlighting that stathmin regulates TEM through ROCK. Stathmin suppression increased the activation of upstream RhoA. Examination of the microtubule-bound GEF-H1 highlighted that stathmin influences RhoA activation via another means.

Stathmin's interaction with many different partners suggests stathmin regulates RhoA activation and metastasis microtubule independently. Restoration of stathmin levels with either wild-type stathmin or 4E:mutant (defective tubulin-binding ability) stathmin returned cell migration back to controls indicating that stathmin influences migration in neuroblastoma cells independently of tubulin binding.

To target stathmin therapeutically in metastatic neuroblastoma, stathmin siRNA was delivered, using InvivoFectamineTM, to suppress stathmin *in vivo*. Stathmin siRNA was delivered and reduced stathmin expression in tumour cells. Despite this, stathmin suppression did not influence metastasis.

In conclusion, this study demonstrates that stathmin regulates neuroblastoma cell migration and invasion, and TEM via ROCK signalling. Moreover, stathmin regulates ROCK signalling via RhoA activation. Furthermore, stathmin's influence on cell migration is independent of tubulin binding. Additionally, therapeutic targeting of stathmin did not influence metastasis. Further investigation is required to determine how stathmin is regulating these phenotypes in a microtubule independent manner and how to enhance stathmin therapeutic targeting through exploitation of key metastasis-related signalling pathways.

Chapter 1. Introduction

1 Introduction

1.1. Neuroblastoma

Neuroblastoma, the most common extra-cranial solid tumour in children, accounts for 6-10% of all malignancies in patients under 15 years and disproportionately 15% of all paediatric cancer deaths (Gutierrez, Fischer et al. 2007). Median age at diagnosis is 18 months and approximately 75% of neuroblastomas occur prior to 5 years of age (Brodeur 2003). Improved outcome for neuroblastoma patients has occurred over recent decades though these improvements are attributable mainly to increasing cure rates amongst patients with localised disease (Maris, Hogarty et al. 2007). The survival rate for high-risk patients with widespread disseminated disease has achieved only modest improvement. A high-risk classification, carrying a depressing 5-year survival rate of 40-50% highlights the urgent need to tackle metastatic neuroblastoma (Maris 2010). Unfortunately, the mechanisms driving metastasis in neuroblastoma are poorly understood.

1.1.1. Clinical Presentation

Approximately 40% of patients will present to the clinic with localised disease that may encompass intra-adrenal masses observed on ultra-sonography to large sympathetic chain locally invasive tumours (Musarella, Chan et al. 1984). Many localised tumours have favourable biological features and these tumours are often treated with surgery alone. A subset of neuroblastoma tumours will spontaneously regress (Plantaz, Rubie et al. 1996). Children who present with metastatic disease tend to have considerable tumour burden and are generally ill. About 70% of patients at clinical presentation have widely-disseminated metastatic disease, which confers a poor prognosis with 5 year survival rates of less than 50%

(Maris 2010). The most common sites of metastasis include bone, bone marrow, lymph nodes and liver (Ara and DeClerck 2006). Neuroblastoma metastatic involvement in the bone or bone marrow can result in bone pain, limping or irritability. Furthermore, there may be signs of marrow failure [reviewed in (Stevens, Johnson et al. 2014)].

1.1.2 Neuroblastoma Staging and Treatment Strategies

Neuroblastoma is staged using the International Neuroblastoma Risk Group (INRG) Staging System, which is heavily based on the degree of metastasis (Monclair, Brodeur et al. 2009). The INRG was developed from the older International Neuroblastoma Staging System (INSS) as the INSS is a postsurgical staging system and a pretreatment risk classification system (i.e. INRG) is preferred. A major goal in therapy is to, at diagnosis, precisely predict each patient's individual risk. Risk stratification involves the use of a number of markers that have clear prognostic impact, such as disease stage, MYCN status (amplified versus single copy), tumour histopathology, DNA index (ploidy) and age at diagnosis (Oberthuer, Theissen et al. 2009).

According to the INRG staging system, stage L1 disease consists of a localised tumour confined to one body compartment that does not involve vital structures. Stage L2 disease is defined as a locoregional tumour with the presence of image-defined risk factors (e.g. infiltration of adjacent organs/structures) (Monclair, Brodeur et al. 2009). Stage M disease is defined as distant metastatic disease (i.e. non-contiguous with primary tumour) (e.g. distant lymph node involvement). Stage MS disease is a special class of metastatic disease where

patients are younger than 18 months with metastatic lesions confined to skin, liver, and/or bone marrow (Monclair, Brodeur et al. 2009).

Improvements in neuroblastoma survival rates over the decades are attributable mainly to increasing cure rates amongst patients with localised disease, where most are successfully treated with surgery alone or combined with chemotherapy when complete tumour removal has not been achieved (Castleberry 1997). Additionally, bone marrow transplants have markedly improved survival rates for neuroblastoma patients over the recent decades ((Gutierrez, Fischer et al. 2007). Despite these improvements in neuroblastoma survival rates, almost half of all patients with neuroblastoma have metastatic disease at diagnosis conferring a dismal 5-year survival rate of 40-50% (Maris 2010). In an attempt to improve outcomes for high-risk patients intensive induction therapy is utilised. The most commonly utilised chemotherapeutics comprise the DNA alkylating agent cisplatin, the topoisomerase II inhibitor etoposide, the DNA intercalating agent doxorubicin and the tubulin-binding agent vincristine (Pearson, Pinkerton et al. 2008). The DNA-targeted pro-drugs, topotecan and cyclophosphamide are frequently used at neuroblastoma relapse (Park, Scott et al. 2011). Due to the frequent occurrence of relapse, biological therapy, with retinoids to induce tumour cell differentiation, has been added to treatment regimes. The synthetic retinoid isotretinoin (13-*cis*-retinoic acid) has been used to treat high-risk patients periodically for 6 months to appreciably increase survival rates for these patients (Matthay, Villablanca et al. 1999, Pearson, Pinkerton et al. 2008). Furthermore, radioactive meta-iodobenzyl-guanidine (MIBG) is employed in monitoring primary and secondary tumour growth during therapy (Maris, Hogarty et al. 2007). Emerging therapies undergoing neuroblastoma clinical trials include the synthetic retinoid derivative fenretinide and monoclonal antibodies targeted to the disialoganglioside G_{D2} (Maris, Hogarty et al. 2007).

1.1.3. Biological Variables and Carcinoma-related Pathways

Genomic amplification of the transcription factor MYCN, which regulates multiple genes controlling cell cycle progression, cell death and drug transport, is most consistently associated with poor outcome and advanced stage metastatic disease in neuroblastoma (Seeger, Brodeur et al. 1985, Brodeur and Seeger 1986). Whole chromosomal gain (e.g. chromosome 17) is typically associated with low stage disease. In contrast, unbalanced chromosomal gain (e.g. chromosome 17q) is associated with poor outcome (Ara and DeClerck 2006, Vermeulen, De Preter et al. 2010). Additionally, loss of chromosome (e.g. 1p, 3p and 11q) is typically indicative of metastatic behaviour (Morowitz, Shusterman et al. 2003, Vermeulen, De Preter et al. 2010).

The carcinoma-related genes most commonly associated with adult carcinogenesis, such as TP53, CDKN2A and Ras, are rarely altered in neuroblastoma. In neuroblastoma, p53 mutations at diagnosis are rare, occurring in <2% of cases [reviewed in (Tweddle, Pearson et al. 2003)]. Despite the above-mentioned biological variables, the most extensively studied biological variable in neuroblastoma is that of the aforementioned MYCN transcription factor and its corresponding target genes. Recently anaplastic lymphoma kinase (ALK) has been an area of great interest due to its ability to promote the expression of MYCN in neuroblastoma [reviewed in (Umapathy, El Wakil et al. 2014)]. Tyrosine kinase inhibitors abrogating ALK activity are currently in clinical use for the treatment of ALK-positive disease (Umapathy, El Wakil et al. 2014).

1.1.4. Cellular Heterogeneity in Neuroblastoma

Clinical response and cellular composition heterogeneity has been recognised as a hallmark of neuroblastoma. Neuroblastoma tumours consist of three distinct cell types: I-type stem cells, N-type neuroblastic/neuroendocrine precursors, and S-type Schwannian/melanoblastic precursors. I-type stem cells have the greatest malignant potential and their frequency is associated with clinical relapse (Ross, Biedler et al. 2003). The presence of abundant stroma characterises tumours with a good prognosis, whereas predominance of undifferentiated neuroblasts, indicates a poor clinical outcome (Ross, Biedler et al. 2003). Tumour histology is classified as favourable or unfavourable depending on the amount of Schwannian stroma content, neuroblast differentiation, age at diagnosis, and the mitosis-karyorrhexis index (Shimada, Ambros et al. 1999).

1.1.5. Metastatic Disease

The majority of cancer deaths are due to metastatic disease (Schroeder, Heller et al. 2012). Metastasis is defined as the movement of disease from one site to another not directly connected with it via a highly selective process consisting of a series of discrete and sequential steps, which have been modeled into a “metastatic cascade”. To generate clinically relevant metastatic lesions, tumour cells must successfully complete all steps of this process: growth of primary tumour → detachment from the primary tumour → cell migration and invasion → anoikis evasion → intravasation-transport through vessels-extravasation → growth of secondary tumour (reviewed in (Stegg 2006)) (Figure 1.1). During each step of the metastatic cascade the cell cytoskeleton undergoes dramatic remodeling. Mutations in or

aberrant expression of the various components of the cytoskeleton (actin, microtubules and intermediate filaments) can contribute to metastatic progression.

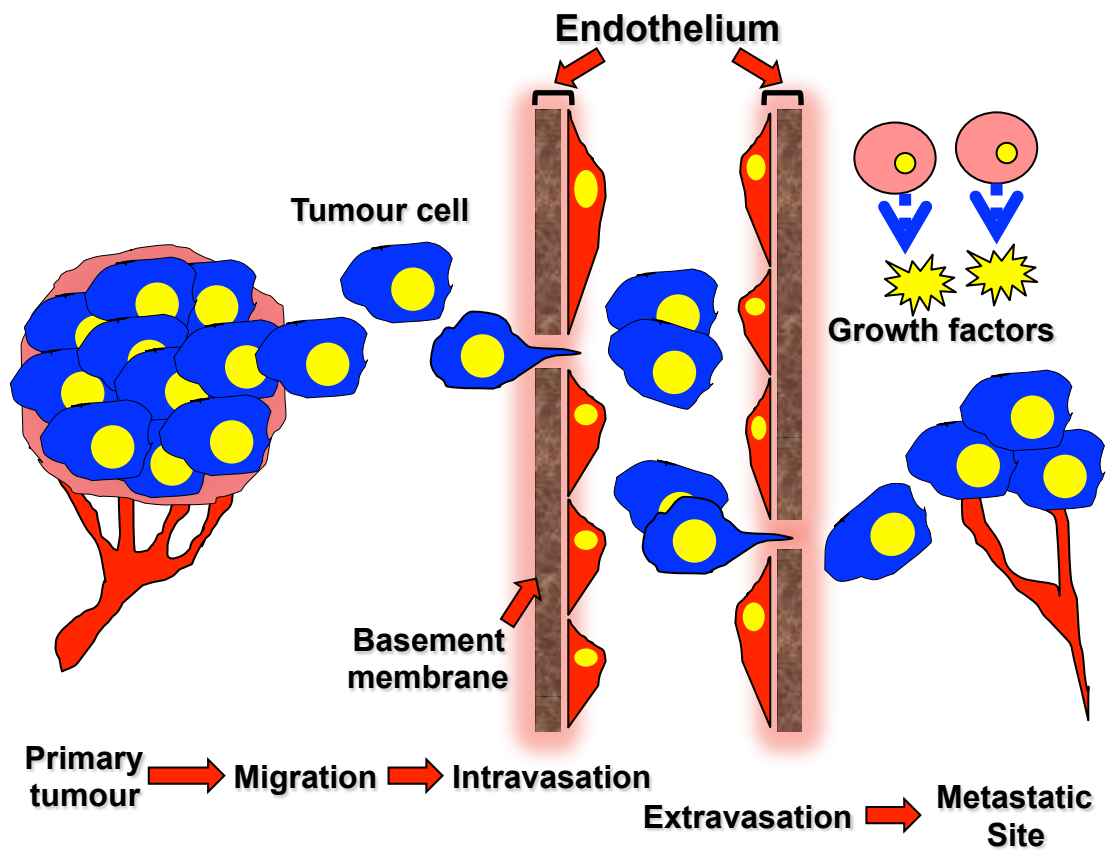
Specifically, neuroblastoma metastatic disease is highly prevalent with greater than 70% of patients exhibiting widely disseminated disease at clinical presentation/diagnosis (Ara and DeClerck 2006). The most frequent locations for neuroblastoma metastases are the bone marrow (70%), bone (56%), lymph nodes (31%), liver (30%), orbital or intracranial sites (18%), lung (3%), and central nervous system (>1%) (DuBois, Kalika et al. 1999, Dubois, London et al. 2008). Different metastatic disease locations carry varying prognoses where patients with metastatic tumour involvement in the bone marrow, lung or central nervous system possess decreased event free survival when compared to patients with liver or skin metastases (DuBois, Kalika et al. 1999).

The MYCN transcription factor is a key regulator of neuroblastoma metastasis where MYCN amplification correlates strongly with advanced stage disease (DuBois, Kalika et al. 1999). Though the observation that 70% of patients with advanced stage metastatic neuroblastoma do not possess amplification of MYCN highlights the multifaceted nature of the metastatic process where a complexity of factors, that when aberrantly regulated, influence metastatic disease progression.

Figure 1.1 The metastatic cascade

For cancer cells to metastasise they must successfully complete all steps of the metastatic cascade. 1) Cancer cells in the primary tumour acquire the ability to detach from the primary tumour and migrate through the surrounding extracellular matrix (ECM) and stroma. 2) Degradation of the vascular basement membrane and travel across the endothelium, termed intravasation. 3) Tumour cells transport through the vasculature, arrest in a capillary bed and cross the vasculature, termed extravasation. 4) Disseminated cells grow and interact with the extracellular environment to form metastatic tumours. Adapted from Ara & DeClerk 2006.

Metastatic Cascade



Recently our laboratory has identified the microtubule destabilising protein stathmin as a key player in neuroblastoma metastasis (Byrne, Yang et al. 2014). Silencing of stathmin expression using RNA interference significantly reduced *in vitro* neuroblastoma cell migration and invasion, and importantly, significantly reduced neuroblastoma metastasis to the lung by 71% in a clinically relevant orthotopic neuroblastoma mouse model (Byrne, Yang et al. 2014). To facilitate the rational design of anti-metastatic therapies targeted against stathmin an understanding of it's role in the cytoskeleton and cell migration and metastasis is required.

1.2 Cell Migration and Metastasis

Metastasis is a complex and multifaceted process. Fundamental to the understanding of tumour cell metastasis is an appreciation of the process of cell motility, and the different manners in which tumour cells migrate and invade. Whilst cell migration is necessary for numerous biological processes, such as embryonic morphogenesis, immune surveillance and tissue repair, aberrant control of cell migration promotes progression of many diseases, notably, cancer invasion and metastasis [reviewed in (Yamaguchi and Condeelis 2007)]. Broadly speaking, and as depicted in Figure 1.2, the process of cell motility can be broken down into four steps: protrusion, adhesion, contraction and retraction. Cells initiate cell motility, in response to an extracellular gradient of growth factors or chemokines, by polarising and extending cytoskeletal actin polymerisation-driven cell membrane protrusions towards the extracellular cue (Small, Stradal et al. 2002, Pollard and Borisy 2003). The protrusions are then stabilised by adhesions linking the actin cytoskeleton to the ECM proteins and actomyosin contraction produces forces on the substratum. Contraction encourages the disassembly of adhesions at the rear of the cell allowing retraction of the

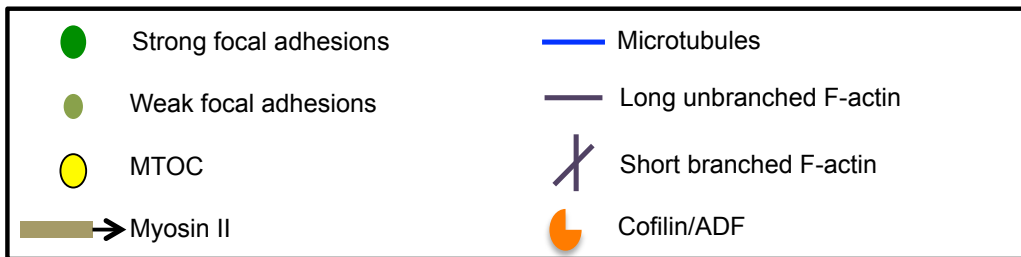
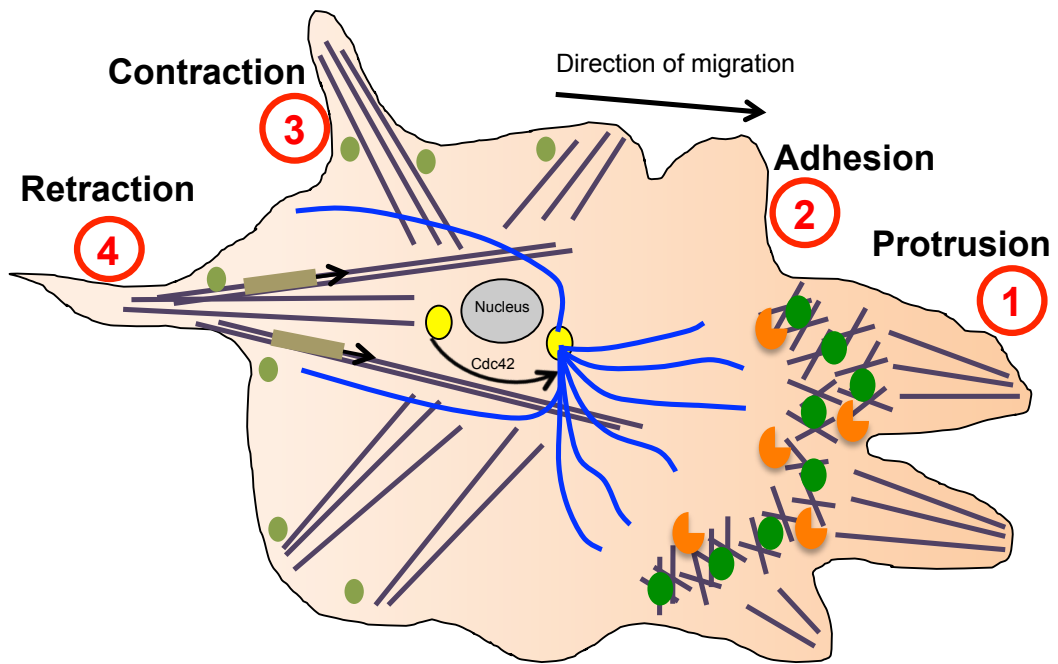
trailing cell body towards the direction of cell movement (Ridley, Schwartz et al. 2003). Key to the regulation of the processes involved in cell motility is the control of cytoskeletal dynamics, which is underpinned by critical cellular signalling pathways, such as the Rho GTPase signalling pathway.

Though despite the complicated nature of tumour cell motility (or migration) encompassing the above four steps, it is often studied in a simplified two-dimensional, planar manner where cells move towards a chemoattractant on an ECM utilising filopodial- and lamellipodial-protrusive structures. Alternatively, cell invasion involves the movement of cells into or in a three-dimensional ECM matrix. Successfully crossing many of the physiological barriers to tumour cell metastasis (such as basement membranes) requires specialised structures, such as invadopodia and podosomes [reviewed in (Yamaguchi and Condeelis 2007)]. There exist different modes of cell migration, such as mesenchymal and amoeboid movement. Mesenchymal motility is associated with F-actin rich protrusions where cell morphology is elongated, whereas, amoeboid motility is a rounded bleb-associated mode of motility (Sahai and Marshall 2003).

Given the complicated nature of tumour cell migration and metastasis it is not surprising that there exists a complex array of regulatory processes, particularly cytoskeletal and cytoskeletal-associated processes where pharmacological intervention may allow opportunities to treat metastatic disease.

Figure 1.2 The cell cytoskeleton and 4 steps of cell migration

A cartoon schematic shows a migrating cell (direction of migration is indicated by the arrow). 4 steps of cell migration shown: protrusion, adhesion, contraction, retraction. F-actin is shown in purple (short, branched F-actin at the leading edge, and long, unbranched F-actin stress fibres at the rear). Microtubules are shown in blue, with ends emanating from the MTOC (yellow circle) near the nucleus (grey ellipse). Strong and weak focal adhesions are shown as either dark or light green circles respectively. The cytoskeletal regulatory proteins, myosin II and cofilin/Actin Depolymerising factor (ADF) are shown. Adapted from Akhshi, *et al.*, 2013.



1.3 Cytoskeletal Structure/Function

Microtubule and microfilaments are polymer structures that orchestrate cellular division and movement, and intracellular signalling and transport via an intricate cross-talking network that involves interaction with a diverse range of proteins and signalling molecules.

1.3.1 Microtubules

1.3.1.1 Microtubule Structure, Dynamics and Function

Microtubules, composed of α/β -tubulin heterodimers that self-associate into polymers, form a network of dynamic structures that are vital for various cellular functions including cell division, motility and polarisation. α/β -tubulin heterodimers interact head-to-tail to form protofilaments, which form microtubule cylinders through the lateral interactions of 13 protofilaments (Wade 2009). Microtubule dynamics and polarity are controlled by the heterodimer repeat pattern where the rapidly growing microtubule plus end is capped by β -tubulin subunits and the slowly growing microtubule minus end is capped by α -tubulin subunits (Wade 2009) (Figure 1.3). Despite the high homology in the six α -tubulin and seven β -tubulin isotypes there is considerable variation in the last 15 amino acids at the C-terminus (Luduena 2013). These differences are believed to affect interactions with microtubule-associated proteins (MAPs) to ultimately impact microtubule dynamics (Nogales 2000).

Microtubules, being highly dynamic structures rapidly alternate between stages of polymerisation (growth) and depolymerisation (shortening), a characteristic named ‘dynamic instability’. Microtubules can switch between phases of growth and shortening termed ‘catastrophe’ and the opposite is termed ‘rescue’ [reviewed in (Wade 2009)] (Figure 1.3). An

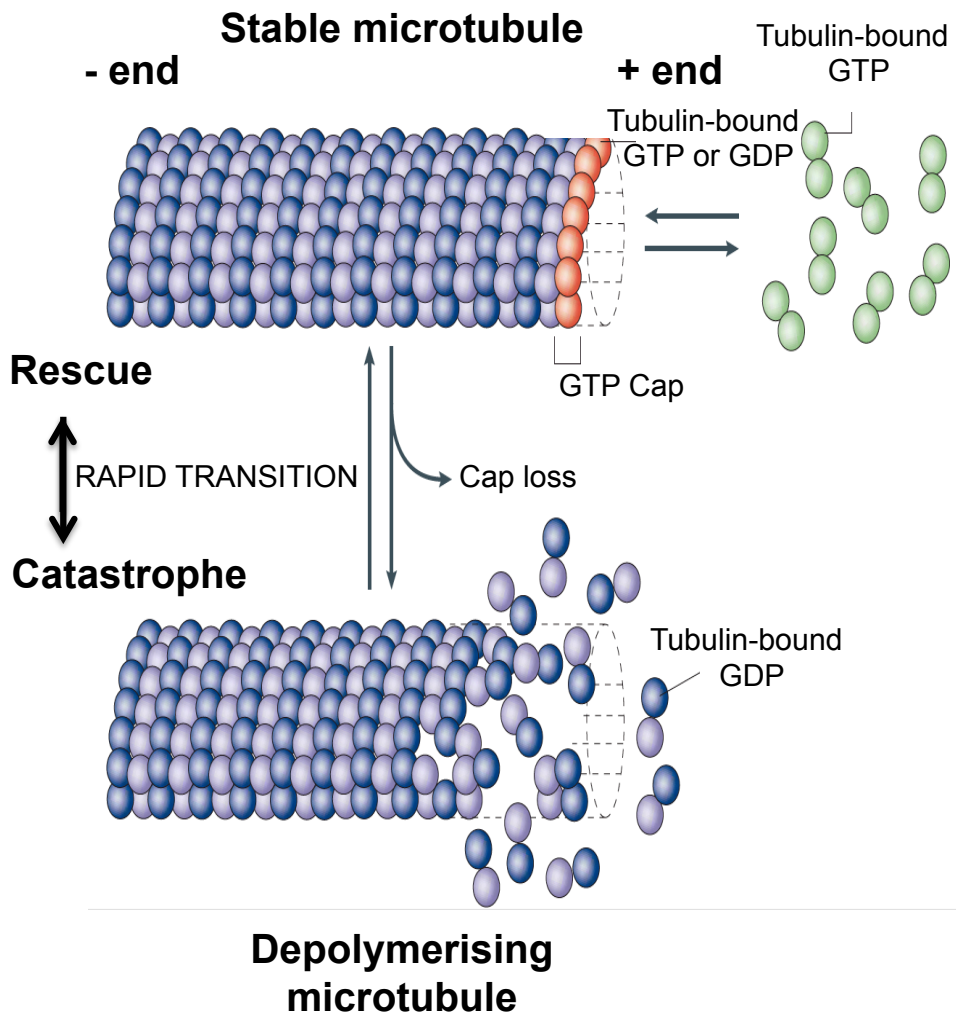
aspect of microtubule dynamics that doesn't influence microtubule length is the movement of tubulin subunits from the plus to minus end; a process termed 'treadmilling' (Nogales 2000).

The highly dynamic polymerisation and depolymerisation ability of microtubules in a regulated manner underpins the key roles microtubules play in intracellular vesicular transport and cell division. In an interphase cell, microtubules begin at the centrosome to form a hub and spoke-type network, which is important for vesicular transport. Throughout mitosis the interphase microtubule network is dramatically reorganised to form the mitotic spindles. Upon completion of mitosis, the mitotic spindle is disassembled and the interphase microtubule network reforms [reviewed in (Jordan and Wilson 2004)].

Whilst the abundance of literature on the role of the cytoskeleton in tumour cell migration and metastasis centers on the actin cytoskeleton, there is increasing evidence highlighting the microtubule system in these processes. The functions of the microtubule system during interphase and mitosis are dependent on their assembly, structure and dynamics, which are influenced by microtubule interactions with various microtubule interacting proteins (Nogales 2000).

Figure 1.3 Microtubule ‘dynamic instability’ is dictated by GTP hydrolysis

A GTP-cap, formed by GTP-loaded tubulin heterodimers at the microtubule plus end prevents microtubule depolymerisation. GTP hydrolysis at the catalytic loop on α -tubulin induces conformational changes that weaken lateral protofilament interactions resulting in depolymerisation. The change in microtubule dynamics from growth to shortening is labelled ‘catastrophe’, whereas shortening to growth is termed ‘rescue’. Adapted from Jordan 2004.



1.3.1.1 Microtubule Interacting Proteins

i) Motor Proteins

One of the vital roles of microtubules is cargo transport around the cell. This microtubule-mediated transport is driven by the kinesin and dynein motor protein families (Verhey and Gaertig 2007). The kinesin and dynein family motor proteins both contain microtubule-binding sites and use ATP hydrolysis to drive their activity, though a key difference is that kinesins ‘walk’ along microtubules towards the microtubule minus end, whereas dyneins ‘walk’ towards the microtubule plus end [reviewed in (Wade 2009)]. A key function of the motor proteins is the transport of proteins (e.g. focal adhesion proteins) to the leading edge of migrating cells (Verhey and Gaertig 2007).

ii) Microtubule Stabilising Proteins

Microtubule stabilisation is largely controlled through the interaction of microtubules with microtubule-associated proteins (MAPs). There are many cellular MAPs such as MAP1A-1C, MAP2a-2c, MAP3, MAP4 and tau, all of which facilitate microtubule stabilisation by binding to the C-terminus of tubulin [reviewed in (Bhat and Setaluri 2007)]. There is increasing interest in how the crosstalk between the microtubule and actin networks influences tumour cell metastasis. Importantly, MAPs can also link microtubules to other cytoskeletal networks, for example, MAP2c can bind to microtubules promoting microtubule stabilisation but also MAP2c can interact with the actin cytoskeleton (Rodriguez, Schaefer et al. 2003). Microtubule plus-end tracking proteins (+TIPs) accumulate at the ends of microtubules to facilitate microtubule stabilisation (Akhmanova and Steinmetz 2008). +TIPs move from older microtubule structures, allowing microtubule depolymerisation, and move to newer growing microtubule ends to assist in microtubule polymerisation via increased

microtubule stabilisation, this movement is controlled in part by the microtubule interacting motor proteins [reviewed in (Akhmanova and Hoogenraad 2005)].

An important microtubule interacting protein, which regulates microtubule dynamics, is end-binding protein 1 (EB1). EB1, a microtubule plus-end binding protein that colocalises and interacts with both cytoplasmic and spindle microtubules in interphase and mitotic cells respectively. Functionally, EB1 acts as an enhancer of microtubule stability. EB1 binds to the extreme plus-end tips of growing microtubules (Morrison, Wardleworth et al. 1998). EB1 is important for the stabilisation of microtubules as it contributes to the formation of stable detyrosinated microtubules (Glu-MTs) thus protecting them from depolymerisation [reviewed in (Zhang, Zaal et al. 2009)]. In addition to EB1, ATIP3 is involved in the regulation of microtubule dynamics. ATIP3 is a potent microtubule-stabilising protein whose depletion increases microtubule dynamics (Molina, Velot et al. 2013). ATIP3 was reported to be a prognostic marker for overall survival in breast cancer, where low ATIP3 levels in metastatic tumours is associated with decreased patient survival (Rodrigues-Ferreira, Di Tommaso et al. 2009). Functionally, ATIP3 was found to mediate cell motility and directionality, and influence the number and size of metastases (Molina, Velot et al. 2013). By reducing microtubule dynamics, ATIP3 regulates the ability of microtubule tips to reach the cell cortex during migration, which may account for decreased cancer cell motility and metastasis.

iii) Microtubule Destabilising Proteins

Similar to microtubule stabilisation, there exist a complex variety of cellular proteins that control microtubule depolymerisation. The main microtubule destabiliser proteins during interphase and mitosis are the kinesin-like proteins, XKCM1 and XKIF2, which bind microtubules inducing a conformational change in tubulin that destabilises microtubules

(Kline-Smith and Walczak 2002). Katanin acts to destabilise microtubules by cleaving microtubules and eliminating the microtubule stabilizing GTP cap (Nogales 2000). The echinoderm microtubule-associated protein (EMAP) destabilises microtubules by reducing microtubule elongation rate and increasing catastrophe frequency (Eichenmuller, Everley et al. 2002). The stathmin-like protein family members are small phosphoproteins that destabilise microtubules (Curmi, Gavet et al. 1999). Recent studies, including those from our laboratory, have implicated the microtubule destabilising protein stathmin in metastasis in 7 different malignancies (see Section 1.4.4), including neuroblastoma (Rana, Maples et al. 2008, Byrne, Yang et al. 2014). Stathmin will be discussed in more detail in Section 1.4.

1.3.2 Actin

Microfilaments are composed of actin polymers and a large array of actin-binding proteins (ABPs). In cells, actin exists either in monomeric (G-actin) or polymeric forms (F-actin). Each actin subunit is able to bind ATP, which is hydrolysed to ADP shortly after incorporation of the actin into a growing filament. Actin filaments consist of double helical polymers that are arranged head to tail and also contain a tropomyosin polymer which runs along the major groove in the microfilament (Gunning, O'Neill et al. 2008). The tropomyosin does not have any van der Waals interactions with actin and hence, 'floats' over the surface of the actin filament (Gunning, O'Neill et al. 2008).

The actin cytoskeleton, underpinned by the selective interaction with a variety of actin-binding proteins, plays important roles in cellular events such as differentiation, division, membrane organisation and notably, cell motility, all of which require the coordinated turnover and remodelling of actin filaments [reviewed in (Gunning, O'Neill et al. 2008)].

Altered cellular motility is a hallmark feature of metastasis, facilitating the advancement of

tumour cells to both local and distant sites in the body [reviewed in (Hanahan and Weinberg 2011)]. A key requirement of this process is the dynamic reorganisation of the actin cytoskeleton. Reorganisation of the actin cytoskeleton is critical for transdifferentiation of epithelial-like cells into motile mesenchymal-like cells, a process known as epithelial-mesenchymal transition (EMT), which is important during development, wound healing and cancer progression (Thiery, Acloque et al. 2009). During EMT, cells reorganise their actin cytoskeleton, enabling dynamic cell elongation and directional motility, altogether increasing the migratory phenotype [reviewed in (Lamouille, Xu et al. 2014)]. The leading edge of the mesenchymal-like migrating cells contains flat membranous lamellipodia, where protrusive force is generated by localised actin polymerisation at the plasma membrane. Dynamic actin cytoskeletal remodelling underlies the formation of typical protrusive structures in invasive cells and is controlled by key cellular signalling pathways (e.g. Rho GTPases) (Fig. 1.4).

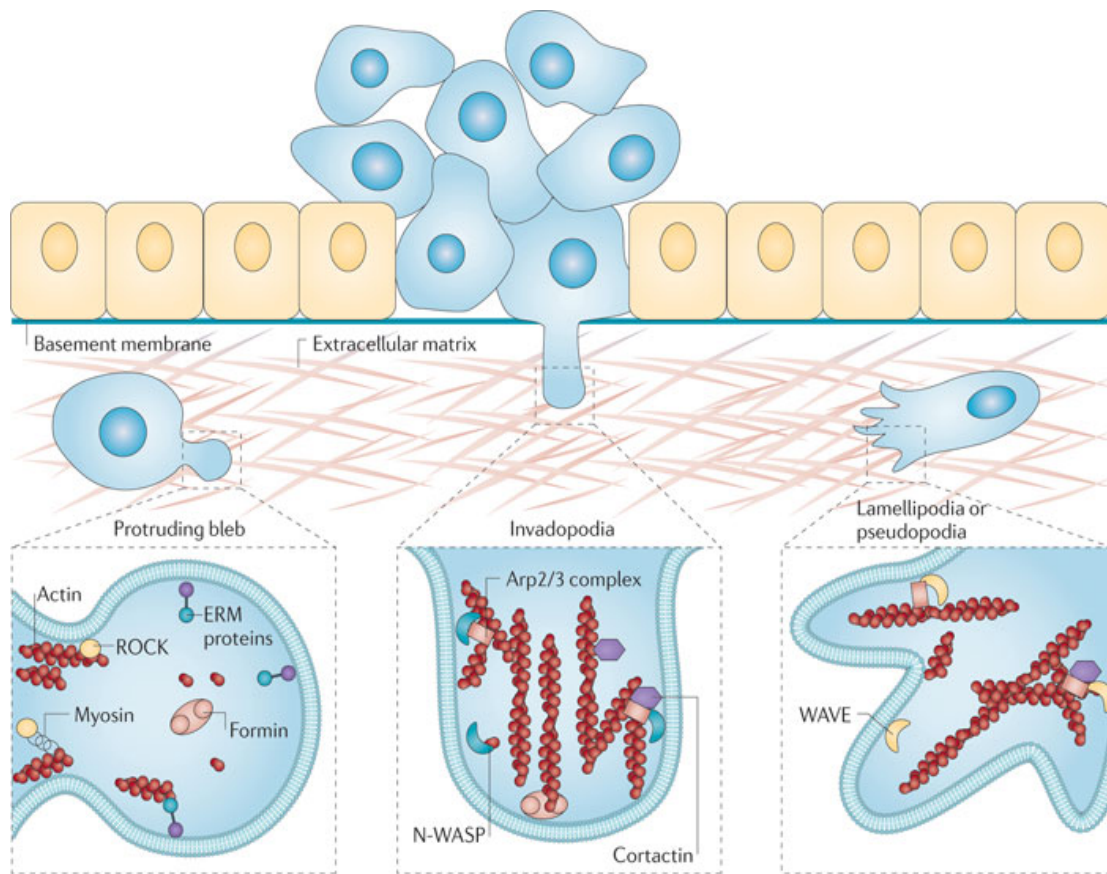
1.3.3 Rho GTPases as Cytoskeletal Regulators of Migration

One of the major cellular signalling pathways that regulates the cytoskeleton is the Rho family GTPase signalling pathway. At the cell membrane, integrins, Receptor Tyrosine Kinases (RTKs), G-Protein Coupled Receptors (GPCRs) and Cadherins receive extracellular signals which then influence the activity of Rho GTPase Guanine Nucleotide Exchange Factors (GEFs), which in turn influence activity of the Rho GTPases (Figure 1.5).

Rho GTPases have strongly emerged as fundamental players in the control of several biochemical pathways underlying migration, such as cytoskeletal dynamics, directional sensing, cell-cell junction assembly/disassembly and integrin-matrix adhesion.

Figure 1.4 Typical protrusive structures in invasive cancer cells

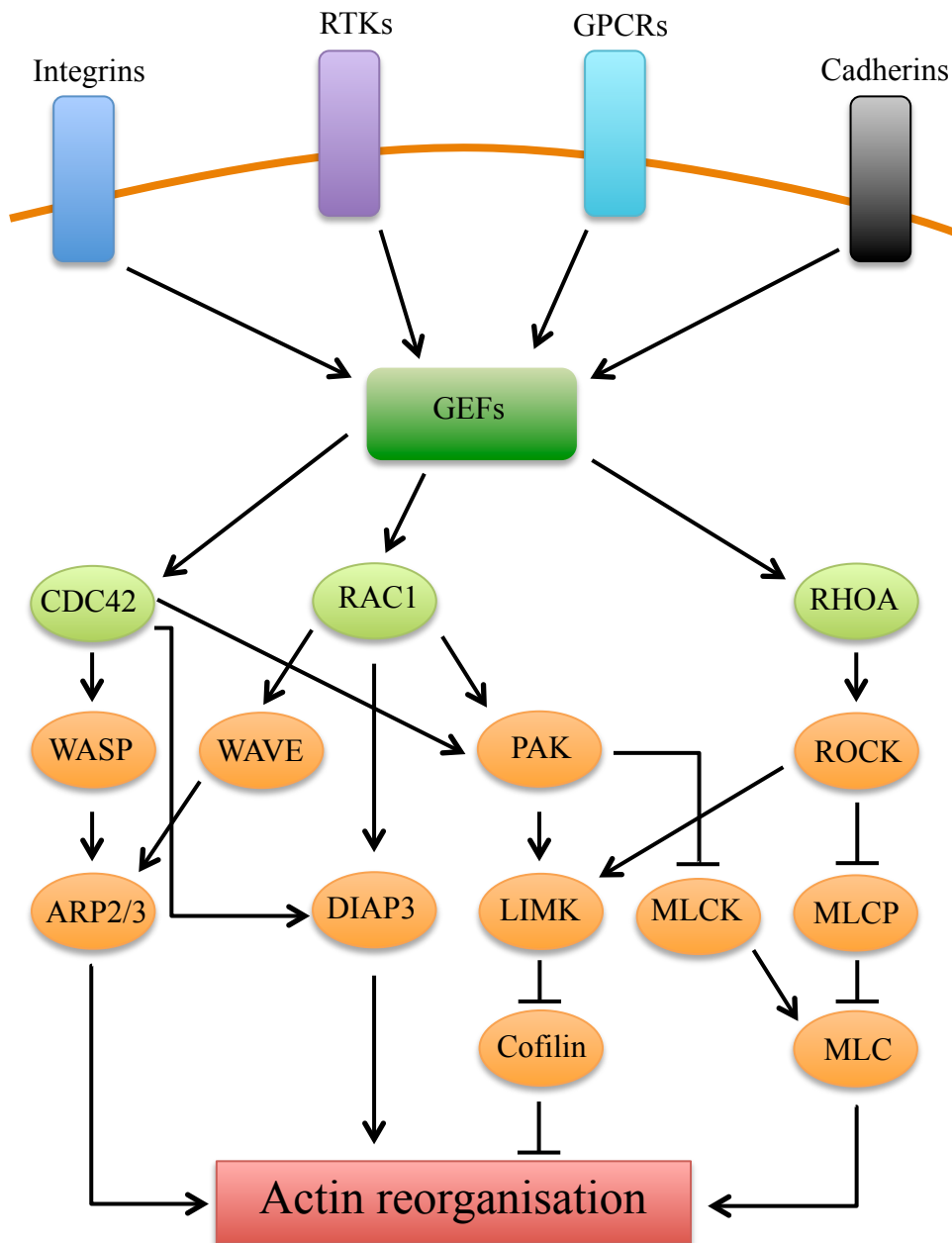
Cancer cell invasive phenotypes involve the formation of typical protrusive structures, such as plasma membrane blebs, invadopodia or pseudopodia, which are dependent on the nucleation and assembly of filamentous actin. Non-apoptotic blebs are highly dynamic protrusions in which the plasma membrane bulks out owing to increased hydrostatic pressure on regions of weak cortical actin [176]. The initial, protruding bleb is devoid of detectable F-actin, which becomes repolymerized during bleb retraction by unknown actin nucleation factors. Ezrin is recruited into the growing bleb, and formins seem to have a role in bleb formation through mechanisms that still need to be defined [177]. Invadopodia are actin-rich cellular protrusions that are tailored for the degradation of the extracellular matrix. The formation of invadopodia relies on N-WASP–Arp2/3-driven actin assembly and requires cortactin for invadopodia initiation and stabilization. Pseudopodia of cancer cells are lamellipodia-like structures and depend on the polymerization and assembly of actin by the WAVE–Arp2/3 nucleation machinery. Reprinted by permission from Macmillan Publishers Ltd: [Nature Reviews Cancer] (Nürnberg, Alexander, Thomas Kitzing, and Robert Grosse. "Nucleating actin for invasion." 11(3): 177-187, copyright (2011).



Nature Reviews | [Cancer](#)

Figure 1.5 Rho GTPases and their effector proteins that mediate actin cytoskeletal regulation

Integrins, Receptor Tyrosine Kinases (RTKs), G-Protein Coupled Receptors (GPCRs) and Cadherins influence activity of Rho GTPase Guanine Nucleotide Exchange Factors (GEFs), which in turn influence activity of the Rho GTPases. Actin cytoskeletal regulation downstream of the Rho GTPases Cdc42, Rac1 and RhoA is facilitated by numerous effector proteins. Cdc42, via activation of WASP (Wiskott-Aldrich syndrome protein), activates the ARP2/3 complex result in actin polymerisation and branched actin structures. Rac1 also activates the ARP2/3 complex via the WASP-related WAVE (WASP family verprolin homologous protein) family of proteins. Both Cdc42 and Rac1 activate DIAP3 (or mDIA2), resulting in unbranched actin filament nucleation. Additionally, Cdc42 and Rac1 activate the PAK family kinases, which, via phosphorylation, activate LIMK (LIM domain kinase), which subsequently, via phosphorylation, inhibits cofilin. Cofilin facilitates actin filament severing and depolymerisation, therefore its inhibition results in elevated polymerised actin stability. Additionally, LIMK is also activated by ROCK (RHO-associated coiled-coil-containing protein kinase), which is a downstream kinase effector of RhoA. ROCK elevated myosin light chain (MLC) phosphorylation via the inhibition of myosin light chain phosphatase (MLCP). MLC phosphorylation results in its increased association with actin filaments. Lastly, PAK lessens ROCK function via MLC kinase (MLCK) inhibition, thus reducing MLC phosphorylation. Adapted from Tybulewicz & Henderson, *Nat. Rev. Imm.*, 2009.



Rho GTPases are a family of small G proteins that, through the action of their downstream effector proteins, regulate the cytoskeleton and thereby influence the cell cycle, cell polarity and cell migration (Jaffe and Hall 2005). Importantly, human tumours from numerous cancer types show elevated expression of Rho GTPase genes, which correlates with an increased invasive and metastatic phenotype [reviewed in (Karlsson, Pedersen et al. 2009)].

Rho GTPases work as molecular switches existing in either an inactive, GDP-bound form or an active, GTP-bound form (Jaffe and Hall 2005). Regulation of GTPase activity is a complex affair with mammalian Rho GTPase inactivation regulated by a family of 67 GTPase activating proteins (GAPs), while activation is mediated by a family of 69 guanine nucleotide exchange factors (GEFs) (Rossman, Der et al. 2005). In their active state they interact with various different effector proteins to mediate the functions of Rho GTPases.

The three most extensively examined Rho GTPases, Rho, Rac and Cdc42 regulate the assembly and organisation of the cytoskeleton in eukaryotic cells [reviewed in (Hall 2012)]. Broadly speaking, Rho can recruit the ROCK (also known as Rho associated coiled-coil forming protein kinase, or Rho kinase) family of kinases that phosphorylate various cytoskeletal proteins promoting actin stress fibre formation and the generation of contractile force [reviewed in (Hall 2012)], Rac reorganises the actin cytoskeleton to promote formation of large membrane protrusions, called lamellipodia, that drive motility in many cell types, and Cdc42 signalling promotes the formation of actin-rich micro-spikes to sense extracellular chemotactic gradients and initiate directed cell movement. A major downstream effector of the Rho GTPase family of proteins is Rho kinase. Rho kinase is an effector of the small GTPase Rho and plays a key role in the regulation of actin remodeling, through the phosphorylation of cofilin and myosin light chain (MLC).

1.3.4 Cofilin, cell motility and metastasis

Downstream of various Rho GTPases is the cofilin pathway consisting of the actin-related protein 2/3 (Arp2/3) complex and cofilin that collectively play principle roles in the generation of free actin filament ends leading to enhanced actin filament remodelling (Edwards, Sanders et al. 1999). The expression of the Arp2/3 complex-regulator protein WAVE2 is highly correlated with greater metastatic risk in several cancer types (Sahai and Marshall 2002, Wang, Goswami et al. 2004, Vega and Ridley 2008). Furthermore, increased expression of cofilin has been observed in numerous malignancies [e.g. glioma, ovarian and lung cancer, and oral squamous cell carcinoma (Sinha, Hutter et al. 1999, Gunnensen, Spirkoska et al. 2000, Martoglio, Tom et al. 2000, Wang, Goswami et al. 2004, Keshamouni, Michailidis et al. 2006, Turhani, Krapfenbauer et al. 2006, Dowling, Meleady et al. 2007)] and is associated with chemotherapy resistance, invasive and metastatic disease. Recently, cofilin has been identified as a key driver of the cell invasive phenotype in prostate cancer (Collazo, Zhu et al. 2014).

Cofilin is inactivated via LIM Kinase 1 (LIMK)-mediated phosphorylation (Mouneimne, DesMarais et al. 2006). Together, LIMK, through cofilin inactivation, and phospholipase C (PLC), through cofilin activation, regulate cofilin in a synchronised manner to spatially restrict its activity (Mouneimne, DesMarais et al. 2006). The spatial restriction of cofilin activity is required for chemotaxis (directed cell movement towards a chemoattractant) as it leads to reorganisation of the actin filaments, which is required for movement towards a chemoattractant (Mouneimne, Soon et al. 2004, Mouneimne, DesMarais et al. 2006). The role of cofilin and its regulatory counterparts in chemotaxis highlights a possible role for cofilin activity regulation in the metastatic process. In support of this, components from both

the activation and inactivation arms of cofilin activity regulation are observed to be over-expressed in numerous invasive carcinomas (Wang, Goswami et al. 2004, Wang, Eddy et al. 2007). Recently, it has been observed that cofilin regulates the formation of actin-barbed ends in invasive tumour cells in a temporal manner (Tania, Prosk et al. 2011). Additionally, results from our laboratory highlighted that suppression of the microtubule destabilising protein stathmin altering neuroblastoma metastasis also altered cofilin phosphorylation levels and hence likely altered cofilin activity levels in neuroblastoma cells (Byrne, Yang et al. 2014).

Congruous with the role of LIMK1 activity in the regulation of actin cytoskeletal dynamics there is expanding evidence indicating an important role of LIMK1 in tumour cell invasion and metastasis. Elevated LIMK1 expression has been observed in numerous tumour types (reviewed in (Kavallaris 2012)). Downregulation of LIMK1 activity is associated with a decreased invasive phenotype and conversely, overexpression of LIMK1 activity is associated with increased invasion (Bagheri-Yarmand, Mazumdar et al. 2006, Horita, Ohashi et al. 2008, Ross-Macdonald, de Silva et al. 2008, Scott, Hooper et al. 2010). Additionally, the influence of elevated LIMK1 levels on cell motility and invasion are reversed by overexpression of cofilin (Wang, Mouneimne et al. 2006), therefore it is apparent that the LIMK1/cofilin ratio is the cellular response determinant and that small changes in actin dynamics could either increase or decrease invasiveness (Scott, Hooper et al. 2010).

The activity of LIMK proteins is controlled for the most part by phosphorylation of the Rho-GTPase effector proteins Rho-associated kinase 1 and 2 (ROCK1 and ROCK2) [reviewed in (Bernard 2007)]. In addition to LIMK and cofilin phosphorylation, active ROCK exerts its influence on cell migration by affecting myosin light chain (MLC) phosphorylation and hence activity. ROCK phosphorylates MLC directly, though the principal effect of ROCK on MLC phosphorylation is its ability to block the dephosphorylation of MLC via MLC

phosphatase (MLCP) inhibition [reviewed in (Mierke, Rosel et al. 2008)]. The increase in MLC phosphorylation, via ROCK's influence, contributes to actin reorganisation and stress fibre formation [reviewed in (Maekawa, Ishizaki et al. 1999)], these in turn are important for invasive cell behavior during metastasis (Yee, Melton et al. 2001, Wyckoff, Pinner et al. 2006, Mierke, Rosel et al. 2008). Recent findings from our laboratory have implicated a role for stathmin in the regulation of MLC phosphorylation in neuroblastoma cells (Byrne, Yang et al. 2014). Altogether ROCK signalling influences various aspects of actin cytoskeletal remodeling during cell migration and metastasis.

1.3.5 Intermediate Filaments

Intermediate filaments (IFs) are 10-nm-thick cytoskeletal structures formed by the self-assembly of members of the IF superfamily of proteins, which are encoded by about 70 genes and classified into 5 classes: keratins, neurofilaments, desmin, laminin and vimentin [reviewed in (Sihag, Inagaki et al. 2007)]. IFs are linked to the ECM and extend to the cytoplasmic interior that surrounds the nucleus. This extensive network allows IFs to coordinate cytoskeletal activities by relaying information from the cell surface to the inner compartments of the cell (Chang and Goldman 2004).

Whilst the vast majority of IF research focuses on diseases other than cancer, there exists evidence providing exciting insights into the involvement of IFs in tumour cell metastasis. Connections between the cytoskeleton and plasma membrane are vital in controlling cell migration [reviewed in (Pan, Jing et al. 2008)]. IFs provide prominent connections in epithelial cells, where keratin IFs are anchored at the cell-cell junctions by desmosomes and hemidesmosomes, and in myocytes, where desmin IFs are secured at costameres (Green and Jones 1996, Capetanaki, Bloch et al. 2007). Whilst many proteins (such as FAK and

Tm5NM1) influence tumour cell migration largely via their control of cell-ECM interactions, cell-cell interactions are also imperative and are commonly aberrantly regulated during metastasis (Hanahan and Weinberg 2011).

Nestin is an IF protein that has been reported as being overexpressed in various tumour types. Additionally, nestin expression correlates with aggressive growth and metastasis, and poor prognosis in pancreatic and prostate cancer, melanoma and glioblastoma [reviewed in (Ishiwata, Matsuda et al. 2011)]. Despite these findings, nestin's role in cancer has not been well characterised. Another IF that has been observed to be overexpressed in various cancers and correlates with tumour invasion and poor prognosis is vimentin (Satelli and Li 2011). Similar to nestin, the role of vimentin in cancer progression remains obscure. Despite this, Satelli *et al.*, have identified a vimentin-binding mini-peptide that has potential as a vimentin-targeted tumour-specific therapy (Satelli and Li 2011). However, more knowledge is required to investigate the suitability of this target and other IF targets in metastatic disease.

1.4 Stathmin

Stathmin, also known as p17, p18, p19 and metablastin, is a small cytosolic phosphoprotein that was discovered in 1983. (Feuerstein and Cooper 1983, Pasmantier, Danoff et al. 1986, Hanash, Strahler et al. 1988, Schubart, Xu et al. 1992). Stathmin is phosphorylated in response to numerous stimuli such as growth factors, antigen receptor stimulation, hormones and heat shock (Sobel and Tashjian 1983, Imboden, Weiss et al. 1985, Doye, Boutterin et al. 1990, Beretta, Dubois et al. 1995). Stathmin is the founding member of the highly conserved stathmin-like protein family. Other family members are the superior cervical ganglion-10 protein (SCG10) (*STMN2*), SCG10-like protein (SCLIP) (*STMN3*), RB3 (*STMN4*) and its splice variants RB3' and RB3'' (Koppel, Boutterin et al. 1990, Curmi, Gavet et al. 1999).

SCG10 and RB3 exhibit neural specific expression, whereas stathmin and SCLIP are ubiquitously expressed (Sobel, Bouterin et al. 1989, Bieche, Maucuer et al. 2003). Stathmin is principally expressed in the central nervous system (Chneiweiss, Beretta et al. 1989, Bieche, Maucuer et al. 2003). High amino acid homology and shared function has raised speculation that the stathmin-like proteins may be functionally redundant and that stathmin expression loss may result in increased compensatory expression of the other stathmin-like family members. Recent findings have demonstrated that upon stathmin suppression in neuroblastoma cells there is no observable compensatory changes in expression levels of the other stathmin-like family members (Byrne, Yang et al. 2014).

1.4.1. Structure and Function

The stathmin gene (STMN1) consisting of four introns and five exons, spans 6.3 kilobases (kb) on chromosome 1 (p35-36.1) (Ferrari, Seunanez et al. 1990, Melhem, Strahler et al. 1991). Stathmin's unstructured N-terminal domain encompasses multiple phosphorylation sites leading to the principle that it is a 'signal-integrating domain' whereas the C-terminus is structured possessing an α -helical structure which is thought to be the region of stathmin that is engaged in coiled-coil protein-protein interactions (e.g. binding of stathmin along two adjacent α/β -tubulin heterodimers) (Figure 1.6) (Maucuer, Camonis et al. 1995). This binding creates the T2S complex (one stathmin molecule: two tubulin heterodimers), where stathmin can influence microtubule dynamics by two separate pH-dependent mechanisms: tubulin heterodimer sequestration and promotion of microtubule catastrophe (Howell, Larsson et al. 1999, Steinmetz 2007) (Figure 1.7). Stathmin functions in healthy nervous system development where it promotes human embryonic stem cell differentiation and neurogenesis in the brain (Jin, Mao et al. 2004, Giampietro, Luzzati et al. 2005, Delaloy, Liu et al. 2010).

Figure 1.6 The T2S complex

Ternary T2S complex X-ray crystal structure (3.5 Å resolution) formed between a portion of the stathmin homologue and two α/β -tubulin heterodimers. The N-terminus interferes with longitudinal tubulin heterodimers contacts, whereas the C-terminus is essential for tubulin sequestering. Adapted from (Steinmetz 2007).

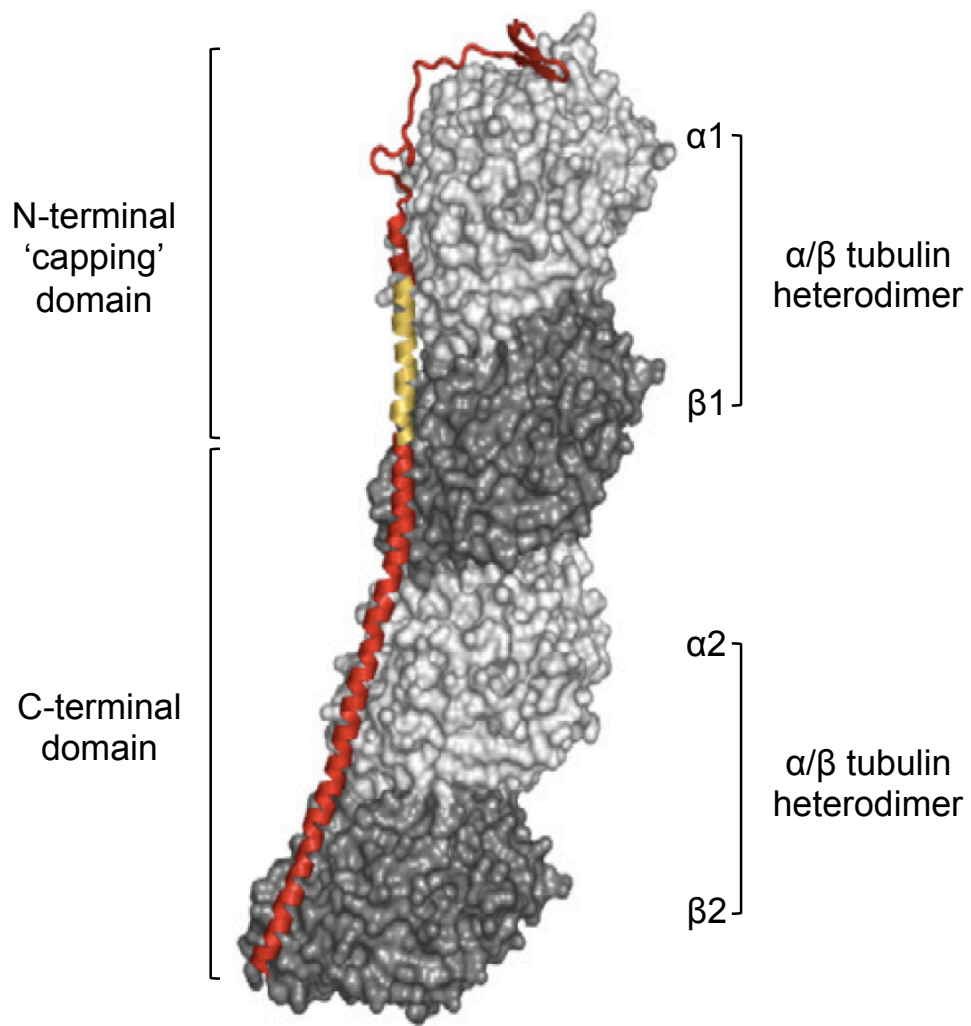
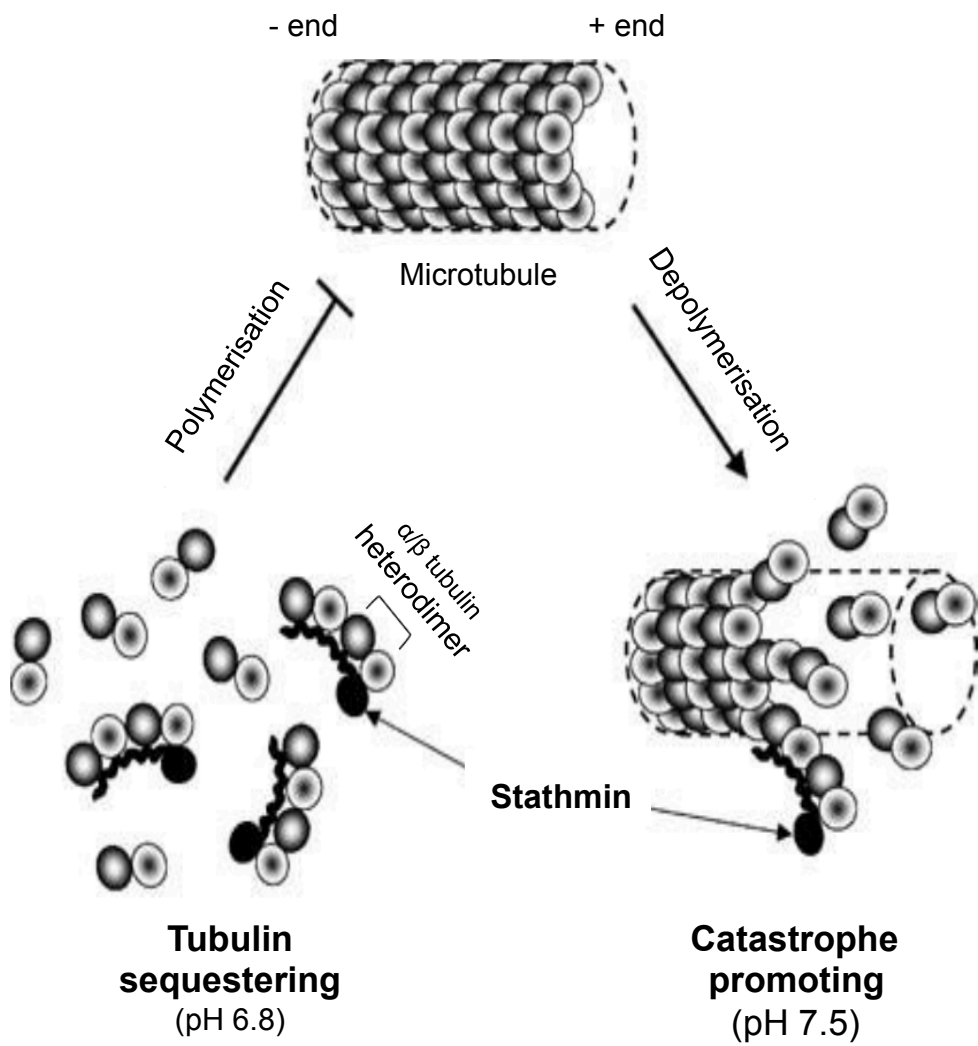


Figure 1.7 Stathmin mediates microtubule dynamics by sequestering tubulin and/or increasing microtubule catastrophe

At pH 6.8, stathmin sequesters tubulin heterodimers therefore interfering with microtubule polymerisation. At pH 7.5, stathmin destabilises microtubules by promoting microtubule catastrophes (Howell, Larsson et al. 1999). PDB ID code: 1SA0. Adapted from (Rubin and Atweh 2004).

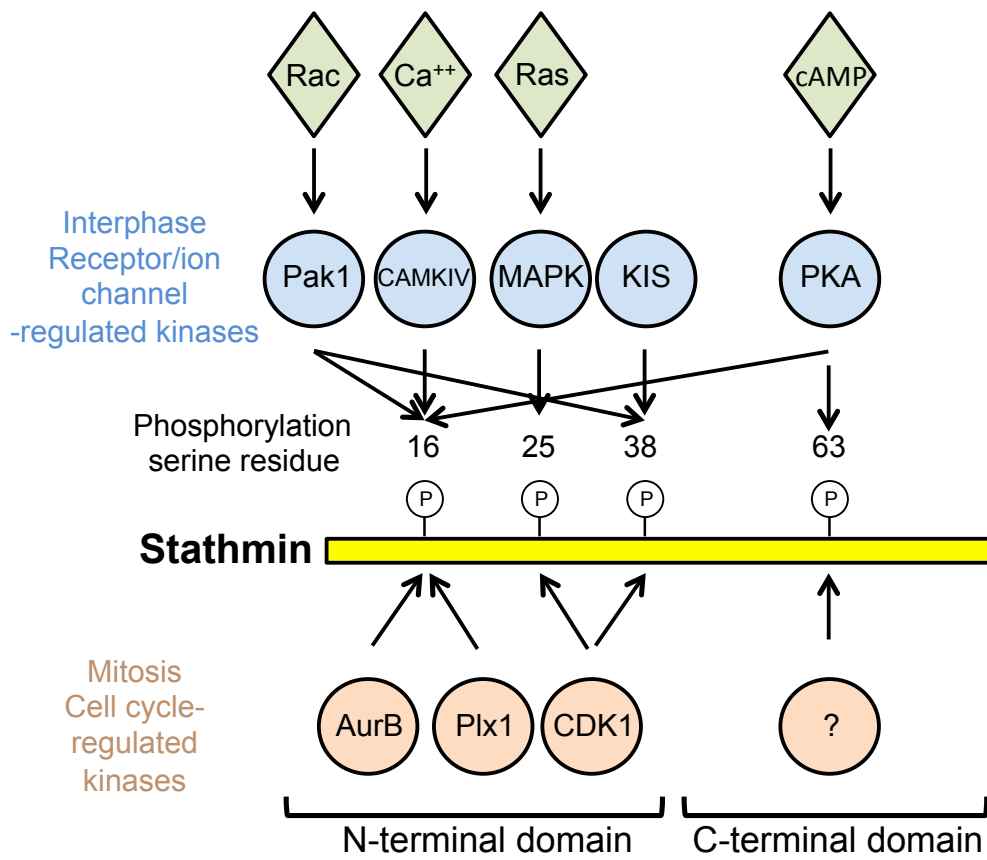


1.4.2 Phosphorylation

Stathmin's tubulin-binding affinity is spatially and temporally controlled by phosphorylation on four serine residues: three in the N-terminal domain (Ser16, Ser25, Ser38) and one in the C-terminal domain (Ser63) (Steinmetz 2007) (Figure 1.8). An array of kinases phosphorylate stathmin during mitosis, including polo-like kinase 1 (PLK1), the cyclin dependent kinase 1 (CDK1)/p34cdc2 and the calcium-calmodium dependent protein kinase (Beretta, Dobransky et al. 1993, Budde, Kumagai et al. 2001). Alternatively, stathmin's activity is controlled in interphase by numerous growth factor-induced kinases including kinase interacting with stathmin (KIS), p21-activated kinase (PAK1) and cyclic adenosine monophosphate-dependent kinase (PKA) (Cassimeris 2002, Wittmann, Bokoch et al. 2004, Langenickel, Olive et al. 2008) (Figure 1.8). Each of the four phosphorylation sites are phosphorylated sequentially where Ser25 and Ser38 phosphorylation is vital for Ser16 and Ser63 phosphorylation (Steinmetz 2007). Phosphorylation of each of the phosphorylation sites generates a grade of tubulin-binding affinity where complete phosphorylation leads to complete inactivation of stathmin's tubulin binding affinity [reviewed in (Steinmetz 2007)].

Figure 1.8 Signalling pathways that influence stathmin phosphorylation

Various ion-channel, receptor and mitotically activated kinases promote stathmin phosphorylation, including p21-activated kinase (Pak1) (Wittman, Bokock et al. 2004; Takahashi and Suzuki 2009), calcium-calmodium dependent protein kinases (CAMKIV), mitogen-activated protein kinase (MAPK) (Ng, Zhao et al. 2010), kinase interacting with stathmin (KIS) (Langenickel, Olive et al. 2008), cyclic adenosine monophosphate-dependent kinase (PKA) (Cassimeris 2002), aurora kinase B (AurB) (Liedtke, Leman et al. 2002), polo-like kinase 1 (Plx1) (Budde, Kumagai et al. 1993). The kinase responsible for Ser63 phosphorylation during mitosis is currently unknown. Adapted from (Holmfeldt, Sellin et al. 2009).



1.4.3 Cell Cycle Regulation

Inactivation of stathmin's tubulin-binding affinity upon complete phosphorylation has the most importance during cell cycle progression (Steinmetz 2007). Upon cells entering mitosis, stathmin is completely phosphorylated in regions proximal to the mitotic spindle (Brattsand, Marklund et al. 1994, Niethammer, Bastiaens et al. 2004). In contrast, as cells exit mitosis, stathmin is completely dephosphorylated resulting in reactivation of stathmin's tubulin-binding ability. Stathmin is dephosphorylated by the okadaic-acid sensitive protein phosphatases PP1, PP2A and PP2B (Mistry, Li et al. 1998, Rubin and Atweh 2004). Impaired stathmin phosphorylation has been observed to influence cell cycle progression in leukemic cells where expression of a Ser16 phosphorylation-impaired mutation led to prometaphase arrest and mitotic spindle microtubule destabilisation (Misek, Chang et al. 2002, Holmfeldt, Sellin et al. 2010). Additionally, mutation of the cyclin-dependent kinase target site responsible for Ser25/Ser38 phosphorylation caused a G2-M delay and subsequent endoreduplication from S phase progression without correct chromosomal separation (Marklund, Osterman et al. 1994, Rubin and Atweh 2004). Furthermore, it has been proposed that excessive stathmin activity results in evasion of the spindle assembly checkpoint preceding the metaphase-anaphase transition and consequently highly controlled regulation of stathmin activity is considered vital for mitosis. Though given stathmin's apparent importance during cell mitosis, stathmin loss can also interfere with mitosis where suppression of stathmin expression can induce a G2-M delay and subsequent growth arrest in various non-neuronal cells (Mistry, Bank et al. 2005, Wang, Dong et al. 2007, Singer, Malz et al. 2009). Stathmin's role in cell proliferation appears to be cell type specific whereby alteration of stathmin expression in various leukaemia cells did not influence mitotic spindle assembly for cell proliferation (Holmfeldt, Brannstrom et al. 2006, Holmfeldt, Sellin et al.

2010). Additionally, recent published findings from our laboratory highlight that stathmin suppression, using RNAi, does not influence cell cycle or cell proliferation in neuroblastoma cells, or primary tumour growth in a clinically-relevant neuroblastoma orthotopic xenograft mouse model (Byrne, Yang et al. 2014).

1.4.4. Stathmin and its Role in Metastasis

In addition to the role of stathmin in cell cycle regulation and nervous system development, growing evidence has highlighted a significant role for stathmin in the migration of various healthy cells, including mouse embryonic fibroblasts (Baldassarre, Belletti et al. 2005), *Drosophila* germ cells (Ozon, Guichet et al. 2002), rat neuronal cells (Jin, Mao et al. 2004) and human endothelial cells (Mistry, Bank et al. 2007). Furthermore, stathmin has been observed to play a role in the migration of numerous tumour cell types, including hepatocellular carcinoma (Gan, Guo et al. 2010), gastric cancer (Jeon, Han et al. 2010), sarcoma (Baldassarre, Belletti et al. 2005), non-small cell lung cancer (Singer, Malz et al. 2009) and oesophageal squamous cell carcinoma (Liu, Sun et al. 2013). Additionally, it has been suggested that stathmin is involved in *in vivo* cell invasion where stathmin is highly expressed in invasive hepatocellular carcinoma (Hsieh, Huang et al. 2010), gastric cancer (Jeon, Han et al. 2010) and endometrial carcinoma (Salvesen, Carter et al. 2009). Therefore, it is not surprising that stathmin over-expression has been observed to correlate strongly with metastatic disease progression in numerous cancer types (Xi, Rui et al. 2009, Hsieh, Huang et al. 2010, Kuramitsu, Taba et al. 2010, Trovik, Wik et al. 2011). Notably, in endometrial carcinoma, pronounced stathmin immunohistochemistry staining is a strong predictor of lymph node metastasis and poor survival (Trovik, Wik et al. 2011).

Whilst stathmin expression is increased in highly migratory, invasive and metastatic

malignancies, altered activity of stathmin due to somatic mutations, where stathmin is present in a more 'active' (unphosphorylated) state has been observed to enhance sarcoma *in vitro* cell invasion and *in vivo* metastasis (Belletti, Nicoloso et al. 2008). Though despite this finding, somatic stathmin mutations are infrequent suggesting that alternative mechanisms to disturb stathmin activity in cancer metastasis may be present. In addition to somatic mutations, an additional way stathmin's phosphorylation state can be altered to influence cell migratory phenotype is via stathmin's interaction with particular proteins. Notably, kinase interacting with stathmin (KIS) influences vascular smooth muscle cell migration through its effect on stathmin Ser38 phosphorylation (Langenickel, Olive et al. 2008). Another protein interacting with stathmin that influences cell migration is STAT3 (Ng, Lin et al. 2006). STAT3 influences microtubule dynamics and migration of mouse embryonic fibroblasts and T cells by interacting with stathmin's C-terminal domain (Ng, Lin et al. 2006, Verma, Dourlat et al. 2009). Furthermore, STAT3 also interacts with the stathmin-like family protein member SCLIP to influence breast cancer invasion (Ng, Lin et al. 2006).

1.4.5 Stathmin in Neuroblastoma

Stathmin is highly expressed in neuroblastoma (Hailat, Strahler et al. 1990). In MYCN-amplified primary neuroblastoma tumours stathmin exhibits aberrant phosphorylation suggesting altered stathmin activity (Hailat, Strahler et al. 1990). MYCN amplification is strongly associated with genetic alterations in chromosome 1p36, which is the genetic location of stathmin leading to the suggestion that stathmin may be genetically altered in neuroblastoma (Brodeur 2003). Importantly, our laboratory has observed that suppression of stathmin, using RNA interference, significantly reduced *in vitro* cell migration and invasion, and *in vivo* neuroblastoma metastasis to the lung by 71% in a clinically relevant orthotopic

neuroblastoma mouse model (Byrne, Yang et al. 2014). Therefore, elevated stathmin levels may contribute to a more aggressive neuroblastoma phenotype. However, at what stages in the metastatic cascade stathmin exerts these effects remains unknown.

1.5 Thesis Aims

The overall objective of this thesis is to investigate the role of stathmin in neuroblastoma metastasis. The major aims are four-fold. Firstly, to determine stathmin's contribution to specific steps of metastasis in neuroblastoma *in vitro*, including cell migration, invasion, anoikis and transendothelial migration. The second aim is to determine how stathmin mediates its influence on metastasis in neuroblastoma by examination of key cellular signalling pathways. The third aim of this thesis is to utilise an experimental mouse model of neuroblastoma metastasis to determine if stathmin's influence to neuroblastoma metastasis *in vivo*, is related to the extravasation step of metastasis. The final aim of this thesis is to examine the therapeutic potential of targeting stathmin in metastatic neuroblastoma. Altogether, these aims have the overall theme of increasing the understanding of stathmin's role in neuroblastoma metastasis and examining stathmin as a potential therapeutic target in metastatic neuroblastoma.

Chapter 2. Materials & Methods

2. Materials & Methods

2.1. Cell Culture

A panel of neuroblastoma cell lines, including SK-N-BE(2), IMR-32, NBL-S, NBL-W, SH-EP and SH-SY5Y were screened for stathmin expression in initial experiments. The human neuroblastoma cell line SK-N-BE(2) was a generous gift from Dr. Sylvain Baruchel (The Hospital for Sick Children, Toronto). IMR-32 was obtained from the American Type Culture Collection (ATCC). SH-EP and SH-SY5Y were obtained from Dr. June Biedler, Fordham University, New York. NBL-S and NBL-W cell lines were kindly provided by Dr S. Cohn (Northwestern University, Chicago, IL). The human normal foetal lung fibroblast cell line MRC-5 was used in initial stathmin experiments and was obtained from the American Type Culture Collection (ATCC). The immortalized human dermal microvascular endothelial (HMEC-1) cell line, used in transendothelial migration experiments was obtained from Dr Eddy Pasquier.

The bulk of experiments conducted in this thesis utilised SK-N-BE(2) and SH-SY5Y neuroblastoma cells, which were all originally derived from bone marrow biopsies of relapsed patients with advanced (stage 4) disease, their clonal derivation has been previously described by (Pacuszka, Duffard et al. 1978). The SK-N-BE(2) and SH-SY5Y cell lines were all validated by short tandem repeat (STR) profiling (CellBank Australia, Westmead, New South Wales). All neuroblastoma cells and MRC-5 cells were grown in 10% foetal calf serum (FCS)/Dulbecco's Modified Eagle Media (DMEM) (Gibco-Invitrogen, Carlsbad, CA, USA) at 37°C in a humidified atmosphere with 5% CO₂. HMEC-1 cells were grown in 10%FCS/MCDB-131 containing 2 mmol/L glutamine (Life Technologies, Paisley, United Kingdom), 1% penicillin, and streptomycin (Life Technologies, Paisley, United Kingdom), 1

$\mu\text{g}/\text{mL}$ hydrocortisone (Pharmacia & Upjohn, St-Quentin- Yvelines, France), and $10 \text{ ng}/\text{mL}$ epithelial growth factor (R&D Systems, Minneapolis, MN). HMEC-1 were used between passages 11 and 16 and MRC-5 between passage 5 and 10. Cells were grown as monolayers and passaged 2-3 times per week using phosphate buffered saline (PBS)/Trypsin. All cells were regularly screened and observed to be free of mycoplasma.

2.2. siRNA-mediated stathmin suppression

RNA interference (RNAi) is an evolutionary-conserved, post-transcriptional gene silencing mechanism found in most eukaryotes. Synthetic small interfering RNA (siRNA), usually 20-25 base pairs long, can be used to activate RNAi and silence target gene expression. For human stathmin (STMN1) suppression studies, neuroblastoma cells were transfected separately with one of four STMN1 ON-TARGETplus siRNA sequences or ON-TARGETplus non-targeting (control) reagent (ThermoFisher Scientific, Lafayette, CO). The ON-TARGETplus siRNA reagents are modified to minimise potential off-target effects by preventing the interaction of the sense strand with the RNA-induced silencing complex (RISC), favouring antisense strand uptake, and the minimisation of seed-related off-target effect by modification of the antisense strand (Dharmacon RNAi Technologies, ThermoFisher Scientific). All siRNAs were reconstituted in 1x siRNA buffer ($20 \text{ mmol}/\text{L}$ KCl, $6 \text{ mmol}/\text{L}$ HEPES pH 7.5, $0.2 \text{ mmol}/\text{L}$ MgCl_2) (ThermoFisher Scientific) to a working concentration of $20 \mu\text{mol}/\text{L}$. The STMN1 ON-TARGETplus siRNA sequences contain four separate, individual siRNA sequences that target STMN1, transcript variant 2 (NM_203399) (See Table 2.2 for siRNA sequences). These four sequences also target the three other STMN1 transcript variants (NM_203401, NM_001145454 and NM_005563) as they are

homologous in these regions. The STMN1 ON-TARGETplus siRNA sequences have been confirmed to have minimal targeting of known genes in human cells.

Table 2.1 Stathmin siRNA sequences

Target gene/Accession #	siRNA Seq.	siRNA sequence	Gene location
STMN1/ *NM_203401, NM_203399, NM_005563, NM_001145454	1	GAAGAGAAACUGACCCACA	Exon 3-4
	2	GAAACGAGAGCACGAGAAA	Exon 4
	3	UAAAGAGAACCGAGAGGCA	Exon 4
	4	GAAAGACGCAAGUCCCAUG	Exon 4
Non-applicable	Non-effective control	GCACTACCAGAGCTAACTCA GATAGTACT	Non-applicable

*All four stathmin siRNA sequences target all four stathmin gene transcripts

Lipofectamine 2000 (Invitrogen, Carlsbad, CA, USA), a cationic liposome-based reagent, was used to deliver siRNA into cells. Cells were seeded into 6 well plates at a density of 1.8×10^5 cells/well for SK-N-BE(2) and 2.5×10^5 cells/well for SH-SY5Y. To maximise and extend stathmin suppression, neuroblastoma cells were double-transfected where cells were transfected with siRNA and Lipofectamine 2000 (2 μ g/well) at 24 and 48 h post-seeding, as previously described (Byrne, Yang et al. 2014). The optimal concentration of stathmin siRNA was 5 nmol/L for SK-N-BE(2) and 50 nmol/L for SH-SY5Y cells.

2.3. RNA isolation and cDNA synthesis – Cell culture

Total RNA from tissue culture cells was isolated using an RNeasyPlus Maxi Kit (Qiagen, Valencia, CA). Neuroblastoma cells were harvested 48 h post-siRNA transfection, washed once with PBS and 600 μ L of RLT plus buffer (Qiagen) including 6 μ L β -mercaptoethanol (Sigma Aldrich Pty. Ltd. Sydney, Australia) was added and samples placed at -80°C for at

least 1 h. Samples were thawed and 600 μL /well added into different gDNA eliminator columns. Columns were centrifuged at maximum speed for 1 min at RT. After disposing of the gDNA column, 600 μL of 70% ethanol was added and the resulting mixture added to different RNA collection columns. Columns were centrifuged at maximum speed (14000 rpm) for 1 min at RT. The columns were transferred to fresh collection tubes and 600 μL of RW1 (wash1) buffer (Qiagen) was added followed by centrifugation at maximum speed for 1 min at RT. RNA columns were transferred to fresh collection tubes and 500 μL of RPE (ethanol-containing wash buffer) was added to the columns followed by centrifugation at maximum speed for 1 min at RT. RNA columns were transferred to fresh 1.5 mL microfuge tubes, 30 μL of RNase/DNase free H_2O added and columns centrifuged at maximum speed for 2 min at RT. Resulting total RNA isolates were quantified using a Nanodrop (Thermo Scientific) and 0.5 μg of RNA was reverse transcribed using a High Capacity cDNA Reverse Transcription Kit (Applied Biosystems, Foster City, CA). 0.5 μg of RNA was diluted to a total volume of 10 μL using RNase/DNase free H_2O . 10 μL of Applied Biosystem cDNA Reverse Transcription Kit master mix was added containing 2 μL /reaction 10xRT buffer, 0.8 μL /reaction 25xdNTPs, 2 μL /reaction 10xRT random primers, 1 μL /reaction Multiscribe[®] reverse transcriptase and 4.2 μL /reaction RNase/DNase free H_2O . The resulting 20 μL reaction mixture was incubated for 10 min at 25°C, 120 min at 37°C and 5 min at 85°C. Resulting cDNA samples were subsequently used in quantitative PCR (qPCR) experiments (see Section 2.5).

2.4. RNA isolation and cDNA synthesis –

Animal tissues

Tumour tissues were cut into small pieces (approx. 100 mg) and homogenized in 1 mL ice-cold Trizol using a tissue homogenizer (TissueRuptor™, Qiagen, Valencia, CA). Tissue debris was removed by centrifugation at 12,000 g for 10 min at 4°C. Tissue homogenate was transferred to a tube containing 200 µL chloroform and mixed vigorously by hand for 15 s followed by centrifugation at 14,000 g for 15 min at 4°C. The aqueous (upper) phase was transferred to a fresh tube and mixed with 500 µL isopropanol followed by 10 min incubation at RT. Samples were centrifuged at 12,000 g for 10 min at 4°C and the resulting RNA pellet washed with 1 mL of 75% ethanol followed by centrifugation at 7,500 g for 5 min at 4°C. Samples were washed again with 1 mL of 75% ethanol. Samples were centrifuged at 7,500 g for 5 min at 4°C and supernatant removed. RNA pellet was air-dried by evaporation in a fume cupboard. Once the RNA pellet was dry it was dissolved by adding 50 µL of RNase/DNase free H₂O and heated to 60°C for 10 min. RNA isolates were quantified using a Nanodrop (Thermoscientific). RNA was reverse transcribed using a Quantitect® reverse transcription kit (Qiagen). 0.5 µg of RNA was diluted to a total of 12 µL in RNase/DNase free H₂O. 2 µL of gDNA wipeout buffer (Qiagen) was added and the 14 µL solution incubated for 2 min at 42°C to remove residual genomic DNA contamination. 1 µL of Quantiscript® reverse transcriptase (Qiagen), 4 µL of Quantiscript® RT buffer (Qiagen) and 1 µL RT primer mix (Qiagen) was added to bring the total reaction volume to 20 µL. Samples were heated to 42°C for 15 min followed by incubation at 95°C for 3 min. Resulting cDNA samples were subsequently used in quantitative PCR (qPCR) experiments (see Section 2.5).

2.5. Quantitative PCR (qPCR)

Quantitative PCR (qPCR) was performed to assess stathmin, the housekeeping gene beta-2-microglobulin (β 2M) and green fluorescent protein (GFP) mRNA expression in tissue culture and animal tissue samples. qPCR was performed in a total volume of 25 μ L consisting of 2 μ L cDNA, 12.5 μ L Quantitect SYBR green (Qiagen, Valencia, CA), 2.5 μ L Quantitect Primer assay (for either stathmin, beta-2-microglobulin or GFP primers, containing both forward and reverse primers) and 8 μ L RNase/DNase free H₂O. Samples were loaded into a 96-well plate and centrifuged at 1,500 g for 2 min. Samples were subsequently analysed on an Applied Biosystems 7900 PCR system using the following thermocycling conditions: 1) 50°C for 2 min, 2) 95°C for 15 min, 3) 40 cycles of 95°C for 15 seconds and 60°C for 1 minute, 4) 95°C for 15 s, 5) 60°C for 1 min and 6) 95°C for 15 s. In tissue culture based experiments, stathmin mRNA was normalised to the house keeping gene β 2M. In animal tissue based experiments, stathmin mRNA was normalised to both β 2M and GFP. Normalisation to GFP was included as GFP is specifically expressed in the SK-N-BE(2)/TGL cells and not expressed in the mouse liver tissue.

2.6. Protein expression analysis

Cells were washed once with PBS and lysed using radio-immunoprecipitation assay (RIPA) buffer containing 150 mM NaCl, 50 mmol/L Tris (pH 7.5), 0.1% sodium dodecyl sulphate (SDS), 0.5% sodium deoxycholate, 10 mmol/L nonylphenoxypolyethoxyethanol (NP-40) and 1% protease inhibitors (Roche Diagnostics, Australia) and then centrifuged at 14,000 g for 7 min at 4°C followed by transferring the cleared lysate to a fresh tube to remove cell debris. Samples were stored at -80°C. For Rho GTPase (Rac1, Cdc42 and RhoA) experiments, cells were harvested on ice, washed with PBS and the cells lysed in Cell Lysis Buffer

(Cytoskeleton Inc., Denver, CO) and cell debris was removed by centrifugation at 14,000 g for 5 min at 4°C and cleared cell lysates transferred to a fresh eppendorf tube and snap frozen immediately in liquid nitrogen. For all experiments total protein content was determined using a BCA protein assay kit (Pierce Biotechnology Inc.) Cell lysates were diluted in 4x reducing sample buffer [130 mM Tris pH 8, 129.65 mmol/L dithiothreitol, 20% (v/v) glycerol, 4.6% (w/v) SDS and 0.02% bromophenol blue] and then boiled at 96°C for 6 min to denature the proteins. Total cellular proteins (15 µg/lane) were resolved on 12% SDS-polyacrylamide gel electrophoresis (PAGE) gels (Bio-Rad Laboratories, Hercules, CA) and electro-transferred, using the Bio-Rad Transfer unit (Bio-Rad Laboratories, Hercules, CA) containing ice-cold transfer buffer (0.025 M Tris-Glycine, 20% methanol) to nitrocellulose membrane (GE Healthcare). Transfer was performed at either 200 milliamps (mA) for 90 min or 70 mA overnight, both at 4°C. Post-transfer membranes were stained with 0.5% Ponceau S (in 1% acetic acid) to assess sufficient protein transfer and equal protein loading and then blocked for 40 minutes in 5% skim milk powder (SMP)/Tris-buffered saline with 0.5% Tween-20 (TBS-T). Membranes were briefly rinsed once with TBS-T and proteins detected using the antibodies listed in Table 2.2. Primary antibodies were either incubated overnight at 4°C or 2 h at RT, and were detected using horseradish peroxidase (HRP)-conjugated polyclonal antibodies (GE Healthcare Life Sciences, Uppsala, Sweden). HRP-conjugated secondary antibodies were incubated for 60 minutes at RT. Membranes were developed using ECL PRIME Western blotting reagent (GE Healthcare) and chemiluminescent signal was detected and imaged using an X-ray developer (Okamoto, China) or Typhoon 9410 laser scanner (GE Healthcare).

Table 2.2 Antibody dilutions for western blots

Primary	Supplier	Dilution	Secondary	Dilution	Diluent
Stathmin	BD	1:1000	Goat α -mouse	1:2500	TBS-T
GAPDH	Abcam	1:5000	Goat α -mouse	1:5000	TBS-T
RhoA (total lysate)	Cytoskeleton	1:2500	Goat α -mouse	1:10000	TBS-T
RhoA (pull-down)	Cytoskeleton	1:1000	Goat α -mouse	1:5000	TBS-T
Rac1 (total lysate)	Cytoskeleton	1:1000	Goat α -mouse	1:1000	TBS-T
Rac1 (pull-down)	Cytoskeleton	1:1000	Goat α -mouse	1:1000	TBS-T
Cdc42 (total lysate)	Cytoskeleton	1:250	Goat α -mouse	1:1000	TBS-T
Cdc42 (pull-down)	Cytoskeleton	1:250	Goat α -mouse	1:1000	TBS-T
GEF-H1	Cell Signalling	1:1000	Donkey α -rabbit	1:10000	TBS-T

*Phospho antibody

2.7 Bromo deoxyuridine (BrdU) cell proliferation assay

Cell proliferation assays were performed to determine whether stathmin suppression influenced SK-N-BE(2) cell growth. SK-N-BE(2) cells were seeded into 96-well plates (Greiner Bio-One, Frickenhausen, Germany) at a density of 2×10^3 cells/well. Cells were transfected with siRNA as previously described (see Section 2.2) in a final volume of 100 μ L/well. Cell proliferation was performed using a BrdU kit as instructed by the manufacturer (Roche Diagnostics, Indianapolis, IN, USA). 48 hours after the second siRNA transfection, 10 μ L of BrdU labeling reagent (10 mM bromo deoxyuridine in PBS, pH 7.4) was added to

give a final concentration of 10 μ M and cells were incubated at 37°C for 2 hours. Fixation of cells was performed by addition of 200 μ L/well FixDenat solution (provided in the kit) and followed by incubation for 30 min at RT. The monoclonal antibody from mouse-mouse hybrid cells [clone BMG, 6H8, Fab fragments] conjugated with peroxidase (POD) (anti-BrdU-POD working solution) was added to the cells and incubated for 90 min at RT, followed by three washes of 1xPBS. The substrate solution (tetramethyl-benzidine, TMP) was added and incubated for up to 30 min at RT until a blue colour of suitable intensity developed (12 minute incubation was optimised for analysis). The plate was read at 370 nm (with a reference wavelength: 492 nm). The proliferation rate was determined by quantifying the amount BrdU incorporation during DNA synthesis. The mean absorbance was determined by subtracting the absorbance of the non-BrdU treated cells (background) from the absorbance value of the BrdU-treated cells.

2.8. Chemotactic migration & invasion assays

Neuroblastoma cells were double-siRNA transfected with control or stathmin siRNA and 48 h later cells were serum starved by incubation in serum-free DMEM media for 2 h. The bottom of 8 μ m BD PET migration chambers (BD Biosciences) and 8 μ m BD Biocoat™ BD Matrigel™ 24-well invasion chambers (BD Biosciences) were coated with 10 μ g/mL collagen IV (BD Biosciences) and incubated at room temperature for 1 h. Inserts were then equilibrated in 1 mL serum-free DMEM for 30 minutes in companion plate wells. Cells were harvested using PBS/trypsin, counted, resuspended in 500 μ L serum-free DMEM into the top chamber at 25,000 cells/insert and 50,000 cells/insert for SK-N-BE(2) and SH-SY5Y cells respectively for both migration and invasion assays. In addition to the collagen IV chemoattractant, the lower chamber contained 25 ng/mL human recombinant platelet-derived

growth factor (PDGF) (Sigma Aldrich Pty. Ltd. Sydney, Australia) diluted in 10% FCS/DMEM to act as an additional chemoattractant in invasion assays. After cells were seeded in the top chamber they were incubated at 37°C for 24 h or 48 h for SK-N-BE(2) and SH-SY5Y cells respectively. Inserts were removed and cells fixed with 100% methanol for 20 min at RT. Inserts were removed from methanol and dried for 1 h. After drying, the cells were stained with (0.45 µm filtered) May-Grunwald (Sigma Aldrich) diluted 1:3 in milliQ-H₂O and (0.45 µm filtered) Giemsa (Sigma Aldrich) diluted 1:25 in milliQ-H₂O. Inserts were dried and membranes removed from inserts with a scalpel and mounted onto glass slides and covered with glass coverslips. At least 10 random images were acquired of each membrane (both top and bottom surfaces) with an Olympus BH-2 inverted microscope using a 20x objective. To identify the cells on the top versus the bottom surface of the transwell membrane insert, images were acquired in slightly different focal planes. For one focal plane, the cells on top were in focus and cells on bottom were out of focus. For the other focal plane, the cells on top were out of focus and cells on bottom were in focus. Results are displayed as either a migration or invasion index [(number of cells on under surface of membrane divided by total number of cells on both surfaces of the membrane) x 100] where control cells are 100% and all other treatments are expressed as a percentage of control.

2.9. 3D Tumour spheroid culture

SK-N-BE(2) cells were seeded at 2,500 cells/well into round-bottomed, ultra-low attachment 96-well plates (Corning, Victoria, Australia) and incubated for up to 7 days at 37°C. If the incubation was longer than 96 h a 50% media exchange was performed, where 50% of the media in the wells (i.e. 50 µL) was aspirated and 50 µL of fresh 10% FCS/DMEM added to each well. For tumour spheroid growth experiments, images were acquired of each spheroid

at 2, 4 and 7 d post-seeding using an Axiovert 200M fluorescent microscope (Zeiss, Oberkochen, Germany) and a 63x 1.4 NA Plan lens, coupled to an AxioCamMR3 camera and driven by the Axio Vision software (Zeiss). Spheroid diameter was quantified using Axio Vision software (Zeiss).

2.10. 3D Tumour spheroid outgrowth into extracellular matrices

After 4 d of tumour spheroid growth, spheroids with an average diameter of ~400-500 μm were subjected to outgrowth into extracellular matrices assays. 80 μL of Collagen I mixture [0.5 mg/mL Rat tail Collagen I (Life Technologies, Paisley, United Kingdom), 1X phosphate-buffered saline, 5.0% (v/v) sodium hydroxide] was added to each well in a flat-bottomed 96-well plate. The plate was placed for 1 h at 37°C to allow polymerisation of collagen I matrix. One spheroid was transferred into each well. An additional 80 μL Collagen I mixture was added to the top of the spheroid. The plate was placed for 1 h at 37°C to allow top layer of Collagen I matrix polymerisation. 100 μL of 10% FCS-containing DMEM was added to each well. Plates were incubated for 48 h at 37°C to allow spheroid invasion into the surrounding collagen I matrix. Images were acquired as above (see Section 2.8). Spheroid invasion (number and length of protrusions) was quantified using Axio Vision software (Zeiss).

2.11. Anoikis Assay

The level of anoikis in siRNA-transfected cells was determined by flow cytometry. 48 hours post-siRNA transfection; cells were harvested and seeded at 70,000 cells/well (6-well plate format) in 12 mg/mL poly(2-hydroxyethyl methacrylate)-coated wells (preventing cell

attachment, forcing cells to remain suspended). After 24 and 12 h incubation at 37°C for SK-N-BE(2) and SH-SY5Y respectively, cells were harvested, washed with warm PBS and stained with propidium iodide (PI) (BD Biosciences), 7-Aminoactinomycin D (7-AAD) (BD Biosciences), both PI and 7-AAD or neither for 15 min at 37°C in the dark. Apoptosis levels were measured by flow cytometry (FACSCanto, BD Biosciences, Franklin Lakes, NJ) and analysed using FlowJo (Tree Star Inc., Ashland, OR, USA).

2.12. Transendothelial migration assay

HMEC-1 cells were harvested using PBS/trypsin and 50,000 cells seeded in 500 µL 10%FCS/MCDB 131 (additional supplements see Section 2.1) in Cytoselect™ tumor transendothelial migration assay inserts (Cell Biolabs Inc., San Diego, CA). After seeding, HMEC-1 cells were incubated for 72 h at 37°C until a confluent monolayer formed. To confirm a confluent endothelial monolayer was present, immunofluorescence staining of the nuclei and cell membranes was performed (see Section 2.13.2), confirming tightly packed cells. The HMEC-1-containing transendothelial migration inserts were incubated with 10 ng/mL TNF-α for 4 h prior to adding neuroblastoma cells to the inserts. Neuroblastoma cells were double-siRNA transfected with control or stathmin siRNA and incubated for 48 h in 10%FCS/DMEM at 37°C. For experiments not including ROCK inhibitors, cells were serum starved by changing media to serum-free DMEM and incubating for 2 h at 37°C.

For experiments including ROCK inhibitors, the effect of ROCK inhibition on endothelial permeability was assessed. A confluent HMEC-1 monolayer was formed and pretreated with TNF-α as above. 500 µL of 1 mg/mL fluorescent dextran (Sigma) serum-free DMEM (either containing or not containing 10 µmol/L Y-27632 or 10 µmol/L H-1152) was added to the top chamber. 500 µL of 10%FCS/DMEM was added to the bottom chamber. Inserts were

incubated at 37°C for 2 h. 20 µL from the bottom chamber was diluted 5X and added in duplicate to Corning® 96 well flat clear bottom black polystyrene Microplates (In Vitro Technologies). Plates were read on a Perkin Elmer Victor³ fluorescent plate reader supported by Wallac 1420 Workstation software with fluorescein (485nm/535nm, 0.1 s) read from bottom to top. Additionally, a logarithmic dilution of fluorescent dextran concentrations was performed to determine whether the experimental sample fluorescent measurements were within the instrument's fluorescence dynamic range. In both experimental and fluorescent dextran dilution samples a sample where no fluorescent dextran was added was used as a blank and its value subtracted from all other values.

Table 2.3 Fluorescent dextran dilution and fluorescence measurements

Relative Fluorescence Units (RFU)			
Fluorescent dextran conc.	N=1	N=2	N=3
10 mg/mL	*	*	*
1 mg/mL	*	*	*
100 µg/mL	2338656	2208248	2210644
10 µg/mL	298619	253838	263938
1 µg/mL	27904	23068	23597
100 ng/mL	5166	2080	2191
10 ng/mL	*	*	*
1 ng/mL	*	*	*

* denotes the RFU value is outside of the instrument's fluorescent dynamic range.

The following fluorescent dextran concentrations were within the instrument's dynamic range: 100 µg/mL, 10 µg/mL, 1 µg/mL and 100 ng/mL. Values above or below these values were outside the instrument's dynamic range. An $R^2=0.99923$ confirms a linear relationship between fluorescent dextran concentration and RFU within the fluorescent dextran concentrations of 100 µg/mL and 100 ng/mL. RFUs obtained in experimental samples (See Chapter 4, Section 4.2, Figure 4.1) were within the linear dynamic range.

Additionally, for experiments including ROCK inhibitors, cells were incubated with either 10 µmol/L Y-27632-containing or 10 µmol/L H-1152-containing serum-free DMEM. Neuroblastoma cells were harvested using PBS/trypsin, counted and resuspended in 500 µL serum-free DMEM including 1x CytoTracker™ (Cell Biolabs Inc., San Diego, CA) at 330,000 cells/500 µL and 550,000 cells/500 µL for SK-N-BE(2) and SH-SY5Y cells respectively and incubated for 2 h at 37°C. To remove residual CytoTracker™, cells were washed twice with serum-free DMEM and resuspended in 300 µL of serum-free DMEM (either containing or not containing 10 µmol/L Y-27632 or 10 µmol/L H-1152) and 300,000 SK-N-BE(2) cells/insert and 500,000 SH-SY5Y cells/insert were seeded into the top chamber of HMEC-1-containing inserts. For experiments including ROCK inhibitors the bottom chamber contained either 500 µL of 10 µmol/L Y-27632-containing or 10 µmol/L H-1152-containing 10%FCS/DMEM where the 10% FCS acts as a chemoattractant. For experiments not including ROCK inhibitors the bottom chamber contained 500 µL of 10%FCS/DMEM. After seeding, cells were incubated for 24 h at 37°C. The inserts were removed from the companion plate and media aspirated from inside the insert. Non-migrated neuroblastoma cells and endothelial cells were removed from inside the insert using damp cotton tips. Inserts were transferred to clean wells in 200 µL of 1X lysis buffer (Cell Biolabs Inc., San Diego, CA) and incubated shaking (Orbit™ P4 digital shaker, Labnet International Inc., Edison, NJ)

at 120 rpm for 5 min. Inserts were removed from companion plate and 80 μ L of solution added in duplicate to Corning[®] 96 well flat clear bottom black polystyrene Microplates (In Vitro Technologies). Plates were read on a Perkin Elmer Victor³ fluorescent plate reader supported by Wallac 1420 Workstation software with fluorescein (485nm/535nm, 0.1 s) read from bottom to top.

2.13. HMEC-1 immunofluorescence staining

HMEC-1 endothelial cells were seeded at a density of 50,000 cells (in 500 μ L 10%FCS/MCDB 131 (additional supplements see Sec 2.1) in Cytoselect[™] tumor transendothelial migration assay inserts (Cell Biolabs Inc., San Diego, CA). After seeding, HMEC-1 cells were incubated for 72 h at 37°C to form a confluent monolayer formed. To assess if a 100% confluent monolayer was formed, cells were fixed and stained with DAPI and Alexa Fluor[®] 568 Phalloidin, as described below. Cells were fixed in 4% PFM/PBS for 10 minutes and then rinsed 3 times in PBS. PFM-fixed cells were permeabilised with 0.2% Triton-X/PBS for 10 minutes and rinsed 3 times in PBS. PFM-fixed cells were blocked in 2%BSA/PBS for 40 minutes. Cells were then incubated with Alexa Fluor[®] 568 Phalloidin (Invitrogen) diluted 1:50 in 0.5%BSA/PBS and incubated for 15 minutes at room temperature, and then rinsed 3 times in PBS. Slides were then washed in milliQ-H₂O and then mounted using VECTASHIELD[®] mounting medium with 4',6-diamidino-2-phenylindole (DAPI) (Vector Laboratories, Burlingame, CA). HMEC-1 endothelial cells were then visualised and imaged using a Zeiss[™] 780 confocal microscope with a 63X 1.35 NA oil objective.

2.14. Rho GTPase (Rac1, Cdc42 and RhoA) activation assays

SK-N-BE(2) cells were seeded into 100 mm tissue culture dishes (Greiner Bio One, GmbH, Frickenhausen, Germany) at 180,000 cells/dish and incubated for 48 h at 37°C. Cells were serum starved by replacing media with serum-free DMEM and incubating cells for 24 h at 37°C. Cells were harvested on ice, washed with ice-cold PBS and then lysed in Cell Lysis Buffer (Cytoskeleton Inc., Denver, CO) and harvested using a cell scraper. Cell debris was removed by centrifugation at 14,000 g for 5 minutes at 4°C and cleared cell lysates transferred to a fresh eppendorf tube and an aliquot dispensed into another tube for stathmin and total lysate Rac1, Cdc42 and RhoA western blotting. Both tubes were immediately snap frozen in liquid nitrogen (to prevent hydrolysis of active Rac1, Cdc42 or RhoA). Protein concentration was quantified using a BCA assay and western blotting performed (see Section 2.6) for stathmin, GAPDH and total Rac1, Cdc42 and RhoA. For active Rac1, Cdc42 and RhoA pull-downs, 450 µg of protein lysate was incubated for 1 h at 4°C (gentle shaking) with 50 µg of Pak1-RBD, Pak1-RBD and rhotekin-RBD beads respectively. Beads were pelleted by centrifugation at 5000 g at 4°C for 3 min. Beads were carefully washed with Wash Buffer (Cytoskeleton Inc., Denver, CO). Washed beads were diluted in 15 µL of 4x reducing sample buffer [130 mM Tris pH 8, 129.65 mmol/L dithiothreitol, 20% (v/v) glycerol, 4.6% (w/v) SDS and 0.02% bromophenol blue] and then boiled at 96°C for 10 min to denature the proteins and remove proteins bound to beads. Samples were analysed by western blotting as described in Section 2.6 for active Rac1, Cdc42 and RhoA.

2.15 Tubulin polymerisation assay

Polymerised and soluble tubulin fractions were isolated as previously described with minor modifications (Kavallaris, Tait et al. 2001). Neuroblastoma cells were grown in 6 well plates for 48 h at 37°C in 10%FCS/DMEM. For serum starvation, media was changed to serum free/DMEM and cells incubated for a further 24 h. Cells were washed twice with warm PBS prior to lysis in 80 µL/well of pre-warmed hypotonic buffer (1 mM MgCl₂, 2 mM ethylene glycol tetraacetic acid (EGTA), 0.5% NP-40, 1x protease inhibitor cocktail and 20 mM Tris HCl, pH 6.8). The cellular residues were scraped from the wells and transferred to 1.5 mL microfuge tubes. The fractions were separated using centrifugation at 14,000 g for 10 minutes at RT. The resulting supernatants (soluble fractions) were transferred to fresh microfuge tubes and placed on ice. The cell pellet (polymerised fraction) was resuspended in 300 µL hypotonic buffer. 100 µL of 4x reducing sample buffer [130 mM Tris pH 8, 129.65 mmol/L dithiothreitol, 20% (v/v) glycerol, 4.6% (w/v) SDS and 0.02% bromophenol blue] was added to both soluble and cell pellet fractions. The soluble fraction was then sonicated for 5 seconds on ice using the Microson™ Ultrasonic homogenizer (Misonix Inc.). The polymerised fraction was sonicated until the cell pellet dissolved (typically 20-45 seconds). All samples were boiled for 10 min at 96°C and 45 µL of each fraction was resolved by 12% SDS-PAGE. Tubulin and GEF-H1 levels in each fraction (soluble 'S' and polymerised 'P') were detected by western blotting using α -tubulin and GEF-H1 antibodies respectively (see Section 2.6).

2.16. Restoration of stathmin levels with wild-type or 4E:mutant stathmin in SK-N-BE(2)/TGL neuroblastoma cells

DNA vectors used to restore stathmin levels with wild-type or 4E:mutant stathmin are built from the mCherry-C1 vector background and contain kanamycin and geneticin antibiotic resistance genes and an mCherry:stathmin fusion gene. 1 μ g of DNA was transfected by electroporation into JM109 competent cells (Promega, Madison, WI). DNA vectors were kindly provided by Dr Dominic Ng from Bio21 and the University of Melbourne, Australia. Selection of positive clones was performed by addition of 50 μ g/mL kanamycin to the bacterial plates. A positive colony was selected and a 200 mL LB broth starter culture prepared by incubating overnight at 37°C with agitation. A maxi-prep was performed using a Qiagen Maxi-prep kit as per manufacturer's instructions (Qiagen). Resulting DNA concentration quantified using the Nanodrop (Thermo Scientific). To generate a kill curve for geneticin in SK-N-BE(2)/TGL cells, 4×10^5 SK-N-BE(2)/TGL cells/well were seeded into 6-well plates and 24 h post-seeding were subjected to a range of geneticin concentrations (0-2000 μ g/mL). Every 48 h fresh 10%FCS/DMEM and geneticin was added. Cells were incubated with geneticin-containing 10%FCS/DMEM for 7-10 days. 750 μ g/mL geneticin was chosen for future experiments. 4×10^5 SK-N-BE(2)/TGL cells/well were seeded into 6-well plates and 24 h-post cell seeding 10 μ L/well Lipofectamine 2000 (Invitrogen, Carlsbad, CA) used to transfect 2 μ g of each DNA vector. 24 h later solution was changed to 10%FCS/DMEM. After another 24 h media was changed to geneticin (750 μ g/mL)-containing 10%FCS/DMEM. Geneticin-containing media was changed every 48 h and

selection was performed for 7-10 days. Following transfection and subsequent geneticin selection, cells positive for mCherry were selected by flow assisted cell sorting (FACS) using the BD Influx™ (BD Biosciences) FACS machine at the Mark Wainwright Analytical Centre Flow Cytometry Facility (University of New South Wales). Cells were amplified in 10%FCS/DMEM for 48 h and then subjected to another round (7-10 days) of selection in 750 µg/mL of geneticin. Following selection cells were plated at 1.8×10^5 cells/well in 6-well plates and harvested 72 h later and assessed for expression of the mCherry:stathmin fusion protein, endogenous stathmin and the house-keeping gene GAPDH. Cells were plated at 1.8×10^5 cells/well in a 6-well plate and 48 h post-seeding were harvested and subjected to chemotactic-induced transwell cell migration assays (see Chapter 2, Section 2.8). The exogenously expressed stathmin has been modified (at the nucleotide sequence, mRNA) and hence it is not recognized by the shRNA target sequence. The wild-type vector expresses stathmin, which has an amino acid sequence that is identical to the endogenous protein. In contrast, the 4E stathmin mutant expresses stathmin, which has glutamic acid substitutions at each of the phosphorylation sites of stathmin (i.e. S16, S25, S38, S63).

2.17. Experimental metastasis neuroblastoma *in vivo* mouse model

1×10^6 SK-N-BE(2)-luciferase expressing cells were injected under normal pressure into the lateral tail vein (total volume 200 µL) of 6-8 week old, severe combined immunodeficient (SCID) Beige mice using a 1 mL syringe attached to a 27-gauge needle. All *in vivo* experiments conducted in this thesis were carried out under approved AEC UNSW #13/116B. All mice were closely monitored each day following neuroblastoma cells injection for any signs of adverse effects (weight loss equal to or greater than 20% or 23 days post-

neuroblastoma cell injection; whichever occurred first).

2.18. *In vivo* & *Ex vivo* imaging of tumour growth in mice

Luciferase-expressing neuroblastoma cells were visualised 7, 15 and 23 days-post neuroblastoma cell injection into mice. 150 mg/kg of the luciferase substrate, D-luciferin (Gold Biotechnology) diluted in Dulbecco's Phosphate-Buffered Saline (DPBS) was injected via intraperitoneal (i.p.) injection. Animals were anaesthetised using 4% and 2% isoflurane (Abbott Laboratories, North Chicago, Illinois) for induction and maintenance respectively and placed onto the warmed stage inside the IVIS Imaging System. Eight minutes after injection mice were imaged on the dorsal, left lateral, right lateral and ventral sides (medium binning, F-stop 1). For *ex vivo* imaging, 150 mg/kg D-luciferin was injected via i.p. Animals were subsequently humanely killed by CO₂ asphyxiation and organs placed in 6-well plates for imaging. Organs were covered with D-luciferin (300 µg/mL in DPBS) for 30 seconds prior to imaging (F-stop 1; medium binning for livers, large binning for all other organs) using the IVIS imaging system. To ascertain animal and tissue background bioluminescence, 3 naïve mice and their organs were imaged using the IVIS Imaging System as described above. The bioluminescence signal from the naïve mice and their organs was subtracted from the signal obtained from similarly sized region of interests (ROIs) from whole animals and their organs of mice injected with luciferase-expressing neuroblastoma cells. Bioluminescent images of mice and organs were electronically presented as a pseudocolour overlay onto a grey scale animal image on the LIVINGIMAGE (v.32) software (Xenogen). Bioluminescent signal was quantified from the ventral side of the live animal, and liver and lungs post-humane kill using the ROI method.

2.19. Immunohistochemistry

Tissues were fixed in 10% neutral-buffered formalin (Sigma, St. Louis, MO, USA) for 24 h and then washed with PBS and placed in 70% ethanol before being placed in histology cassettes (ProSciTech). Cassettes were kept submerged in 70% ethanol and sent to the Histology and Microscopy Unit at the University of New South Wales, Australia for processing. Tissues were paraffin-embedded, 5 μ m sections cut and stained with haematoxylin and eosin (H&E) or prepared on aminoalkylsilane-treated glass slides for subsequent immunohistochemistry (IHC) analysis. For IHC experiments, slides were incubated for 30 min at 60°C to promote tissue section attachment throughout the IHC processing. Tissues were deparaffinised using 3x 5 min incubations in xylene and rehydrated through a series of ethanol incubations (100%, 95% and 70%; 5 minutes each) and 2x 5 min washes in milliQ-H₂O. Slides were placed in 400 mL antigen retrieval buffer (10 mM sodium citrate, 0.05% Tween-20 pH 6) and heated in a microwave oven for 4 min. Subsequently, slides and antigen retrieval buffer were incubated at 104°C for 15 min. The slides and buffer were allowed to cool for 40 min at RT and slides were then washed 2x 5 min in milliQ-H₂O. Slides were incubated for 10 min in a peroxidase blocking solution (1% H₂O₂, 3.3% methanol) to block endogenous peroxidase activity. Tissue sections were outlined with a PAP pen and then blocked with either 10% goat serum or mouse IgG blocking reagent (Vector Laboratories, Burlingame, CA, USA) for 1 h for luciferase and stathmin staining respectively. To detect luciferase and stathmin expression, tissue sections were incubated for overnight at 4°C with either a rabbit polyclonal antibody against luciferase (Fitzgerald, Actin, MA, USA) diluted in 1% goat serum, or mouse monoclonal antibody against stathmin (Abcam, Cambridge, UK) diluted in mouse-on-mouse diluent (600 μ l protein concentrate in 7.5 mL PBS) (Vector Laboratories) at 1:100 and 1:250 respectively. To guarantee secondary

antibody specificity, a tissue section was incubated with either a rabbit or mouse IgG control antibody at equivalent concentrations to the respective primary antibodies. Slides were washed 3x 5 min in 0.05% Tween-20/PBS (PBS-T) followed by 1x 5 min wash in PBS. Tissue sections were incubated for 45 min at RT with either an anti-rabbit biotinylated secondary antibody (Vector Laboratories) diluted 1:200 in 1% goat serum, or anti-mouse biotinylated secondary antibody (Vector Laboratories) diluted in mouse-on-mouse diluent (Vector Laboratories) to detect luciferase and stathmin expression respectively. Slides were washed in PBS-T and PBS as described above and incubated for 5 min with avidin-biotin peroxidase complex from the Vectastain ABC Kit (Vector Laboratories). Slides were washed 1x 5 min in PBS and incubated with ImmPACT™ DAB substrate (Vector Laboratories) at RT until the desired colour intensity developed (20 or 40 seconds for stathmin or luciferase detection respectively). Slides were rinsed 1x 1 min in milliQ-H₂O, nuclear counterstained for 30 s with Mayer's haematoxylin, dehydrated and then mounted with EUKITT mounting medium (O. Kindler GmbH and Co, Freiburg, Germany). Slides were sent for scanning at the Histology and Microscopy Unit at the University of New South Wales, Australia using an Aperio ScanScope XT Slide Scanner and images were subsequently analysed using the ImageScope software (Aperio, Vista, CA, USA).

2.20. Delivery of Invivofectamine®:stathmin sequence 3 siRNA *in vivo*

For experiments carried out in Chapter 6 Invivofectamine® was utilised as a delivery vehicle for stathmin sequence 3 siRNA (STMN1 Seq.3_{SI}) to human neuroblastoma tumours inside mouse liver tissue generated using the tail vein experimental neuroblastoma mouse model

(see Section 2.16). Note: All InvivoFectamine®:siRNA complex injections in this thesis were prepared and injected to deliver a dose of 2 mg of siRNA/kg of mouse tissue.

2.20.1. Visualisation of uptake of InvivoFectamine®:STMN1 Seq.3_{SI} siRNA

Tumour bearing mice (22 days post-neuroblastoma tail vein cell injection) were injected under normal pressure into the lateral tail vein (total volume 100 µL) using a 1 mL syringe attached to a 27-gauge needle with either InvivoFectamine®:Alexa Fluor 647-conjugated siRNA (fluorescent) complexes or InvivoFectamine®:siRNA (non-fluorescent) complexes and 4 h later mice were humanely killed by CO₂ asphyxiation and livers placed in 6-well plates for imaging using the IVIS Imaging System. The fluorescent signal from the non-fluorescent complex treated mouse livers was subtracted from the signal obtained from the fluorescent complex treated mouse livers using similarly sized ROIs. Fluorescent images of livers are electronically presented as a pseudocolour overlay onto a grey scale liver animal image on the LIVINGIMAGE (v.32) software (Xenogen). Uptake of InvivoFectamine®:Alexa Fluor 647-conjugated siRNA complexes (2 mg/kg siRNA) was also assessed by fluorescence microscopy. After livers were imaged using the IVIS Imaging System they were frozen in Tissue-Tek® OCT Compound (ProSciTech, Australia) and sent to the Histology and Microscopy Unit at the University of New South Wales, Australia for sectioning and DAPI staining. Slides were analysed using a Zeiss™ 780 confocal microscope with a 63X 1.35 NA oil objective.

2.20.2. Stathmin gene silencing efficacy using Invivofectamine®:STMN1 Seq.3_{SI} siRNA *in vivo*

Tumour bearing mice (20 days post-neuroblastoma cell tail vein injection) were injected under normal pressure into the lateral tail vein (total volume 100 μ L) using a 1 mL syringe attached to a 27-gauge needle with either Invivofectamine®:STMN1 Seq.3_{SI} complexes or Invivofectamine®:control-siRNA complexes (2 mg/kg siRNA) once daily for 3 consecutive days as previously described by our group (Boyer, Teo et al. 2013). 24 h after the third injection mice were humanely killed by CO₂ asphyxiation and livers were placed in the RNA stabilisation reagent RNeasy Lysis Buffer (Qiagen, Valencia, CA) for 24 h at RT and then stored at -80°C. RNA isolation, cDNA synthesis and qPCR to examine stathmin, GFP and β 2M expression was performed as per Sections 2.4-5. Additionally, liver tissue from naïve mice (no neuroblastoma cells injected) was included to assess species specificity of stathmin, GFP and β 2M qPCR primers.

2.20.3. Effect of STMN1 Seq.3_{SI} delivery on metastatic neuroblastoma tumour burden *in vivo*

SCID-Beige mice were injected with neuroblastoma cells as per Section 2.16. Starting 48 h post-neuroblastoma cell injection, each mouse was injected under normal pressure into the lateral tail vein (total volume 100 μ L) using a 1 mL syringe attached to a 27-gauge

needle once daily for three days with either InvivoFectamine®:STMN1 Seq.3_{SI} complexes or InvivoFectamine®:control-siRNA complexes. Twelve days post-neuroblastoma cell injection, each mouse was injected as above once daily for three days with either InvivoFectamine®:STMN1 Seq.3_{SI} complexes or InvivoFectamine®:control-siRNA complexes. 23 days post-neuroblastoma cell injection mice were imaged using the IVIS Imaging System as per Section 2.17, humanely killed by CO₂ asphyxiation and the livers imaged using the IVIS Imaging System as per Section 2.17 to determine *in vivo* abdominal and *ex vivo* liver tumour burden respectively.

2.21. Statistical analyses

Statistical analyses were performed using the GraphPad Prism v6 software. Unpaired, two-tailed Student's t-tests were used to determine statistical differences between control and experimental groups, where p-values of <0.05 were deemed statistically significant. Results were expressed as means of the number of independent experiments performed (at least 3) ± standard error of mean (SEM).

Chapter 3.

3 Evaluation of stathmin's role in the steps of the metastatic cascade in neuroblastoma cells

3.1 Introduction

Improvements in neuroblastoma survival rates over the decades are attributable mainly to increasing cure rates amongst patients with localised disease (Maris, Hogarty et al. 2007). The survival rates for patients with distant metastases, classified as high-risk, have achieved only modest improvement where a high-risk classification carries a dismal 5-year survival rate of 40-50% (Maris 2010). This depressing survival rate highlights the need to address metastatic neuroblastoma. Unfortunately, the mechanisms driving metastasis in neuroblastoma are poorly understood.

Metastasis is the dissemination of tumour cells from one site to another consisting of a series of discrete and successive steps; modeled into a “metastatic cascade” [reviewed in (Fife 2014)]. During each step of the metastatic cascade, the cytoskeleton of the tumour cell undergoes remarkable remodelling. Alterations in the components of the cytoskeleton (actin, microtubules and intermediate filaments) or their interacting partners can promote metastasis [reviewed in (Fife 2014)].

Stathmin is an important microtubule destabilising protein whose overexpression has been closely associated with highly metastatic disease in numerous malignancies (reviewed in Chapter 1). Additionally, elevated levels of stathmin have been associated with advanced-stage disease in neuroblastoma (Hailat, Strahler et al. 1990). Furthermore, recent findings from our laboratory have revealed a role for stathmin in neuroblastoma metastasis where

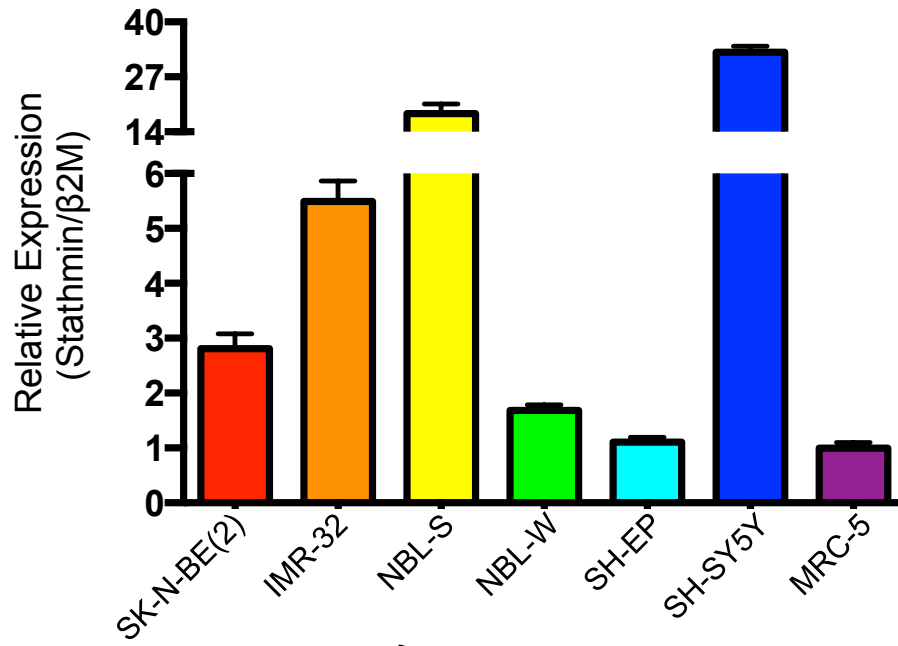
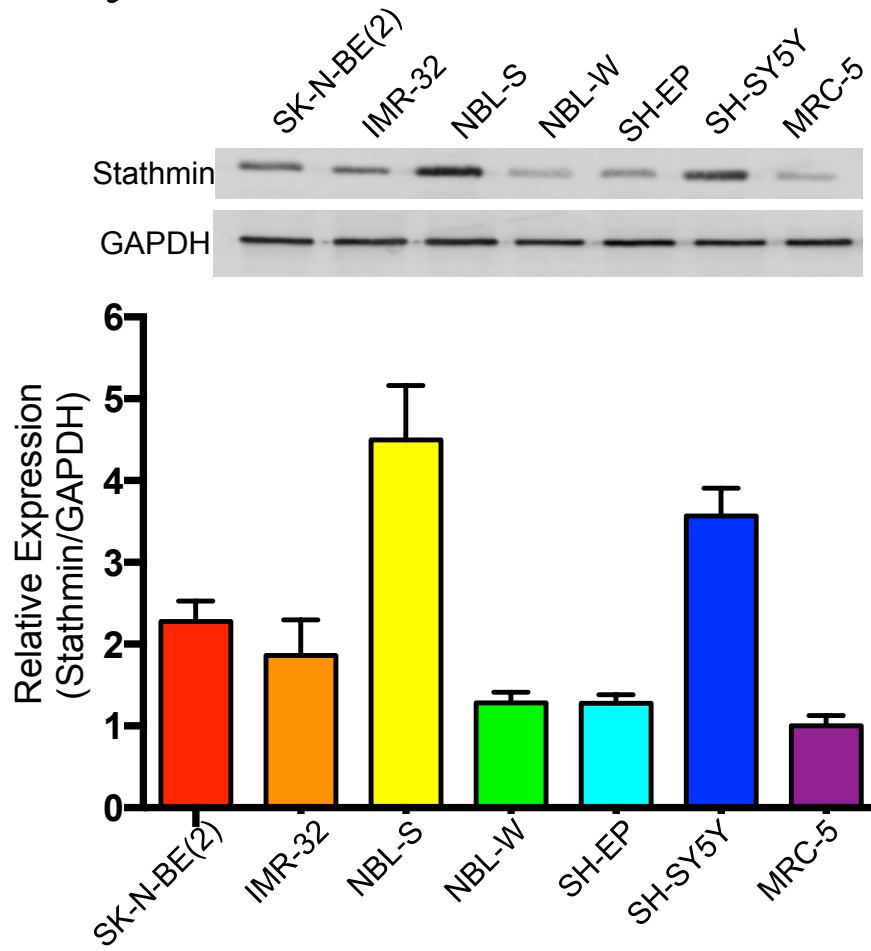
suppression of stathmin expression significantly reduced neuroblastoma metastatic tumour burden in the lungs in a clinically relevant neuroblastoma mouse model (Byrne, Yang et al. 2014). Despite evidence linking stathmin with neuroblastoma metastasis, there is limited knowledge of the role of stathmin in specific stages of the metastatic cascade. To address this, small-interfering and short-hairpin RNA (siRNA and shRNA) approaches were utilised to potently suppress stathmin expression and subsequently examine stathmin's role in specific steps of the metastatic cascade in neuroblastoma.

3.2 Stathmin expression in neuroblastoma cell lines

In order to investigate stathmin's role in the neuroblastoma metastatic cascade a panel of neuroblastoma cell lines were initially screened for stathmin gene (Fig. 3.1a) and protein expression (Fig. 3.1B) by real-time quantitative PCR, and western blot respectively. The neuroblastoma cell lines examined expressed varying levels of stathmin (Fig. 3.1). Two cell lines, SK-N-BE(2) and SH-SY5Y, were selected for experiments in this thesis as they expressed moderate to high levels of stathmin respectively. Additionally, these cell lines were selected, as they possess different genetic features that may influence stathmin's role in the neuroblastoma metastatic cascade. For example SK-N-BE(2) cells have MYCN amplification (Carr, Bown et al. 2007) and mutant p53 (Tweddle, Malcolm et al. 2001) whereas SH-SY5Y cells have single copy MYCN and wild-type p53 (Chesler, Goldenberg et al. 2008). MRC-5 cells isolated from a normal lung expressed the lowest levels of stathmin mRNA and protein relative to the neuroblastoma cell lines examined (Fig 3.1a-b).

Figure 3.1 Stathmin mRNA and protein expression in neuroblastoma cell lines

(a) Stathmin gene levels in a panel of neuroblastoma cell lines, normalised to the lung fibroblast cell line, MRC-5. Stathmin mRNA was normalised to the housekeeping gene β 2-microglobulin (β 2M). (b) A representative western blot showing stathmin protein expression in a panel of neuroblastoma cell lines, including the lung fibroblast cell line MRC-5. GAPDH was used as a protein loading control. Lower graph shows corresponding protein quantitation of stathmin protein expression. Data represents the mean \pm SEM (error bars) of three independent experiments.

a**b**

3.3 Stathmin gene silencing using siRNA in neuroblastoma cells

Small interfering RNAs (siRNAs), typically 20-25 base pairs in length, silence their target gene's expression by utilising the native RNA interference (RNAi) machinery in a cell (Wilson and Doudna 2013). An siRNA approach was used in this thesis to investigate stathmin's role in the neuroblastoma metastatic cascade. Prior published work from our laboratory highlighted that stathmin suppression, using siRNA, decreased neuroblastoma cell migration and invasion (Byrne, Yang et al. 2014). This was performed using an siRNA pool (where 4 separate siRNA sequences targeting stathmin were pooled). In chapter 6 of this thesis, the therapeutic potential of suppressing stathmin on neuroblastoma metastasis will be examined and in order to suppress stathmin *in vivo*, single siRNA sequences will be needed. Optimisation of the stathmin suppression capabilities of the 4 separate stathmin siRNA sequences from the siRNA pool will enable the selection of the siRNA sequence that provides optimal stathmin suppression. This will allow the delivery of the most potent siRNA sequence to suppress stathmin expression *in vivo*.

In addition to using siRNA, we have also used short-hairpin RNA (shRNA). Importantly, we have previously described neuroblastoma cells that possess stable stathmin suppression using shRNA (Byrne, Yang et al. 2014). Additionally, these shRNA-expressing SK-N-BE(2) cells express luciferase. These cells were generated by the retroviral transduction with a vector containing a fusion gene (consisting of herpes simplex virus type 1 thymidine kinase [HSV-tk], enhanced-green fluorescent protein (eGFP) and firefly luciferase). These cells are herein named SK-N-BE(2)/TGL cells and are used in most *in vitro* experiments in this chapter, unless stated otherwise. Examples where the SK-N-BE(2)/TGL cells were not used are the

anoikis and transendothelial migration experiments in Chapter 3 as the green fluorescence from eGFP expression interferes with the fluorescence aspects of these particular assays.

For experiments utilising siRNA-mediated stathmin suppression optimisation of stathmin gene silencing is required. Initially the four aforementioned siRNA sequences were evaluated by transfecting SK-N-BE(2)/TGL cells with 100 nmol/L of siRNA that targets different regions of the STMN1 gene. This led to a significant suppression of stathmin mRNA expression ($82.6 \pm 5.27\%$, $p < 0.0001$; $84.6 \pm 5.25\%$, $p < 0.0001$; $94.7 \pm 5.23\%$, $p < 0.0001$; $90.3 \pm 5.23\%$, $p < 0.0001$ for stathmin siRNA sequences 1, 2, 3 and 4 respectively) compared to control non-targeting siRNA (Fig. 3.2a) Additionally, 100 nmol/L of the 4 separate stathmin siRNA sequences significantly suppressed stathmin protein expression ($50.3 \pm 12.10\%$, $p < 0.05$; $50.2 \pm 14.95\%$, $p < 0.05$; $68.8 \pm 12.29\%$, $p < 0.005$; $64.8 \pm 12.95\%$, $p < 0.005$ for stathmin siRNA sequences 1, 2, 3 and 4 respectively) compared to control siRNA (Fig. 3.2b). Stathmin siRNA sequences 3 and 4 achieved the most potent suppression of stathmin at both the mRNA and protein level in SK-N-BE(2)/TGL cells and hence were chosen for subsequent experiments.

Similar to SK-N-BE(2)/TGL cells, the SH-SY5Y cells also showed significant reduction in stathmin mRNA expression ($64.0 \pm 2.99\%$, $p < 0.0001$; $59.0 \pm 5.31\%$, $p < 0.0005$; $84.3 \pm 2.92\%$, $p < 0.0001$; $69.5 \pm 3.83\%$, $p < 0.0001$ for stathmin siRNA sequences 1, 2, 3 and 4 respectively) compared to control siRNA (Fig. 3.3a). This was also reflected in significantly reduced protein levels ($43.3 \pm 10.70\%$, $p < 0.05$; $44.1 \pm 13.90\%$, $p < 0.05$; $63.6 \pm 15.79\%$, $p < 0.05$; $62.3 \pm 11.79\%$, $p < 0.005$ for stathmin siRNA sequences 1, 2, 3 and 4 respectively) compared to control siRNA (Fig. 3.3b). Altogether, stathmin siRNA sequences 3 and 4 displayed the most

Figure 3.2 Stathmin siRNA sequence selection in SK-N-BE(2)/TGL neuroblastoma cells

The gene silencing efficacy of four independent stathmin siRNA sequences were evaluated in SK-N-BE(2)/TGL cells. **(a)** Stathmin mRNA levels in SK-N-BE(2)/TGL cells 72 h post transfection with 100 nmol/L stathmin siRNA sequence 1 (Seq1), sequence 2 (Seq2), sequence 3 (Seq3), sequence 4 (Seq4) or non-functional control (Ctrl_{SI}) siRNA. Stathmin mRNA was normalised to the housekeeping gene β 2-microglobulin (β 2M). **(b)** A representative western blot and corresponding quantitation (lower graph) of stathmin protein expression in SK-N-BE(2)/TGL cells 72 h post transfection with 100 nmol/L stathmin siRNA sequence 1 (Seq1), sequence 2 (Seq2), sequence 3 (Seq3), sequence 4 (Seq4) or non-functional control (Ctrl_{SI}) siRNA. Stathmin protein expression was normalised to GAPDH (loading control). Data represents the mean \pm SEM (error bars) of three independent experiments, * $p < 0.05$; ** $p < 0.005$; **** $p < 0.0001$.

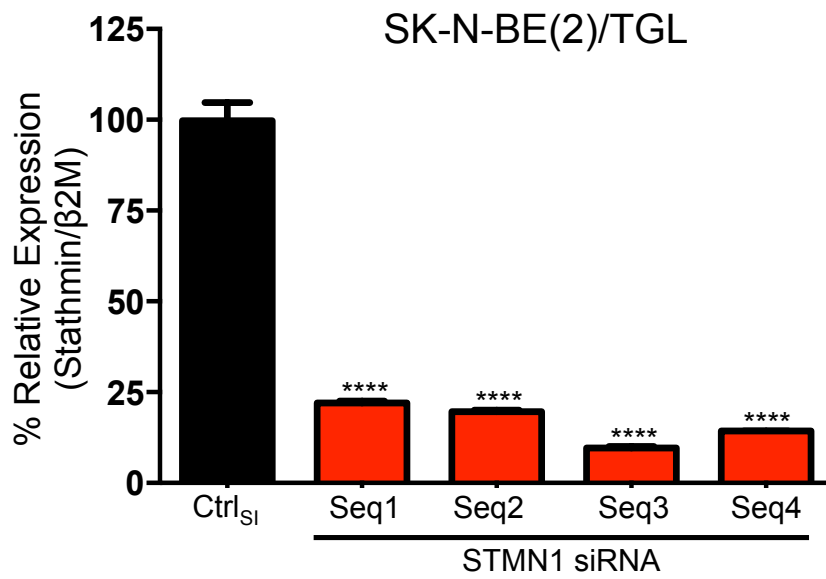
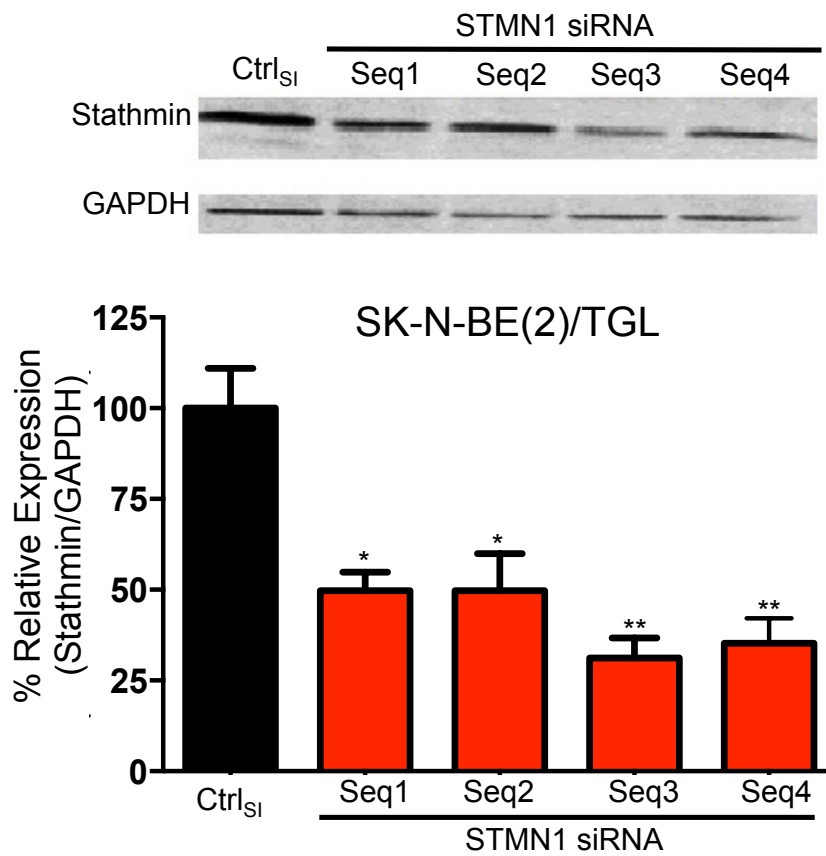
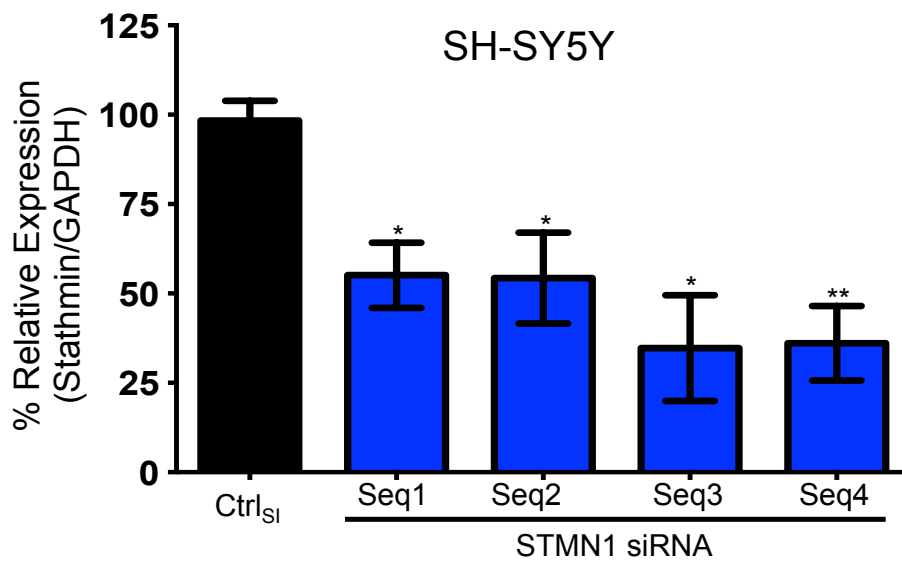
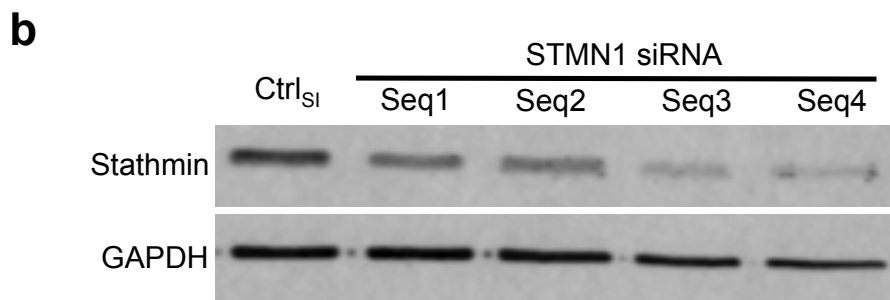
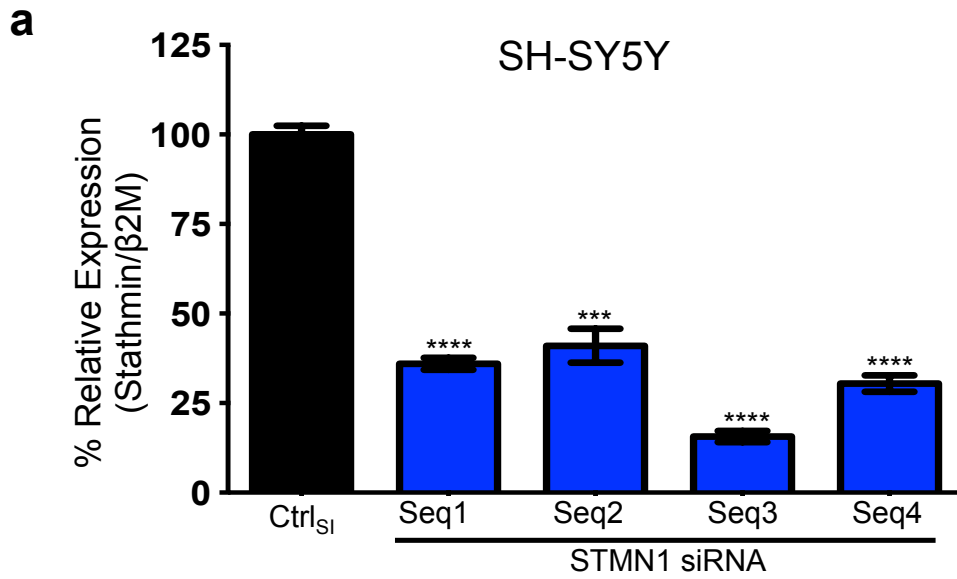
a**b**

Figure 3.3 Stathmin siRNA sequence selection in SH-SY5Y neuroblastoma cells

Similar to SK-N-BE(2)/TGL cells, the gene silencing efficacy of four independent stathmin siRNA sequences were evaluated in SH-SY5Y cells. **(a)** Stathmin mRNA levels in SH-SY5Y cells 72 h post transfection with 100 nmol/L stathmin siRNA sequence 1 (Seq1), sequence 2 (Seq2), sequence 3 (Seq3), sequence 4 (Seq4) or non-functional control (Ctrl_{si}) siRNA. Stathmin mRNA was normalised to the housekeeping gene β 2-microglobulin (β 2M). **(b)** A representative western blot and corresponding quantitation (lower graph) of stathmin protein expression in SH-SY5Y cells 72 h post transfection with 100 nmol/L stathmin siRNA sequence 1 (Seq1), sequence 2 (Seq2), sequence 3 (Seq3), sequence 4 (Seq4) or control (Ctrl_{si}) siRNA. Stathmin protein expression was normalised to GAPDH (loading control). Data represents the mean \pm SEM (error bars) of three independent experiments, * $p < 0.05$; ** $p < 0.005$, *** $p < 0.001$; **** $p < 0.0001$.



potent suppression of stathmin expression and both the mRNA and protein level in SH-SY5Y cells and hence were chosen for subsequent experiments. Additionally, stathmin siRNA sequences 3 and 4 are hereafter referred to as STMN1 Seq.3_{SI} and STMN1 Seq.4_{SI} respectively. To determine the lowest effective siRNA concentration, a concentration gradient was performed (using 5, 10, 50 and 100 nmol/L siRNA). In SK-N-BE(2)/TGL cells, all concentrations tested of STMN1 Seq.3_{SI} significantly suppressed stathmin mRNA expression by at least 80% (Fig. 3.4a) and protein expression by at least 56% (Fig. 3.4c). Additionally, STMN1 Seq.4_{SI} achieved similar suppression of stathmin as STMN1 Seq.3_{SI} at all concentrations tested in SK-N-BE(2)/TGL cells at both the mRNA and protein levels compared to control siRNA (Fig. 3.4b,d).

Similar to SK-N-BE(2) cells, in SH-SY5Y cells, all concentrations of STMN1 Seq.3_{SI} significantly suppressed stathmin mRNA expression by 58% (Fig. 3.5a). Additionally, 50 and 100 nmol/L STMN1 Seq.3_{SI} significantly reduced stathmin protein expression by (67.2±19.47%, p<0.05; and 69.2±19.95%, p<0.05) (Fig. 3.5c). Although, 5 and 10 nmol/L of STMN1 Seq.3_{SI} suppressed stathmin protein expression this did not reach statistical significance (37.6±19.65%, p=0.128; 43.5±21.06%, p=0.108) (Fig. 3.5c). Moreover, STMN1 Seq.4_{SI} displayed similar significant suppression of stathmin at the mRNA level using all siRNA concentrations tested but only 50 and 100 nmol/L STMN1 Seq.4_{SI} achieved significant suppression of stathmin at the protein level (Fig. 3.5b,d).

In summation, 5 and 50nM of both siRNA sequences achieved similar effective suppression of stathmin expression at both the mRNA and protein level in SK-N-BE(2)/TGL and SH-SY5Y cells respectively, and hence were chosen for subsequent experiments with these cells.

Figure 3.4 Stathmin siRNA sequence concentration optimisation in SK-N-BE(2)/TGL neuroblastoma cells

To determine the lowest effective siRNA concentration, the efficacy of STMN1 Seq.3_{SI} and STMN1 Seq.4_{SI} at 5, 10, 50 and 100 nmol/L was evaluated in SK-N-BE(2)/TGL cells. Stathmin mRNA levels in SK-N-BE(2)/TGL cells 72 h post transfection with 5, 10, 50 or 100 nmol/L of STMN1 Seq.3_{SI} (**a**), STMN1 Seq.4_{SI} (**b**) or 100 nmol/L control (Ctrl_{SI}) siRNA. Stathmin mRNA was normalised to β 2-microglobulin (β 2M). A representative western blot and corresponding quantitation (lower graph) of stathmin protein expression in SK-N-BE(2)/TGL cells 72 h post transfection with 5, 10, 50 or 100 nmol/L STMN1 Seq.3_{SI} (**c**), STMN1 Seq.4_{SI} (**d**) or 100 nmol/L Ctrl_{SI}. Stathmin protein expression was normalised to GAPDH (loading control). Data represents the mean \pm SEM (error bars) of three independent experiments, * $p < 0.05$; **** $p < 0.0001$.

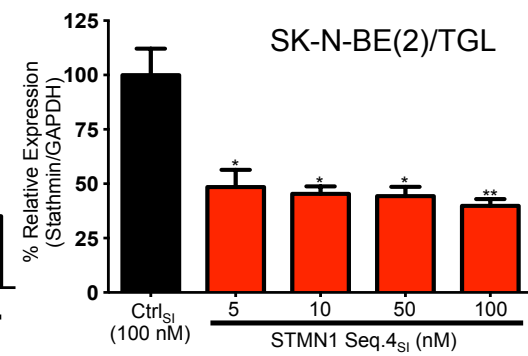
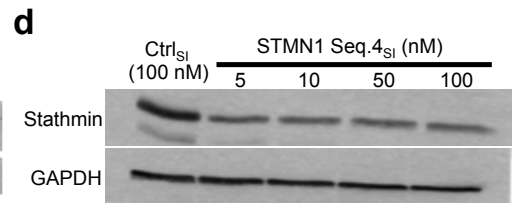
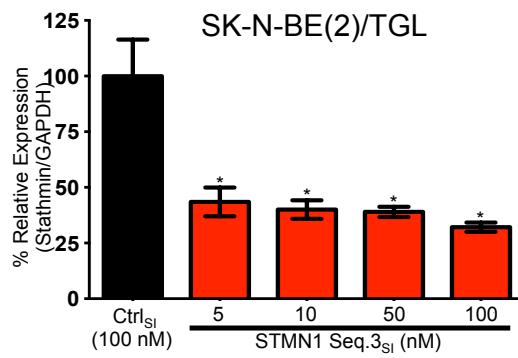
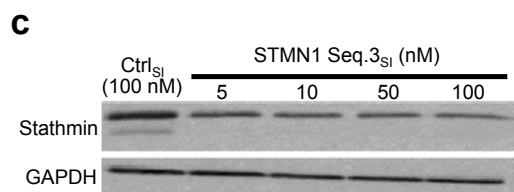
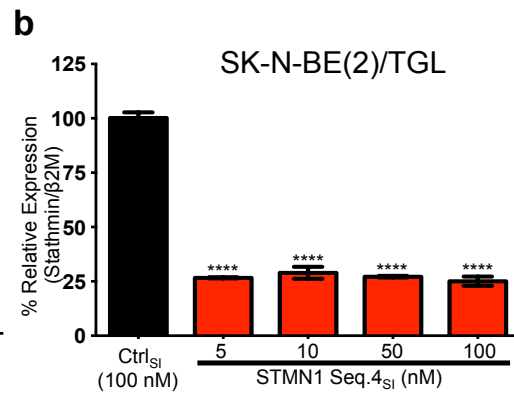
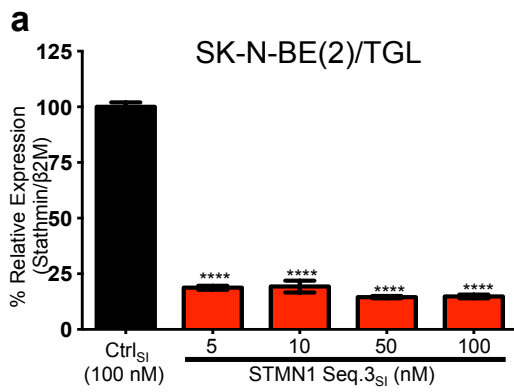
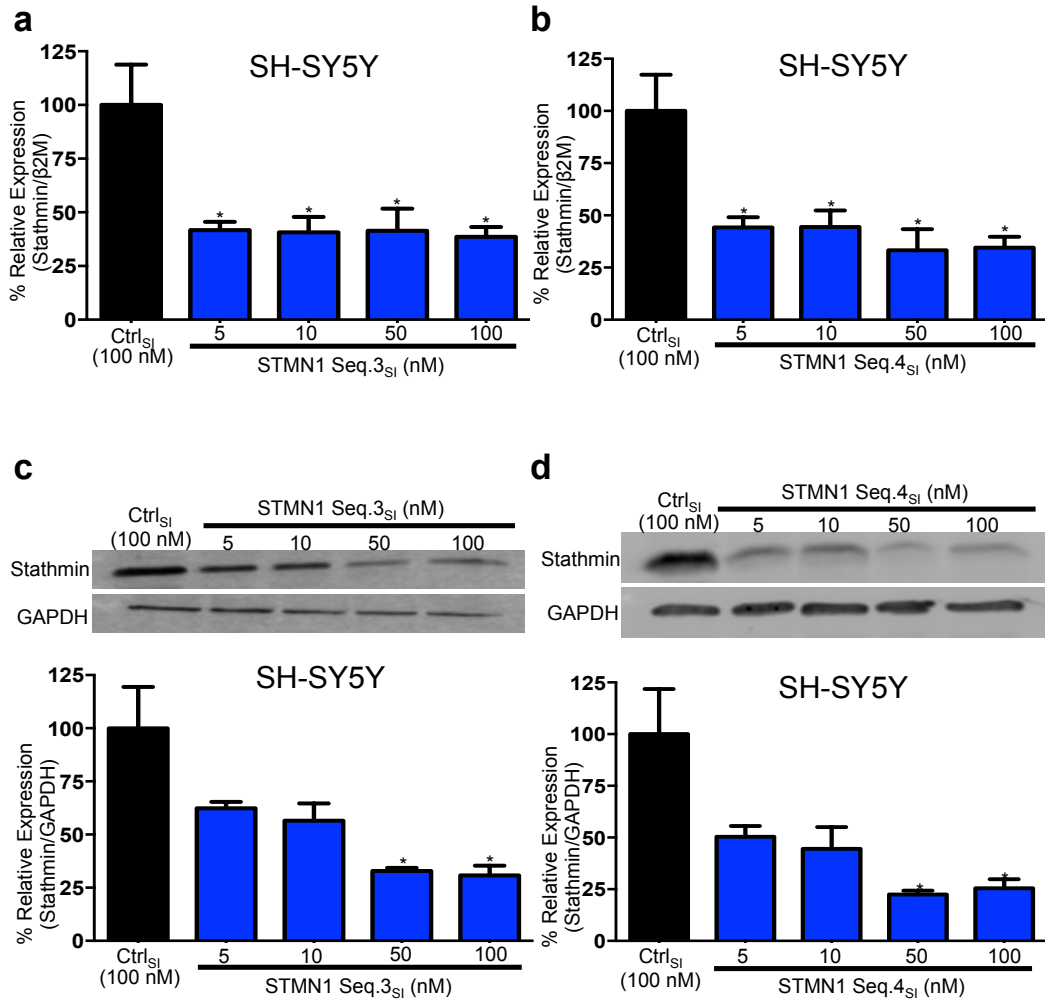


Figure 3.5 Stathmin siRNA sequence concentration optimisation in SH-SY5Y neuroblastoma cells

To determine the lowest effective siRNA concentration, the efficacy of STMN1 Seq.3_{SI} and STMN1 Seq.4_{SI} at 5, 10, 50 and 100 nmol/L was evaluated in SH-SY5Y cells. Stathmin mRNA levels in SH-SY5Y cells 72 h post transfection with 5, 10, 50 or 100 nmol/L of STMN1 Seq.3_{SI} (**a**), STMN1 Seq.4_{SI} (**b**) or 100 nmol/L control (Ctrl_{SI}) siRNA. Stathmin mRNA was normalised to β 2-microglobulin (β 2M). A representative western blot and corresponding quantitation (lower graph) of stathmin protein expression in SH-SY5Y cells 72 h post transfection with 5, 10, 50 or 100 nmol/L STMN1 Seq.3_{SI} (**c**), STMN1 Seq.4_{SI} (**d**) or 100 nmol/L Ctrl_{SI}. Stathmin protein expression was normalised to GAPDH (loading control). Data represents the mean \pm SEM (error bars) of three independent experiments, * $p < 0.05$; **** $p < 0.0001$.



3.4 Stathmin suppression does not affect neuroblastoma cell proliferation in 2-dimensional or 3-dimensional culture

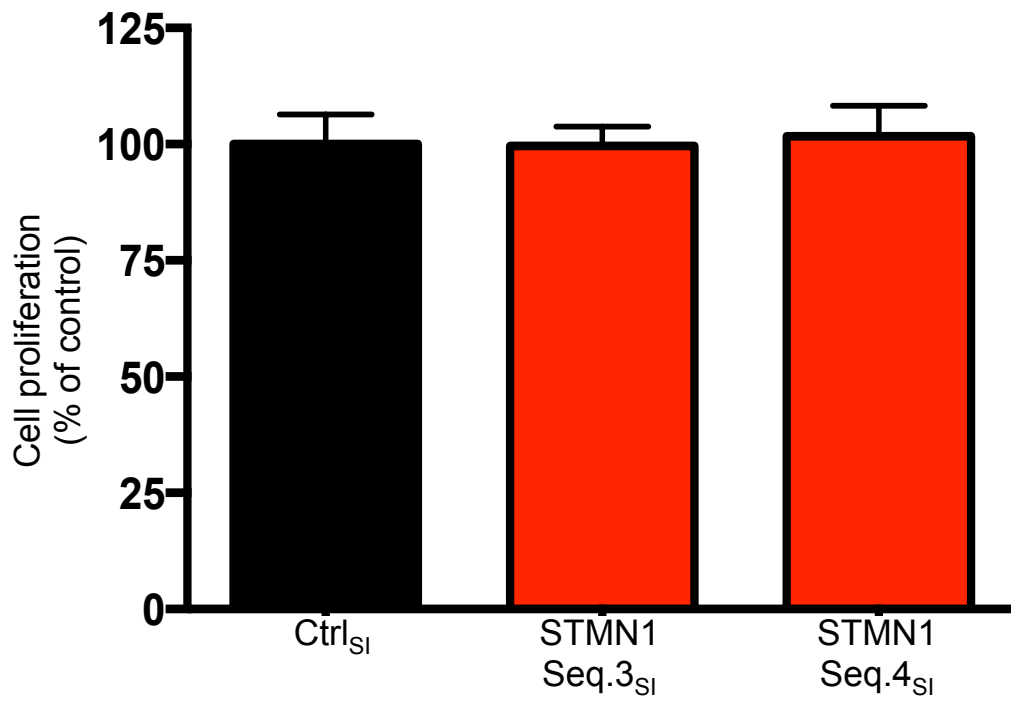
An initial step of the metastatic cascade is the growth of the primary tumour. In several non-neuronal malignancies, suppression of stathmin expression results in a tumour cell growth decrease (Mistry, Bank et al. 2005, Singer, Ehemann et al. 2007, Wang, Dong et al. 2007, Mitra, Kandalam et al. 2011). However, suppression of stathmin expression does not appear to influence cell proliferation in a panel of leukaemia cells leading to the hypothesis that stathmin's role in cell proliferation may be cell-type specific (Holmfeldt, Sellin et al. 2010). Recently our laboratory showed that suppressing stathmin, using pooled siRNA sequences, did not markedly alter neuroblastoma cell proliferation using an alamar blue-based assay (Byrne, Yang et al. 2014). To ascertain whether stathmin suppression using individual siRNA sequences can alter cell proliferation of neuroblastoma cells in a 2-dimensional (2D) cell monolayer culture, stathmin siRNA-suppressed cells were subjected to an *in vitro* cell proliferation (BrdU incorporation) assay. Stathmin suppression did not significantly influence *in vitro* SK-N-BE(2)/TGL cell proliferation in 2D-cell culture ($99.6 \pm 2.40\%$, $p=0.94$; $101.7 \pm 3.84\%$, $p=0.77$ for STMN1 Seq.3_{SI} and STMN1 Seq.4_{SI} cells respectively compared to $100.0 \pm 3.69\%$ (normalised) Ctrl_{SI} cells) (Fig. 3.6).

3D tumour spheroid models better mimic the 3D *in vivo* tumour microenvironment compared to 2D monolayer cultures with respect to nutrient and oxygen gradients, cell-cell interactions,

Figure 3.6 Stathmin does not influence SK-N-BE(2)/TGL cell proliferation in 2D monolayer culture

Cell proliferation of STMN1 Seq.3_{SI}, STMN1 Seq.4_{SI} and Ctrl_{SI} siRNA-transfected SK-N-BE(2)/TGL cells as measured using the bromo deoxyuridine (BrdU) cell proliferation assay. Data represents the mean of three independent experiments \pm SEM (error bars).

SK-N-BE(2)/TGL



signalling pathway activity and gene expression profiles [reviewed in (Vinci, Gowan et al. 2012)].

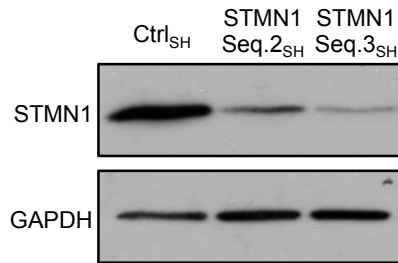
To address the effect of stathmin suppression on 3D growth, a gene silencing approach was used. Due to the length of the 3D spheroid experiments, neuroblastoma cells stably expressing stathmin shRNA that were previously described by our laboratory were used for these experiments (Byrne, Yang et al. 2014). Fig. 3.7a validates that stathmin is effectively suppressed using two independent stathmin shRNA sequences, denoted as stathmin shRNA sequence 2 and stathmin shRNA sequence 3, compared to controls (herein referred to as STMN1 Seq.2_{SH}, STMN1 Seq.3_{SH} and Ctrl_{SH} SK-N-BE(2)/TGL cells respectively).

To examine the effect of stathmin suppression on tumour spheroid growth stathmin- and control-shRNA-expressing SK-N-BE(2)/TGL tumour spheroids were grown for 7 days (with diameter measurements acquired at 2, 4 and 7 days post-cell seeding). Stathmin suppression did not significantly influence tumour spheroid growth at any of the above-mentioned timepoints (Figure 3.7b-c). Collectively, these results are congruous with previous findings where stathmin was observed not to influence both neuroblastoma cell 2D monolayer cell proliferation (alamar blue assay) and orthotopic xenograft primary tumour growth (Byrne, Yang et al. 2014). Altogether, these findings indicate that stathmin does not play a major role in regulating neuroblastoma cell proliferation in both *in vitro* and *in vivo* environments.

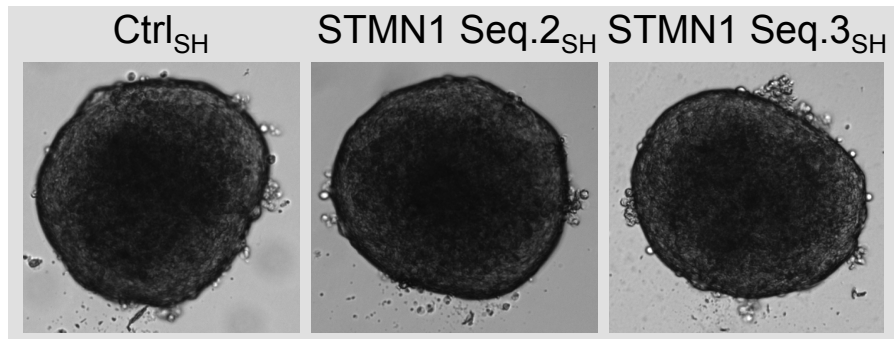
Figure 3.7 Stathmin does not influence neuroblastoma 3D tumour spheroid growth

To determine stathmin's influence on 3D tumour spheroid growth, SK-N-BE(2)/TGL cells expressing either stable stathmin or non-targeting short-hairpin RNA (shRNA) were seeded at 2,500 cells/well in round-bottomed low-attachment 96-well plates and incubated at 37°C for 7 d with diameter measurements acquired 2, 4 and 7 d post-seeding. **(a)** A representative western blot of stathmin protein expression in STMN1 Seq.2_{SH}, STMN1 Seq.3_{SH} and Ctrl_{SH} SK-N-BE(2)/TGL cells. **(b)** Representative tumour spheroid phase contrast microscopy images of Ctrl_{SH}, STMN1 Seq.2_{SH} and STMN1 Seq.3_{SH} tumour spheroids acquired 4 d post-seeding. **(c)** Tumour spheroid diameter was measured at 2, 4 and 7 d post-seeding using a Zeiss Axiovert 200M microscope and measurements subsequently analysed using Axiovision 4.8 software. Data represents the mean \pm SEM (error bars) of three independent experiments.

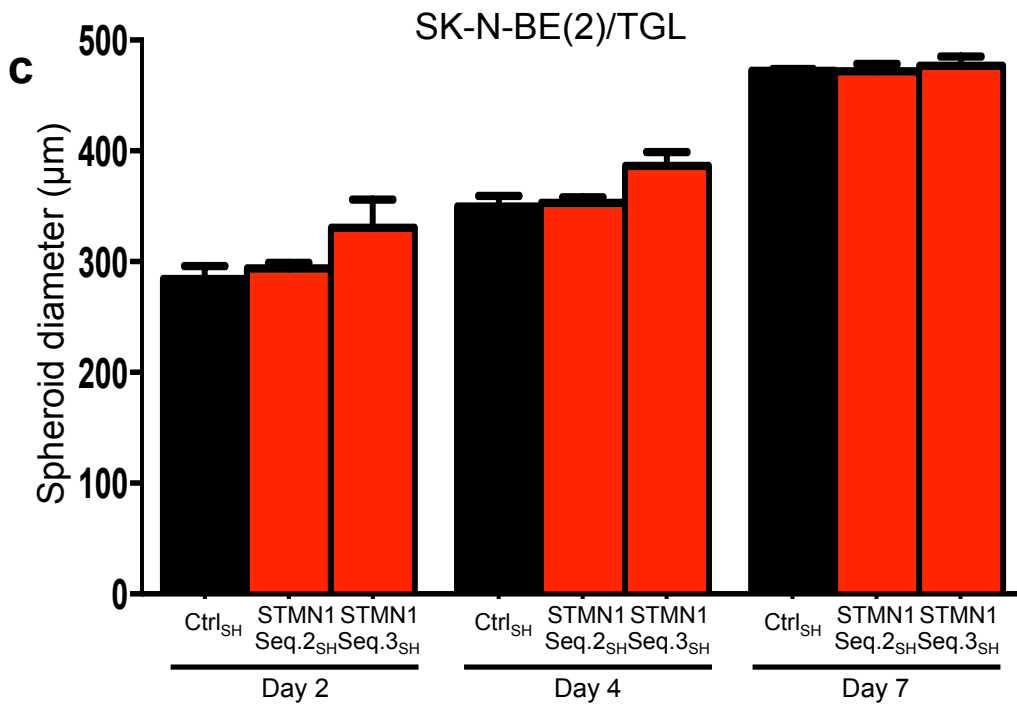
a



b



c



3.5 Stathmin mediates chemotactic-induced neuroblastoma cell migration and invasion

In an *in vivo* environment, cancer cells are constantly experiencing concentration gradients in chemoattractants (such as growth factors and cytokines). These gradients can influence cell migratory and invasive behaviour (Mouneimne, DesMarais et al. 2006). Previous results from our laboratory highlight that stathmin suppressed neuroblastoma cells exhibit a decreased migratory and invasive phenotype compared to controls (Byrne, Yang et al. 2014). These previous experiments were conducted using separate siRNA sequences combined in a pooled sample. One of the aims of this thesis is to investigate the therapeutic targeting of stathmin using a single siRNA sequence. The two most effective siRNA sequences identified in Section 3.3 were chosen to determine whether they would influence the migratory and invasive phenotype and corroborate the previous findings.

To determine whether stathmin was influencing chemotactic-induced neuroblastoma cell migration and invasion, stathmin siRNA-suppressed neuroblastoma cells were subjected to transwell migration and invasion assays, which are commonly used to reproduce *in vivo* chemotactic-induced cell migration and invasion in an *in vitro* setting (Valster, Tran et al. 2005). Stathmin suppression significantly reduced the migratory ability of SK-N-BE(2)/TGL cells (migration index of $29.9 \pm 2.94\%$, $p < 0.005$; $31.2 \pm 3.96\%$, $p < 0.05$; $48.9 \pm 2.53\%$ for STMN1 Seq.3_{SI} and STMN1 Seq.4_{SI} compared to Ctrl_{SI} respectively) (Figure 3.8a). Similarly, in SH-SY5Y cells, stathmin suppression significantly reduced migration (migration index of $6.5 \pm 0.43\%$, $p < 0.005$; $6.5 \pm 0.51\%$, $p < 0.005$; 10.8 ± 0.35 for STMN1 Seq.3_{SI}

Figure 3.8 Stathmin regulates chemotactic-induced neuroblastoma cell migration

To determine stathmin's influence on chemotactic-induced neuroblastoma cell migration, stathmin siRNA-suppressed neuroblastoma cells were subjected to transwell migration assays. Serum and collagen IV were used as chemo-attractants (see Chapter 2, Section 2.6). Chemotactic-induced migration of Ctrl_{SI}, STMN1 Seq.3_{SI} and STMN1 Seq.4_{SI} siRNA-transfected SK-N-BE(2)/TGL **(a)** and SH-SY5Y **(b)** cells. Data displayed as a migration index, which is the percentage of total cells that successfully migrate from the top to the bottom chamber. Migration index = [(number of cells on under surface of membrane divided by total number of cells on both surfaces of the membrane) x 100]. Data represents the mean of three independent experiments ±SEM (error bars). * p<0.05, ** p<0.005.

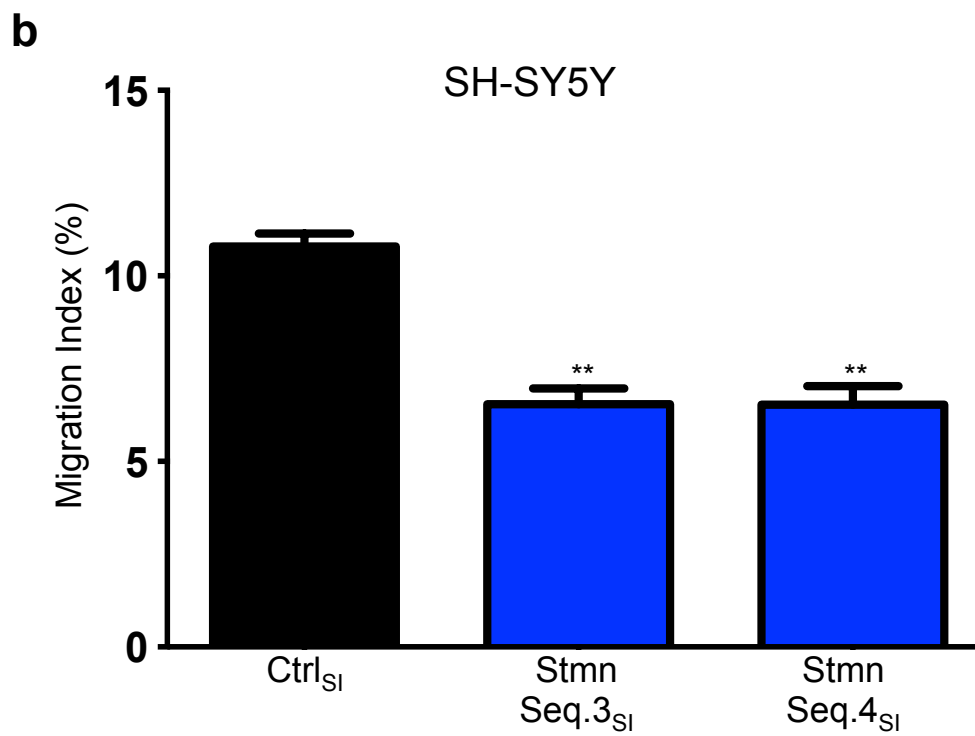
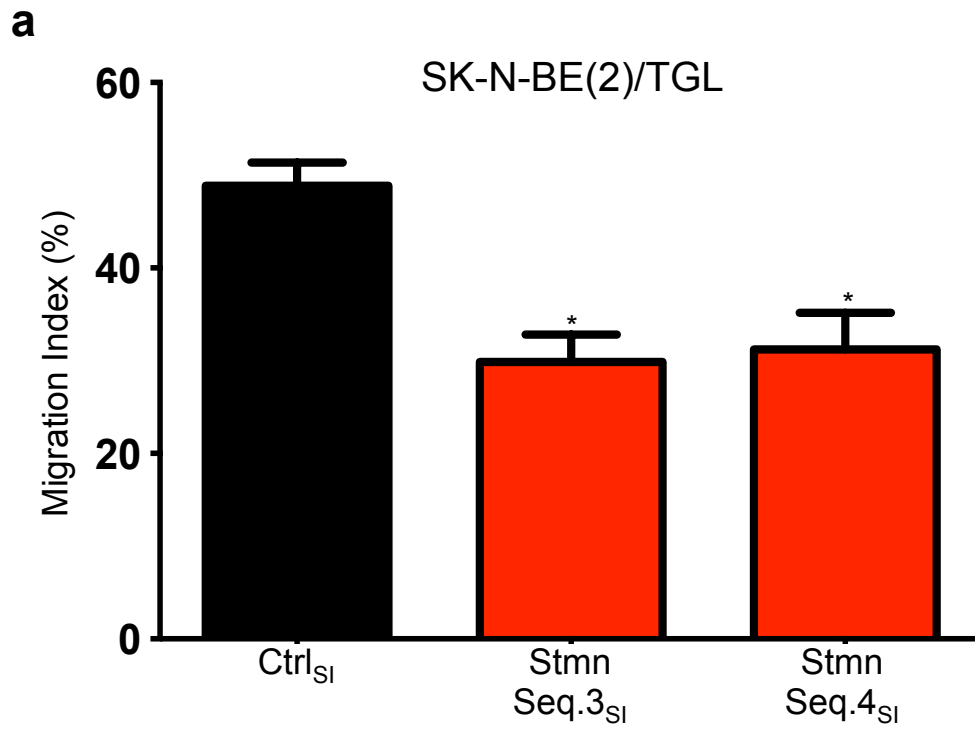
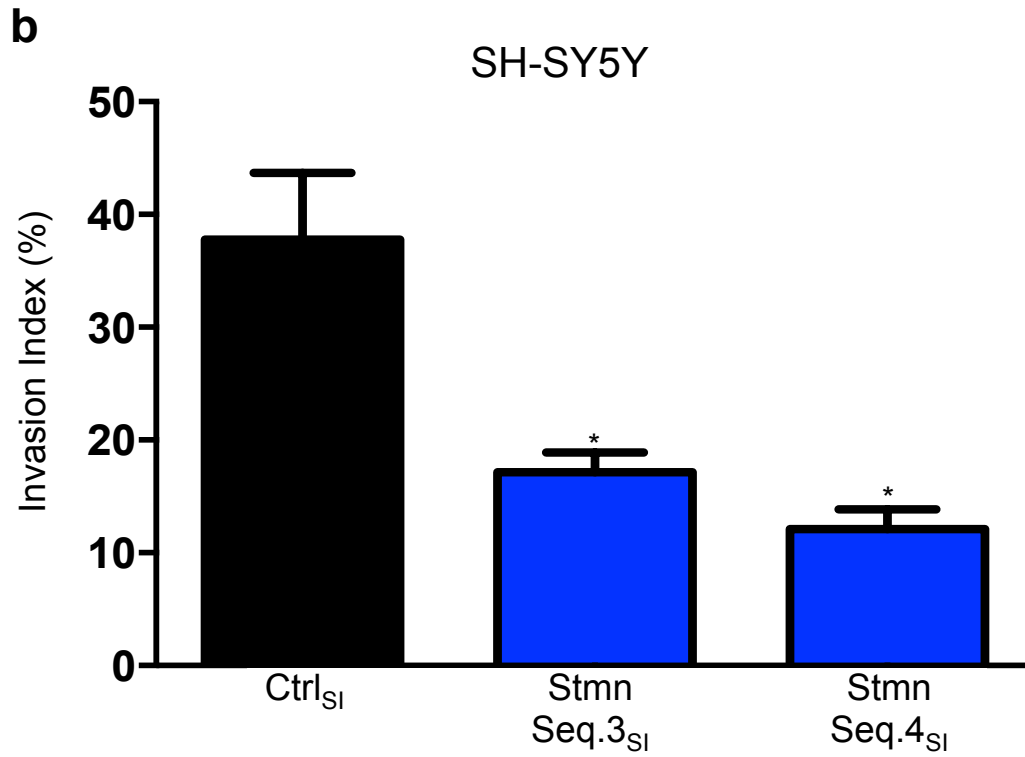
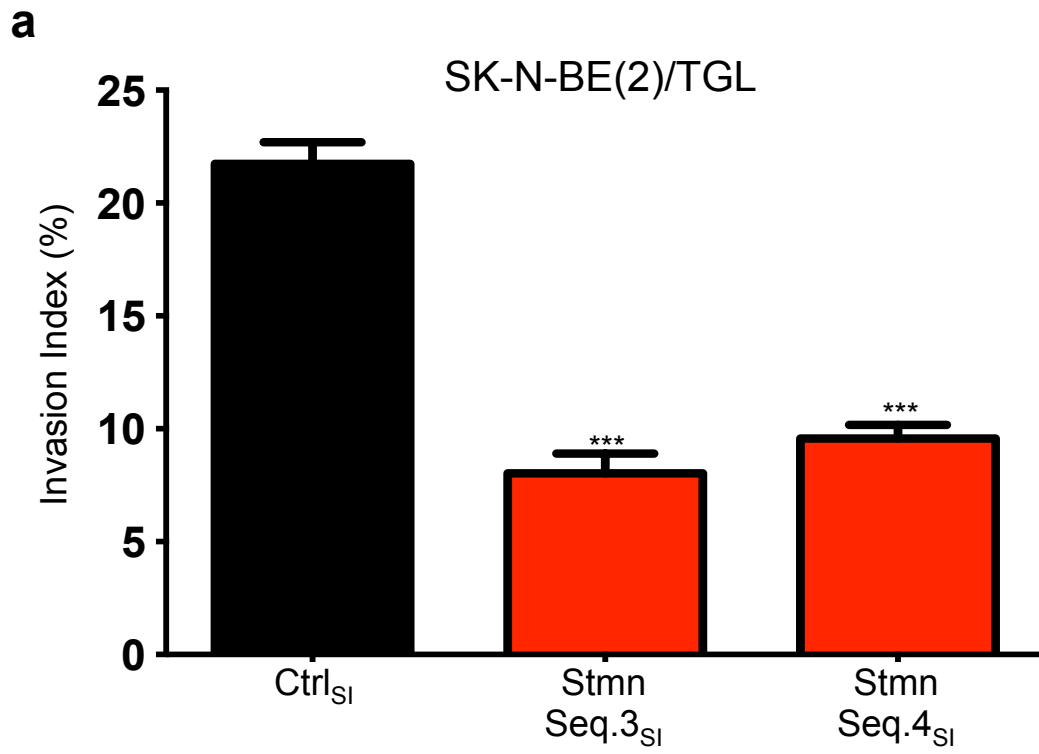


Figure 3.9 Stathmin regulates chemotactic-induced neuroblastoma cell invasion

To determine stathmin's influence on chemotactic-induced neuroblastoma cell invasion, stathmin siRNA-suppressed neuroblastoma cells were subjected to transwell invasion assays. Transwell invasion assays are similar to transwell migration assays where tumour cells are required to cross a porous membrane. However, in transwell invasion assays there is a matrigel coating on top of the porous membrane. For tumour cells to cross into the bottom chamber they need to digest and invade through the matrigel layer before crossing the porous membrane. Serum, PDGF and collagen IV were used as chemo-attractants (see Chapter 2, Section 2.6). PDGF was used in invasion assays (and not migration assays) due to the ability of PDGF to promote cell invasion. Chemotactic-induced cell invasion of Ctrl_{SI}, STMN1 Seq.3_{SI} and STMN1 Seq.4_{SI} siRNA-transfected SK-N-BE(2)/TGL **(a)** and SH-SY5Y **(b)** cells. Data displayed as an invasion index, which is the percentage of total cells that successfully migrate from the top to the bottom chamber. Invasion index = [(number of cells on under surface of membrane divided by total number of cells on both surfaces of the membrane) x 100]. Data represents the mean of three independent experiments ±SEM (error bars). * p<0.05, *** p<0.0005.



and STMN1 Seq.4_{SI} compared to Ctrl_{SI} respectively) (Figure 3.8b). Moreover, stathmin suppression significantly reduced the invasive ability of SK-N-BE(2)/TGL cells (invasion index of $8.0 \pm 0.86\%$, $p < 0.05$; $9.6 \pm 0.60\%$, $p < 0.005$; $21.7 \pm 0.96\%$ for STMN1 Seq.3_{SI} and STMN1 Seq.4_{SI} compared to Ctrl_{SI} respectively) (Figure 3.9a). Furthermore, stathmin suppression significantly reduced SH-SY5Y invasive ability (invasion index of 17.2 ± 1.73 , $p < 0.05$; $12.1 \pm 1.76\%$, $p < 0.05$; $37.8 \pm 5.9\%$ for STMN1 Seq.3_{SI} and STMN1 Seq.4_{SI} compared to Ctrl_{SI} respectively) (Figure 3.9b). These results demonstrate that two independent stathmin siRNA sequences can suppress stathmin and reduce neuroblastoma cell chemotactic-induced migration and invasion.

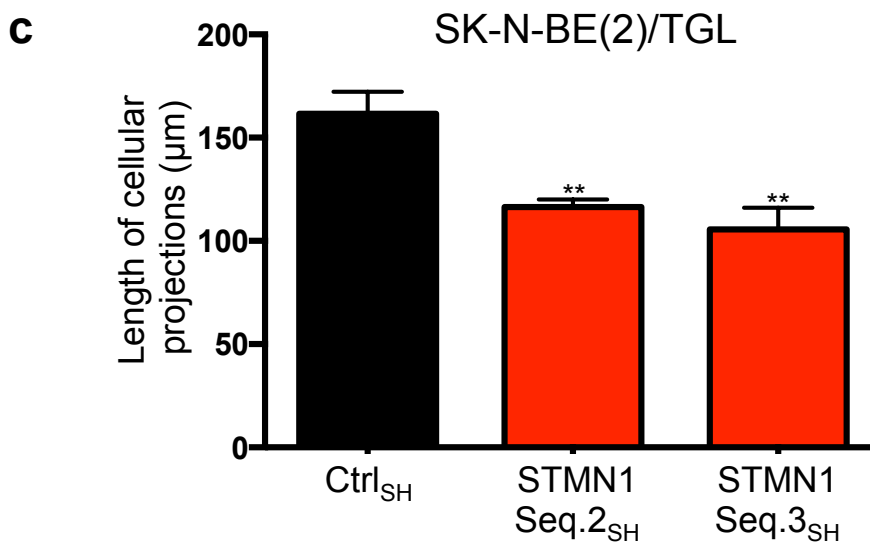
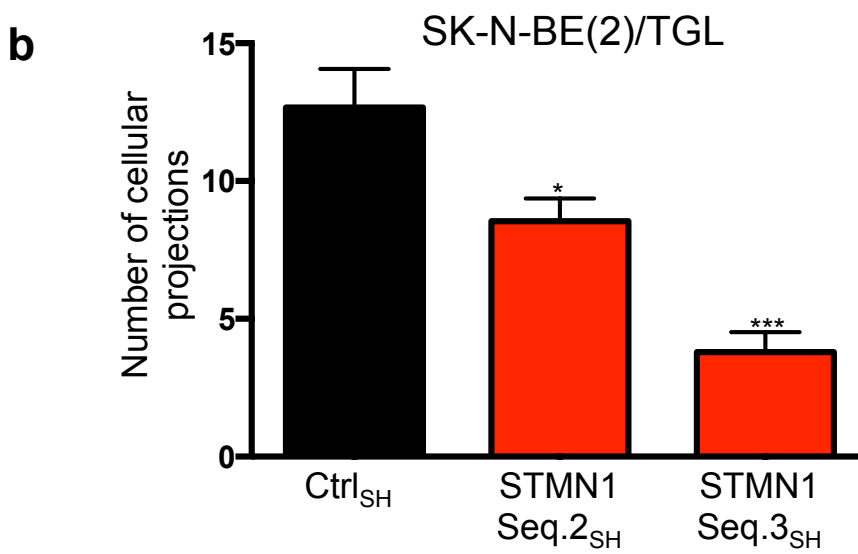
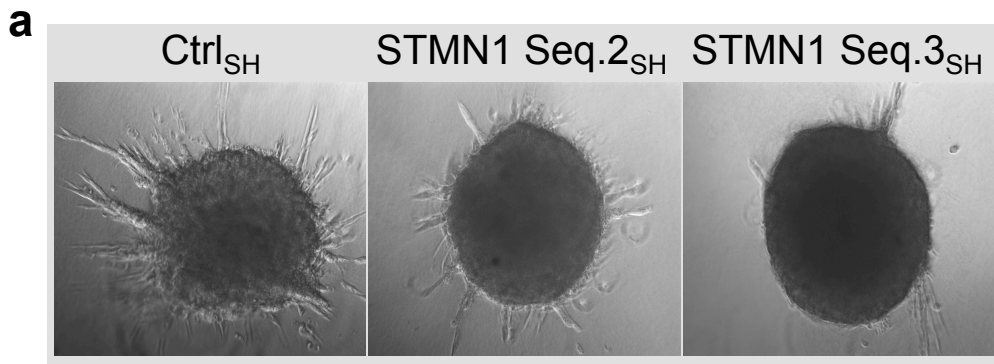
3.6 Stathmin suppression reduces 3D tumour spheroid invasion into 3D extracellular matrices

To investigate and visualize the impact of stathmin suppression on the migratory and invasive phenotype a 3D spheroid outgrowth assay was developed (see Section 2.8). Briefly, SK-N-BE(2)/TGL spheroids were grown and then embedded in a collagen I extracellular matrix and subsequently their invasive phenotype was imaged and measured. Unlike the transwell invasion assays, this 3D tumour spheroid invasion assay more closely resembles *in vivo* tumour cell invasion away from the primary tumour, as the neuroblastoma cells are required to break free from considerable neuroblastoma cell-cell interactions. Furthermore, in this assay, the tumour cells are embedded in a matrix rather than sitting on top of a matrix and invading into a 3D matrix.

Similar to tumour spheroid experiments presented in Section 3.4, neuroblastoma SK-N-BE(2) stathmin- and control-shRNA-expressing and luciferase-expressing cells previously described by our laboratory were used for the 3D tumour spheroid invasion experiments (Byrne, Yang et al. 2014). After a 48 h incubation, allowing the cells to invade into the surrounding collagen I matrix, stathmin suppressed spheroids (both STMN1 Seq.2_{SH} and STMN1 Seq.3_{SH}) exhibited a decreased invasive phenotype compared to Ctrl_{SH} spheroids (Figure 3.10a). To quantify this effect, the number of cellular outgrowths was measured and it showed that stathmin suppression significantly reduced the number of invasive cellular protrusions ($32.6 \pm 1.16\%$, $p < 0.05$; and $70.0 \pm 1.12\%$, $p < 0.0005$) for STMN1 Seq.2_{SH} and STMN1 Seq.3_{SH} respectively compared to Ctrl_{SH} (Figure 3.10b). Another parameter that was measured was the length of cellular protrusions. Stathmin suppression significantly reduced

Figure 3.10 Stathmin suppression reduces 3D tumour spheroid invasion into 3D extracellular matrices

To determine stathmin's influence on 3D tumour spheroid invasion into a 3D extracellular matrix stathmin- and control-shRNA-expressing SK-N-BE(2)/TGL neuroblastoma cells (STMN1 Seq.2_{SH}, STMN1 Seq.3_{SH} and Ctrl_{SH}) were seeded at 2500 cells/well in round-bottomed 96-well plates and incubated at 37°C for 4 days. Spheroids were transferred into a collagen I (1 mg/mL) matrix and incubated at 37°C for 48 h. **(a)** Spheroids were imaged using a Zeiss Axiovert 200M microscope. The number **(b)** and length **(c)** of cellular protrusions were measured using Axiovision 4.8 software. Data represents the mean \pm SEM (error bars) of three independent experiments.



the length of the invasive cellular protrusions ($28.0 \pm 1.06\%$, $p < 0.005$; and $34.7 \pm 1.40\%$, $p < 0.005$) for STMN1 Seq.2_{SH} and STMN1 Seq.3_{SH} respectively compared to Ctrl_{SH} (Figure 3.10c). Collectively, these results further demonstrate the importance of stathmin in neuroblastoma cell migration and invasion during metastasis.

3.7 Stathmin does not affect neuroblastoma cell sensitivity to anoikis

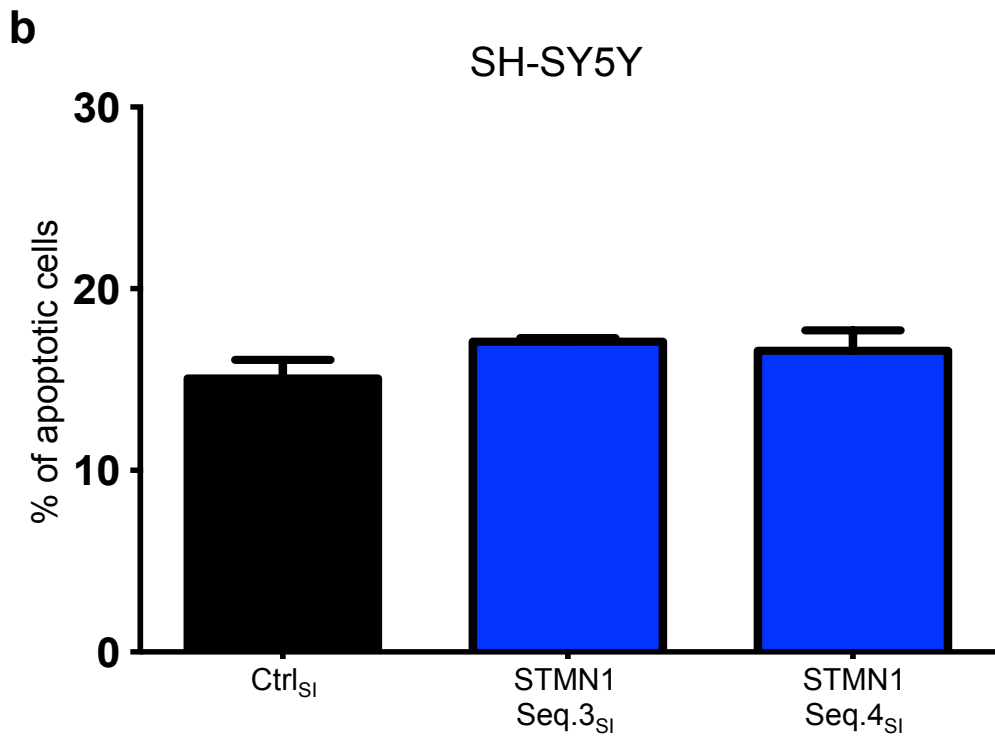
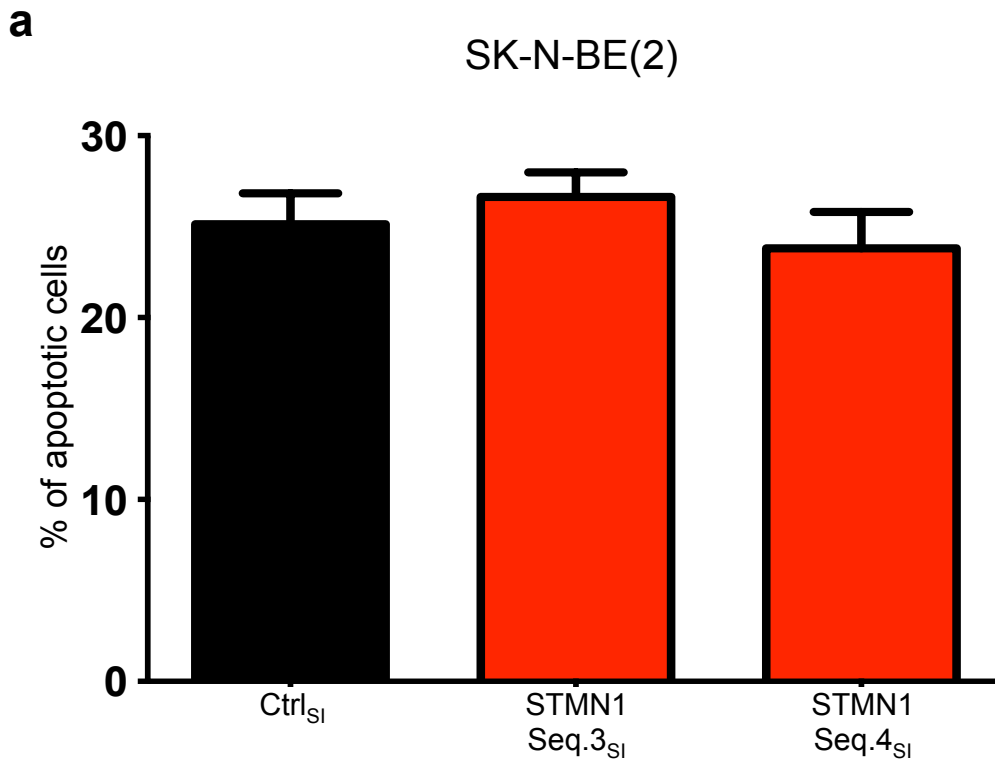
As tumour cells lose contact with the basement membrane during invasion and proceeding intravasation into blood and lymph vessels, and extravasation at distant sites they encounter a critical barrier against metastasis: anoikis (apoptotic cell death induced by loss or inadequate cell adhesion in anchorage-dependent cells) (Frisch and Screaton 2001). It is generally accepted that anoikis hampers metastasis by inducing apoptosis when tumour cells enter ‘foreign’ environments. Therefore, anoikis suppression is expected to be important for tumour cells to metastasise successfully. For anoikis and subsequent transendothelial migration experiments, a transient stathmin gene silencing approach instead of stable stathmin suppression, was used due to fluorescence interference between the green fluorescent protein (GFP)-expressing neuroblastoma cells and the assay protocols.

To investigate whether stathmin was involved in anoikis, stathmin suppressed cells were assessed for their ability to survive under anchorage-independent conditions. In order to determine whether stathmin played a role in neuroblastoma cell anoikis, SK-N-BE(2) and SH-SY5Y cells were transfected with either Ctrl_{SI}, STMN1 Seq.3_{SI} or STMN1 Seq.4_{SI} siRNA and were incubated in forced suspension in an anchorage-independent manner for 24 h and 12 h respectively inducing a stress on the anchorage-dependent cells (see Section 2.9). Time

of forced suspension incubation was determined based on degree on apoptosis. It was evident that SH-SY5Y cells were more sensitive to apoptosis at comparable time-points and hence a shorter incubation time was used. Stathmin suppression, using STMN1 Seq.3_{SI} and STMN1 Seq.4_{SI} in SK-N-BE(2) (Figure 3.11a) and SH-SY5Y (Figure 3.11b) did not significantly affect levels of neuroblastoma cell apoptosis compared to Ctrl_{SI}. These results indicate that stathmin is not likely involved in the anoikis step of the metastatic cascade in neuroblastoma.

Figure 3.11 Stathmin suppression does not alter sensitivity to anoikis

Neuroblastoma cells, SK-N-BE(2) and SH-SY5Y, were transfected with Ctrl_{SI}, STMN1 Seq.3_{SI} or STMN1 Seq.4_{SI} and then incubated in suspension for 24 h (for SK-N-BE(2)) or 12 h (for SH-SY5Y). % Apoptosis was measured using annexin V staining and flow cytometry (see Section 2.9). Anoikis (% apoptotic cells) of Ctrl_{SI}, STMN1 Seq.3_{SI} and STMN1 Seq.4_{SI} siRNA-transfected **(a)** SK-N-BE(2) and **(b)** SH-SY5Y cells. Data represents the mean of three independent experiments \pm SEM (error bars). * $p < 0.05$, ** $p < 0.005$.



3.8 Stathmin regulates chemotactic-induced neuroblastoma cell transendothelial migration

Another critical step of the metastatic cascade includes the degradation of the vascular basement membrane and subsequent travel across the endothelium (termed intravasation), and once inside the vasculature the arrest of tumour cells in a capillary bed and crossing of the vasculature (termed extravasation) (Ara and DeClerck 2006). Collectively, intravasation and extravasation are termed transendothelial migration.

To examine stathmin's role in neuroblastoma cell transendothelial migration, stathmin suppressed cells were subjected to *in vitro* chemotactic transendothelial migration assays where neuroblastoma cells were required to cross both a confluent endothelial cell monolayer and matrigel matrix (as depicted in Fig. 3.12a). Initially, HMEC-1 endothelial cells were seeded into a transendothelial migration assay chamber and allowed to grow to confluency (See Chapter 2, Section 2.12). A confluent, tight sheet of endothelial cells was confirmed using fluorescent microscopy (Fig. 3.12b). SK-N-BE(2) and SH-SY5Y cells were transfected with Ctrl_{SI}, STMN1 Seq.3_{SI} or STMN1 Seq.4_{SI} siRNA and plated onto the endothelial cells to determine their ability to pass through the tight sheet of endothelial cells, the extracellular matrix and membrane pores to complete transendothelial migration.

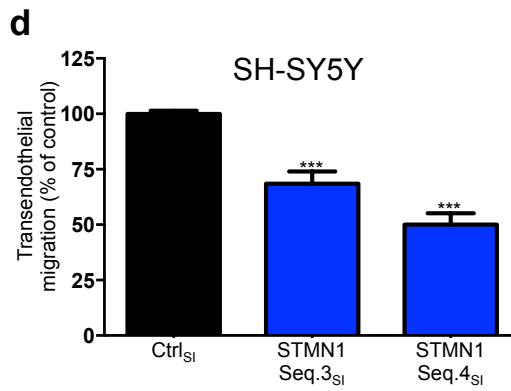
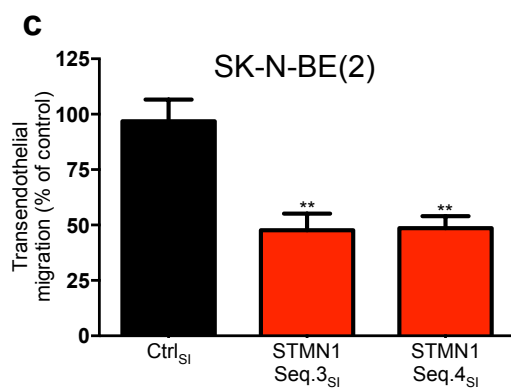
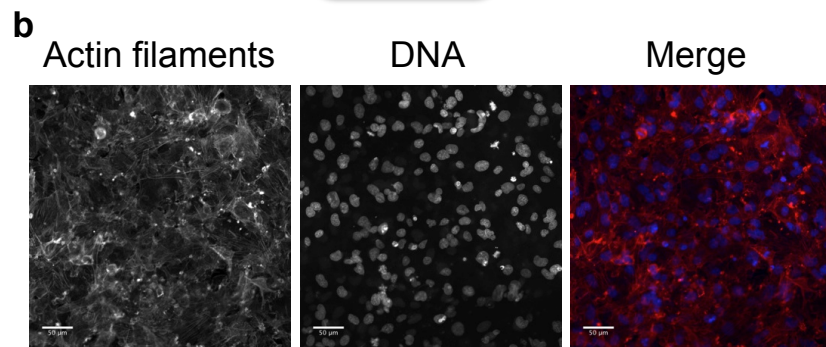
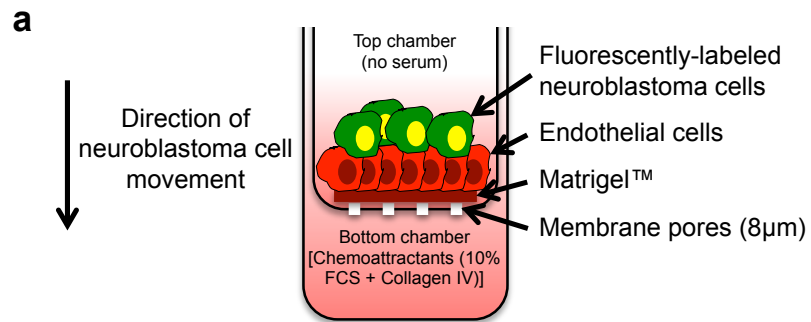
Fluorescence measurements of cells that crossed into the lower chamber showed that stathmin suppression significantly reduced the transendothelial migratory ability of SK-N-BE(2) cells (54.0±9.53%, p<0.0001; and 58.3±9.75%, p<0.0001) for STMN1 Seq.3_{SI} cells and STMN1 Seq.4_{SI} cells respectively compared to Ctrl_{SI} cells (Figure 3.12c). Similarly, stathmin suppression also reduced the transendothelial migratory ability of SH-SY5Y cells

(31.5±5.66%, $p<0.0005$; and 50.0±5.28%, $p<0.0001$) for STMN1 Seq.3_{SI} and STMN1 Seq.4_{SI} respectively compared to Ctrl_{SI} cells (Figure 3.12d). These results provide the first evidence that stathmin plays a role in neuroblastoma cell transendothelial migration and indicate a potential role for stathmin in the intravasation and extravasation steps of the metastatic cascade.

Figure 3.12 Stathmin suppression reduces neuroblastoma cell transendothelial migration

To determine stathmin's influence on neuroblastoma cell transendothelial migration, stathmin siRNA-suppressed neuroblastoma cells were subjected to transendothelial migration assays.

(a) Schematic of the transendothelial migration assay used in this study. Serum-starved and fluorescently-labelled neuroblastoma cells were required to chemotactically migrate and invade through a confluent HMEC-1 endothelial cell monolayer, Matrigel™ barrier and 0.8 µm membrane pores. Serum and collagen IV were used as chemoattractants (see Section 2.10) **(b)** Fluorescent microscopy of a confluent monolayer of HMEC-1 endothelial cells. Actin filaments stained using AF568-phalloidin; DNA stained using DAPI. Merged colour image on right. Scale bar = 50 µm. STMN1 Seq.3_{SI}, STMN1 Seq.4_{SI} and Ctrl_{SI} siRNA-treated SK-N-BE(2) **(c)** and SH-SY5Y **(d)** were subjected to chemotactic transendothelial migration assays. Results are expressed as a relative % of Ctrl_{SI} cells (% of control). Data represents the mean of at least four independent experiments ±SEM (error bars). ** p<0.005, ***p<0.0005.



3.9 Discussion

Stathmin overexpression in multiple malignancies correlates with metastatic disease progression and a poor clinical outcome (Singer, Malz et al. 2009, Hsieh, Huang et al. 2010, Jeon, Han et al. 2010, Trovik, Wik et al. 2011). Recently, our laboratory identified stathmin as an important contributor of cell invasion and metastasis in neuroblastoma (Byrne, Yang et al. 2014). Metastasis is a complex and multi-stepped process that has been modelled into a “metastatic cascade” [reviewed in (Steeg 2006)]. This chapter demonstrates that suppression of stathmin expression influences multiple steps of the metastatic cascade in neuroblastoma, including cell migration and invasion (corroborating our laboratories previous findings (Byrne, Yang et al. 2014)), anoikis and transendothelial migration.

Proliferation of tumour cells, an initial step of the metastatic cascade, is important during metastasis, both for the growth of the primary tumour and also for the establishment and development of secondary metastatic tumours. Stathmin has been largely studied for its role in cell division due to the importance of microtubule depolymerisation and re-polymerisation to form the mitotic spindle during cell division. In some cell types, inhibition of stathmin expression or impairment of stathmin phosphorylation induces a G2-M arrest, which is associated with a reduction in cell proliferation (Mistry, Bank et al. 2005, Singer, Ehemann et al. 2007, Singer, Malz et al. 2009). Despite these findings, stathmin’s role in cell proliferation appears to be cell type specific where alteration of stathmin expression in various leukaemia cells did not influence mitotic spindle assembly nor cell proliferation (Holmfeldt, Brannstrom et al. 2006, Holmfeldt, Sellin et al. 2010). Results from this chapter demonstrate that stathmin suppression, using two separate and independent siRNA sequences, does not significantly influence neuroblastoma 2D monolayer cell proliferation using a BrdU-based assay (Fig. 3.6). This finding corroborates our laboratory’s prior observation that stathmin suppression,

using multiple siRNA sequences combined into a pooled mixture, does not influence neuroblastoma 2D monolayer cell proliferation using an alamar blue-based assay (Byrne, Yang et al. 2014). Similarly, to further replicate the 3D *in vivo* tumour environment a 3D tumour spheroid model was used and it showed that stathmin suppression, using the aforementioned independent stathmin siRNA sequences, did not influence tumour spheroid growth (Fig. 3.7). This finding is congruous with the previous discovery that stathmin suppression does not influence the *in vivo* growth of neuroblastoma xenograft primary tumours (Byrne, Yang et al. 2014). Altogether, these observations provide further support that stathmin does not influence cell proliferation or tumour growth in neuroblastoma.

In addition to stathmin's role in cell division in some cell types, stathmin is emerging as a protein involved in the highly migratory, invasive and metastatic phenotype of multiple malignancies (reviewed in Section 1.5.5). Prior results from our laboratory revealed a role for stathmin in neuroblastoma cell migration and invasion (Byrne, Yang et al. 2014), however the specific steps where stathmin was influencing metastasis were not well understood. Results from this thesis showed that stathmin suppression, using two separate and independent siRNA sequences, reduced both neuroblastoma cell chemotactic-induced migration and invasion (Figs. 3.8-9). Furthermore, a 3D spheroid outgrowth assay was developed (see Section 2.8) to allow further investigation and importantly visualisation of stathmin's role in the invasive phenotype in neuroblastoma. The assay more closely resembles *in vivo* tumour cell invasion away from the primary tumour during metastasis. Suppression of stathmin expression, using two independent shRNA sequences, reduced the neuroblastoma invasive phenotype as measured using two separate parameters (Fig. 3.10). Collectively, these results further demonstrate the importance of stathmin in the cell migratory and invasive phenotype during metastasis.

The ability of tumour cells to resist anoikis (apoptotic cell death induced by loss or inadequate cell adhesion in anchorage-dependent cells) is a key characteristic of metastatic malignancy and has prime importance for tumour cell survival during cell movement through the harsh environment of the bloodstream. Anoikis is thought to confer a selective advantage to tumour cells providing them with an increased survival time in the absence of matrix attachment to facilitate eventual colonisation on secondary sites. Differences between the cytoskeletal structures of attached versus suspended cells indicate that the cytoskeleton may play a role in the regulation of survival signalling in anoikis [reviewed in (Frisch and Screaton 2001)]. A notable connection between the cytoskeleton and anoikis involves the proapoptotic Bcl-2-family protein Bim and the microtubule-stabilising agent taxol (Puthalakath, Huang et al. 1999, Strasser, Puthalakath et al. 2000). In untreated cells, Bim is sequestered by microtubule-associated dynein light chain 1. Though upon treatment with the microtubule-stabilising agent taxol, Bim is released from the microtubules allowing Bim:Bcl-2 interaction, subsequent release of cytochrome c from mitochondria and eventual induction of anoikis (Puthalakath, Huang et al. 1999, Strasser, Puthalakath et al. 2000). Interestingly, treatment of breast cancer and melanoma cells with the microtubule-destabilising drug vinblastine provokes anoikis induction by decreasing cell adhesion via the generation of disorganized focal adhesion and actin stress fibres (Deschesnes, Patenaude et al. 2007). Thus it is apparent that disruption of the microtubule system, by either a microtubule stabilising or destabilising agent, promotes anoikis induction though it is unclear whether perturbation of microtubule dynamics by aberrant expression of an endogenous microtubule destabilising protein (such as stathmin) may influence anoikis however, results from this chapter indicate that stathmin is not likely playing a role in the anoikis step of the metastatic cascade in neuroblastoma (Fig. 3.11).

If a tumour cell survives the harsh environment of the bloodstream a critical step for metastatic disease progression is the crossing of the vasculature from the bloodstream into secondary tissue sites (a process known as transendothelial migration). The majority of research into transendothelial migration centers on lymphocyte transmigration from the bloodstream into tissues. The process of leukocyte transmigration from the bloodstream into tissues has provided some new insights into how cancer cells cross into secondary tissues during metastasis. Leukocyte transmigration regulation is intimately related to cytoskeletal regulation. During leukocyte transmigration, leukocytes extend an F-actin rich lamellipodium, which constitutes the leading edge, and a trailing edge where both the microtubule and intermediate filament networks are retracted [reviewed in (Vicente-Manzanares and Sanchez-Madrid 2004)]. Remodelling of the actin cytoskeleton during actin polymerisation-mediated lamellipodial protrusion has been shown to play a key role in leukocyte transmigration (Vicente-Manzanares and Sanchez-Madrid 2004). In addition to actin cytoskeletal changes, it is apparent that microtubule polymerisation can influence transendothelial migration where the calcium-binding protein MRP14 through forming a complex with MRP8, promotes the polymerisation of microtubules by direct binding to tubulin to promote transendothelial migration (Vogl, Ludwig et al. 2004).

Cytoskeletal remodelling alterations that influence transendothelial migration fuel the hypothesis that the microtubule destabilising protein stathmin, through its direct effects on the microtubule system and indirect effects on the actin network, may be involved in tumour cell transendothelial migration. Importantly, results from this chapter support the hypothesis that stathmin mediates transendothelial migration in neuroblastoma (Fig. 12c-d) thus indicating that stathmin plays a critical role during this vital step of metastasis.

This chapter has examined the role of the microtubule destabilising protein stathmin on key

steps of the metastatic cascade in neuroblastoma. It is apparent that stathmin does not likely influence neuroblastoma cell proliferation or sensitivity to anoikis. In contrast, it has been shown that stathmin is important during tumour cell migration, invasion and transendothelial migration in neuroblastoma. Altogether, these results demonstrate that stathmin influences multiple key steps of the metastatic cascade in neuroblastoma. The signalling pathways in which stathmin mediates its influence will be examined in Chapter 4.

Chapter 4.

4 Stathmin and its role in signalling in cell migration in neuroblastoma cells

4.1 Introduction

Tumour cell metastasis is a multifaceted, complex affair and there exists a complex array of cell regulatory events to modulate this process. *In vitro* studies in Chapter 3 revealed a role for stathmin in multiple key steps of the metastatic cascade in neuroblastoma, however, the basis by which stathmin exerts these effects is not understood. Rho GTPases have strongly emerged as important participants in the regulation of several biochemical pathways controlling migration, such as cytoskeletal dynamics, directional sensing, cell-cell junction assembly/disassembly and integrin-matrix adhesion (Jaffe and Hall 2005). The three most comprehensively studied Rho GTPases, RhoA, Rac1 and Cdc42 regulate the assembly and organisation of the cytoskeleton in eukaryotic cells [reviewed in (Hall 2012)]. Rho GTPases function as molecular switches existing in either an inactive, GDP-bound form or an active, GTP-bound form (Jaffe and Hall 2005). Regulation of GTPase activity is complex with Rho GTPase inactivation regulated by 67 GTPase activating proteins (GAPs), while activation is mediated by 69 guanine nucleotide exchange factors (GEFs) (Rossman, Der et al. 2005). It is only in their GTP-bound state that they interact with their various respective effector proteins to mediate the functions of Rho GTPases (reviewed in Chapter 1, Section 1.3.3; Figure 1.5).

Previous results from our laboratory demonstrated a connection between stathmin's function in the invasive phenotype in neuroblastoma cells with RhoGTPase signalling where pharmacological inhibition of ROCK, a downstream effector of the Rho GTPase RhoA returned cell invasion back to control levels indicating that stathmin was acting, at least in

part, via ROCK (Byrne, Yang et al. 2014). Consequently, stathmin suppression influenced the phosphorylation of the key actin remodelling proteins cofilin and myosin light chain (MLC) both of which are downstream effectors of ROCK (Byrne, Yang et al. 2014).

Despite evidence linking stathmin with key steps of the metastatic cascade, there is limited knowledge of the role of stathmin in the regulation of Rho GTPase signalling. Additionally, it is unknown whether stathmin's influence on neuroblastoma cell transendothelial migration is via Rho GTPase or ROCK signalling. To address this, short-interfering and short-hairpin (siRNA and shRNA) approaches were utilised to suppress stathmin expression and then examine stathmin's role in the regulation of Rho GTPase signalling in neuroblastoma.

4.2 Stathmin regulates chemotactic-induced neuroblastoma cell transendothelial migration via ROCK signalling

Results from this thesis highlighted a role for stathmin in the regulation of transendothelial migration in neuroblastoma (see Section 3.8, Fig. 3.12c, d). To determine whether stathmin's influence on transendothelial migration is operating through ROCK signalling, stathmin suppressed cells were either treated separately with the ROCK inhibitors, Y-27632 or H-1152, or left untreated. ROCK inhibitors were both used at 10 $\mu\text{mol/L}$ as previously optimised (Byrne, Yang et al. 2014). For comparative purposes, Figure 3.12 panels c and d have been reproduced in Figure 4.2 panels a and b as samples that were not treated with ROCK inhibitors. Untreated and ROCK inhibitor-treated samples were performed at the same time to allow for comparison. Initially, HMEC-1 endothelial cells were exposed to ROCK inhibitors to determine whether this would affect endothelial permeability in the

absence of neuroblastoma cells. The effect of ROCK inhibitor treatment on permeability was assessed by measuring fluorescent dextran movement through the endothelial layer. This method has previously been used to assess endothelial permeability (Martin-Padura, Lostaglio et al. 1998). As shown in Figure 4.1 treatment of HMEC-1 cells with either of the two ROCK inhibitors (Y-27632, H-1152) did not significantly alter endothelial permeability when compared to an untreated control (Fig. 4.1). This confirms that any change that is observed in transendothelial migration of neuroblastoma cells in ROCK treated samples is due to the neuroblastoma cells and not to ROCK inhibition-induced alterations in the permeability of the endothelial layer. As shown in Chapter 3.8, Figure 3.12c (and also reproduced in Fig. 4.2a for comparative purposes) stathmin suppression decreased transendothelial migration in SK-N-BE(2) cells. Treatment of stathmin siRNA-transfected SK-N-BE(2) cells with Y-27632 returned transendothelial migration levels of stathmin-suppressed SK-N-BE(2) cells back to that of Ctrl_{SI} cells (STMN Seq.3_{SI}: 86.0±4.88%, p=0.68; STMN1 Seq.4_{SI}: 66.2±4.54%, p=0.26; Ctrl_{SI}: 81.0±10.85%) (Figure 4.1c). Additionally, as shown in Chapter 3.8, Figure 3.12d (and also reproduced in Fig. 4.2b for comparative purposes) stathmin suppression decreased transendothelial migration in SH-SY5Y cells. Treatment of stathmin siRNA-transfected SH-SY5Y cells with Y-27632 returned transendothelial migration back to that of Ctrl_{SI} cells (STMN1 Seq.3_{SI}: 89.2±4.23%, p=0.06; STMN1 Seq.4_{SI}: 83.3±7.60%, p=0.07; Ctrl_{SI}: 100.1±2.93%) (Figure 4.2d). Similarly, treatment of stathmin siRNA-transfected SK-N-BE(2) and SH-SY5Y cells with the ROCK inhibitor H-1152 returned transendothelial migration levels of stathmin-suppressed SK-N-BE(2) and SH-SY5Y cells back to that of Ctrl_{SI} cells (Figure 4.2e, f). Altogether, these results indicate that stathmin's influence on neuroblastoma cell transendothelial migration is due, at least in part, to an influence on ROCK signalling.

Figure 4.1 The effect of ROCK inhibitor treatment on endothelial permeability

To examine the effect of ROCK inhibition on HMEC-1 endothelial permeability, HMEC-1 endothelial cells were (1) seeded into transendothelial migration inserts and allowed to form a confluent monolayer, (2) treated with either Y-27632, H-1152 or left untreated, (3) incubated with fluorescent dextran and (4) the amount of fluorescent dextran movement from the top to bottom chamber measured. Results are expressed as a relative % of untreated control. Data represents the mean of at least three independent experiments \pm SEM (error bars).

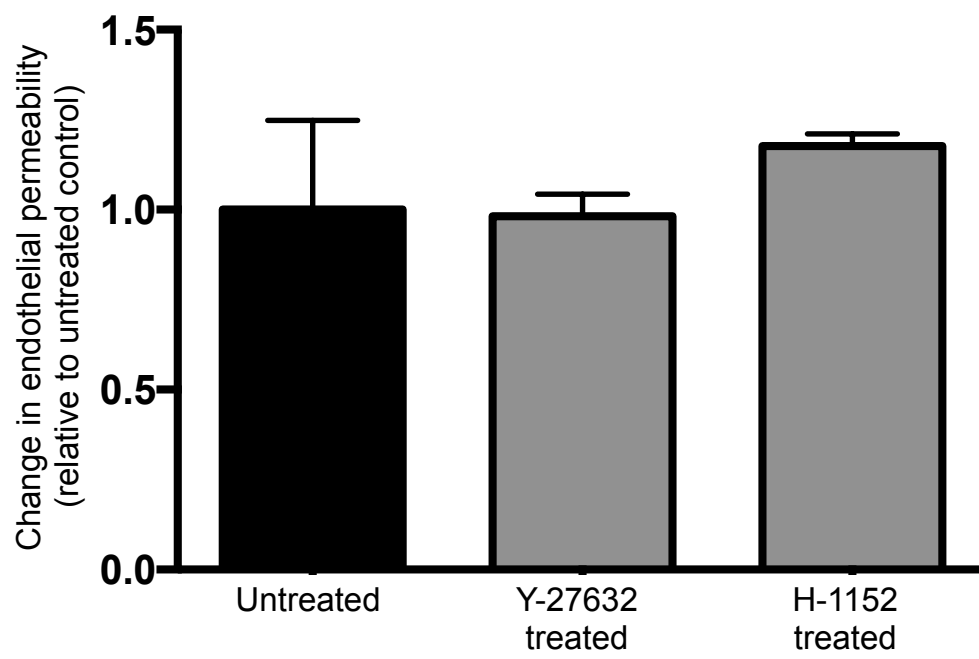
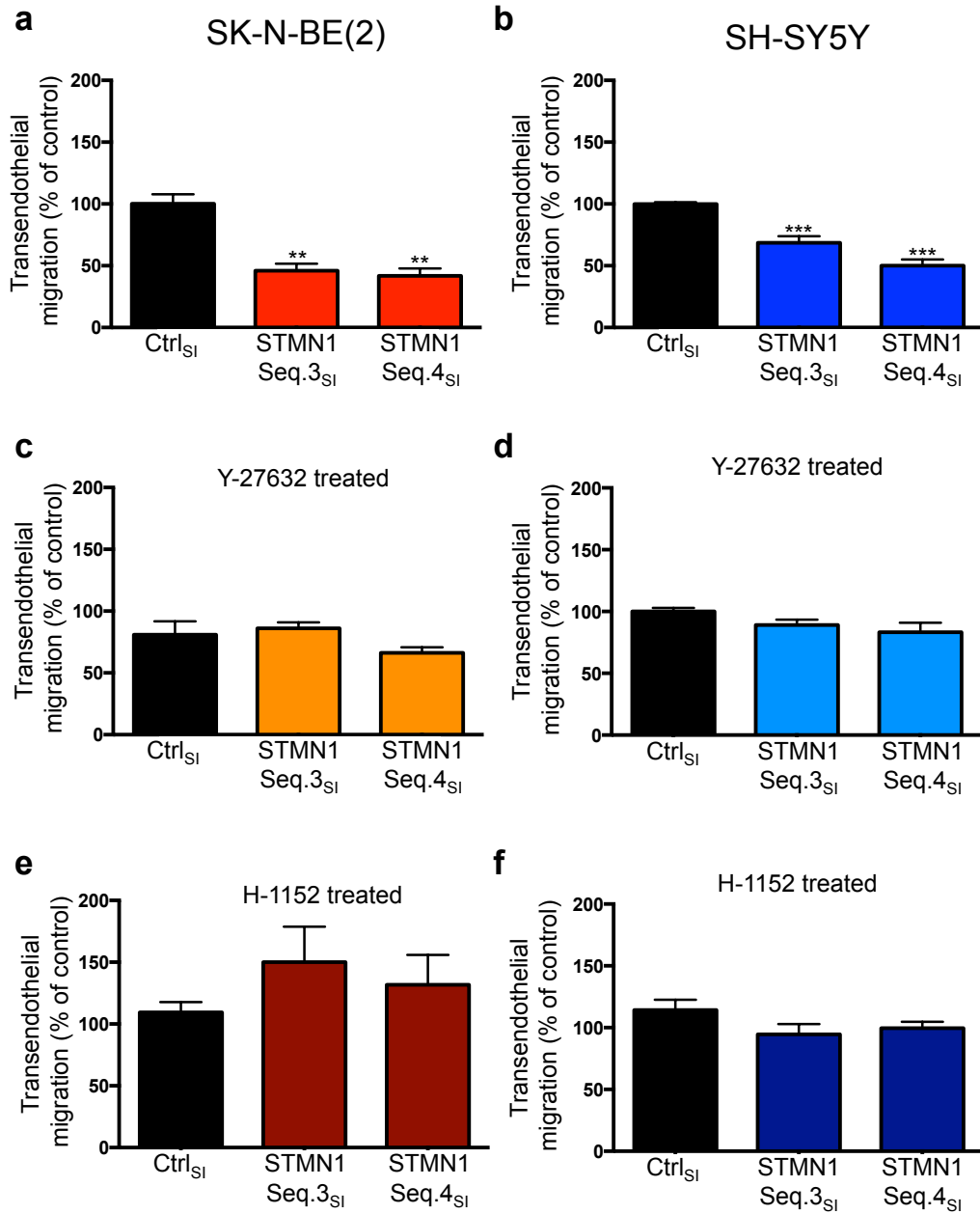


Figure 4.2 Stathmin suppression-induced reduction of cell transendothelial migration is reversed by ROCK inhibition

The effect of ROCK signalling on stathmin suppression-induced transendothelial migration was evaluated in SK-N-BE(2) and SH-SY5Y cells using the ROCK inhibitors, Y-27632 or H-1152. For comparative purposes, panels a and b are reproduced from Fig. 3.12c,d as these are the non-ROCK inhibitor treated samples. Transendothelial migration assays for untreated and ROCK inhibitor-treated samples were performed at the same time. STMN1 Seq.3_{SI}, STMN1 Seq.4_{SI} and Ctrl_{SI} siRNA-transfected SK-N-BE(2) cells were left untreated (**a**) or treated with 10 μ mol/L Y-27632 (**c**) or H-1152 (**e**) and subjected to chemotactic transendothelial migration assays. Transendothelial migration assays were also performed on siRNA-transfected SH-SY5Y cells in untreated (**b**), Y-27632 (**d**) and H-1152 (**f**) treated conditions. Results are expressed as a percentage of untreated Ctrl_{SI} cells (% of control). Data represents the mean of at least 4 independent experiments \pm SEM (error bars). ** p<0.005, ***p<0.0005.



4.3 Stathmin does not influence Rac1 activation

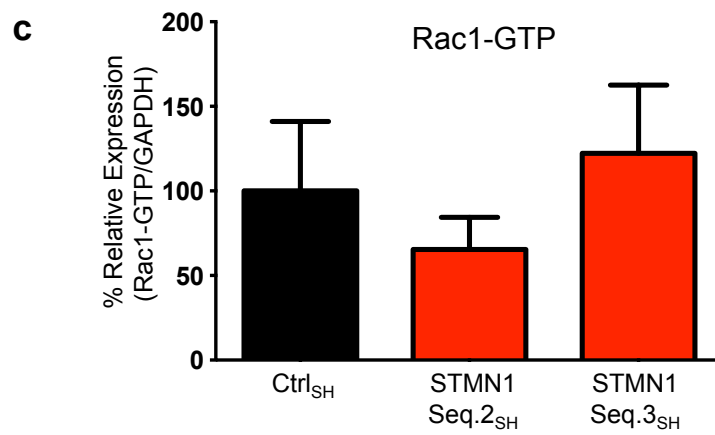
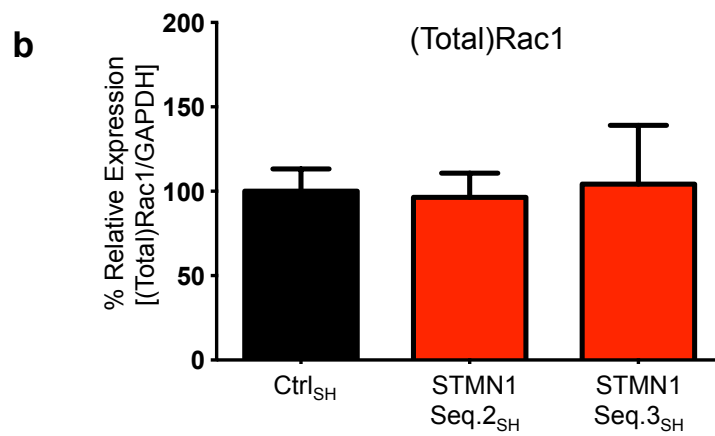
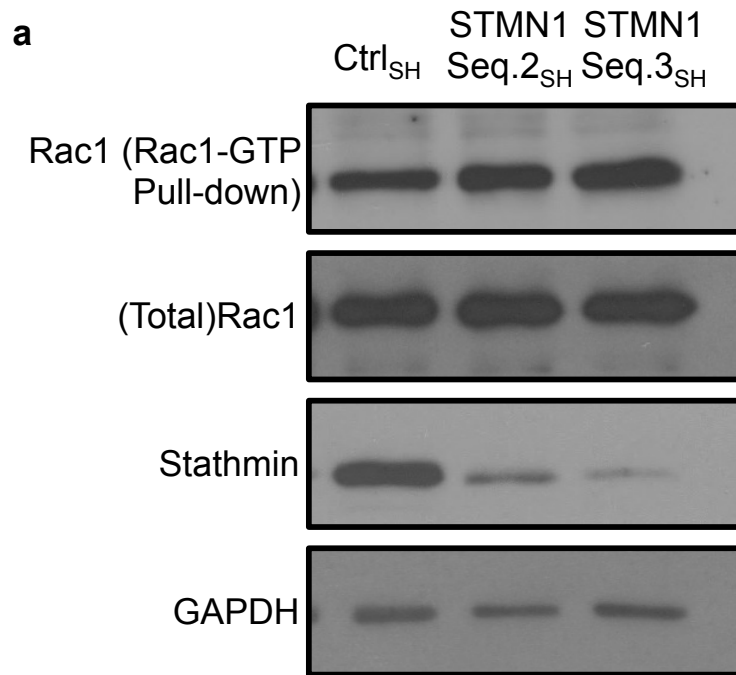
In order to understand the potential mechanisms by which stathmin is influencing neuroblastoma cell transendothelial migration, we examined the Rho GTPases RhoA, Rac1 and Cdc42 in stathmin suppressed SK-N-BE(2)/TGL cells.

Broadly speaking, Rac1 reorganises the actin cytoskeleton to promote the formation of large membrane protrusions, called lamellipodia, that drive motility in many cell types [reviewed in (Hall 2012)]. To determine if stathmin had a role in the regulation of Rac1 in neuroblastoma, total Rac1 levels and Rac1 activation (Rac1-GTP) levels were assessed (as described in Chapter 2, Section 2.14). SK-N-BE(2)/TGL cells were grown and serum-starved prior to harvesting. Protein lysates were harvested and total Rac1 levels assessed by western blotting. Analysis of total Rac1 levels by western blotting showed that stathmin suppression did not markedly influence total Rac1 levels compared to control in SK-N-BE(2)/TGL cells (Figure 4.3a). To quantify this, densitometry was performed on the western blots and showed that stathmin suppression did not significantly alter total Rac1 levels compared to controls (Figure 4.3b).

To determine stathmin's influence on Rac1 activation, a pull-down experiment was performed. The Rac1 pull-down activation assay utilizes the Rac1 effector protein, p21 activated kinase I (PAK)'s interactive binding region (also called the p21 Binding Domain, PBD). The PBD protein motif has been shown to bind specifically to the GTP-bound form of Rac1 protein (Burbelo, Drechsel et al. 1995). The PBD region of PAK is an ideal tool for affinity purification of GTP-Rac1 from cell lysates as PAK has a high affinity for GTP-Rac1 and that PAK binding significantly reduces intrinsic and catalytic rate of Rac1 hydrolysis

Figure 4.3 Stathmin suppression does not markedly influence total Rac1 or Rac1 activation levels

To determine stathmin's role in the regulation of Rac1 in neuroblastoma, total Rac1 levels and Rac1 activation (Rac-GTP) levels were assessed. Ctrl_{SH}, STMN1 Seq.2_{SH} and STMN1 Seq.3_{SH} SK-N-BE(2)/TGL cells were grown and serum-starved prior to harvesting. Protein lysates were harvested and total Rac1 levels assessed by western blotting. Rac1 activation levels were assessed using a Rac1 activation assay pulldown experiment followed by western blotting for Rac1. Additionally, western blotting assessed stathmin and GAPDH levels. **(a)** A representative western blot has been selected and is shown from at least 4 independent experiments. **(b) and (c)** corresponding western blot densitometry quantitation of total Rac1 and active Rac1 levels, **respectively**. Data represents the mean of at least 4 independent experiments \pm SEM (error bars).



(Zhang, Chernoff et al. 1998). This assay utilizes PAK-PBD in the form of a GST fusion protein whereby the PAK-PBD/GTP-Rac1 complex can be ‘pulled-down’ with glutathione affinity beads to provide a simple means of quantifying Rac1 activation in cells. Subsequently, the amount of activated Rac1 can be determined by western blotting using a Rac1 specific antibody. The active Rac1 pulldown assay and subsequent western blotting for Rac1 was performed on control and stathmin-suppressed SK-N-BE(2)/TGL cells and it showed that stathmin suppression does not markedly alter Rac1 activation compared to controls (Figure 4.3a). Quantitation of western blots showed that stathmin suppression did not significantly alter Rac1 activation compared to controls (Figure 4.3c). Altogether, these results indicate that stathmin is not likely playing a role in the regulation of Rac1 signalling in neuroblastoma.

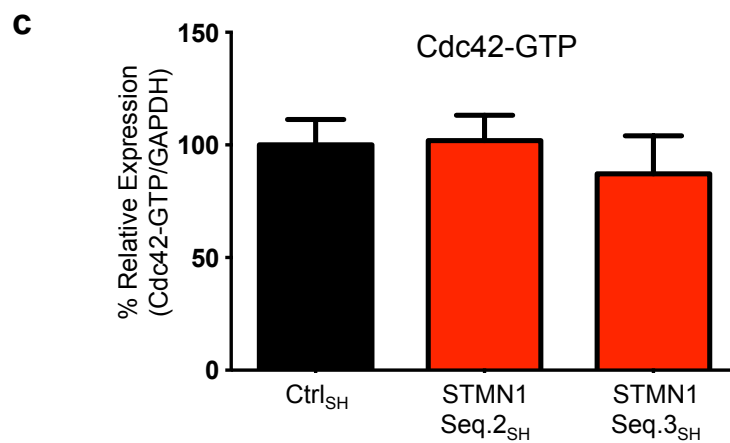
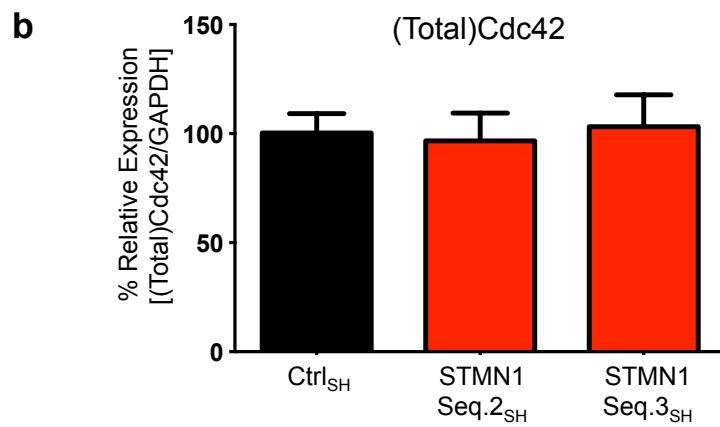
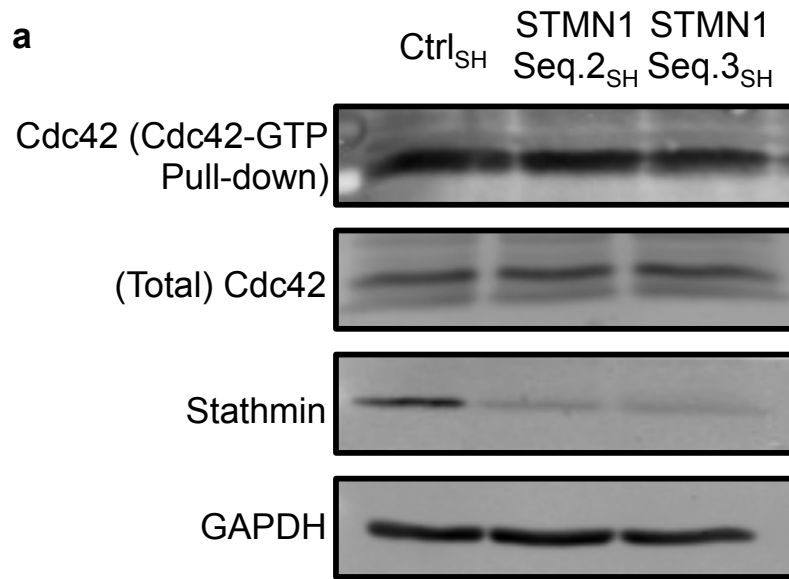
4.4 Stathmin does not influence Cdc42 activation

Another well-studied Rho GTPase that plays crucial roles in the regulation of the cytoskeleton during cell migration is Cdc42. Cdc42 regulates both the actin network and microtubule system where Cdc42 signalling promotes the formation of actin-rich microspikes to sense extracellular gradients and initiate directed cell movement [reviewed in (Hall 2012)]. Cdc42 signalling has been shown to influence the downstream effector proteins cofilin and MLC; both of which our laboratory has previously identified as possessing altered phosphorylation levels in stathmin suppressed cells compared to controls (Byrne, Yang et al. 2014).

To determine stathmin’s role in the regulation of Cdc42 in neuroblastoma, total Cdc42 levels and Cdc42 activation (Cdc42-GTP) levels were assessed. Ctrl_{SH}, STMN1 Seq.2_{SH} and

Figure 4.4 Stathmin suppression does not markedly influence total Cdc42 or Cdc42 activation levels

To determine stathmin's role in the regulation of Cdc42 signalling in neuroblastoma, total Cdc42 levels and Cdc42 activation (Cdc42-GTP) levels were assessed. Ctrl_{SH}, STMN1 Seq.2_{SH} and STMN1 Seq.3_{SH} SK-N-BE(2)/TGL cells were grown and serum-starved prior to harvesting. Protein lysates were harvested and total Cdc42 levels assessed by western blotting. Cdc42 activation levels were assessed using a Cdc42 activation assay pulldown experiment followed by western blotting for Cdc42. Additionally, western blotting assessed stathmin and GAPDH levels. **(a)** A representative western blot has been selected and is shown from at least 4 independent experiments. **(b) and (c)** corresponding western blot densitometry quantitation of total Cdc42 and active Cdc42 levels, **respectively**. Data represents the mean of at least 4 independent experiments \pm SEM (error bars).



STMN1 Seq.3^{SH} SK-N-BE(2)/TGL cells were grown and serum-starved prior to protein lysate harvesting. Western blotting and corresponding densitometry quantitation showed that stathmin suppression did not influence total Cdc42 levels compared to controls in SK-N-BE(2)/TGL cells (Figure 4.4a,b).

To determine stathmin's influence on Cdc42 activation, a pull-down experiment similar to that performed to analyse Rac1 activation was performed using the PBD of PAK to pull-down active Cdc42 (see Section 4.4). The active Cdc42 pull-down assay and subsequent western blotting for Cdc42 was performed on control and stathmin-suppressed SK-N-BE(2)/TGL cells and it showed that stathmin suppression does not markedly alter Cdc42 activation compared to controls (Fig. 4.4a). This was confirmed by densitometry of western blots (Fig. 4.4c). Altogether, these results indicate that stathmin is not likely playing a role in the regulation of Cdc42 signalling in neuroblastoma.

4.5 Stathmin suppression increases RhoA activation

A key Rho GTPase that plays vital roles in the regulation of the cytoskeleton and cell migration and invasion is RhoA. RhoA signalling regulates the phosphorylation of various cytoskeletal-remodelling proteins to promote actin stress fibre formation and the generation of contractile force [reviewed in (Hall 2012)]. RhoA performs these functions largely through activation of the downstream protein ROCK (also known as Rho-associated coiled-coil forming protein kinase, or Rho kinase) where ROCK can influence downstream phosphorylation, and hence activity, of the actin severing protein cofilin and the actin stress fibre contractility protein MLC [reviewed in (Hall 2012)]. Importantly, our laboratory has collectively shown, through results previously published and those presented in this thesis, that stathmin's influence on neuroblastoma cell invasion and transendothelial migration is, at

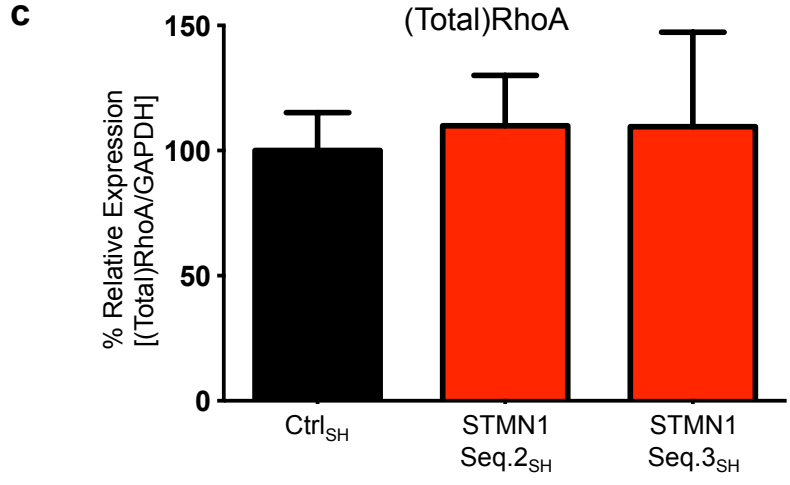
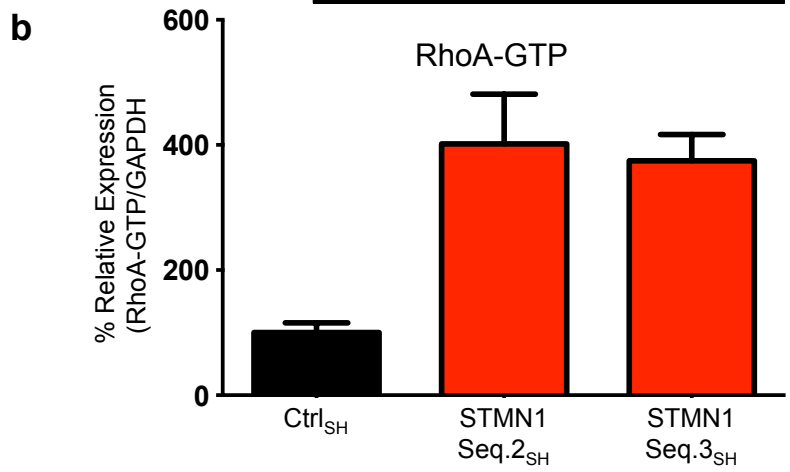
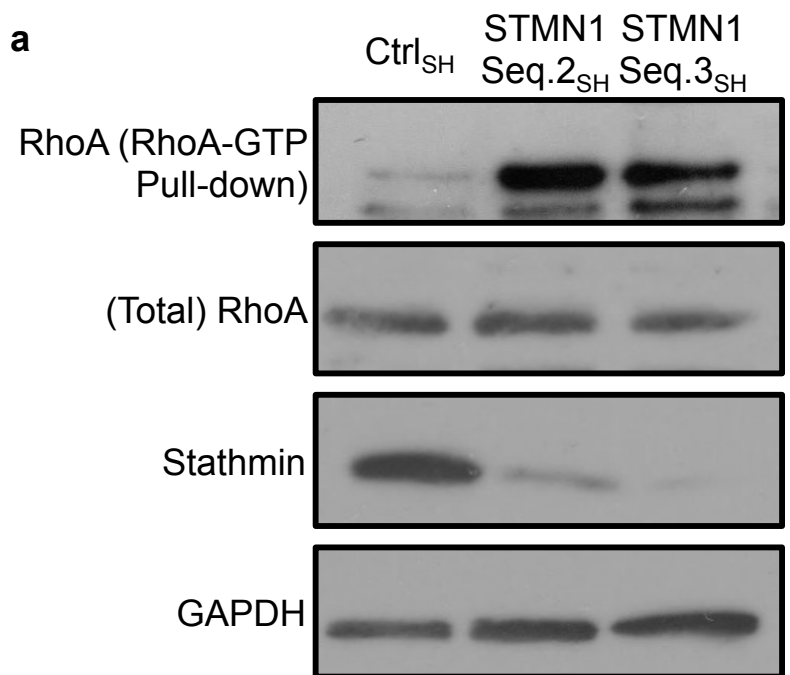
least in part, via regulation of ROCK signalling. Additionally, stathmin suppressed neuroblastoma cells exhibit altered phosphorylation, and hence likely altered activity, of both the RhoA/ROCK signalling pathway downstream effector proteins cofilin and MLC (Byrne, Yang et al. 2014).

To determine if stathmin influences RhoA regulation in neuroblastoma, total RhoA levels and RhoA activation (RhoA-GTP) levels were assessed. Ctrl_{SH}, STMN1 Seq.2_{SH} and STMN1 Seq.3_{SH} SK-N-BE(2)/TGL cells were grown, subsequently serum starved and protein lysates harvested. Western blotting analysis highlighted that stathmin suppression, with either of the independent shRNA sequences STMN1 Seq.2_{SH} or STMN1 Seq.3_{SH}, did not alter total RhoA levels compared to controls in SK-N-BE(2)/TGL cells (Figure 4.5a). To quantify this, western blotting densitometry showed that stathmin suppression did not significantly alter total RhoA levels compared to controls (Figure 4.5b).

Whilst it is evident that stathmin does not influence total RhoA protein levels in neuroblastoma, this does not preclude stathmin from influencing RhoA-GTP levels and hence RhoA activation in neuroblastoma. To determine if stathmin suppression influences RhoA activation, a pull-down experiment similar to that performed to analyse both Rac1 and Cdc42 activation was performed (see Chapter 4, Section 4.3-4.4; Chapter 2, Section 2.14). The RhoA activation pull-down assay possesses a few notable differences such as the use of the RhoA binding domain (also called the RBD) of the RhoA effector protein, rhotekin to specifically bind to the GTP-bound form of RhoA. The amount of activated RhoA is determined by western blotting using a RhoA specific antibody. The active RhoA pull-down assay and subsequent western blotting for RhoA was performed on control and stathmin

Figure 4.5 Stathmin suppression increases RhoA activation

To determine stathmin's role in the regulation of RhoA signalling in neuroblastoma, total RhoA levels and RhoA activation (RhoA-GTP) levels were assessed. Ctrl_{SH}, STMN1 Seq.2_{SH} and STMN1 Seq.3_{SH} SK-N-BE(2)/TGL cells were grown and serum-starved prior to harvesting. Protein lysates were harvested and total RhoA levels assessed by western blotting. RhoA activation levels were assessed using a RhoA activation assay pulldown experiment followed by western blotting for RhoA. Additionally, western blotting assessed stathmin and GAPDH levels. **(a)** A representative western blot has been selected and is shown from at least 4 independent experiments. **(b)** and **(c)** corresponding western blot densitometry quantitation of total RhoA and active RhoA levels, **respectively**. Data represents the mean of at least 4 independent experiments \pm SEM (error bars).



suppressed SK-N-BE(2)/TGL cells and it showed a marked increase in RhoA-GTP levels in stathmin suppressed cells, both STMN1 Seq.2_{SH} and STMN1 Seq.3_{SH}, compared to controls (Figure 4.5). Western blotting densitometry and quantitation showed that stathmin suppression significantly increased RhoA activation compared to controls (3.0 fold, $p < 0.01$; and 2.7 fold, $p < 0.001$ for STMN1 Seq.2_{SH} and STMN1 Seq.3_{SH} respectively (Figure 4.5c). This demonstrates that stathmin is likely playing a key role either directly or indirectly, in the regulation of RhoA activation and hence RhoA signalling in neuroblastoma. Furthermore, this highlights that stathmin's influence on neuroblastoma cell invasion and transendothelial migration may indeed be upstream of ROCK by affecting the activation of the upstream Rho GTPase RhoA. This data provides the first evidence that stathmin suppression can influence ROCK signalling via activation of RhoA in neuroblastoma cells.

4.6 Stathmin does not influence guanine nucleotide exchange factor H1 microtubule association

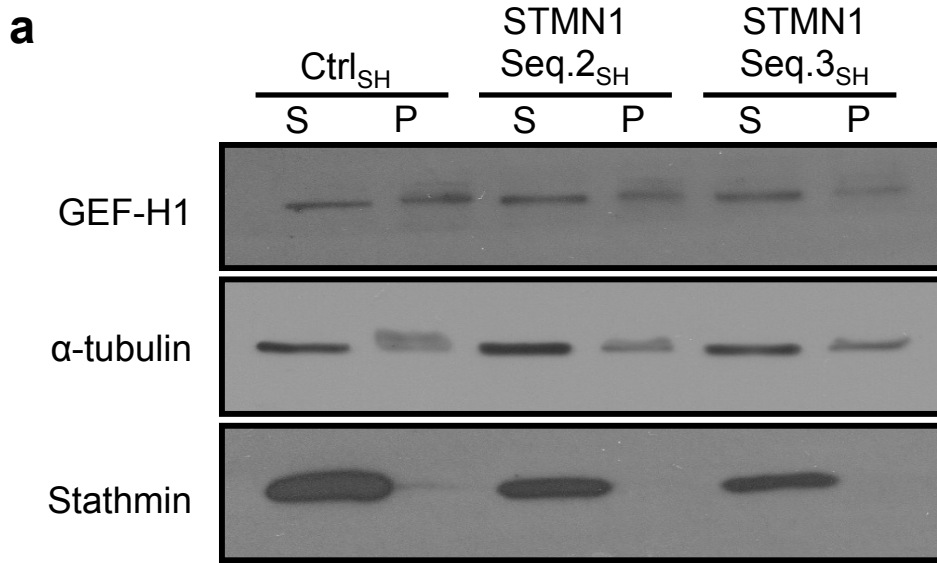
In order to examine how stathmin is influencing RhoA activation the guanine nucleotide exchange factor H1 (GEF-H1) was selected for analysis due to its important connection to microtubule dynamics. GEF-H1 is able to bind microtubules and it is in this microtubule-bound state that the guanine nucleotide exchange activity of GEF-H1 is suppressed. Upon microtubule disruption GEF-H1 is released from microtubules resulting in stimulation of RhoA activation (Krendel, Zenke et al. 2002). It has been shown that microtubule disassembly induced by thrombin, TNF- α or nocodazole led to the GEF-H1-dependent activation of RhoA signalling resulting in subsequent stress-fibre mediated cell contraction (Birukova, Adyshev et al. 2006, Chang, Nalbant et al. 2008, Kakiashvili, Speight et al. 2009).

Therefore, it is possible that stathmin's function as a microtubule destabilising protein may be influencing RhoA activation in neuroblastoma via affecting GEF-H1 microtubule binding.

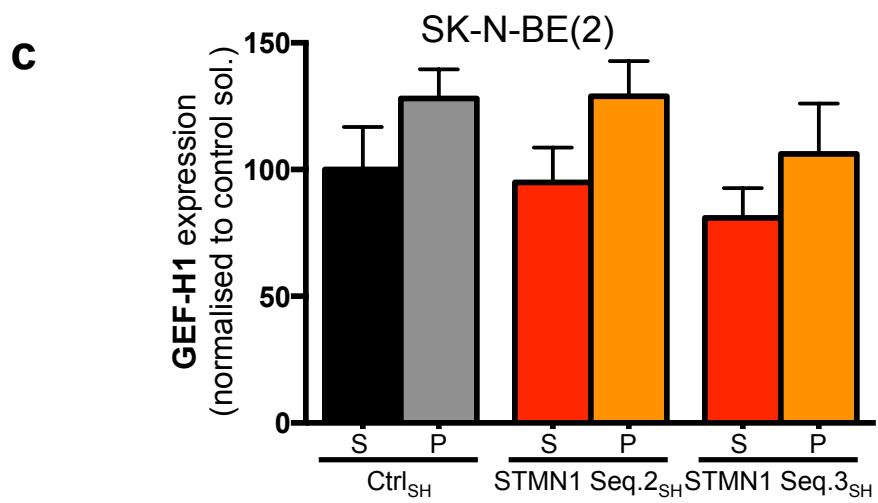
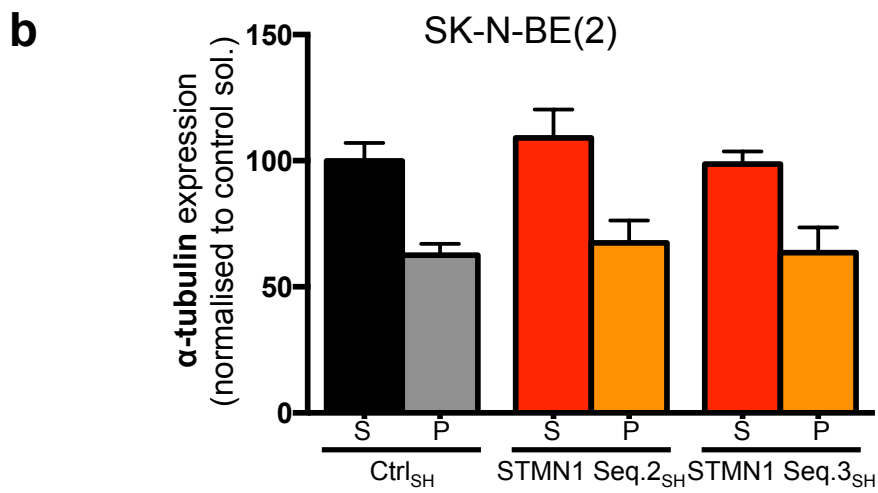
To examine stathmin's influence on GEF-H1 microtubule binding, a tubulin polymerisation assay was performed, where the polymerised and soluble tubulin fraction was isolated separately and the amount of particular proteins (in this case GEF-H1) analysed by western blotting to determine whether there exists any change in the association of GEF-H1 with microtubules (see Chapter 2, Section 2.13). Western blotting and corresponding densitometry quantitation showed that stathmin suppression did not influence tubulin polymer levels compared to control cells (Fig. 4.6a,b). In the soluble tubulin fraction, stathmin suppression does not appear to alter GEF-H1 levels (Fig.4.6a,c). It is evident that there is a small decrease in GEF-H1 in the polymerised tubulin fraction of STMN1 Seq.3_{SH} cells compared to Ctrl_{SH} and STMN1 Seq.2_{SH} (Fig. 4.6). However, in corresponding western blot densitometry quantitation of the eight separate experiments, the amount of GEF-H1 in the polymerised tubulin fractions does not significantly change (Fig. 4.6c). Altogether, these results indicate that stathmin is not likely playing a role in GEF-H1 microtubule association. Therefore, stathmin's influence on RhoA activation is likely not due to alterations in the association of microtubules and GEF-H1.

Figure 4.6 Stathmin does not influence GEF-H1 microtubule association

To examine stathmin's influence on GEF-H1 microtubule binding, a tubulin polymerisation assay was performed. Ctrl_{SH}, STMN1 Seq.2_{SH} and STMN1 Seq.3_{SH} SK-N-BE(2)/TGL cells were grown and serum-starved prior to harvesting. Protein lysates were harvested using a hypotonic buffer where subsequent centrifugation of the resulting protein lysate led to separation into 2 fractions: a soluble tubulin fraction (denoted as "S") and a polymerised tubulin fraction (denoted as "P"). **(a)** GEF-H1, α -tubulin and stathmin levels were measured using western blotting. A representative western blot has been selected and is shown from at least 8 independent experiments. **(b)** Corresponding western blotting quantitation of α -tubulin levels in Ctrl and stathmin suppressed cells. **(c)** Corresponding western blot densitometry quantitation of GEF-H1 levels in Ctrl and stathmin suppressed cells. Data represents the mean \pm SEM (error bars) of 8 independent experiments.



Note: **S** denotes **soluble** tubulin fraction; **P** denotes **polymerised** tubulin fraction



4.7 Stathmin's influence on cell migration is independent of its tubulin-binding ability

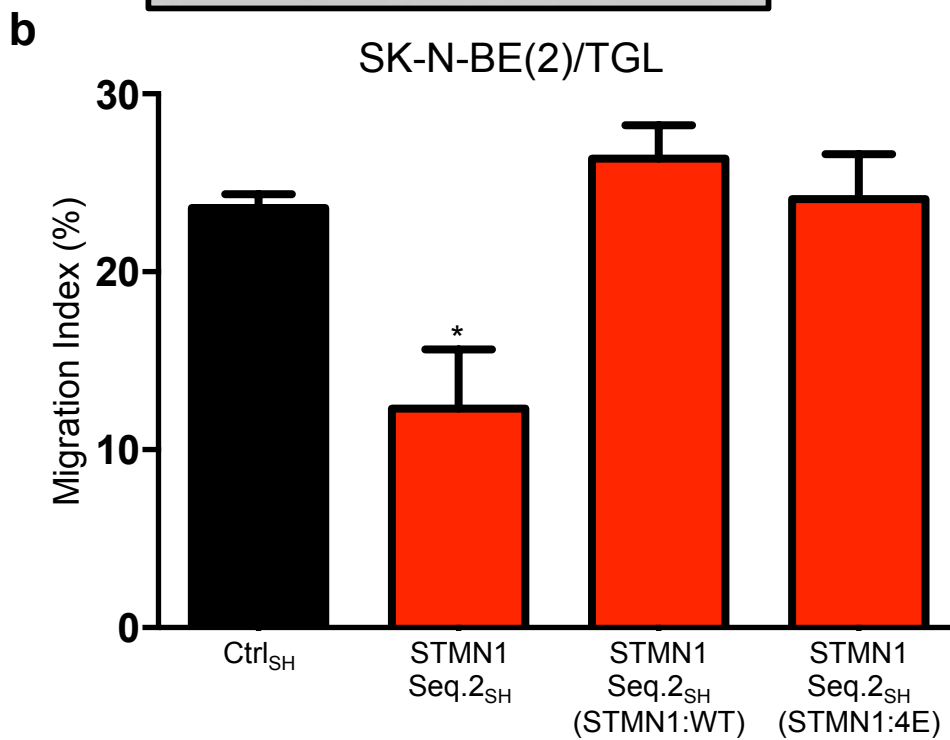
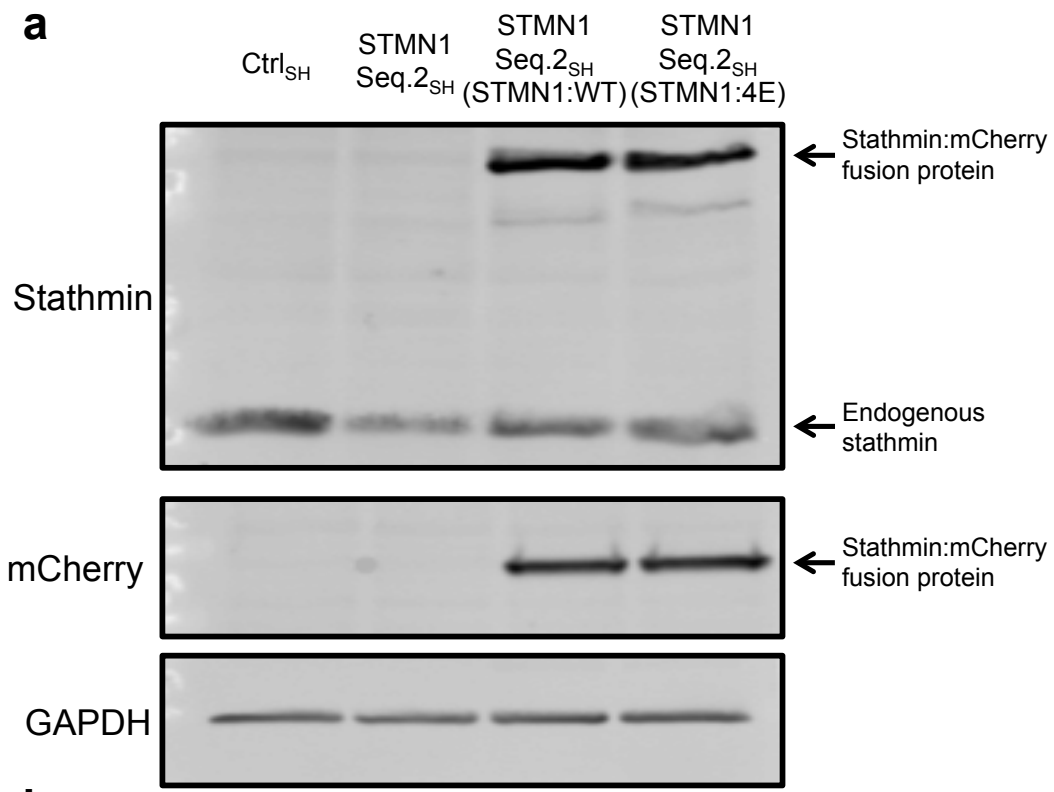
This thesis highlights that stathmin is important in multiple key steps of the metastatic cascade in neuroblastoma and that stathmin is mediating its role, at least in part, via its effects on RhoA activation and RhoA signalling downstream effector proteins. However, it is unknown at this stage whether stathmin's effect on these phenotypes is dependent or independent of its tubulin-binding ability. Investigation of the above matter requires an appreciation of how stathmin interacts with tubulin and microtubules. Stathmin's tubulin-binding affinity is controlled by phosphorylation on four serine residues (Steinmetz 2007). Phosphorylation of each site generates a grade of tubulin-binding affinity where complete phosphorylation leads to complete inactivation of stathmin's tubulin binding affinity [reviewed in (Steinmetz 2007)]. It is unknown whether altered stathmin phosphorylation, and hence impaired stathmin tubulin-binding affinity, influences stathmin's effects on cell migration.

To investigate whether stathmin was influencing neuroblastoma cell migration in a microtubule dependent or independent manner a 4E:stathmin mutant was employed. The 4E:stathmin mutant has impaired tubulin binding and is effectively considered inactive (Amayed, Pantaloni et al. 2002, Niethammer, Bastiaens et al. 2004). To determine if restoring stathmin expression with either a wild-type or 4E:stathmin mutant construct in the stathmin-suppressed cells will return cell migration back to controls, SK-N-BE(2)/TGL STMN1 Seq.2_{SH} cells were stably transfected separately with two constructs; containing either a wild-type stathmin or the 4E:stathmin mutant [hereafter referred to as STMN1 Seq.2_{SH} (STMN1:WT) and STMN1 Seq.2_{SH} (STMN1:4E) respectively]. Both constructs contained a

geneticin antibiotic resistance gene for antibiotic selection and both the wild-type stathmin and 4E:stathmin mutant proteins were fused with mCherry for FACS processing. Utilising both geneticin antibiotic treatment and subsequent FACS for selection of high mCherry expressing cells allowed the generation of stable cell populations. Once stable cell populations were generated they were assessed for expression of the relevant mCherry:stathmin fusion protein. STMN1 Seq.2_{SH} (STMN1:WT) and STMN1 Seq.2_{SH} (STMN1:4E) both expressed mCherry protein at the expected fusion protein size (~50 kDa) and the stathmin fusion protein (~50 kDa) and maintained endogenous stathmin suppression similar to STMN1 Seq.2_{SH} and distinct from STMN1 Ctrl_{SH} (Fig. 4.7a). Each cell population was subjected to chemotactic-induced cell migration assays (see Section 2.8). As previously found, stathmin suppression significantly reduced the migratory ability of SK-N-BE(2)/TGL cells compared to controls (migration index of 23.6±0.77%; 12.3±3.34%, p<0.05 for Ctrl_{SH} and STMN1 Seq.2_{SH} respectively) (Fig. 4.7b). Importantly, expression of the wild-type stathmin protein returned the migration index back to controls [migration index of 23.6±0.77%; 26.4±1.88%, p=0.25 for Ctrl_{SH} and STMN1 Seq.2_{SH} (STMN1:WT) respectively] indicating that ectopic stathmin expression is functioning similarly to endogenous stathmin in respect to cell migration. This result provides the first evidence that stathmin is having a direct influence on cell migration in neuroblastoma where restoration of stathmin levels returned migration levels back to controls. Interestingly, expression of the 4E:stathmin mutant also returned the migration index back to controls [migration index of 23.6±0.77%; 24.1±2.53%, p=0.86 for Ctrl_{SH} and STMN1 Seq.2_{SH} (STMN1:4E) respectively] (Fig. 4.7b). This finding provides for the first time direct evidence that stathmin's role in neuroblastoma cell migration is independent of its tubulin-binding ability.

Figure 4.7 Stathmin's influence on cell migration is independent of its tubulin-binding ability

To determine if stathmin was influencing neuroblastoma cell migration in a microtubule dependent or independent manner SK-N-BE(2)/TGL STMN1 Seq.2_{SH} cells were stably transfected separately with vectors expressing either a wild-type stathmin protein or a pseudophosphorylated 4E stathmin mutant fused to mCherry [designated as STMN1 Seq.2_{SH} (STMN1:WT) and STMN1 Seq.2_{SH} (STMN1:4E) respectively]. Ctrl_{SH}, STMN1 Seq.2_{SH} and the above mentioned vector transfected cells were assessed for expression of the mCherry and stathmin fusion protein, endogenous stathmin and the loading control GAPDH **(a)** A representative western blot of stathmin, mCherry and GAPDH protein expression. **(b)** Chemotactic-induced migration of Ctrl_{SH}, STMN1 Seq.2_{SH}, STMN1 Seq.2_{SH} (STMN1:WT) and STMN1 Seq.2_{SH} (STMN1:4E). Data displayed as a migration index, which is the percentage of total cells that successfully migrate from the top to the bottom chamber. Migration index = [(number of cells on under surface of membrane divided by the total number of cell on both surfaces of the membrane) *100]. Data represents the mean of three independent experiments ±SEM (error bars). * p<0.05.



4.8 Discussion

Results from this thesis have demonstrated an important role for stathmin during multiple steps of the metastatic cascade in neuroblastoma. However, the precise cell signalling pathways regulating stathmin's influence on neuroblastoma metastasis are not well understood. In this chapter, stathmin has been shown to influence tumour cell transendothelial migration via regulation of the Rho GTPase RhoA and subsequent ROCK signalling and that these effects are independent of stathmin's tubulin-binding ability.

Tumour cell movement across the vasculature from the bloodstream into secondary tissue sites (a process known as transendothelial migration) is important during haematogenous metastatic spread of disease. Results from this thesis highlighted a key role for stathmin during transendothelial migration in neuroblastoma (see Section 3.8). Previous published findings from our laboratory revealed that stathmin's influence on tumour cell migration in neuroblastoma was, at least in part, via regulation of ROCK and downstream effector proteins cofilin and MLC (Byrne, Yang et al. 2014). This finding drove interest into whether stathmin was influencing tumour cell transendothelial migration in a similar manner. Importantly, results from this chapter reveal that the treatment of stathmin suppressed neuroblastoma cells with two independent pharmacological ROCK inhibitors returned transendothelial migration levels back to Ctrl_{SI}-treated cells indicating that stathmin mediates its influence on transendothelial migration in neuroblastoma cells in a similar manner to cell migration via the regulation of ROCK signalling (Fig. 4.2).

Identification that stathmin may be influencing tumour cell metastasis in neuroblastoma via regulation of ROCK and downstream effector proteins cofilin and MLC raised curiosity as to how stathmin was influencing these signalling events. All three Rho GTPases RhoA, Rac1 and Cdc42 control regulation of cofilin and MLC activity, whereas ROCK activation is

predominantly controlled via the regulation of RhoA [reviewed in (Hall 2012)]. Whilst RhoA principally controls direct ROCK activation this does not preclude Rac1 or Cdc42 from influencing ROCK activation indirectly via affecting RhoA activation. Crosstalk between various Rho GTPases has been observed where the activation state of one or more Rho GTPases can influence the activation state of other Rho GTPases. Rac1 and Cdc42 activation have been shown to activate RhoA (Ridley, Paterson et al. 1992, Kozma, Ahmed et al. 1995, Nobes and Hall 1995). In contrast Sander et al, observed that activation of Rac1 and Cdc42 antagonises RhoA activation to consequently determine cellular morphology and migratory behaviour (Sander, ten Klooster et al. 1999).

This chapter revealed that stathmin suppression does not influence total or active protein levels of Rac1 or Cdc42 in neuroblastoma cells (Figs. 4.3-4.4) indicating that stathmin's influence of ROCK, cofilin and MLC signalling in neuroblastoma cells is not via regulation of Rac1 or Cdc42 activation. This above finding is congruous with evidence in this thesis that stathmin does not influence anoikis in neuroblastoma (see Section 3.7) as Rac1 and Cdc42 have been shown to be key regulators of anoikis (Cheng, Symons et al. 2004). Importantly, stathmin suppression resulted in a marked increase in RhoA activation levels in neuroblastoma cells indicating that stathmin's influence of ROCK, cofilin and MLC is via its regulation of RhoA activation (Fig. 4.5). Furthermore, this result suggests that elevated stathmin levels act to inhibit activation of RhoA signalling and influence associated downstream effector proteins to promote neuroblastoma cell migratory, invasive and metastatic behaviour. Moreover, these results indicate that stathmin suppression-mediated regulation of ROCK activation in neuroblastoma cells is not due to indirect effects from changes in Rac1 or Cdc42 activation but are due to direct effects from marked alterations in RhoA activation.

Traditional mesenchymal cell migration requiring both actin-driven protrusion at the front coordinated with actomyosin contractility at the rear has led to the hypothesis that multiple Rho family members are required in different subcellular locations to promote cell migration (Raftopoulou and Hall 2004). Several groups have developed novel biosensors capable of spatial and temporal visualisation of specific Rho GTPase activation (Yoshizaki, Ohba et al. 2003, Hodgson, Shen et al. 2010). This led to the observation that RhoA and Rac1 are both active at leading edge protrusions of migrating cells (Machacek, Hodgson et al. 2009). Niethammer et al., identified that stathmin is hyperphosphorylated in the lamellipodia of migrating cells indicating that stathmin is inactive in these regions (Niethammer, Bastiaens et al. 2004). This inactivation of stathmin may be responsible for the activation of RhoA at leading edge protrusions of migrating cells. Whilst Rac1 and Cdc42 activation levels were not altered in whole cell lysates of stathmin suppressed neuroblastoma cells (Figs. 4.3-4.4) this does not preclude that stathmin may play a role in the spatial or temporal alteration or restriction of either Rac1 or Cdc42 activation during cellular movement.

Understanding how stathmin is regulating RhoA activation is a complex affair where 23 Rho GEFs display specificity towards RhoA, with 10 of these displaying unique specificity [reviewed in (Rossman, Der et al. 2005)]. From the 23 GEFs exhibiting specificity towards RhoA, GEF-H1 was chosen for analysis, as its ability to activate RhoA is dependent on its ability to bind microtubules where microtubule disruption induced by thrombin, TNF- α or nocodazole treatment led to GEF-H1-dependent activation of RhoA (Krendel, Zenke et al. 2002, Birukova, Adyshev et al. 2006, Chang, Nalbant et al. 2008, Kakiashvili, Speight et al. 2009). Additionally, stathmin's influence on the microtubule network has been shown to regulate the release of GEF-H1 from microtubules and subsequently activate RhoA in thrombin-treated endothelial cells (Tian, Tian et al. 2012). Results from this chapter show

that suppression of the microtubule destabilising protein stathmin in neuroblastoma cells does not influence GEF-H1-microtubule association (Fig. 4.6) indicating that stathmin's influence on RhoA activation is not via alterations in GEF-H1-mediated RhoA activation. This result leaves open the possibility that stathmin may influence RhoA activation via regulation with other GEFs. Due to timing restrictions another GEF was not analysed though a suitable target for future examination may be the microtubule bound GEF p190RhoGEF (van Horck, Ahmadian et al. 2001).

Many activities attributed to stathmin are tied to its ability to modulate microtubule dynamics though stathmin has been observed to interact with a variety of proteins [reviewed in (Belletti and Baldassarre 2011)]. This led to the possibility that stathmin may be influencing cell migration in neuroblastoma cells in a microtubule independent manner. This was addressed by examining whether stathmin was influencing neuroblastoma cell migration in a microtubule dependent or independent manner, by ectopically restoring stathmin with either wild-type stathmin or 4E:stathmin mutant. The 4E:stathmin mutant, where all four serine phosphorylation sites have been mutated to glutamic acid residues acts as a pseudo-phosphorylated protein and has been variously reported to be either active or inactive, depending on whether an *in vitro* cell-based or cell-free, or *in vivo* assay system was used (Curmi, Andersen et al. 1997, Horwitz, Shen et al. 1997, Gavet, Ozon et al. 1998, Larsson, Segerman et al. 1999, Holmfeldt, Larsson et al. 2001, Amayed, Pantaloni et al. 2002, Niethammer, Bastiaens et al. 2004). Whilst glutamic acid substitution only partially recapitulates the effects of real phosphorylation it substantially reduces stathmin's affinity to tubulin where at low free-tubulin concentrations there is a 40-fold increase in K_D for 4E:stathmin compared to wild-type stathmin suggesting that stathmin is effectively considered inactive (Amayed, Pantaloni et al. 2002). Additionally, the findings published in

Science from Niethammer et al., using a 4E:stathmin FRET-based reporter strongly indicate that the 4E:stathmin mutant does not interact with tubulin (Niethammer, Bastiaens et al. 2004). Altogether the 4E:mutant has impaired tubulin binding and is effectively considered inactive. This allowed the determination of whether stathmin's influence on neuroblastoma cell migration is microtubule dependent or independent.

Results from this chapter demonstrated that ectopic restoration of stathmin levels with wild-type stathmin increased stathmin suppression-induced cell migration back to control levels (Fig. 4.7). This result provides the first evidence that stathmin has a direct effect on cell migration. Additionally, restoration of stathmin levels with the pseudophosphorylated 4E:stathmin mutant returned cell migration back to controls (Fig. 4.7). This provides the first evidence that stathmin is influencing the migratory phenotype in neuroblastoma cells independently of its tubulin-binding ability (Fig. 4.7). The evidence that stathmin interacts with multiple proteins involved in many different cellular processes in human cancer opens various potential avenues for how stathmin may be regulating cell migration in neuroblastoma cells. These proteins include NF- κ B, which is widely implicated in tumour cell survival, immunity, inflammation and cell proliferation (Lu, Liu et al. 2014, Vezina, Vaillancourt-Jean et al. 2014); the cell cycle regulatory protein p27^{Kip1} commonly downregulated in cancer which has emerged as a regulator of cell motility and RhoA activation (Besson, Gurian-West et al. 2004, Baldassarre, Belletti et al. 2005, Belletti, Nicoloso et al. 2005); the kinase interacting with stathmin (KIS) controls G1/S transition via p27^{Kip1} phosphorylation (Maucuer, Camonis et al. 1995, Boehm, Yoshimoto et al. 2002); the vesicular recycling protein TSG101 lost in human cancer (Herz and Bergmann 2009); the heat shock protein HSP70, which is involved in numerous facets of malignant progression (Manceau, Gavet et al. 1999, Calderwood, Khaleque et al. 2006) and the oncogene STAT3

which is involved in cell motility and is associated with decreased survival in multiple malignancies (Ng, Lin et al. 2006, Yu, Pardoll et al. 2009). Whether stathmin is able to interact with any of these or other cancer-relevant proteins and influence their activity to regulate the migratory, invasive and metastatic phenotype in neuroblastoma is unknown and is worthy of future investigation.

This chapter has examined key cell signalling pathways that may be involved in stathmin's influence on neuroblastoma metastasis. It is evident that stathmin's influence on transendothelial migration in neuroblastoma cells is, at least in part, via activation of RhoA. Stathmin's influence on RhoA activation is not mediated by GEF-H1-microtubule association though this does not preclude that stathmin may be mediating its effects via other Rho GEFs. Furthermore, stathmin's influence on the migratory phenotype in neuroblastoma cells is independent of its tubulin-binding ability suggesting that stathmin's influence on RhoA/ROCK signalling and cell migration in neuroblastoma cells may be via stathmin's interactions with other proteins.

Chapter 5.

5 Effect of stathmin on transendothelial migration

in vivo

5.1 Introduction

Metastasis is a complex process and to investigate whether stathmin was influencing transendothelial migration *in vivo*, a mouse model of metastasis is required. Xenograft models are extensively used in pre-clinical settings. The experimental metastasis xenograft model, where tumour cells are injected directly into the bloodstream and then are required to extravasate, invade, seed and grow in different tissues assesses survival of tumour cells in the bloodstream and extravasation *in vivo* (Van Sluis, Niers et al. 2009). Based on results from Chapters 3 and 4 demonstrating that stathmin is mediating *in vitro* transendothelial migration in neuroblastoma, the aim of this chapter was to determine whether stathmin regulates neuroblastoma cell extravasation *in vivo* using an experimental metastasis model of neuroblastoma.

5.2 Stathmin suppression reduced whole-body neuroblastoma metastatic tumour burden

To investigate and visualise the impact of stathmin suppression on tumour cell extravasation in an *in vivo* setting SK-N-BE(2)/TGL cells previously described by our laboratory were used. Prior to using the Ctrl_{SH}, STMN1 Seq.2_{SH} and STMN1 Seq.3_{SH} SK-N-BE(2)/TGL cells their luciferase expression levels were examined. The above-mentioned SK-N-BE(2)/TGL cells were plated into 96-well plates at 10,000 cells/well and serially diluted to 78 cells/well.

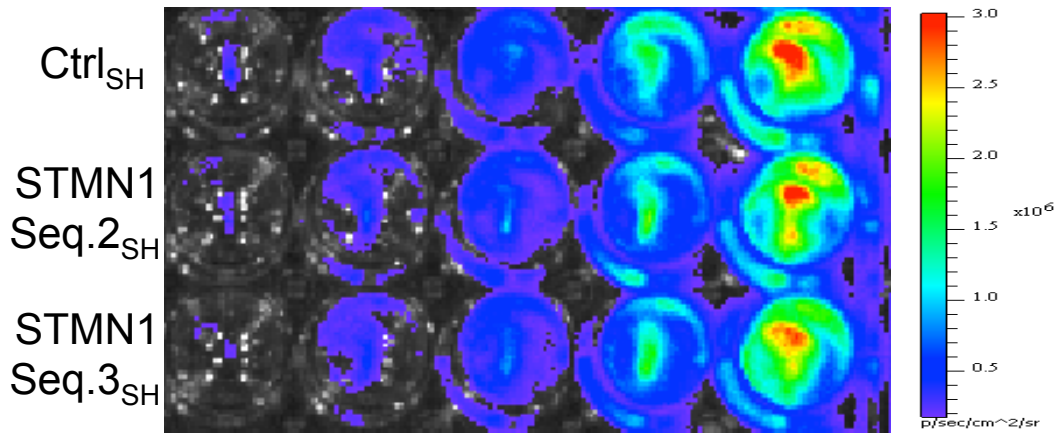
The luciferase substrate, D-luciferin was added to the cells and the resulting bioluminescent signal acquired using the Xenogen IVIS Imaging System. Bioluminescent imaging confirmed Ctrl_{SH}, STMN1 Seq.2_{SH} and STMN1 Seq.3_{SH} SK-N-BE(2)/TGL cells expressed equal amounts of luciferase (Fig. 5.1a-b) making them valuable for quantitative studies to understand the impact of stathmin on metastasis.

Having confirmed equal luciferase expression in the control and stathmin shRNA SK-N-BE(2)/TGL cells, mice were injected with Ctrl_{SH}, STMN1 Seq.2_{SH} and STMN1 Seq.3_{SH} SK-N-BE(2)/TGL cells and metastatic tumours allowed to form and grow over 23 days. Metastatic tumour burden from the whole-body was assessed by peritoneal injection with the luciferase substrate, D-luciferin, and then bioluminescent signal detected using the Xenogen IVIS Imaging System. Figure 5.2a displays representative pseudocolour bioluminescent images overlaid on photographic images of mice (ventrally oriented) and qualitative visualisation shows that stable stathmin suppression with either STMN1 Seq.2_{SH} or STMN1 Seq.3_{SH} reduced whole-body metastatic tumour burden compared to controls (Ctrl_{SH}). To quantify this observation, region of interests (ROIs) were drawn around each mouse and bioluminescent signal measured as total flux (photon/second). Importantly, quantitation of mouse whole-body bioluminescence showed significantly reduced neuroblastoma whole-body metastatic tumour burden compared to controls (Ctrl_{SH}) (STMN1 Seq.2_{SH}: $2.2 \times 10^9 \pm 5.68 \times 10^8$ photons/sec, $p < 0.005$; STMN1 Seq.3_{SH}: $3.6 \times 10^9 \pm 8.21 \times 10^8$ photons/sec, $p < 0.05$; Ctrl_{SH}: $1.9 \times 10^{10} \pm 5.71 \times 10^9$ photons/sec) (Figure 5.2b). Given the experimental metastasis model selectively assesses the extravasation step of cancer metastasis, this data, taken along with *in vitro* data (Fig 3.12c-d), supports a role for stathmin in extravasation in neuroblastoma *in vivo*.

Figure 5.1 shRNA-expressing SK-N-BE(2)/TGL cells express similar levels of luciferase.

To determine luciferase expression levels, Ctrl_{SH}, STMN1 Seq.2_{SH} and STMN1 Seq.3_{SH} SK-N-BE(2)/TGL cells were seeded into 96-well plates and serially diluted in two-fold steps from 10,000 to 78 cells/well. The luciferase substrate, D-luciferin, was incubated with the cells and subsequent bioluminescent signal measured using the Xenogen IVIS Imaging System. **(a)** A representative bioluminescent image of all three serially diluted cell populations is shown. The coloured scale bar displays the degree of bioluminescence emitted from the cells, as measured in photons/second/centimere squared/steradian (p/sec/cm²/sr). **(b)** Quantification of bioluminescent signal emitted from all three cell populations confirmed that each cell population expressed comparable levels of luciferase, measured as total flux (photons/second).

a



b

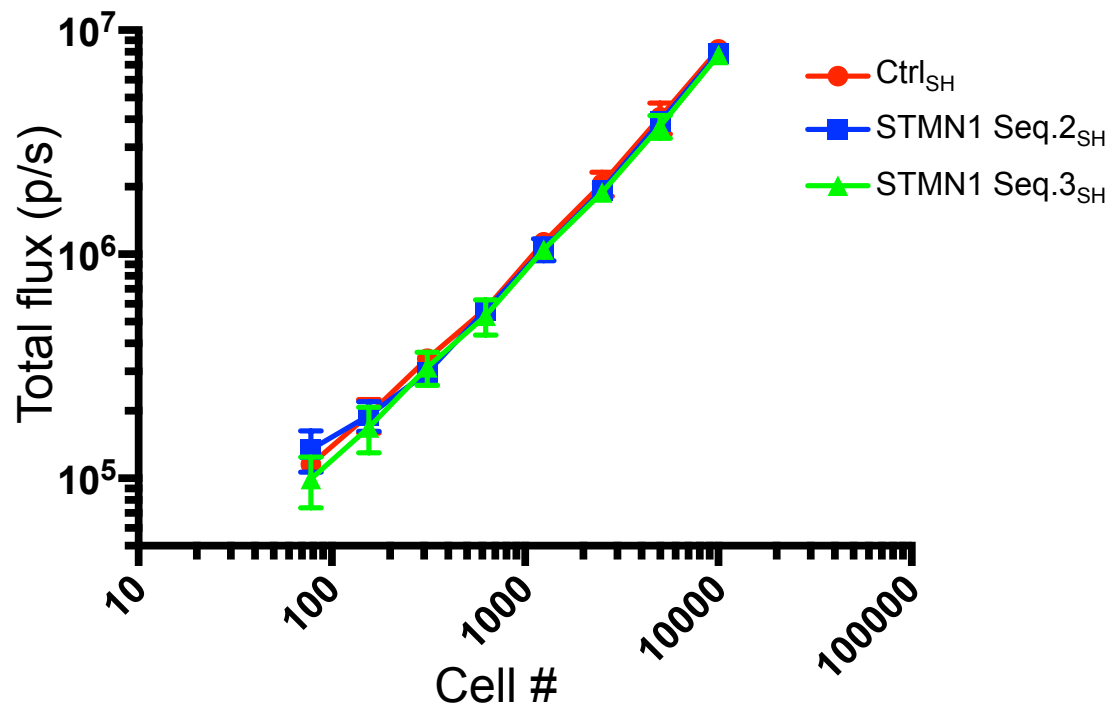
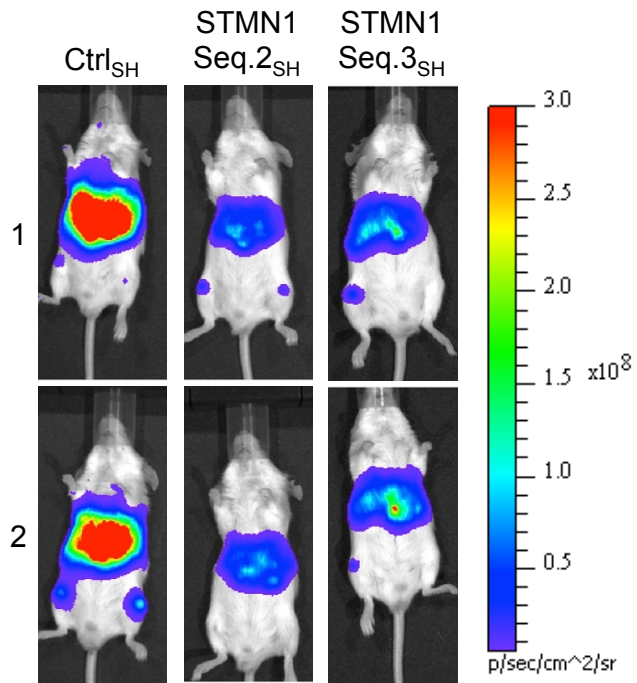


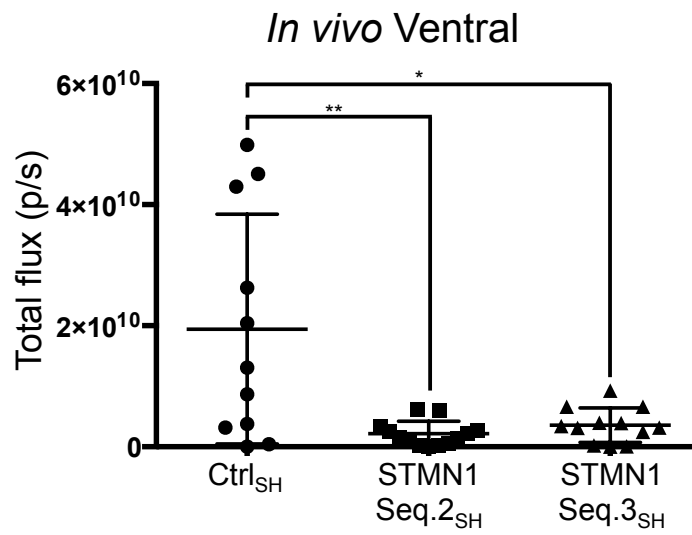
Figure 5.2 Stathmin suppression reduces neuroblastoma metastatic tumour burden in the whole-body of living mice by bioluminescent imaging

To determine the impact of stathmin suppression on tumour cell extravasation *in vivo*, mice were injected intravenously with shRNA-expressing Ctrl_{SH}, STMN1 Seq.2_{SH} and STMN1 Seq.3_{SH} SK-N-BE(2)/TGL cells and whole-body metastatic tumour burden was measured using the Xenogen IVIS Imaging System. **(a)** Representative pseudocolour bioluminescent images of mice from each group are shown. The coloured scale bar displays the degree of bioluminescence emitted from the cells, as measured in photons/second/centimetre squared/steradian (p/sec/cm²/sr). **(b)** Quantitation of bioluminescence emitted from the whole-body of mice from each group. Each dot is representative of one mouse and each bar represents the mean total flux (photons/second) ±SEM (error bars) for each group (n≥11), * p<0.05, ** p<0.005.

a



b



5.3 Stathmin suppression does not reduce neuroblastoma metastasis to the spleen, brain or legs

To further examine stathmin's role on neuroblastoma metastasis, and more specifically extravasation *in vivo*, organ specific locations of metastasis were examined. Following *in vivo* bioluminescence imaging, mice were humanely killed using CO₂ asphyxiation, organs removed and *ex vivo* imaged using the Xenogen IVIS Imaging System. Whilst the major sites of metastasis were the kidneys, lungs and liver, metastatic tumour burden was also observed in the spleen, brain and legs (Figs 5.3, 5.4a, c & e). Figure 5.4 panels a, c and e displays representative pseudocolour bioluminescent images overlaid on photographic images of spleens, brains and legs respectively and qualitative visualisation shows that stable stathmin suppression, using either STMN1 Seq.2_{SH} or STMN1 Seq.3_{SH} resulted in variable neuroblastoma metastatic tumour burden in each site compared to controls (Ctrl_{SH}). Quantitation of bioluminescence signal from each site showed that stathmin suppression with either STMN1 Seq.2_{SH} or STMN1 Seq.3_{SH} did not significantly alter neuroblastoma metastatic tumour burden in the spleen (Fig. 5.4b), brain (Fig. 5.4d) or legs (Fig. 5.4f). These results indicate that stathmin may not play a role in the extravasation of neuroblastoma cells to the spleen, brain or legs in this model.

Figure 5.3 Neuroblastoma metastatic spread in the experimental metastasis model

To explore which organs possessed neuroblastoma metastatic tumour burden in the experimental metastasis model, mice were injected intravenously with SK-N-BE(2)/TGL neuroblastoma cells and 23 days post-neuroblastoma cell injection mice were humanely killed using CO₂ asphyxiation, kidneys, spleen, lungs, brain, legs and liver removed and *ex vivo* imaged using the Xenogen IVIS Imaging System. **(a)** A representative 6-well plate containing kidneys (in separate wells), spleen, lungs, brain and legs is shown. **(b)** A representative image of a liver, which was analysed in a separate plate to prevent interference of liver bioluminescent signal into other organs, is shown. The coloured scale bars display the amount of bioluminescence emitted from the kidneys, spleen, lungs, brain, legs and liver, as measured in photons/second/centimeter squared/steradian (p/sec/cm²/sr).

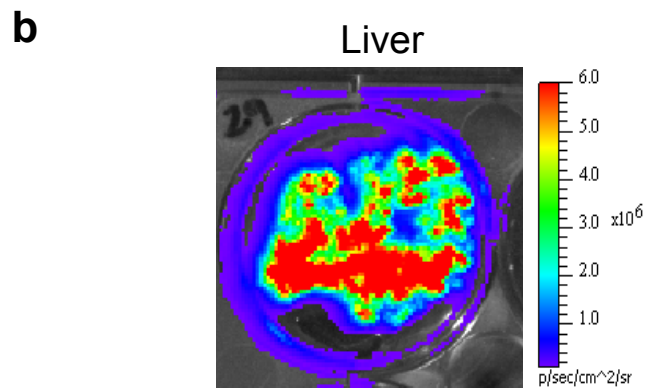
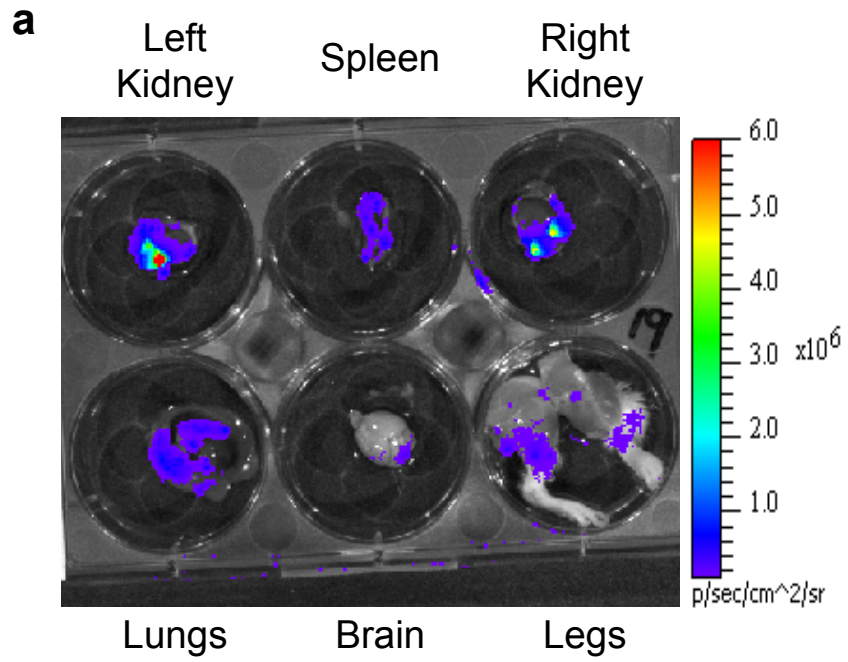
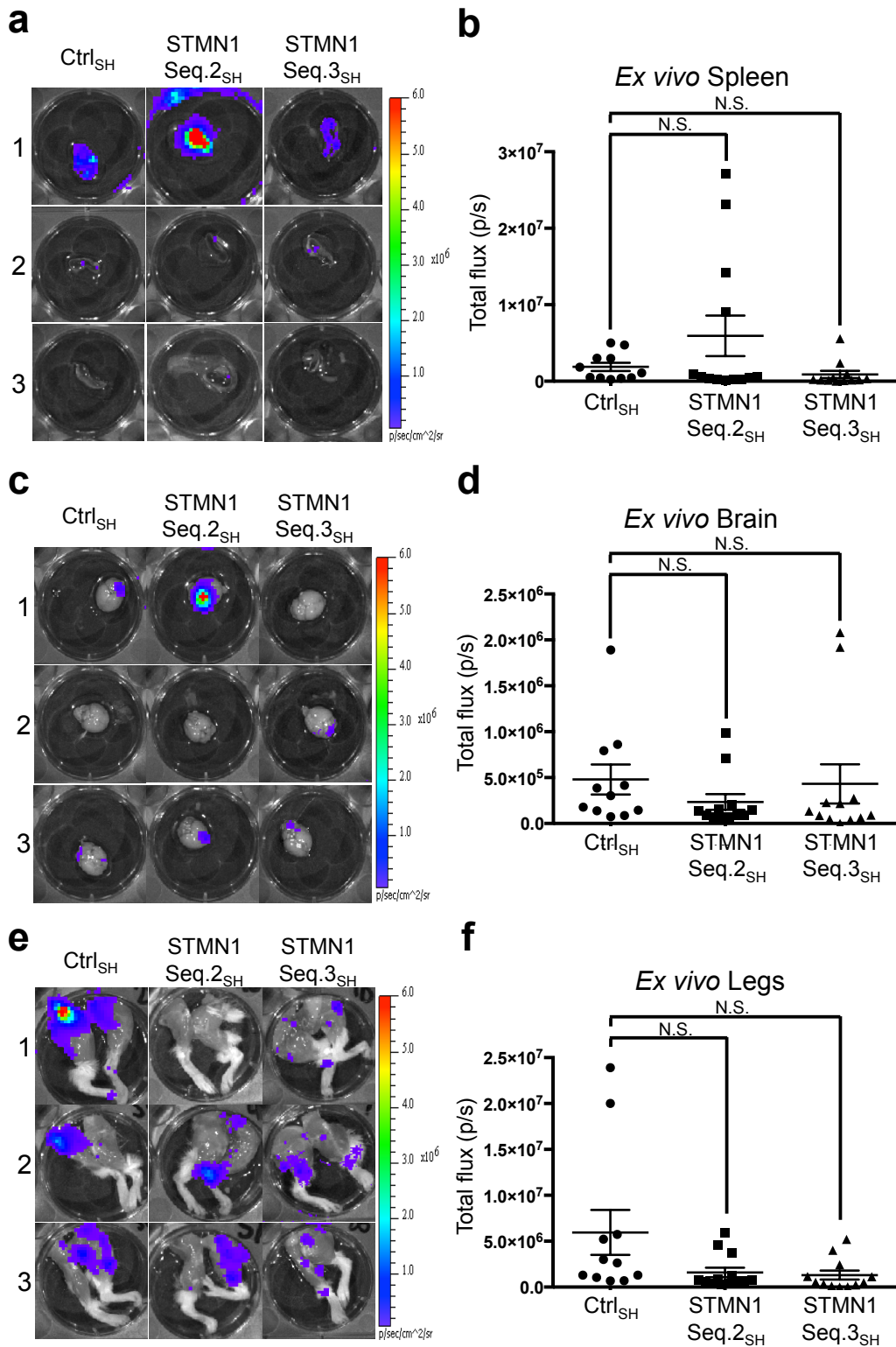


Figure 5.4 Stathmin suppression does not influence neuroblastoma metastatic tumour burden in the spleen, brain or legs of mice measured by bioluminescent imaging

To determine the impact of stathmin suppression on extravasation of neuroblastoma cells into the spleen, brain and legs *in vivo*, mice were injected intravenously with shRNA-expressing Ctrl_{SH}, STMN1 Seq.2_{SH} and STMN1 Seq.3_{SH} SK-N-BE(2)/TGL neuroblastoma cells and 23 days post-neuroblastoma cell injection mice were humanely killed using CO₂ asphyxiation, spleen, brain and leg metastatic tumour burden was measured using the Xenogen IVIS Imaging System. Representative pseudocolour images from the spleen (**a**), brain (**c**) and legs (**e**) of mice from each group are shown. The coloured scale bar displays the amount of bioluminescence emitted from the spleen, brain and legs, as measured in photons/second/centimeter squared/steradian (p/sec/cm²/sr). To quantify neuroblastoma tumour burden in the spleen (**b**), brain (**d**) and legs (**f**) of mice, total flux (photons/sec) was measured from each spleen, brain and pair of legs respectively. Each dot represents one spleen, brain or pair of legs and each bar represents the mean total flux ±SEM (error bars) for each group (n≥11), N.S. denotes not significant.

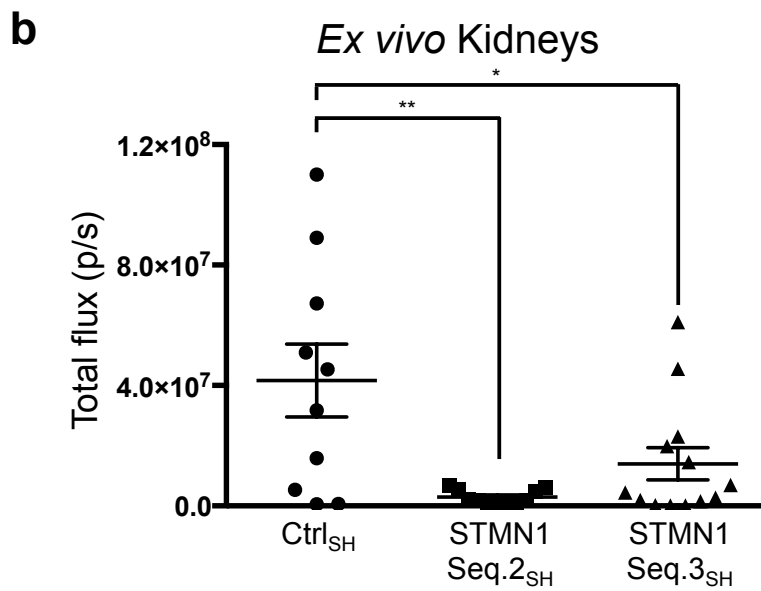
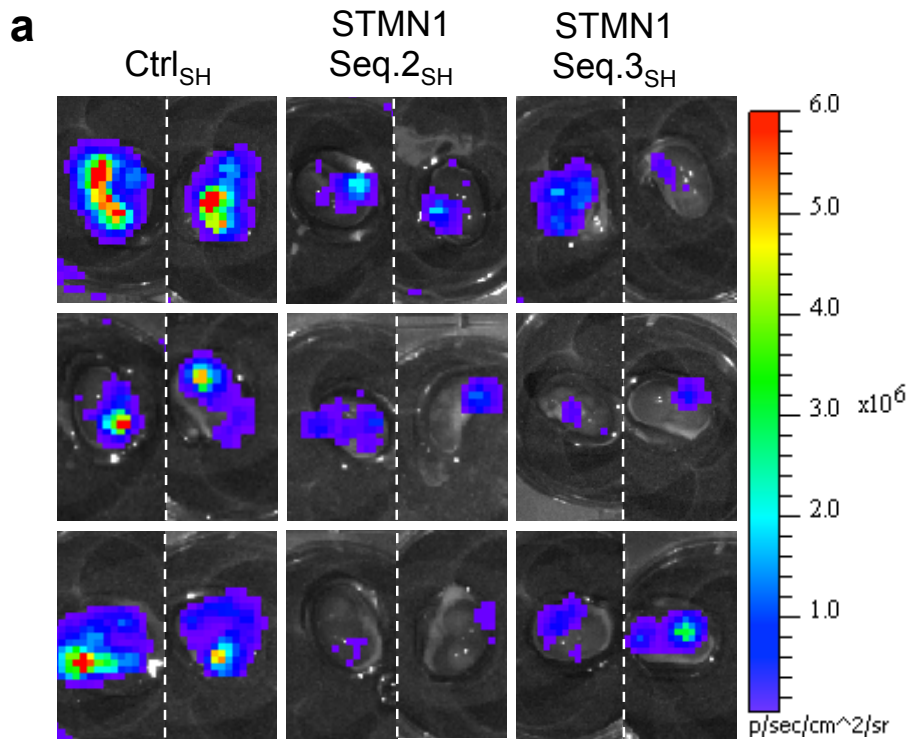


5.4 Stathmin suppression reduces neuroblastoma kidney metastasis

To further investigate the role of stathmin on extravasation *in vivo*, the tumour burden in the kidneys was examined from mice injected with either Ctrl_{SH}, STMN1 Seq.2_{SH} or STMN1 Seq.3_{SH} SK-N-BE(2)/TGL neuroblastoma cells. Neuroblastoma metastases in the kidneys of mice were detected using bioluminescent imaging and Figure 5.5a displays representative pseudocolour bioluminescent images overlaid on photographic images of kidneys and qualitative visualisation shows that stable stathmin suppression with either STMN1 Seq.2_{SH} or STMN1 Seq.3_{SH} reduced neuroblastoma metastatic tumour burden in the kidneys compared to controls (Ctrl_{SH}). Quantitation of this observation by measuring total flux from each set of kidneys showed that stathmin suppression with either STMN1 Seq.2_{SH} or STMN1 Seq.3_{SH} significantly reduced neuroblastoma metastatic tumour burden in the kidneys compared to controls (Ctrl_{SH}) (STMN1 Seq.2_{SH}: $3.0 \times 10^6 \pm 7.19 \times 10^5$ photons/sec, $p < 0.005$; STMN1 Seq.3_{SH}: $1.4 \times 10^7 \pm 5.35 \times 10^6$ photons/sec, $p < 0.05$; Ctrl_{SH}: $4.2 \times 10^7 \pm 1.21 \times 10^7$ photons/sec) (Fig. 5.5b). This observation supports a role for stathmin in extravasation of neuroblastoma cells into the kidneys of mice.

Figure 5.5 Stathmin suppression reduces neuroblastoma metastatic tumour burden in the kidneys of mice by bioluminescent imaging

To determine the influence of stathmin suppression on extravasation of neuroblastoma tumour cells into the kidneys *in vivo*, mice were injected intravenously with shRNA-expressing Ctrl_{SH}, STMN1 Seq.2_{SH} or STMN1 Seq.3_{SH} SK-N-BE(2)/TGL neuroblastoma cells and kidney metastatic tumour burden was measured using the Xenogen IVIS Imaging System. **(a)** Representative pseudocolour bioluminescent images from the kidneys of mice from each group are shown. Dotted white lines indicate kidneys from same mouse and image have been spliced together. The coloured scale bar displays the amount of bioluminescence emitted from the kidneys, as measured in photons/second/centimeter squared/steradian (p/sec/cm²/sr). **(b)** To quantify neuroblastoma tumour burden in the kidneys of mice, total flux (photons/sec) was measured from each set of kidneys. Each dot represents one set of kidneys and each bar represents the mean total flux ±SEM (error bars) for each group (n≥11), * p<0.05, ** p<0.005.



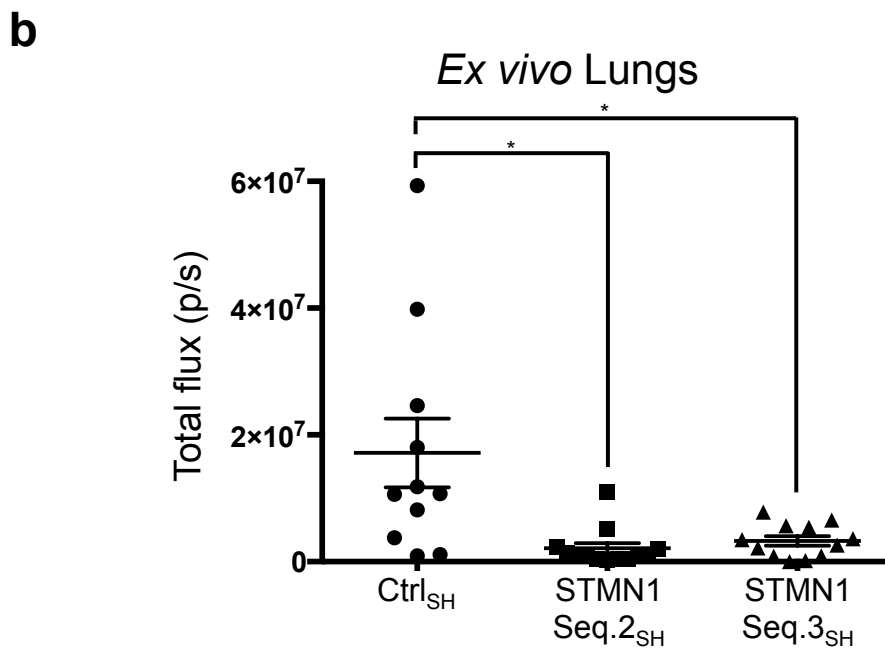
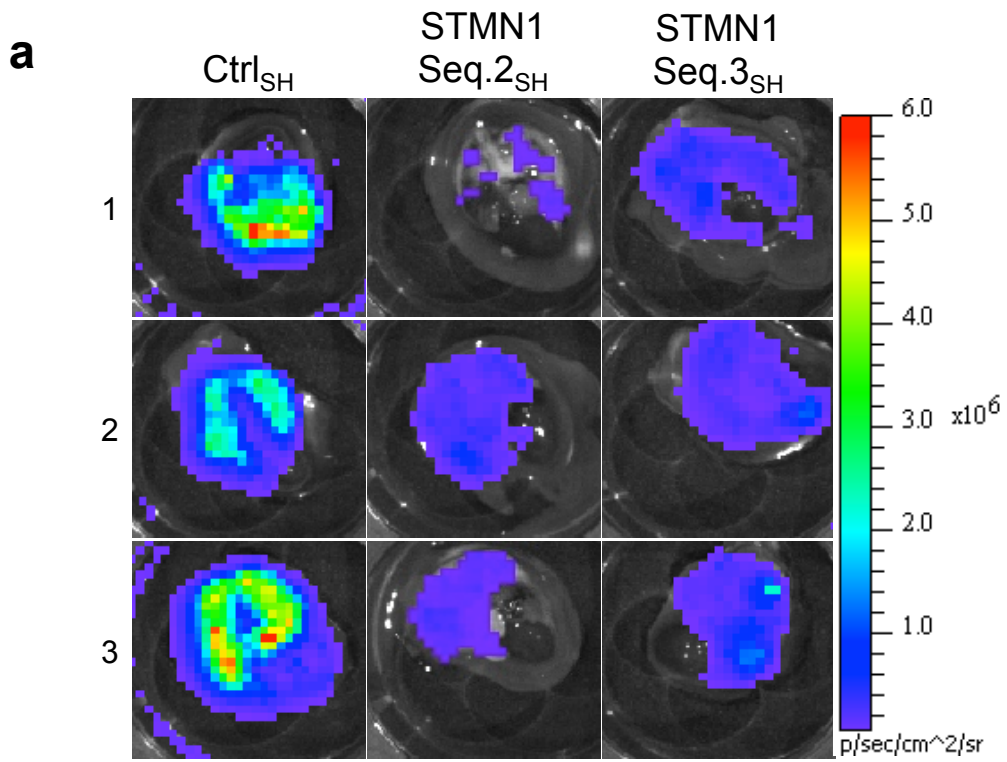
5.5 Stathmin suppression reduces neuroblastoma lung metastasis

To further investigate and visualise the impact of stathmin suppression on tumour cell extravasation in an *in vivo* setting, the lungs of tumour bearing mice were examined *ex vivo*. Following *in vivo* bioluminescence imaging, mice injected with either Ctrl_{SH}, STMN1 Seq.2_{SH} or STMN1 Seq.3_{SH} SK-N-BE(2) neuroblastoma cells were humanely killed using CO₂ asphyxiation, lungs removed and *ex vivo* imaged using the Xenogen IVIS Imaging System.

Figure 5.5a, displaying representative pseudocolour bioluminescent images overlaid on photographic images of sets of lungs, shows that neuroblastoma metastases in the lungs of mice were present. Qualitative visualisation shows that stable suppression of stathmin with either STMN1 Seq.2_{SH} or STMN1 Seq.3_{SH} reduced neuroblastoma metastatic tumour burden in the lungs compared to controls (Ctrl_{SH}). To quantify this observation, the total flux from each set of lungs was measured and it showed that stathmin suppression using either STMN1 Seq.2_{SH} or STMN1 Seq.3_{SH} significantly reduced neuroblastoma metastatic tumour burden in the lungs compared to controls (Ctrl_{SH}) (STMN1 Seq.2_{SH}: $2.1 \times 10^6 \pm 8.23 \times 10^5$ photons/sec, $p < 0.01$; STMN1 Seq.3_{SH}: $3.3 \times 10^6 \pm 7.54 \times 10^5$ photons/sec, $p < 0.05$; Ctrl_{SH}: $1.7 \times 10^7 \pm 5.43 \times 10^6$ photons/sec) (Fig. 5.6b). This data supports a role for stathmin in the extravasation of neuroblastoma cells into the lungs of mice.

Figure 5.6 Stathmin suppression reduces neuroblastoma metastatic tumour burden in the lungs of mice by bioluminescent imaging

To determine the impact of stathmin suppression on extravasation of neuroblastoma cells into the lungs *in vivo*, mice were injected intravenously with shRNA-expressing Ctrl_{SH}, STMN1 Seq.2_{SH} or STMN1 Seq.3_{SH} SK-N-BE(2)/TGL cells and lung metastatic tumour burden was measured using the Xenogen IVIS Imaging System. **(a)** Representative pseudocolour bioluminescent images from the lungs of mice from each group are shown. The coloured scale bar displays the amount of bioluminescence emitted from the tumours, as measured in photons/second/centimetre squared/steradian (p/sec/cm²/sr). **(b)** Neuroblastoma tumour burden in the lungs of mice from each group was quantified by measuring the total flux (photons/sec) from each set of lungs. Each dot represents one set of lungs and each bar represents the mean total flux \pm SEM (error bars) for each group (n \geq 11), * p<0.05.



5.6 Stathmin suppression reduces neuroblastoma liver metastasis

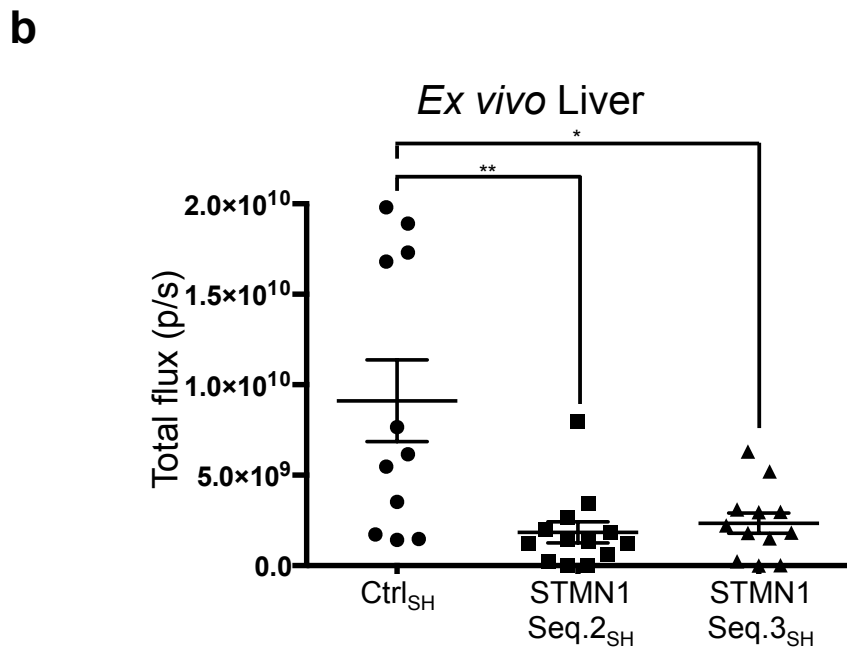
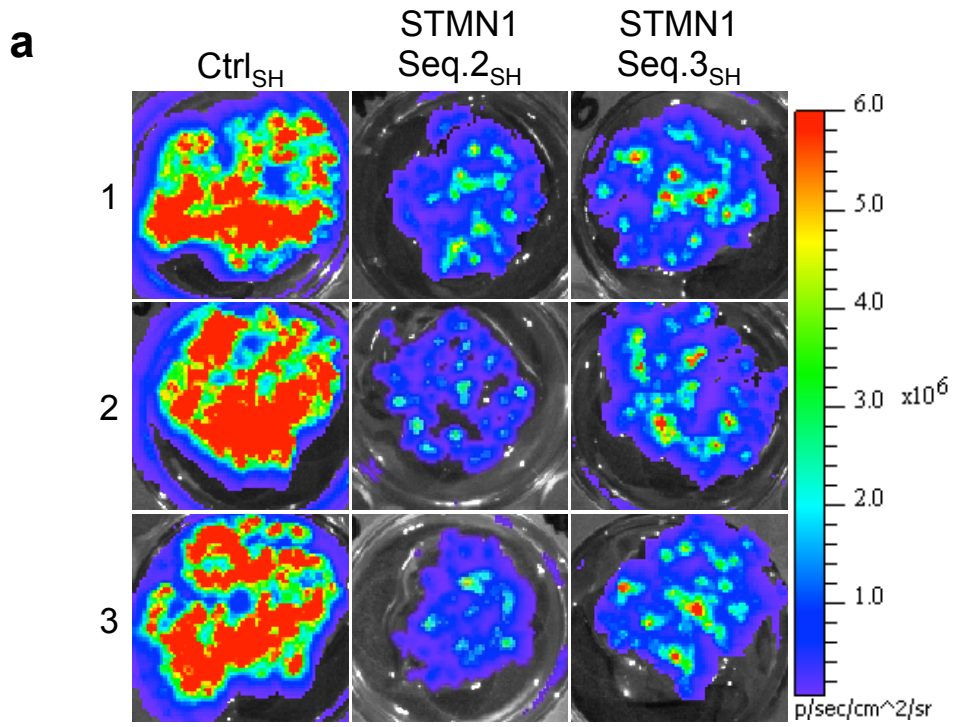
The major neuroblastoma tumour burden in mice injected intravenously with either Ctrl_{SH}, STMN1 Seq.2_{SH} or STMN1 Seq.3_{SH} SK-N-BE(2) neuroblastoma cells was present in the liver. To further examine the role for stathmin in the extravasation of neuroblastoma cells in mice, the livers from the above-mentioned mice were examined using *ex vivo* bioluminescence imaging.

Figure 5.6a shows that neuroblastoma metastases were present in the livers of mice. Qualitative analysis shows that stable stathmin suppression using either STMN1 Seq.2_{SH} or STMN1 Seq.3_{SH} resulted in a marked decrease in metastatic tumour burden in the liver compared to controls (Ctrl_{SH}) (Fig. 5.7a). Quantitation of tumour burden showed that stathmin suppression significantly reduced tumour burden in the liver of mice compared to controls (STMN1 Seq.2_{SH}: $1.8 \times 10^9 \pm 5.84 \times 10^8$ photons/sec, $p < 0.005$; STMN1 Seq.3_{SH}: $2.3 \times 10^9 \pm 5.62 \times 10^8$ photons/sec, $p < 0.01$; Ctrl_{SH}: $9.1 \times 10^9 \pm 2.26 \times 10^9$ photons/sec) (Fig. 5.7b). Given the experimental metastasis model selectively assesses the extravasation step of cancer metastasis, this data, taken along with *ex vivo* analysis of tumour burden in the kidneys and lungs (Figs. 5.6-5.7), supports a role for stathmin in the extravasation of neuroblastoma cells *in vivo*.

To determine if the luciferase expression levels measured *in vitro* (Fig. 5.1) reflected the actual levels *in vivo*, histological analysis of neuroblastoma tumours in mouse liver tissue was performed by paraffin-embedding, sectioning and staining livers from tumour-bearing mice with haematoxylin-eosin (H&E) and by performing immunohistochemistry

Figure 5.7 Stathmin suppression reduces neuroblastoma metastatic tumour burden in the livers of mice by bioluminescent imaging

To determine the impact of stathmin suppression on extravasation and eventual metastasis of neuroblastoma cells to the liver *in vivo*, mice were injected intravenously with shRNA-expressing Ctrl_{SH}, STMN1 Seq.2_{SH} or STMN1 Seq.3_{SH} SK-N-BE(2)/TGL cells and metastatic tumour burden in the liver was measured using Xenogen IVIS bioluminescent imaging. **(a)** Representative pseudocolour bioluminescent images from the liver of each mouse from each group are shown. The coloured scale bar displays the amount of bioluminescence emitted from the tumours, as measured in photons/second/centimetre squared/steradian (p/sec/cm²/sr). **(b)** Neuroblastoma tumour burden in the liver of each mouse from each group was quantified by measuring the total flux (photons/sec) from each liver. Each dot represents one liver and each bar represents the mean total flux \pm SEM (error bars) for each group (n \geq 11), * p<0.05, ** p<0.01.



separately probing for luciferase and stathmin (Fig. 5.8). H&E staining confirmed the presence of neuroblastoma tumour nodules as distinct regions of intense purple staining compared to the normal mouse liver tissue, which stained strongly as pink (Fig. 5.8). Negative staining using relevant isotype control antibodies confirmed suitable specificity of the stathmin and luciferase antibodies (Fig. 5.8). Immunohistochemical analysis confirmed that tumour nodules from mice of all treatment groups (Ctrl_{SH}, STMN1 Seq.2_{SH} and STMN1 Seq.3_{SH}) expressed similar levels of luciferase, this data further confirms the aforementioned *in vitro* cell-based luciferase expression results shown in Fig. 5.1. Furthermore, Immunohistochemical analysis confirmed stathmin expression with the observation of high expression of stathmin in liver tumours of Ctrl_{SH}-treated mice and decreased stathmin suppression in STMN1 Seq.2_{SH}- and STMN1 Seq.3_{SH}-treated mice (Fig 5.8).

To quantify the maintenance of stable stathmin suppression in the metastatic neuroblastoma tumours of STMN1 Seq.2_{SH} and STMN1 Seq.3_{SH} tumour-bearing mice compared to Ctrl_{SH} mice, stathmin gene expression was measured using qPCR. Beta-2-microglobulin was used as a housekeeping gene and GFP was analysed as a human cell specific gene (as the TGL vector contains GFP) to account for the large amount of mouse liver tissue contaminating the RNA isolates.

Quantitative PCR analysis confirmed that stathmin suppression was maintained in the metastatic neuroblastoma tumours in STMN1 Seq.2_{SH}- and STMN1 Seq.3_{SH}-treated mice where 62% and 69% stathmin suppression was achieved respectively compared to Ctrl_{SH}-treated mice (STMN1 Seq.2_{SH}: 62.6±10.78%, p<0.0005; STMN1 Seq.3_{SH}: 69.4±13.06%, p<0.0005; Ctrl_{SH}: 100.0±10.28%) (Fig. 5.9). This data, taken with qualitative data in Fig. 5.8., confirms that stable stathmin suppression was maintained in STMN1 Seq.2_{SH}- and STMN1 Seq.3_{SH}-treated mice compared to Ctrl_{SH}-treated mice.

Figure 5.8 Luciferase and stathmin expression in neuroblastoma metastatic tumours in mouse liver tissue by immunohistochemistry staining

To determine whether the luciferase signal represents neuroblastoma tumour burden, whole livers from mice were fixed, paraffin-embedded and sectioned prior to staining with H&E and immunohistochemistry. Immunohistochemistry was performed probing for stathmin and luciferase expression. No staining was present in the isotype control, which confirmed specificity of the secondary antibody. Luciferase expression was similar in all treatment groups. Stathmin expression was qualitatively decreased in the STMN1 Seq.2_{SH}- and STMN1 Seq.3_{SH}-treated mice compared to Ctrl_{SH}-treated mice.

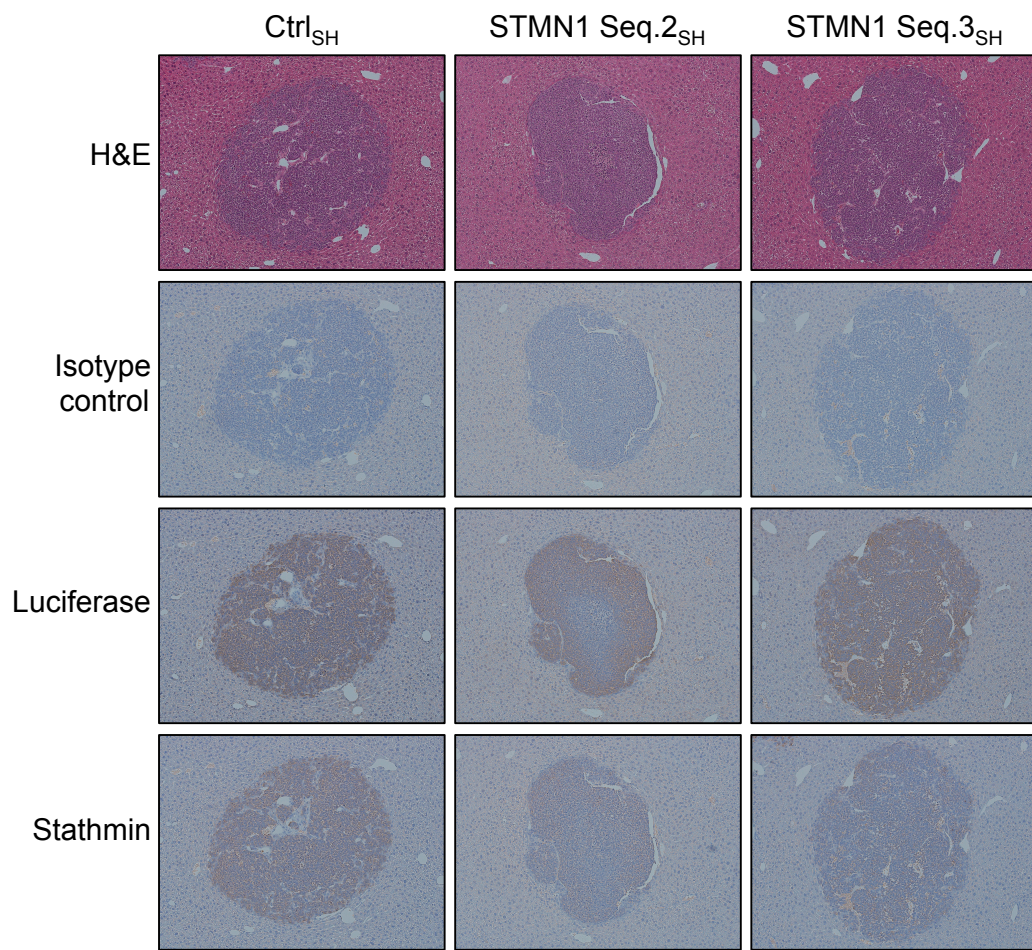
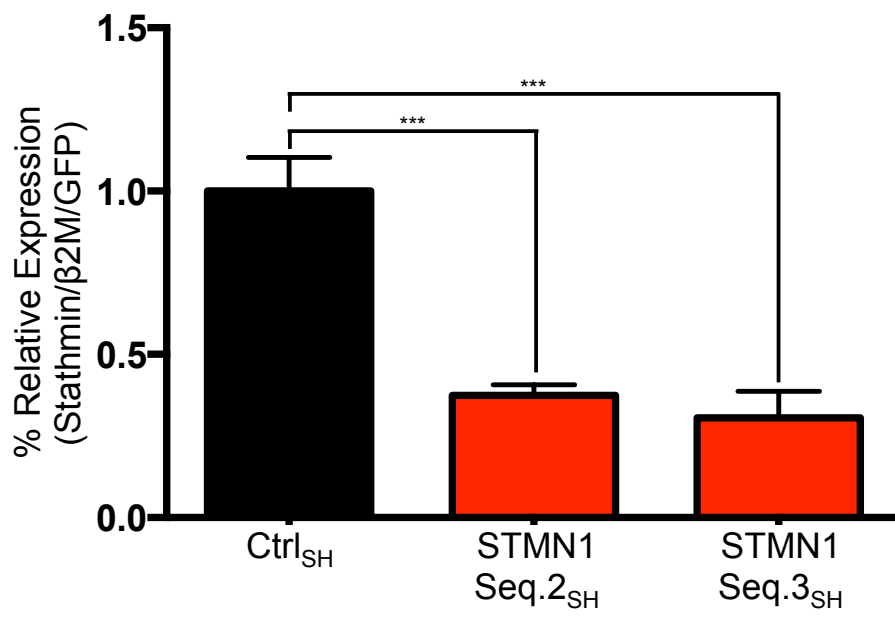


Figure 5.9 Stathmin gene suppression was maintained in metastatic neuroblastoma tumours

To quantify stathmin suppression maintenance in the metastatic neuroblastoma tumours of Ctrl_{SH}, STMN1 Seq.2_{SH}, STMN1 Seq.3_{SH} tumour-bearing mice, stathmin gene expression was measured using qPCR. Stathmin mRNA was normalized to the housekeeping gene beta-2-microglobulin. Additionally, stathmin mRNA was normalized to GFP, which was analysed as a human cell specific gene to account for the large amount of mouse liver tissue contaminating the RNA isolates. Data represents the mean \pm SEM (error bars) of 6 individual livers from mice from the Ctrl_{SH}, STMN1 Seq.2_{SH} and STMN1 Seq.3_{SH} treatment groups.

*** p<0.001.

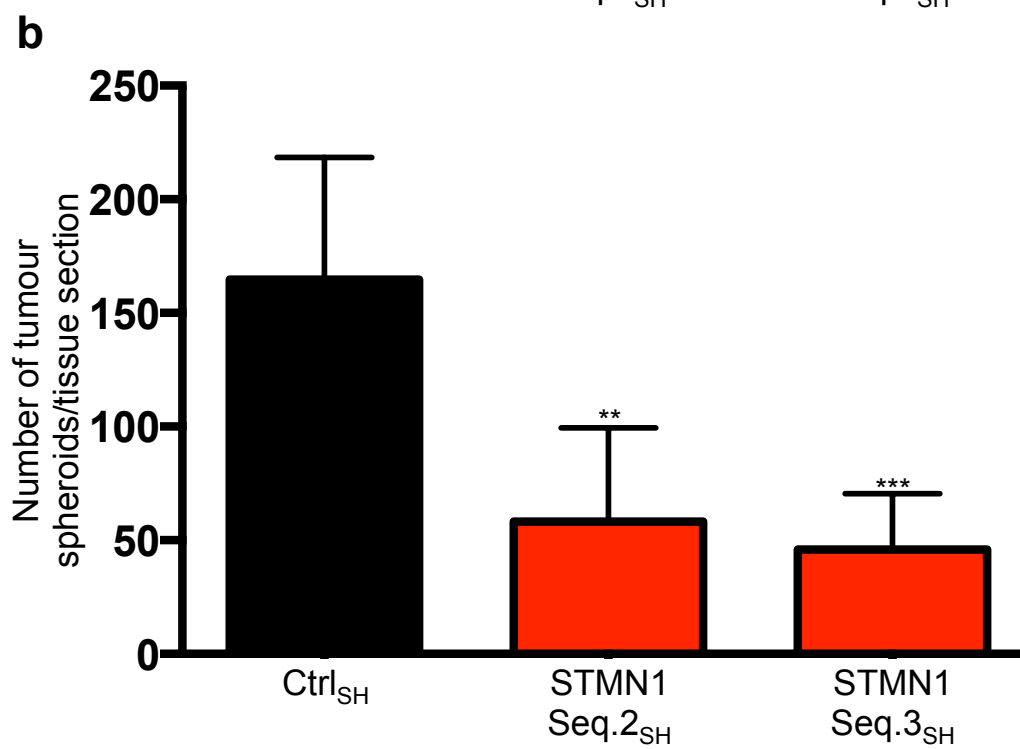
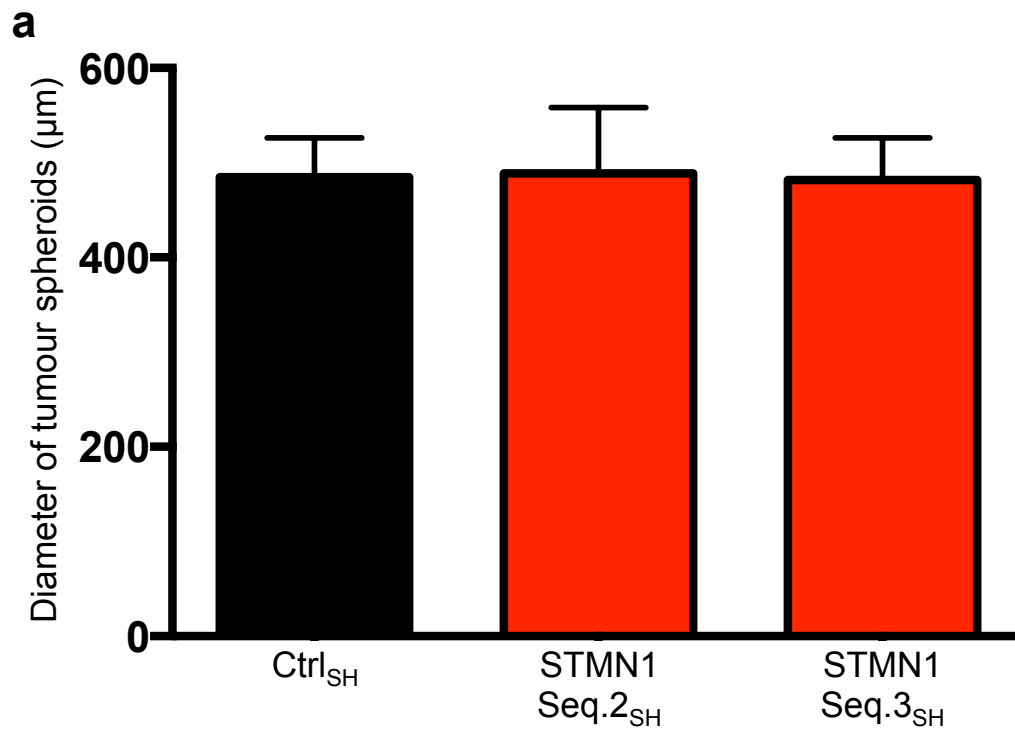


To determine if the decrease in bioluminescence reflected the actual tumour burden in the livers of mice, histology and H&E staining was performed followed by measurement of tumour nodule size and number. Quantitation of tumour nodule size showed that stathmin suppression did not significantly influence tumour nodule size compared to controls (STMN1 Seq.2_{SH}: 488±28.31 μm , $p=0.91$; STMN1 Seq.3_{SH}: 481.5±18.25 μm , $p=0.89$; Ctrl_{SH}: 484.9±16.97 μm) (Fig. 5.10a) suggesting that once neuroblastoma cells have extravasated into the liver tissue that their growth is unaffected by stathmin suppression. This result further corroborates results from this thesis (Chapter 3, Section 3.4) and our laboratory's previously published results (Byrne, Yang et al. 2014) suggesting that stathmin is not involved in the proliferation of neuroblastoma cells in 2D- and 3D-based *in vitro* experiments or the growth of neuroblastoma primary tumours *in vivo* (Byrne, Yang et al. 2014).

Quantitation of tumour nodule number showed that stathmin suppression using either STMN1 Seq.2_{SH} or STMN1 Seq.3_{SH} significantly reduced neuroblastoma tumour nodule number per tissue section compared to controls (Ctrl_{SH}) (STMN1 Seq.2_{SH}: 58.2±16.90, $p<0.005$; STMN1 Seq.3_{SH}: 46.0±10.03, $p<0.001$; Ctrl_{SH}: 164.7±21.99) (Fig. 5.10b). This result suggests that stathmin is important for the extravasation, or the seeding of tumour cells, from the bloodstream into liver tissue *in vivo* to generate metastatic tumours. This data, taken along with bioluminescent measurements quantified from the kidneys (Fig. 5.5b), lungs (Fig. 5.6b) and liver (Fig. 5.7b), support a role for stathmin in the extravasation of neuroblastoma cells *in vivo*.

Figure 5.10 Stathmin suppression reduces neuroblastoma metastatic tumour burden in the liver of mice by histological quantification

To investigate the influence of stathmin suppression on the extravasation of neuroblastoma cells to the liver *in vivo*, mice were injected intravenously with shRNA-expressing Ctrl_{SH}, STMN1 Seq.2_{SH} or STMN1 Seq.3_{SH} SK-N-BE(2)/TGL cells and metastatic tumour burden in the liver was measured by histological analysis. Using H&E stained tumour-bearing liver sections from the Ctrl_{SH}, STMN1 Seq.2_{SH} and STMN1 Seq.3_{SH} treatment groups, the size and number of tumour nodules was measured. Results are expressed as average tumour nodule size **(a)** and number of tumour nodules per tissue section **(b)**. Data represents the mean \pm SEM (error bars) of 6 individual livers from mice from the Ctrl_{SH}, STMN1 Seq.2_{SH} and STMN1 Seq.3_{SH} treatment groups. ** p<0.005; *** p<0.001.



5.7 Discussion

Results from this thesis have identified a defect in *in vitro* neuroblastoma transendothelial migration upon stathmin suppression (Fig. 3.12c-d). To further understand how stathmin is controlling this phenotype, an *in vivo* model of metastasis was established specifically to examine stathmin's role in *in vivo* neuroblastoma transendothelial migration. The outlined findings have provided the first evidence that stathmin is important in *in vivo* neuroblastoma transendothelial migration.

Bioluminescent imaging analysis of the whole-body of mice injected intravenously with Ctrl_{SH}, STMN1 Seq.2_{SH} or STMN1 Seq.3_{SH} SK-N-BE(2)/TGL neuroblastoma cells suggested that stathmin may be important for transendothelial migration of neuroblastoma cells *in vivo* (Fig. 5.2). What was unclear was whether the effects on transendothelial migration were organ specific. *Ex vivo* bioluminescent imaging of various organs revealed the presence of luciferase-expressing neuroblastoma cells in the spleen, brain, legs, kidneys, lungs and liver (Fig. 5.3). The kidneys, lungs and liver showed high levels of metastatic tumour burden with the liver being the predominant site of metastasis. Quantitation of bioluminescent analysis of the spleen, brain and legs suggested that stathmin is not important in the extravasation of neuroblastoma cells to these sites (Fig. 5.4). Examination of metastatic tumour burden in the legs from Ctrl_{SH}-treated mice revealed the presence of two samples that displayed markedly increased tumour burden relative to the means of all three groups but the comparison between the Ctrl_{SH}-treated mice and either STMN1 Seq.2_{SH}- or STMN1 Seq.3_{SH}-treated mice did not reach statistical significance. An increase in the number of mice per group size may allow a more complete examination of stathmin's role in extravasation to the legs of mice.

Quantitation of bioluminescent signal from the kidneys, lungs and liver indicated that stathmin is important in transendothelial migration of neuroblastoma cells *in vivo* to these sites (Fig. 5.5-5.7). To determine if the decrease in bioluminescence in the liver between Ctrl_{SH}-treated and STMN1 Seq.2_{SH}- or STMN1 Seq.3_{SH}-treated mice was due to changes in the actual tumour burden in the liver, tumour nodules were examined by histology and H&E staining. The observation that stathmin suppression did not influence tumour nodule size (Fig. 5.10a) suggested that once neuroblastoma cells have seeded and established metastatic foci that stathmin suppression does not influence the proliferation of neuroblastoma cells to generate metastatic tumour nodules and is aligned with our previous findings that stathmin is not involved in the *in vitro* or *in vivo* growth of neuroblastoma cells (Byrne, Yang et al. 2014). In contrast to tumour nodule size, the number of tumour nodules was decreased upon stathmin suppression (Fig. 5.10b) suggesting that stathmin is important for the extravasation, or seeding of tumour cells, from the bloodstream into liver tissue *in vivo* in the generation of metastatic tumours. The reduction in the number of tumour nodules is congruous with the observation in the *in vitro* transendothelial migration experiments where stathmin suppression reduced the number of cells that crossed the endothelial barrier (Fig. 3.12c-d). This finding, combined with the bioluminescent measurements from the kidneys (Fig. 5.5b), lungs (Fig. 5.6b) and liver (Fig. 5.7b), collectively provide the first evidence that stathmin plays a key role in the extravasation of neuroblastoma cells (into at least) the kidneys, lung and liver *in vivo*.

Multiple studies, including one from our laboratory, have highlighted the effectiveness of reducing stathmin expression in the primary tumour to prevent metastatic spread (Belletti, Nicoloso et al. 2008, Singer, Malz et al. 2009, Byrne, Yang et al. 2014). The observation that suppression of stathmin can significantly reduce metastasis beyond the primary tumour (such

as during extravasation of tumour cells into metastatic sites) suggests a possible multifaceted role that stathmin may play during the complex process of metastasis.

In conclusion, this chapter, through the analysis of multiple organs has revealed an important role for stathmin in the extravasation of neuroblastoma cells *in vivo*.

Chapter 6.

6 Therapeutic potential of targeting stathmin to reduce metastasis in neuroblastoma *in vivo*

6.1 Introduction

The survival rates for neuroblastoma patients with distant metastases, classified as high-risk, have achieved only modest improvement over recent decades where a high-risk classification carries a dismal 5-year survival rate of 40-50% (Maris 2010). This depressing survival rate highlights the need to address treatments for metastatic neuroblastoma. This thesis has revealed that stathmin plays a role in multiple steps of the metastatic cascade in neuroblastoma and has provided key insights into how stathmin regulates these phenotypes including regulation of RhoA signalling, and cell migration in a microtubule-independent manner. Suppression of stathmin expression *in vivo* by the delivery of siRNA is an attractive proposition though the macromolecular and polar form of naked siRNA impedes its ability to gain access to cancer cells to exert its effect. In addition, serum nucleases facilitate the rapid degradation of naked siRNA (Williford, Wu et al. 2014). A promising new therapeutic strategy for the treatment of many cancers involves systemic delivery of siRNA to suppress key cancer-related genes using nanoparticle-mediated delivery systems (Williford, Wu et al. 2014).

Nanoparticles have been utilised to deliver siRNA in the laboratory to a variety of malignancies and have shown efficacy in stalling tumour growth, inducing sensitization to chemotherapeutics and increasing survival rates in multiple malignancies, including neuroblastoma [reviewed in (Williford, Wu et al. 2014)]. Notably, nanoparticles have been used to deliver VEGF siRNA to reduce *in vivo* tumour growth and angiogenesis in

neuroblastoma (Schiffelers, Ansari et al. 2004). A breakthrough study published by Davis *et al.* in Nature provided the first-in-human evidence of target gene suppression using nanoparticle-mediated siRNA delivery (Davis, Zuckerman et al. 2010). Additionally, recently Taberero *et al.* published the first-in-human evidence that RNA interference therapeutic targeting in endometrial carcinoma patients led to complete regression of liver metastases (Taberero, Shapiro et al. 2013).

In order to investigate the therapeutic potential of targeting stathmin gene expression using nanoparticles to reduce metastasis in neuroblastoma *in vivo*, the siRNA delivery vehicle InvivoFectamine® was used to deliver stathmin siRNA to neuroblastoma metastases in the experimental model of neuroblastoma metastasis that was established in Chapter 5. Suppression of stathmin expression in tumour tissue and impact on metastatic tumour burden in the liver was evaluated.

6.2 Determining the ability to deliver stathmin siRNA to metastatic neuroblastoma

To determine whether stathmin siRNA could be delivered effectively to metastatic tumours in the experimental neuroblastoma mouse model established in Chapter 5, 1×10^6 SK-N-BE(2) neuroblastoma cells were injected via the lateral tail vein into SCID Beige mice. These cells were chosen as they express stathmin and are the parental cells of those used in the shRNA studies. The presence of tumours was confirmed using the Xenogen IVIS Imaging system and at 23 days post-neuroblastoma cell injection mice were treated once with fluorescently labelled siRNA. Four hours after injection, mice were culled, Xenogen IVIS

fluorescent imaging performed and fluorescent microscopy used to assess the uptake of fluorescent siRNA in the mouse liver tumour tissue.

Figure 6.1 highlights the biodistribution of the fluorescently labelled siRNA to the liver, kidneys, lungs and spleen of tumour-bearing SCID Beige mice. As expected, no fluorescent signal is present in the mice injected with the InvivoFectamine®:unlabelled-siRNA complexes. In the InvivoFectamine®:Alexa Fluor™ 647-labelled siRNA complex treated mice no signal was detected in the kidneys, lungs or spleen. In contrast, a substantial signal was present in the liver (Fig. 6.1).

To further demonstrate the ability of InvivoFectamine® to deliver siRNA to neuroblastoma tumour tissue in the livers of mice, fluorescent microscopy was used. Briefly, tumour-bearing livers post-*ex vivo* imaging were frozen, sectioned, DAPI stained and imaged using a fluorescent microscope. Initially, the presence of neuroblastoma tumour cells in the liver of mice was confirmed as these cells express GFP, while the normal mouse tissue does not express GFP (Fig. 6.2). The fluorescently labelled-siRNA was able to accumulate in the metastatic neuroblastoma tumour in the liver of mice. This highlights that siRNA can be effectively delivered to the metastatic tumours in the mouse livers.

Figure 6.1 Uptake of fluorescently labelled siRNA, using InvivoFectamine®, to metastatic neuroblastoma tumours in mouse liver

To determine the ability of InvivoFectamine® to deliver fluorescently-labelled siRNA to mouse liver, kidneys, lungs and spleen *in vivo*, tumour-bearing SCID Beige mice, at 23 days-post neuroblastoma cell lateral tail vein injection were injected once with InvivoFectamine®:fluorescently labelled non-targeting siRNA (Alexa Fluor™ 647-conjugated siRNA) (at 2 mg siRNA/kg of mouse weight). Four hours after the injection mice were humanely killed, and the amount of fluorescent signal emitted from liver, kidney, lung and spleen tissues was evaluated using the Xenogen IVIS imaging system. Representative *ex vivo* pseudocolour fluorescent images from the liver, kidneys, lungs and spleen of mice from each group are shown. The coloured scale bar displays the amount of fluorescence emitted from each tissue, as measured in efficiency.

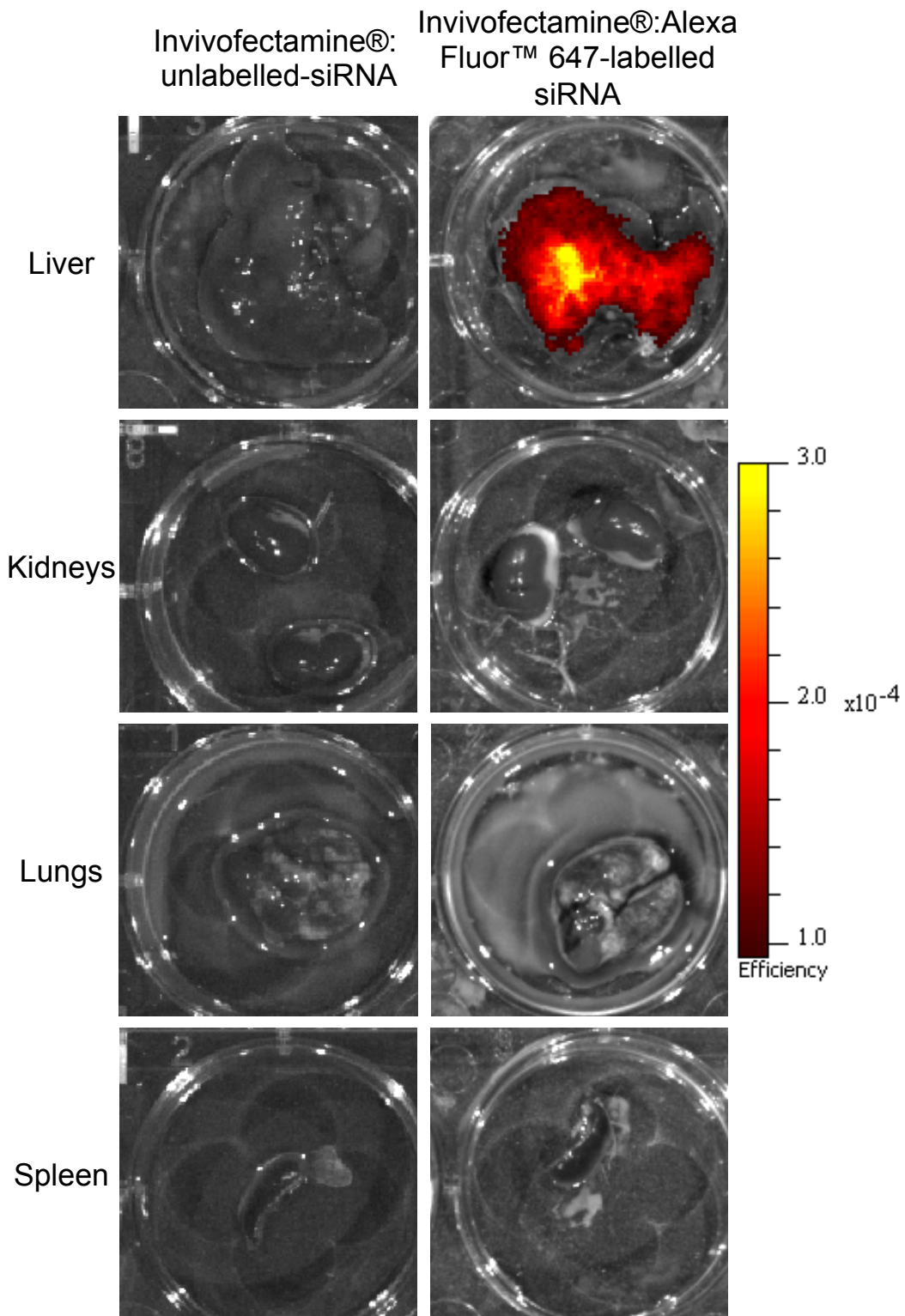
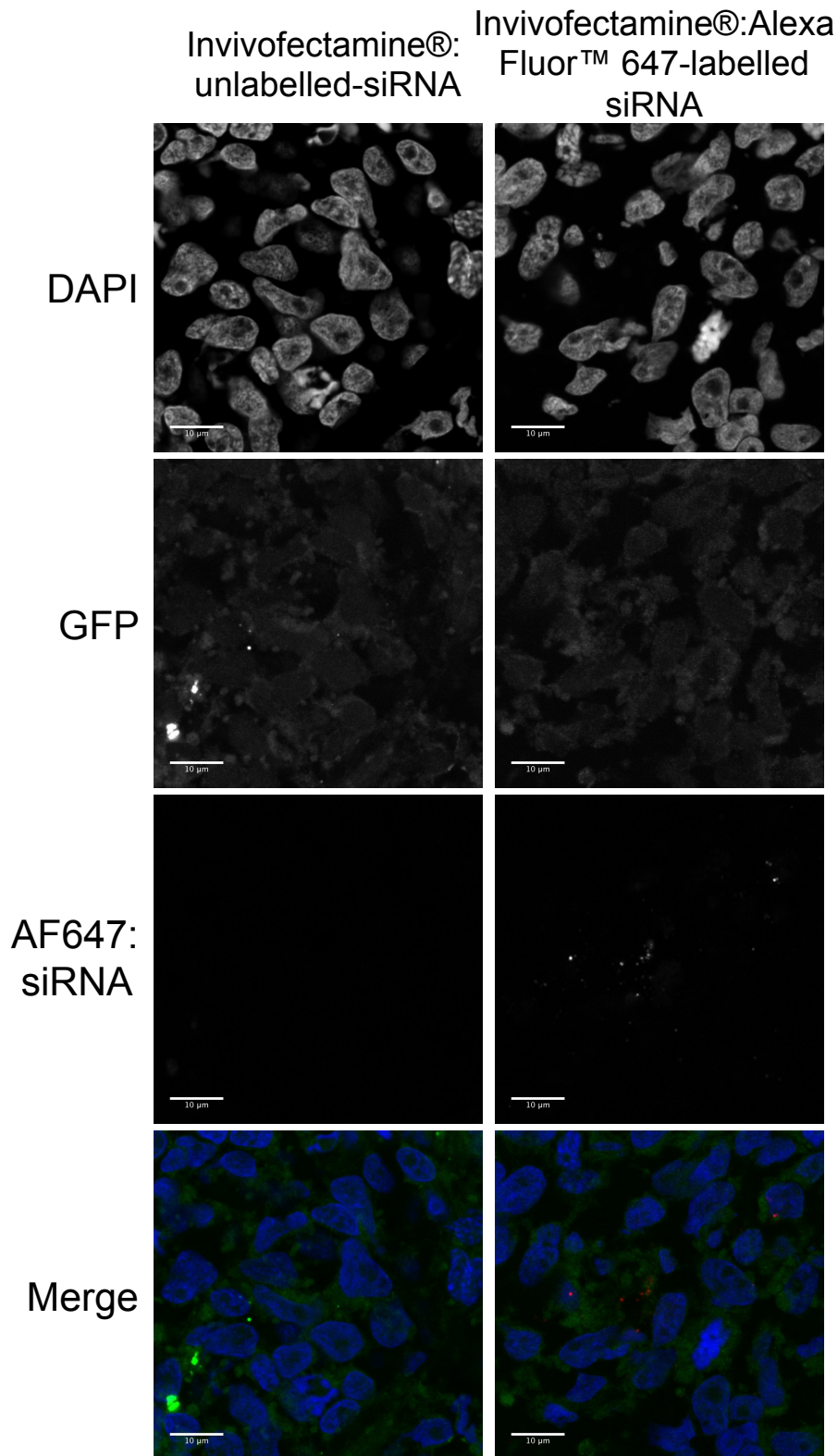


Figure 6.2 Uptake of fluorescently labelled siRNA, using InvivoFectamine®, to metastatic neuroblastoma tumours in mouse liver measured using confocal microscopy

To further confirm the ability of InvivoFectamine® to deliver siRNA to metastatic neuroblastoma tumours in mouse liver *in vivo*, tumours were initially established using the metastatic model described in Chapter 2, Section 2.17. Twenty-three days post tumour cell seeding, tumour burden was confirmed using the Xenogen IVIS Imaging System and mice were injected with InvivoFectamine®:fluorescently labelled non-targeting siRNA (Alexa Fluor™ 647-conjugated siRNA; 2 mg siRNA/kg of mouse weight). Four hours after the injection mice were humanely killed, tumour-bearing liver tissue was frozen in OCT compound, livers were sectioned, stained for DAPI and analysed using a Zeiss™ 780 confocal microscope with a 63X 1.35 NA oil objective. DAPI, GFP and Alexa Fluor™ 647:siRNA are shown in greyscale and merged channels in pseudocolour. Scale bar = 10 µm. Representative microscopy images were selected from one tumour-bearing liver out of at least 3 tumour-bearing mice.

Metastatic neuroblastoma tumours in mouse liver

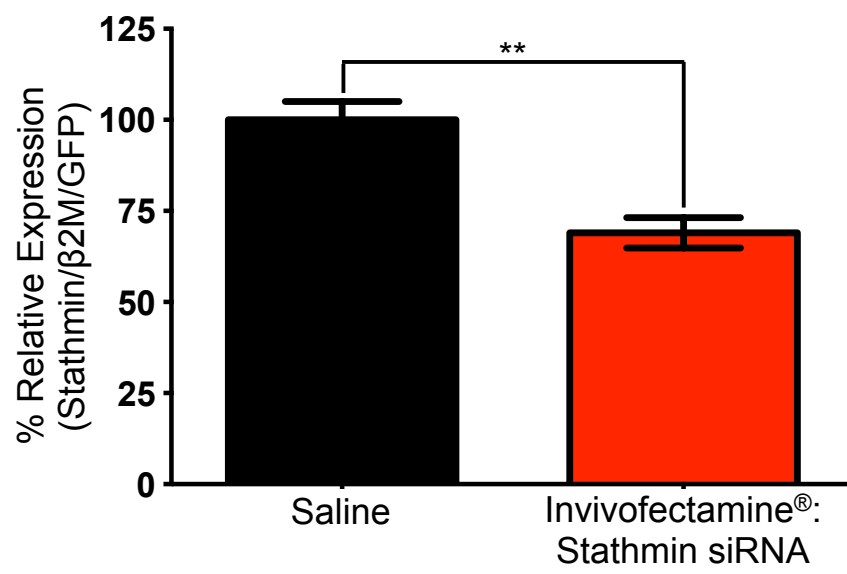


6.3 Invivofectamine®:stathmin siRNA complexes silence stathmin expression in liver metastatic tumours

Having shown that Invivofectamine® is effectively delivering siRNA to metastatic neuroblastoma tumours in mouse liver (Chapter 6, Section 6.2), it was important to determine whether Invivofectamine®:stathmin-siRNA complexes can suppress stathmin gene expression in neuroblastoma tumour tissue. Briefly, mice at 20 days-post neuroblastoma cell injection were injected once daily for 3 consecutive days with Invivofectamine®:stathmin-siRNA complexes (at 2 mg siRNA/kg of mouse weight). Twenty-four hours after the third injection, mice were culled and tumour-bearing livers were harvested and placed in RNA later. Subsequent qPCR analysis of stathmin, the house-keeping gene beta-2-microglobulin, and the human-cell specific gene GFP (as the TGL vector contains GFP), showed that administration of Invivofectamine®:stathmin-siRNA complexes significantly reduced stathmin mRNA expression by $30.97 \pm 6.5\%$ ($p < 0.005$) compared to saline-treated controls (Fig. 6.3). This indicates that Invivofectamine® effectively delivers stathmin siRNA to neuroblastoma tumour tissue *in vivo* and silences stathmin gene expression.

Figure 6.3 Invivofectamine®:stathmin-siRNA complexes silence stathmin gene expression in liver metastatic tumours

To determine the efficacy of Invivofectamine®:stathmin-siRNA delivery, tumour-bearing SCID Beige mice at 20 days-post neuroblastoma cell lateral tail vein injection were injected with Invivofectamine®:stathmin siRNA complexes (at 2 mg siRNA/kg mouse weight) once daily for 3 consecutive days. Mice were humanely killed, liver tissue harvested and qPCR was performed. Stathmin mRNA was normalised to the housekeeping gene beta-2-microglobulin (β 2M) and the human cell specific gene GFP (as the TGL vector contains GFP) to remove signal from contaminating mouse liver cells in the RNA isolates. Data represents the mean \pm SEM (error bars) of 5 individual livers from mice from the saline and Invivofectamine®:stathmin-siRNA treatment groups. ** $p < 0.005$.



6.4 Therapeutic evaluation of *in vivo* stathmin suppression on neuroblastoma metastatic tumour burden in the liver of mice

In order to investigate the influence of *in vivo* stathmin suppression on neuroblastoma metastatic tumour burden, mice at 48 h post-neuroblastoma cell injection were injected once daily for 3 consecutive days with InvivoFectamine®:stathmin-siRNA complexes (at 2 mg of siRNA/kg of mouse weight). In order to enhance, and potentially lengthen the duration of stathmin suppression, the same mice at 12 days post-neuroblastoma cell injection were injected once daily for 3 consecutive days using the above-mentioned complexes. At 23 days-post neuroblastoma cell injection, metastatic tumour burden in the abdomen was assessed by injection with the luciferase substrate, D-luciferin, via intraperitoneal injection and then bioluminescent signal detected using the Xenogen IVIS Imaging System. To quantify metastatic tumour burden, regions of interest (ROIs) were drawn around each mouse and the bioluminescent signal measured as total flux (photons/second). Quantification of mouse abdominal bioluminescence showed that stathmin suppression, using the InvivoFectamine®:stathmin-siRNA complexes, did not significantly influence neuroblastoma metastatic tumour burden compared to InvivoFectamine®:control-siRNA treated mice ($p=0.69$).

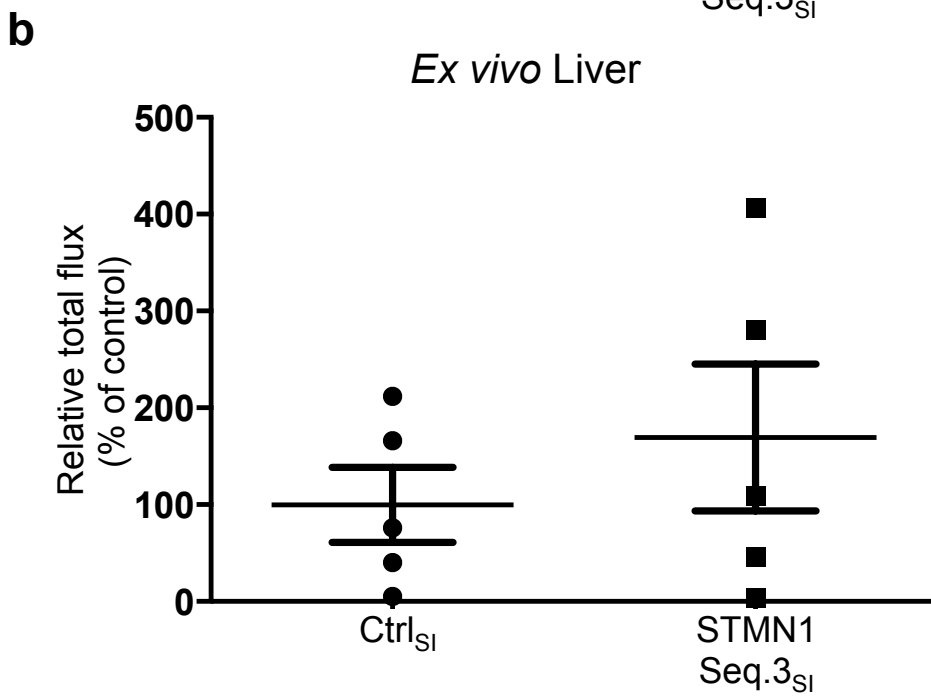
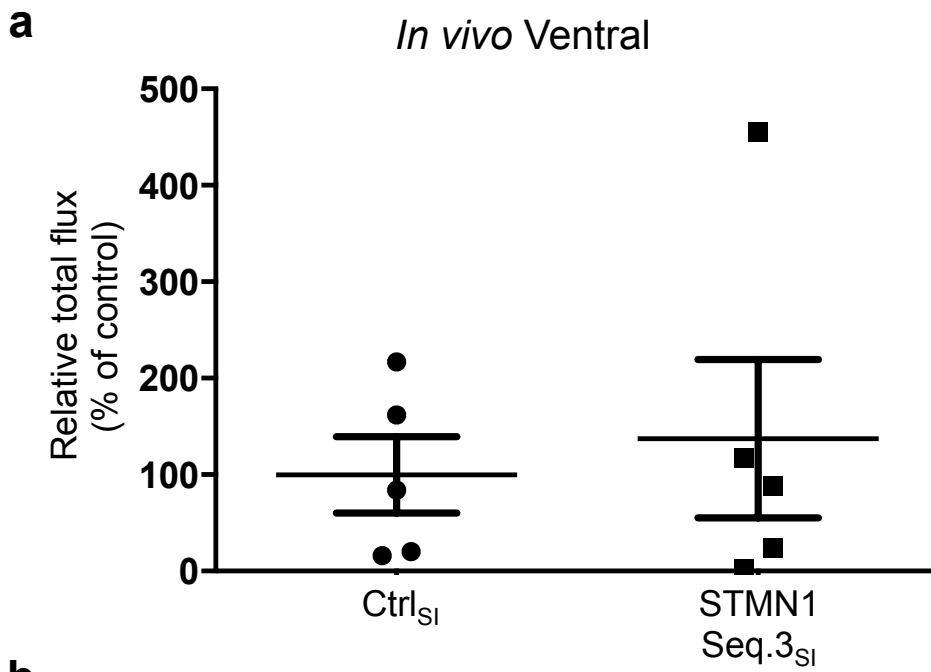
To further investigate the influence of therapeutic stathmin gene suppression on neuroblastoma metastatic tumour burden, *ex vivo* bioluminescence imaging was performed. Shortly after *in vivo* abdominal bioluminescence images were acquired, mice were humanely killed by CO₂ asphyxiation, livers removed and subsequently imaged using the Xenogen

IVIS Imaging System. Neuroblastoma metastases in the liver of mice were detected using bioluminescent imaging. Quantification of mouse liver metastatic tumour burden bioluminescence showed that stathmin suppression, using the InvivoFectamine®:stathmin-siRNA complexes, did not significantly influence neuroblastoma metastatic tumour burden in the liver of mice compared to InvivoFectamine®:control-siRNA treated mice ($p=0.44$).

Altogether, these results indicate that delivering and partially suppressing stathmin expression using a delivery vehicle in neuroblastoma tumour cells does not significantly influence the metastatic tumour burden in the model used in this study.

Figure 6.4 Therapeutic evaluation of stathmin suppression using Invivofectamine™:stathmin siRNA complexes on neuroblastoma metastatic tumour burden in mice

To determine the therapeutic effect of stathmin suppression on neuroblastoma metastatic tumour burden, mice at two and twelve days post-neuroblastoma cell injection were injected once daily for 3 consecutive days with Invivofectamine®:stathmin-siRNA complexes. At 23 days post-neuroblastoma cell injection mice were humanely killed, and *in vivo* abdominal and *ex vivo* liver bioluminescence measured and analysed using the Xenogen IVIS Imaging System. Neuroblastoma tumour burden in the **(a)** abdomen (measured ventrally) of, and **(b)** liver from each mouse from each group was quantified by measuring total flux (photons/sec). Each dot represents one mouse abdomen/liver and each bar represents the mean total flux \pm SEM (error bars) for each group ($n \geq 5$).



6.5 Discussion

This thesis highlighted that stathmin plays a role in multiple steps of the metastatic cascade in neuroblastoma (Chapters 3 and 5) and has given important insights into how stathmin regulates these phenotypes (Chapter 4, Sections 4.5 and 4.7). These findings raised the potential of therapeutically targeting stathmin to decrease neuroblastoma metastasis. To address this, stathmin siRNA was delivered *in vivo* using InvivoFectamine®, which was selected as it has repeatedly been reported in a number of studies to exhibit high levels of liver biodistribution (Piskounova, Polyarchou et al. 2011, Hsu, Yu et al. 2013, Farooq, Hoque et al. 2014, Hattori, Arai et al. 2014, Zhang, Xie et al. 2014). Given in chapter 5 a high metastatic tumour burden was observed in the liver using the metastatic neuroblastoma tumour model, InvivoFectamine® was considered a suitable delivery agent. Importantly, delivery of stathmin siRNA using InvivoFectamine®:stathmin-siRNA significantly reduced stathmin gene expression in metastatic neuroblastoma tumours in mouse liver as measured using qPCR (Fig 6.3).

Suppression of stathmin gene expression did not influence metastatic tumour burden in this model as measured using *in vivo* whole-body and *ex vivo* liver bioluminescence (Fig. 6.4). This result may be due to the limited level of stathmin suppression achieved (~30% at the gene level). This amount of stathmin suppression achieved is markedly different to the experiments using stable stathmin suppression in Chapter 5 (Fig 5.9) and by Byrne *et al.* (Byrne, Yang et al. 2014), where at least 60% stathmin suppression was achieved at the gene level and stathmin suppression was observed to significantly reduce metastasis. This disparity in stathmin suppression levels raises the issue of whether 30% stathmin suppression is sufficient to cause an effect on metastasis in this model. Future experimental changes that

may potentially enhance stathmin gene silencing include increasing the amount of siRNA administered, examination of stathmin suppression duration to ascertain optimal frequency of siRNA administration, and use of active targeting. Active targeting of stathmin siRNA involves the use of a delivery vehicle that is conjugated with a tumour-specific cell surface moiety that may facilitate stathmin siRNA uptake into tumour tissue and enhance stathmin gene suppression. A promising neuroblastoma tumour-specific cell surface moiety is the disialoganglioside G_{D2} , which is ubiquitously expressed on neuroblastoma lesions from all disease stages (Wu, Schwartz et al. 1986) and has very restricted distribution in normal tissues (Svennerholm, Bostrom et al. 1994). Antibodies targeted against G_{D2} have shown efficacy at reducing primary tumour growth and eradicating established metastases in *in vivo* models of neuroblastoma (Mujoo, Cheresch et al. 1987, Pancook, Becker et al. 1996). Additionally, G_{D2} antibodies have successfully been used in the clinic increasing event-free survival and overall survival for patients with highly metastatic disease (Modak and Cheung 2007, Yu, Gilman et al. 2010). Two decades of clinical testing of G_{D2} antibodies have shown that it is safe and results in increased survival for neuroblastoma patients (Ahmed and Cheung 2014).

In addition to the direct effects of G_{D2} antibodies on neuroblastoma tumour cells, the use of G_{D2} antibody targeted therapies has captured recent interest where the conjugation of nanoparticles with G_{D2} antibodies significantly improved the delivery of gene silencing cargo to neuroblastoma cells *in vivo* (Adrian, Wolf et al. 2011, Shen, Gong et al. 2012, Tivnan, Orr et al. 2012). The findings of these studies raise the possibility that conjugation of G_{D2} antibodies to an siRNA delivery vehicle may enable enhanced stathmin suppression. Nanoparticles that have been developed and used by our laboratory that are amenable to conjugation with G_{D2} antibodies include star polymers created using the dimethylaminoethyl

methacrylate monomer, and interfering nanoparticles (iNOPs) composed of functionalized poly-L-lysine dendrimers, which have shown gene silencing efficacy *in vitro* and *in vivo* respectively (Baigude, Su et al. 2013, Boyer, Teo et al. 2013). Additionally, novel phage display-derived neuroblastoma-targeting peptides have recently been developed that bind with high selectivity to patient-derived neuroblastoma cells (Loi, Di Paolo et al. 2013). These neuroblastoma-targeting peptides may increase the transfection efficiency and gene silencing efficacy of nanoparticle:stathmin siRNA complexes.

The lack of effect on metastasis following stathmin suppression should not only be considered in terms of the 30% suppression but also the experimental design. The experiment was designed to deliver stathmin siRNA complexes shortly after neuroblastoma cell injection, and it is possible that tumour cells seeded early before siRNA was delivered and stathmin suppression occurred. Suppression of stathmin after cell seeding would not likely influence tumour burden as I have previously shown, Figs. 3.6 and 3.7, and our laboratory (Byrne, Yang et al. 2014), that stathmin suppression does not influence neuroblastoma cell growth *in vitro* or *in vivo*. Administration of InvivoFectamine®:stathmin-siRNA complexes at the same time as neuroblastoma cell injection may allow stathmin suppression to occur in neuroblastoma cells prior to cell seeding. This would then address whether stathmin is required for the initial seeding phase of metastasis.

Any potential future therapy designed to suppress stathmin expression would be used in combination with other treatments that are already used to treat neuroblastoma such as the chemotherapeutics cisplatin, etoposide, doxorubicin or vincristine (reviewed in Chapter 1, Section 1.1.2). Stathmin expression has been closely associated with chemotherapy drug sensitivity and resistance in numerous malignancies (Iancu, Mistry et al. 2000, Don, Verrills et al. 2004, Mistry and Atweh 2006, Alli, Yang et al. 2007, Kuramitsu, Taba et al. 2010,

Mitra, Kandalam et al. 2011) and therefore further investigation involving the suppression of stathmin expression using InvivoFectamine®:stathmin-siRNA complexes with routine chemotherapeutics will reveal potential effective chemotherapeutic/siRNA combinations.

In addition to combining stathmin targeting and chemotherapeutic drugs, the simultaneous targeting of stathmin with inhibitors against particular members of signalling pathways involved in neuroblastoma metastasis may reduce metastasis in neuroblastoma. Currently our laboratory is investigating how stathmin regulates migration- and metastasis-related proteins which may uncover signalling pathways that when targeted together with stathmin suppression produce a synergistic reduction in metastasis. Furthermore, identification that stathmin is mediating its influence on neuroblastoma cell migration, invasion and metastasis, at least in part via RhoA/ROCK signalling, highlights that targeting certain arms of that pathway such as LIMK or cofilin, may offer novel targeting strategies in combination with stathmin suppression. Moreover, given that stathmin's influence on cell migration in neuroblastoma was shown to be independent of its tubulin binding ability (Chapter 4, Section 4.7), this raises the possibility that stathmin may be mediating its influence via its interacting partners (e.g. p27^{Kip1} see Chapter 4, section 4.8) and that targeting these interacting partners in combination with stathmin suppression may enable enhanced reduction of metastasis in neuroblastoma.

This chapter has examined the therapeutic potential of targeting stathmin using gene silencing. InvivoFectamine® effectively delivered siRNA to neuroblastoma metastatic tumours and partially silenced stathmin gene expression. Whole-body and liver tumour measurements revealed that therapeutic suppression of stathmin expression did not influence neuroblastoma metastasis in this model. However in future, experimental alterations can be made to enhance stathmin gene suppression and simultaneous treatment with

chemotherapeutic agents or pharmacological targeting of other metastasis-related signalling pathways (e.g Rho/ROCK) or stathmin interacting partners (e.g p27^{Kip1}) may collectively enable therapeutic reduction of neuroblastoma metastasis.

Chapter 7. Conclusions and Future Perspectives

Neuroblastoma, the most common extra-cranial solid tumour in children accounts for 6-10% of malignancies under 15 years and disproportionately, 15% of paediatric oncology deaths (Gutierrez, Fischer et al. 2007). Metastatic disease at clinical presentation is highly prevalent and unfortunately carries a dismal 5-year survival rate of 40-50% (Maris 2010). This depressing survival rate highlights the need to address metastatic neuroblastoma. Unfortunately, the mechanisms driving metastasis in neuroblastoma are poorly understood.

Stathmin, a microtubule destabilising protein, is overexpressed and associated with advanced stage disease in numerous malignancies, including neuroblastoma [reviewed in Chapter 1 and (Kavallaris 2012)]. Importantly, a role for stathmin has been identified in neuroblastoma metastasis where suppression of stathmin expression significantly reduced neuroblastoma metastatic tumour burden in the lungs in a clinically relevant orthotopic neuroblastoma mouse model (Byrne, Yang et al. 2014). Despite this, there is limited knowledge of how stathmin is regulating neuroblastoma metastasis.

This thesis addressed the significance of aberrant stathmin expression in neuroblastoma by investigating stathmin's contribution to (1) specific steps of metastasis; (2) potential mechanisms by which stathmin exerts effects in metastasis, and (3) whether stathmin can be therapeutically targeted in metastatic neuroblastoma. Overall, this study increased understanding of the unique role of stathmin in key steps of neuroblastoma metastasis and how it exerts its influence through intracellular signalling pathways.

The studies in this thesis demonstrated that suppression of stathmin expression did not influence neuroblastoma cell proliferation or sensitivity to anoikis. In contrast, stathmin suppression significantly decreased chemotactic-induced cell migration and invasion. This observation supports a previous finding from our laboratory (Byrne, Yang et al. 2014) using four separate siRNA sequences combined in a pooled sample. In the latter parts of this thesis, therapeutic targeting using stathmin siRNA was proposed. For these studies single siRNA sequences (as opposed to pooled sequences) were required. Therefore, as part of the current study the therapeutic targeting of stathmin using single siRNA sequences was investigated. Hence, single siRNA sequences were validated and used for migration and invasion assays. The observation that stathmin suppression reduced neuroblastoma cell migration and invasion is in agreement with the findings showing that stathmin is important in the migration and invasion of various tumour cells [(Belletti, Nicoloso et al. 2008, Singer, Malz et al. 2009, Gan, Guo et al. 2010, Jeon, Han et al. 2010, Liu, Sun et al. 2013) and reviewed in Chapter 1, Section 1.4.4]. These studies variably used either 2D scratch assays (Singer, Malz et al. 2009, Liu, Sun et al. 2013) or 3D transwell migration assays (Belletti, Nicoloso et al. 2008, Gan, Guo et al. 2010, Jeon, Han et al. 2010) and each showed that stathmin suppression reduced cell migration. It is interesting to see the same result (i.e. reduced cell migration upon stathmin suppression) for both 2D and 3D migration assays as the type of motility assay used has, in some situations, led to discrepancies in the results obtained (Baldassarre, Belletti et al. 2005). Notably, previous findings from our laboratory indicated that stathmin does not play a role in 2D neuroblastoma cell migration (unpublished findings) but in contrast stathmin is important in 3D transwell neuroblastoma cell migration (Byrne, Yang et al. 2014). Baldassarre and colleagues have discussed how in 3D based migration assays increased microtubule stability may, through altering cell motility to one lacking polarisation could act

as an inhibitor of cell migration, whereas in 2D based assays increased microtubule stability promotes cell polarisation to promote cell migration (Baldassarre, Belletti et al. 2005). The variability in cell migration results between different types of tumour cell lines and migration assays used suggests that stathmin's role in migration may potentially be cell type specific and that careful consideration needs to be taken when selecting 2D or 3D migration assays as they appear to examine different aspects of cell migration. Additionally, the novel findings in this thesis that showed reduced invasion of neuroblastoma cells from 3D tumour spheroids into a 3D extracellular matrix further exemplifies stathmin's importance in the invasive phenotype in neuroblastoma.

In Chapter 3, Section 3.8 a functional role for stathmin in the extravasation step of metastasis was highlighted, where stathmin suppression significantly reduced *in vitro* transendothelial migration of neuroblastoma cells. Whilst this thesis identified a role for stathmin in *in vitro* transendothelial migration it was unknown whether stathmin was important in *in vivo* transendothelial migration (i.e. extravasation). Use of an experimental metastasis mouse model specifically examining the extravasation step of the metastatic cascade led to the observation that stathmin suppression significantly reduced total whole-body, liver and lung metastatic tumour burden. While the matrix metalloproteinases MMP-2 and MMP-9 (Chantrain, Shimada et al. 2004) and the insulin-like growth factor-1 receptor (van Golen, Schwab et al. 2006) have been shown to be involved in neuroblastoma extravasation, this is the first time that stathmin has been observed to play an important role in the extravasation of neuroblastoma cells *in vivo*.

This thesis highlighted that stathmin was influencing transendothelial migration, at least in part, via ROCK signalling. ROCK activity is a key regulator of the transition between alternative modes of migration and invasion (Sahai and Marshall 2003). A rounded or

elongated cell shape in a 3D environment is generally indicative of different ROCK activity status in a cell (Sahai and Marshall 2003). Belletti and colleagues examined the role of stathmin in the control of sarcoma cell shape in 3D matrices. They observed that increased stathmin activity resulted in a more rounded sarcoma cell phenotype (Belletti, Nicoloso et al. 2008). Unfortunately, the effect of increased stathmin activity on ROCK signalling in sarcoma cells was not examined. The influence of altered stathmin expression levels on regulating mode of invasion in neuroblastoma cells was not presented in this thesis and warrants future investigation.

Whilst this thesis identified that stathmin influenced transendothelial migration, at least in part, via ROCK signalling, it is unknown whether stathmin exerts its effects on transendothelial migration by directly acting upon ROCK or independently through upstream Rho GTPases. Examination of the activation of upstream Rho GTPases identified that stathmin suppression did not influence Rac1 or Cdc42 activation whereas stathmin suppression led to hyperactivation of RhoA suggesting that stathmin regulates ROCK directly or indirectly by activating the upstream Rho GTPase, RhoA. The above observation was performed using whole cell lysates however the activation of Rho GTPases is spatially controlled during cell migration (Etienne-Manneville and Hall 2002). Hence, to gain an understanding of the spatial distribution of RhoA activation, further work is required to determine if stathmin suppression alters the spatial and temporal regulation of RhoA activation. A RhoA activation biosensor has been developed and has shown that RhoA is active at the leading cell edge during migration (Kurokawa and Matsuda 2005, Pertz, Hodgson et al. 2006, Machacek, Hodgson et al. 2009). Future studies using this biosensor could enable the determination of whether stathmin controls RhoA activation in neuroblastoma cells in a spatial and temporal manner.

Whilst no significant alteration in either Rac1 or Cdc42 activation levels in stathmin suppressed cells was observed, this does not preclude that there may be spatial changes in Rac1 or Cdc42 activation upon stathmin suppression that is unable to be resolved or determined using a whole cell lysate-based assay. Biosensors for Rac1 and Cdc42 have also been developed and may help uncover if stathmin regulates Rac1 or Cdc42 activation spatially or temporally (Kraynov, Chamberlain et al. 2000, Nalbant, Hodgson et al. 2004). Moreover, a stathmin-based FRET-biosensor has been developed that enables the examination of spatial and temporal stathmin activation and tubulin-binding ability (Niethammer, Bastiaens et al. 2004). Gradients of stathmin activation have been observed both during interphase in motile lamella protrusions and in mitosis near chromosomes (Niethammer, Bastiaens et al. 2004). These stathmin-tubulin interaction patterns likely echo stathmin phosphorylation in these areas. Local stathmin phosphorylation and inactivation around mitotic chromosomes appears to be required for correct spindle assembly during mitosis. Similarly, inactivation of stathmin at the lamella is likely responsible for microtubule stabilisation and growth in these areas (Niethammer, Bastiaens et al. 2004). If stathmin is regulating RhoA, Rac1 or Cdc42 activation in a spatial or temporal manner the use of the stathmin-based FRET-biosensor will enable the examination of whether stathmin's influence on Rho GTPase activation is due to localised changes in stathmin activation.

To identify how stathmin may be regulating RhoA activation, the relationship between stathmin and the Rho GTPase regulatory proteins, the Rho GEFs, was examined. The regulation of RhoA activation is complex where 23 Rho GEFs display specificity towards RhoA, with 10 of these displaying unique specificity [reviewed in (Rossman, Der et al. 2005)]. Out of these 23 Rho GEFs, GEF-H1 was selected for examination, as the interaction of GEF-H1 with microtubules has been shown to be key to its control of RhoA activation

(Krendel, Zenke et al. 2002, Birukova, Adyshev et al. 2006, Chang, Nalbant et al. 2008, Kakiashvili, Speight et al. 2009). In this thesis, stathmin suppression was found not to influence the association of GEF-H1 with microtubules in neuroblastoma suggesting that stathmin is not regulating RhoA activation via alteration of GEF-H1 microtubule association. In order to further understand how stathmin is regulating RhoA, examination of the only other known Rho GEF that is regulated by microtubule binding, GEF p190RhoGEF (van Horck, Ahmadian et al. 2001) warrants further investigation. Though due to timing restrictions this examination was not performed in this study.

Stathmin's best-studied functions are related to its ability to bind tubulin and regulate microtubule dynamics. Though stathmin has also been shown to bind to other proteins, some of which are involved in cell migration and invasion [reviewed in (Belletti and Baldassarre 2011)], such as p27^{Kip1} (Baldassarre, Belletti et al. 2005, Belletti, Pellizzari et al. 2010) and STAT3 (Ng, Lin et al. 2006, Verma, Dourlat et al. 2009). This raises the possibility that stathmin's influence on neuroblastoma cell migration is via its interaction with proteins other than tubulin and that stathmin is acting independent of tubulin binding. This was addressed by examining whether stathmin was influencing neuroblastoma cell migration in a microtubule dependent or independent manner. Wild-type stathmin, and a stathmin pseudophosphorylated mutant protein with impaired tubulin binding (Niethammer, Bastiaens et al. 2004) were used to restore stathmin levels in the neuroblastoma stathmin shRNA cells. Wild-type stathmin returned the stathmin suppression-induced reduction of cell migration in neuroblastoma cells back to control levels, thus providing the first evidence that stathmin has a direct effect on cell migration. Importantly, restoration of stathmin levels with the mutant pseudophosphorylated stathmin protein with defective tubulin binding also returned cell migration back to control levels. This observation suggests that stathmin's influence on the

cell migratory phenotype in neuroblastoma is microtubule independent. In order to gain further insight into how stathmin is regulating cell migration in a microtubule independent manner, investigation of stathmin-interacting proteins (e.g. p27^{Kip1}) may assist in more wholly identifying stathmin's role in regulating neuroblastoma cell migration and metastasis. p27^{Kip1} is a protein that is largely studied for its role as a cyclin-dependent kinase inhibitor during the cell cycle (Sherr and Roberts 1999). p27^{Kip1} is inactivated in many different types of cancer and has emerged as a regulator of cell motility and RhoA activation (Besson, Gurian-West et al. 2004, Baldassarre, Belletti et al. 2005, Belletti, Nicoloso et al. 2005). p27^{Kip1} is particularly interesting as its ability to regulate cell motility and RhoA activation is tied to its ability to bind to and impair the activity of stathmin (Baldassarre, Belletti et al. 2005). p27^{Kip1} acts as an inhibitor of cell motility in multiple cell types (Goukassian, Diez-Juan et al. 2001, Sun, Marx et al. 2001, Daniel, Pippin et al. 2004, Baldassarre, Belletti et al. 2005). Modulation of p27^{Kip1} and stathmin levels led to alterations in sarcoma migration and invasion leading to the suggestion that the p27^{Kip1}/stathmin ratio is the determinant of migratory and invasive phenotype. Additionally, the p27^{Kip1}/stathmin ratio was observed to be elevated in primary sarcomas in comparison to metastatic disease (Baldassarre, Belletti et al. 2005). Further investigations involving the modulation of p27^{Kip1} and stathmin levels examining cell migration, invasion, transendothelial migration and RhoA activation may provide key insights into whether stathmin is regulating the cell migratory phenotype in neuroblastoma through its interaction with p27^{Kip1}.

Given the evidence that stathmin is involved in neuroblastoma metastasis, this raises the possibility that targeting stathmin may provide a suitable avenue to target metastasis in neuroblastoma. Whilst there are currently no known pharmacological stathmin inhibitors, several studies have examined the therapeutic potential of targeting stathmin through the

delivery of siRNA/shRNA constructs to reduce stathmin expression in multiple malignancies (Zhang, Wang et al. 2006, Phadke, Jay et al. 2011). Moreover, a survivin promoter-driven siRNA expression vector designed to target stathmin for gene knockdown was incubated with cervical cancer and osteosarcoma cells and resulted in significant inhibition of stathmin expression and a marked growth inhibition (Zhang, Wang et al. 2006). Furthermore, miRNA/siRNA composites were highly effective in the suppression of stathmin gene expression in colorectal and melanoma cells *in vitro*. Additionally, injection of the miRNA/siRNA composites into colorectal and melanoma xenografts showed significant xenograft growth inhibition (Phadke, Jay et al. 2011). This thesis examined the therapeutic potential of targeting stathmin to decrease metastasis by delivery of stathmin siRNA using InvivoFectamine®. InvivoFectamine® delivered stathmin siRNA and achieved significant stathmin gene suppression *in vivo*. Though the amount of stathmin gene knockdown was markedly less (~30%) than that achieved in the experiments using stable stathmin suppression (~60%) in this study (Fig. 5.9) and by Byrne *et al.* (Byrne, Yang et al. 2014). Whether more potent *in vivo* knockdown of stathmin expression is required to see an effect remains to be resolved. Potential future investigations that may enhance stathmin gene knockdown might include optimising the dosage regime and exploiting active targeting by conjugating a tumour-specific moiety to the siRNA delivery vehicle. One potential avenue of active targeted siRNA delivery in neuroblastoma is the exploitation of the disialoganglioside G_{D2}, which has high expression on neuroblastoma tumours and very restricted expression elsewhere in the body (Wu, Schwartz et al. 1986, Svennerholm, Bostrom et al. 1994). G_{D2} antibodies are successfully being used in the clinic and have increased event-free survival and overall survival for patients with highly metastatic disease (Modak and Cheung 2007, Yu, Gilman et al. 2010). Additionally, G_{D2} antibodies have recently been used to actively target

nanoparticles to improve gene silencing cargo delivery in neuroblastoma cells *in vivo* (Adrian, Wolf et al. 2011, Shen, Gong et al. 2012, Tivnan, Orr et al. 2012). As outlined above, therapeutic suppression of stathmin expression did not influence metastasis in our model. This may be due to the neuroblastoma cells seeding prior to effective stathmin suppression, and when stathmin suppression occurs after cell seeding it is likely that stathmin gene knockdown doesn't influence the growth of the metastatic tumours as evidenced by the data from this thesis and our laboratory (Byrne, Yang et al. 2014), highlighting that stathmin suppression doesn't influence the growth of neuroblastoma cells *in vitro* and *in vivo*. Injection of InvivoFectamine®:stathmin-siRNA complexes simultaneously with the neuroblastoma cells may enable earlier stathmin suppression to occur and potentially decrease metastasis.

Many modern approaches to cancer therapy are combination therapies targeting multiple targets simultaneously. It is likely any therapies aimed at suppressing stathmin expression would incorporate the concurrent attack of other targets by using routine chemotherapeutics. Indeed, modulation of stathmin levels has been closely associated with the modification of drug sensitivity and resistance in multiple malignancies (Iancu, Mistry et al. 2000, Don, Verrills et al. 2004, Mistry and Atweh 2006, Alli, Yang et al. 2007, Kuramitsu, Taba et al. 2010, Mitra, Kandalam et al. 2011). Further work is now required to determine if altered stathmin expression levels in neuroblastoma influences drug sensitivity or resistance *in vivo*.

Overall, this thesis provides new insights into the role of stathmin in neuroblastoma, including but not limited to it being involved in neuroblastoma cell transendothelial migration, RhoA/ROCK signalling and cell migration in a microtubule independent manner. Results from this thesis may have important therapeutic significance as targeting stathmin,

and in particular in combination with chemotherapy or targeted therapies, could lead to a reduction in neuroblastoma metastasis and ultimately increase patient survival.

Chapter 8. References

- Adrian, J. E., A. Wolf, A. Steinbach, J. Rossler and R. Suss (2011). "Targeted delivery to neuroblastoma of novel siRNA-anti-GD2-liposomes prepared by dual asymmetric centrifugation and sterol-based post-insertion method." Pharm Res **28**(9): 2261-2272.
- Ahmed, M. and N. K. Cheung (2014). "Engineering anti-GD2 monoclonal antibodies for cancer immunotherapy." FEBS Lett **588**(2): 288-297.
- Akhmanova, A. and C. C. Hoogenraad (2005). "Microtubule plus-end-tracking proteins: mechanisms and functions." Curr Opin Cell Biol **17**(1): 47-54.
- Akhmanova, A. and M. O. Steinmetz (2008). "Tracking the ends: a dynamic protein network controls the fate of microtubule tips." Nat Rev Mol Cell Biol **9**(4): 309-322.
- Alli, E., J. M. Yang, J. M. Ford and W. N. Hait (2007). "Reversal of stathmin-mediated resistance to paclitaxel and vinblastine in human breast carcinoma cells." Mol Pharmacol **71**(5): 1233-1240.
- Amayed, P., D. Pantaloni and M. F. Carlier (2002). "The effect of stathmin phosphorylation on microtubule assembly depends on tubulin critical concentration." J Biol Chem **277**(25): 22718-22724.
- Ara, T. and Y. A. DeClerck (2006). "Mechanisms of invasion and metastasis in human neuroblastoma." Cancer Metastasis Rev **25**(4): 645-657.
- Bagheri-Yarmand, R., A. Mazumdar, A. A. Sahin and R. Kumar (2006). "LIM kinase 1 increases tumor metastasis of human breast cancer cells via regulation of the urokinase-type plasminogen activator system." Int J Cancer **118**(11): 2703-2710.
- Baigude, H., J. Su, J. McCarroll and T. M. Rana (2013). "In Vivo Delivery of RNAi by Reducible Interfering Nanoparticles (iNOPs)." ACS Med Chem Lett **4**(8): 720-723.
- Baldassarre, G., B. Belletti, M. S. Nicoloso, M. Schiappacassi, A. Vecchione, P. Spessotto, A. Morrione, V. Canzonieri and A. Colombatti (2005). "p27(Kip1)-stathmin interaction influences sarcoma cell migration and invasion." Cancer Cell **7**(1): 51-63.
- Belletti, B. and G. Baldassarre (2011). "Stathmin: a protein with many tasks. New biomarker and potential target in cancer." Expert opinion on therapeutic targets **15**(11): 1249-1266.
- Belletti, B., M. S. Nicoloso, M. Schiappacassi, S. Berton, F. Lovat, K. Wolf, V. Canzonieri, S. D'Andrea, A. Zucchetto, P. Friedl, A. Colombatti and G. Baldassarre (2008). "Stathmin activity influences sarcoma cell shape, motility, and metastatic potential." Mol Biol Cell **19**(5): 2003-2013.
- Belletti, B., M. S. Nicoloso, M. Schiappacassi, E. Chimienti, S. Berton, F. Lovat, A. Colombatti and G. Baldassarre (2005). "p27(kip1) functional regulation in human cancer: a potential target for therapeutic designs." Curr Med Chem **12**(14): 1589-1605.

Belletti, B., I. Pellizzari, S. Berton, L. Fabris, K. Wolf, F. Lovat, M. Schiappacassi, S. D'Andrea, M. S. Nicoloso, S. Lovisa, M. Sonogo, P. Defilippi, A. Vecchione, A. Colombatti, P. Friedl and G. Baldassarre (2010). "p27kip1 controls cell morphology and motility by regulating microtubule-dependent lipid raft recycling." Mol Cell Biol **30**(9): 2229-2240.

Beretta, L., T. Dobransky and A. Sobel (1993). "Multiple phosphorylation of stathmin. Identification of four sites phosphorylated in intact cells and in vitro by cyclic AMP-dependent protein kinase and p34cdc2." J Biol Chem **268**(27): 20076-20084.

Beretta, L., M. F. Dubois, A. Sobel and O. Bensaude (1995). "Stathmin is a major substrate for mitogen-activated protein kinase during heat shock and chemical stress in HeLa cells." Eur J Biochem **227**(1-2): 388-395.

Bernard, O. (2007). "Lim kinases, regulators of actin dynamics." Int J Biochem Cell Biol **39**(6): 1071-1076.

Besson, A., M. Gurian-West, A. Schmidt, A. Hall and J. M. Roberts (2004). "p27Kip1 modulates cell migration through the regulation of RhoA activation." Genes Dev **18**(8): 862-876.

Bhat, K. M. and V. Setaluri (2007). "Microtubule-associated proteins as targets in cancer chemotherapy." Clin Cancer Res **13**(10): 2849-2854.

Bieche, I., A. Maucuer, I. Laurendeau, S. Lachkar, A. J. Spano, A. Frankfurter, P. Levy, V. Manceau, A. Sobel, M. Vidaud and P. A. Curmi (2003). "Expression of stathmin family genes in human tissues: non-neural-restricted expression for SCLIP." Genomics **81**(4): 400-410.

Birukova, A. A., D. Adyshev, B. Gorshkov, G. M. Bokoch, K. G. Birukov and A. D. Verin (2006). "GEF-H1 is involved in agonist-induced human pulmonary endothelial barrier dysfunction." Am J Physiol Lung Cell Mol Physiol **290**(3): L540-548.

Boehm, M., T. Yoshimoto, M. F. Crook, S. Nallamshetty, A. True, G. J. Nabel and E. G. Nabel (2002). "A growth factor-dependent nuclear kinase phosphorylates p27(Kip1) and regulates cell cycle progression." EMBO J **21**(13): 3390-3401.

Boyer, C., J. Teo, P. Phillips, R. B. Erlich, S. Sagnella, G. Sharbeen, T. Dwarto, H. T. Duong, D. Goldstein, T. P. Davis, M. Kavallaris and J. McCarroll (2013). "Effective delivery of siRNA into cancer cells and tumors using well-defined biodegradable cationic star polymers." Mol Pharm **10**(6): 2435-2444.

Brattsand, G., U. Marklund, K. Nylander, G. Roos and M. Gullberg (1994). "Cell-cycle-regulated phosphorylation of oncoprotein 18 on Ser16, Ser25 and Ser38." Eur J Biochem **220**(2): 359-368.

Brodeur, G. M. (2003). "Neuroblastoma: biological insights into a clinical enigma." Nat Rev Cancer **3**(3): 203-216.

Brodeur, G. M. and R. C. Seeger (1986). "Gene amplification in human neuroblastomas: basic mechanisms and clinical implications." Cancer Genet Cytogenet **19**(1-2): 101-111.

Budde, P. P., A. Kumagai, W. G. Dunphy and R. Heald (2001). "Regulation of Op18 during spindle assembly in *Xenopus* egg extracts." J Cell Biol **153**(1): 149-158.

Burbelo, P. D., D. Drechsel and A. Hall (1995). "A conserved binding motif defines numerous candidate target proteins for both Cdc42 and Rac GTPases." J Biol Chem **270**(49): 29071-29074.

Byrne, F. L., L. Yang, P. A. Phillips, L. M. Hansford, J. I. Fletcher, C. J. Ormandy, J. A. McCarroll and M. Kavallaris (2014). "RNAi-mediated stathmin suppression reduces lung metastasis in an orthotopic neuroblastoma mouse model." Oncogene.

Calderwood, S. K., M. A. Khaleque, D. B. Sawyer and D. R. Ciocca (2006). "Heat shock proteins in cancer: chaperones of tumorigenesis." Trends Biochem Sci **31**(3): 164-172.

Capetanaki, Y., R. J. Bloch, A. Kouloumenta, M. Mavroidis and S. Psarras (2007). "Muscle intermediate filaments and their links to membranes and membranous organelles." Exp Cell Res **313**(10): 2063-2076.

Carr, J., N. P. Bown, M. C. Case, A. G. Hall, J. Lunec and D. A. Tweddle (2007). "High-resolution analysis of allelic imbalance in neuroblastoma cell lines by single nucleotide polymorphism arrays." Cancer Genet Cytogenet **172**(2): 127-138.

Cassimeris, L. (2002). "The oncoprotein 18/stathmin family of microtubule destabilizers." Curr Opin Cell Biol **14**(1): 18-24.

Castleberry, R. P. (1997). "Neuroblastoma." Eur J Cancer **33**(9): 1430-1437; discussion 1437-1438.

Chang, L. and R. D. Goldman (2004). "Intermediate filaments mediate cytoskeletal crosstalk." Nat Rev Mol Cell Biol **5**(8): 601-613.

Chang, Y. C., P. Nalbant, J. Birkenfeld, Z. F. Chang and G. M. Bokoch (2008). "GEF-H1 couples nocodazole-induced microtubule disassembly to cell contractility via RhoA." Mol Biol Cell **19**(5): 2147-2153.

Chantrain, C. F., H. Shimada, S. Jodele, S. Groshen, W. Ye, D. R. Shalinsky, Z. Werb, L. M. Coussens and Y. A. DeClerck (2004). "Stromal matrix metalloproteinase-9 regulates the vascular architecture in neuroblastoma by promoting pericyte recruitment." Cancer Res **64**(5): 1675-1686.

Cheng, T. L., M. Symons and T. S. Jou (2004). "Regulation of anoikis by Cdc42 and Rac1." Exp Cell Res **295**(2): 497-511.

Chesler, L., D. D. Goldenberg, R. Collins, M. Grimmer, G. E. Kim, T. Tihan, K. Nguyen, S. Yakovenko, K. K. Matthay and W. A. Weiss (2008). "Chemotherapy-induced apoptosis in a transgenic model of neuroblastoma proceeds through p53 induction." Neoplasia **10**(11): 1268-1274.

Chneiweiss, H., L. Beretta, J. Cordier, M. C. Bouterin, J. Glowinski and A. Sobel (1989). "Stathmin is a major phosphoprotein and cyclic AMP-dependent protein kinase substrate in

- mouse brain neurons but not in astrocytes in culture: regulation during ontogenesis." J Neurochem **53**(3): 856-863.
- Collazo, J., B. Zhu, S. Larkin, S. K. Martin, H. Pu, C. Horbinski, S. Koochekpour and N. Kyprianou (2014). "Cofilin drives cell-invasive and metastatic responses to TGF-beta in prostate cancer." Cancer Res **74**(8): 2362-2373.
- Curmi, P. A., S. S. Andersen, S. Lachkar, O. Gavet, E. Karsenti, M. Knossow and A. Sobel (1997). "The stathmin/tubulin interaction in vitro." J Biol Chem **272**(40): 25029-25036.
- Curmi, P. A., O. Gavet, E. Charbaut, S. Ozon, S. Lachkar-Colmerauer, V. Manceau, S. Siavoshian, A. Maucuer and A. Sobel (1999). "Stathmin and its phosphoprotein family: general properties, biochemical and functional interaction with tubulin." Cell Struct Funct **24**(5): 345-357.
- Daniel, C., J. Pippin, S. J. Shankland and C. Hugo (2004). "The rapamycin derivative RAD inhibits mesangial cell migration through the CDK-inhibitor p27KIP1." Lab Invest **84**(5): 588-596.
- Davis, M. E., J. E. Zuckerman, C. H. Choi, D. Seligson, A. Tolcher, C. A. Alabi, Y. Yen, J. D. Heidel and A. Ribas (2010). "Evidence of RNAi in humans from systemically administered siRNA via targeted nanoparticles." Nature **464**(7291): 1067-1070.
- Delaloy, C., L. Liu, J. A. Lee, H. Su, F. Shen, G. Y. Yang, W. L. Young, K. N. Ivey and F. B. Gao (2010). "MicroRNA-9 coordinates proliferation and migration of human embryonic stem cell-derived neural progenitors." Cell Stem Cell **6**(4): 323-335.
- Deschesnes, R. G., A. Patenaude, J. L. Rousseau, J. S. Fortin, C. Ricard, M. F. Cote, J. Huot, C. G. R and E. Petitclerc (2007). "Microtubule-destabilizing agents induce focal adhesion structure disorganization and anoikis in cancer cells." J Pharmacol Exp Ther **320**(2): 853-864.
- Don, S., N. M. Verrills, T. Y. Liaw, M. L. Liu, M. D. Norris, M. Haber and M. Kavallaris (2004). "Neuronal-associated microtubule proteins class III beta-tubulin and MAP2c in neuroblastoma: role in resistance to microtubule-targeted drugs." Mol Cancer Ther **3**(9): 1137-1146.
- Dowling, P., P. Meleady, A. Dowd, M. Henry, S. Glynn and M. Clynes (2007). "Proteomic analysis of isolated membrane fractions from superinvasive cancer cells." Biochim Biophys Acta **1774**(1): 93-101.
- Doye, V., M. C. Bouterin and A. Sobel (1990). "Phosphorylation of stathmin and other proteins related to nerve growth factor-induced regulation of PC12 cells." J Biol Chem **265**(20): 11650-11655.
- DuBois, S. G., Y. Kalika, J. N. Lukens, G. M. Brodeur, R. C. Seeger, J. B. Atkinson, G. M. Haase, C. T. Black, C. Perez, H. Shimada, R. Gerbing, D. O. Stram and K. K. Matthay (1999). "Metastatic sites in stage IV and IVS neuroblastoma correlate with age, tumor biology, and survival." J Pediatr Hematol Oncol **21**(3): 181-189.

Dubois, S. G., W. B. London, Y. Zhang, K. K. Matthay, T. Monclair, P. F. Ambros, S. L. Cohn, A. Pearson and L. Diller (2008). "Lung metastases in neuroblastoma at initial diagnosis: A report from the International Neuroblastoma Risk Group (INRG) project." Pediatr Blood Cancer **51**(5): 589-592.

Edwards, D. C., L. C. Sanders, G. M. Bokoch and G. N. Gill (1999). "Activation of LIM-kinase by Pak1 couples Rac/Cdc42 GTPase signalling to actin cytoskeletal dynamics." Nat Cell Biol **1**(5): 253-259.

Eichenmuller, B., P. Everley, J. Palange, D. Lepley and K. A. Suprenant (2002). "The human EMAP-like protein-70 (ELP70) is a microtubule destabilizer that localizes to the mitotic apparatus." J Biol Chem **277**(2): 1301-1309.

Etienne-Manneville, S. and A. Hall (2002). "Rho GTPases in cell biology." Nature **420**(6916): 629-635.

Farooq, A., R. Hoque, X. Ouyang, A. Farooq, A. Ghani, K. Ahsan, M. Guerra and W. Z. Mehal (2014). "Activation of N-methyl-d-aspartate receptor downregulates inflammasome activity and liver inflammation via a beta-arrestin-2 pathway." Am J Physiol Gastrointest Liver Physiol **307**(7): G732-740.

Ferrari, A. C., H. N. Seunanz, S. M. Hanash and G. F. Atweh (1990). "A gene that encodes for a leukemia-associated phosphoprotein (p18) maps to chromosome bands 1p35-36.1." Genes Chromosomes Cancer **2**(2): 125-129.

Feuerstein, N. and H. L. Cooper (1983). "Rapid protein phosphorylation induced by phorbol ester in HL-60 cells. Unique alkali-stable phosphorylation of a 17,000-dalton protein detected by two-dimensional gel electrophoresis." J Biol Chem **258**(17): 10786-10793.

Fife, C. M., McCarroll, J. M., Kavallaris, M. (2014). "Movers and shakers: cell cytoskeleton in cancer metastasis." British Journal of Pharmacology.

Frisch, S. M. and R. A. Screaton (2001). "Anoikis mechanisms." Curr Opin Cell Biol **13**(5): 555-562.

Gan, L., K. Guo, Y. Li, X. Kang, L. Sun, H. Shu and Y. Liu (2010). "Up-regulated expression of stathmin may be associated with hepatocarcinogenesis." Oncol Rep **23**(4): 1037-1043.

Gavet, O., S. Ozon, V. Manceau, S. Lawler, P. Curmi and A. Sobel (1998). "The stathmin phosphoprotein family: intracellular localization and effects on the microtubule network." J Cell Sci **111** (Pt **22**): 3333-3346.

Giampietro, C., F. Luzzati, G. Gambarotta, P. Giacobini, E. Boda, A. Fasolo and I. Perroteau (2005). "Stathmin expression modulates migratory properties of GN-11 neurons in vitro." Endocrinology **146**(4): 1825-1834.

Goukassian, D., A. Diez-Juan, T. Asahara, P. Schratzberger, M. Silver, T. Murayama, J. M. Isner and V. Andres (2001). "Overexpression of p27(Kip1) by doxycycline-regulated

- adenoviral vectors inhibits endothelial cell proliferation and migration and impairs angiogenesis." FASEB J **15**(11): 1877-1885.
- Green, K. J. and J. C. Jones (1996). "Desmosomes and hemidesmosomes: structure and function of molecular components." FASEB J **10**(8): 871-881.
- Gunnensen, J. M., V. Spirkoska, P. E. Smith, R. A. Danks and S. S. Tan (2000). "Growth and migration markers of rat C6 glioma cells identified by serial analysis of gene expression." Glia **32**(2): 146-154.
- Gunning, P., G. O'Neill and E. Hardeman (2008). "Tropomyosin-based regulation of the actin cytoskeleton in time and space." Physiol Rev **88**(1): 1-35.
- Gutierrez, J. C., A. C. Fischer, J. E. Sola, E. A. Perez and L. G. Koniaris (2007). "Markedly improving survival of neuroblastoma: a 30-year analysis of 1,646 patients." Pediatr Surg Int **23**(7): 637-646.
- Hailat, N., J. Strahler, R. Melhem, X. X. Zhu, G. Brodeur, R. C. Seeger, C. P. Reynolds and S. Hanash (1990). "N-myc gene amplification in neuroblastoma is associated with altered phosphorylation of a proliferation related polypeptide (Op18)." Oncogene **5**(11): 1615-1618.
- Hall, A. (2012). "Rho family GTPases." Biochem Soc Trans **40**(6): 1378-1382.
- Hanahan, D. and R. A. Weinberg (2011). "Hallmarks of cancer: the next generation." Cell **144**(5): 646-674.
- Hanash, S. M., J. R. Strahler, R. Kuick, E. H. Chu and D. Nichols (1988). "Identification of a polypeptide associated with the malignant phenotype in acute leukemia." J Biol Chem **263**(26): 12813-12815.
- Hattori, Y., S. Arai, R. Okamoto, M. Hamada, K. Kawano and E. Yonemochi (2014). "Sequential intravenous injection of anionic polymer and cationic lipoplex of siRNA could effectively deliver siRNA to the liver." Int J Pharm **476**(1-2): 289-298.
- Herz, H. M. and A. Bergmann (2009). "Genetic analysis of ESCRT function in Drosophila: a tumour model for human Tsg101." Biochem Soc Trans **37**(Pt 1): 204-207.
- Hodgson, L., F. Shen and K. Hahn (2010). "Biosensors for characterizing the dynamics of rho family GTPases in living cells." Curr Protoc Cell Biol **Chapter 14**: Unit 14 11 11-26.
- Holmfeldt, P., K. Brannstrom, S. Stenmark and M. Gullberg (2006). "Aneugenic activity of Op18/stathmin is potentiated by the somatic Q18-->e mutation in leukemic cells." Mol Biol Cell **17**(7): 2921-2930.
- Holmfeldt, P., N. Larsson, B. Segerman, B. Howell, J. Morabito, L. Cassimeris and M. Gullberg (2001). "The catastrophe-promoting activity of ectopic Op18/stathmin is required for disruption of mitotic spindles but not interphase microtubules." Mol Biol Cell **12**(1): 73-83.

- Holmfeldt, P., M. E. Sellin and M. Gullberg (2010). "Upregulated Op18/stathmin activity causes chromosomal instability through a mechanism that evades the spindle assembly checkpoint." Exp Cell Res **316**(12): 2017-2026.
- Horita, Y., K. Ohashi, M. Mukai, M. Inoue and K. Mizuno (2008). "Suppression of the invasive capacity of rat ascites hepatoma cells by knockdown of Slingshot or LIM kinase." J Biol Chem **283**(10): 6013-6021.
- Horwitz, S. B., H. J. Shen, L. He, P. Dittmar, R. Neef, J. Chen and U. K. Schubart (1997). "The microtubule-destabilizing activity of metablastin (p19) is controlled by phosphorylation." J Biol Chem **272**(13): 8129-8132.
- Howell, B., N. Larsson, M. Gullberg and L. Cassimeris (1999). "Dissociation of the tubulin-sequestering and microtubule catastrophe-promoting activities of oncoprotein 18/stathmin." Mol Biol Cell **10**(1): 105-118.
- Hsieh, S. Y., S. F. Huang, M. C. Yu, T. S. Yeh, T. C. Chen, Y. J. Lin, C. J. Chang, C. M. Sung, Y. L. Lee and C. Y. Hsu (2010). "Stathmin1 overexpression associated with polyploidy, tumor-cell invasion, early recurrence, and poor prognosis in human hepatoma." Mol Carcinog **49**(5): 476-487.
- Hsu, S. H., B. Yu, X. Wang, Y. Lu, C. R. Schmidt, R. J. Lee, L. J. Lee, S. T. Jacob and K. Ghoshal (2013). "Cationic lipid nanoparticles for therapeutic delivery of siRNA and miRNA to murine liver tumor." Nanomedicine **9**(8): 1169-1180.
- Iancu, C., S. J. Mistry, S. Arkin and G. F. Atweh (2000). "Taxol and anti-stathmin therapy: a synergistic combination that targets the mitotic spindle." Cancer Res **60**(13): 3537-3541.
- Imboden, J. B., A. Weiss and J. D. Stobo (1985). "The antigen receptor on a human T cell line initiates activation by increasing cytoplasmic free calcium." J Immunol **134**(2): 663-665.
- Ishiwata, T., Y. Matsuda and Z. Naito (2011). "Nestin in gastrointestinal and other cancers: effects on cells and tumor angiogenesis." World J Gastroenterol **17**(4): 409-418.
- Jaffe, A. B. and A. Hall (2005). "Rho GTPases: biochemistry and biology." Annu Rev Cell Dev Biol **21**: 247-269.
- Jeon, T. Y., M. E. Han, Y. W. Lee, Y. S. Lee, G. H. Kim, G. A. Song, G. Y. Hur, J. Y. Kim, H. J. Kim, S. Yoon, S. Y. Baek, B. S. Kim, J. B. Kim and S. O. Oh (2010). "Overexpression of stathmin1 in the diffuse type of gastric cancer and its roles in proliferation and migration of gastric cancer cells." Br J Cancer **102**(4): 710-718.
- Jin, K., X. O. Mao, B. Cottrell, B. Schilling, L. Xie, R. H. Row, Y. Sun, A. Peel, J. Childs, G. Gendeh, B. W. Gibson and D. A. Greenberg (2004). "Proteomic and immunochemical characterization of a role for stathmin in adult neurogenesis." FASEB J **18**(2): 287-299.
- Jordan, M. A. and L. Wilson (2004). "Microtubules as a target for anticancer drugs." Nat Rev Cancer **4**(4): 253-265.

- Kakiashvili, E., P. Speight, F. Waheed, R. Seth, M. Lodyga, S. Tanimura, M. Kohno, O. D. Rotstein, A. Kapus and K. Szaszi (2009). "GEF-H1 mediates tumor necrosis factor-alpha-induced Rho activation and myosin phosphorylation: role in the regulation of tubular paracellular permeability." *J Biol Chem* **284**(17): 11454-11466.
- Karlsson, R., E. D. Pedersen, Z. Wang and C. Brakebusch (2009). "Rho GTPase function in tumorigenesis." *Biochim Biophys Acta* **1796**(2): 91-98.
- Kavallaris, M., Ed. (2012). *Cytoskeleton and Human Disease*, Humana Press.
- Kavallaris, M., A. S. Tait, B. J. Walsh, L. He, S. B. Horwitz, M. D. Norris and M. Haber (2001). "Multiple microtubule alterations are associated with Vinca alkaloid resistance in human leukemia cells." *Cancer Res* **61**(15): 5803-5809.
- Keshamouni, V. G., G. Michailidis, C. S. Grasso, S. Anthwal, J. R. Strahler, A. Walker, D. A. Arenberg, R. C. Reddy, S. Akulapalli, V. J. Thannickal, T. J. Standiford, P. C. Andrews and G. S. Omenn (2006). "Differential protein expression profiling by iTRAQ-2DLC-MS/MS of lung cancer cells undergoing epithelial-mesenchymal transition reveals a migratory/invasive phenotype." *J Proteome Res* **5**(5): 1143-1154.
- Kline-Smith, S. L. and C. E. Walczak (2002). "The microtubule-destabilizing kinesin XKCM1 regulates microtubule dynamic instability in cells." *Mol Biol Cell* **13**(8): 2718-2731.
- Koppel, J., M. C. Bouterin, V. Doye, H. Peyro-Saint-Paul and A. Sobel (1990). "Developmental tissue expression and phylogenetic conservation of stathmin, a phosphoprotein associated with cell regulations." *J Biol Chem* **265**(7): 3703-3707.
- Kozma, R., S. Ahmed, A. Best and L. Lim (1995). "The Ras-related protein Cdc42Hs and bradykinin promote formation of peripheral actin microspikes and filopodia in Swiss 3T3 fibroblasts." *Mol Cell Biol* **15**(4): 1942-1952.
- Kraynov, V. S., C. Chamberlain, G. M. Bokoch, M. A. Schwartz, S. Slabaugh and K. M. Hahn (2000). "Localized Rac activation dynamics visualized in living cells." *Science* **290**(5490): 333-337.
- Krendel, M., F. T. Zenke and G. M. Bokoch (2002). "Nucleotide exchange factor GEF-H1 mediates cross-talk between microtubules and the actin cytoskeleton." *Nat Cell Biol* **4**(4): 294-301.
- Kuramitsu, Y., K. Taba, S. Ryozaawa, K. Yoshida, X. Zhang, T. Tanaka, S. Maehara, Y. Maehara, I. Sakaida and K. Nakamura (2010). "Identification of up- and down-regulated proteins in gemcitabine-resistant pancreatic cancer cells using two-dimensional gel electrophoresis and mass spectrometry." *Anticancer Res* **30**(9): 3367-3372.
- Kurokawa, K. and M. Matsuda (2005). "Localized RhoA activation as a requirement for the induction of membrane ruffling." *Mol Biol Cell* **16**(9): 4294-4303.
- Lamouille, S., J. Xu and R. Derynck (2014). "Molecular mechanisms of epithelial-mesenchymal transition." *Nat Rev Mol Cell Biol* **15**(3): 178-196.

Langenickel, T. H., M. Olive, M. Boehm, H. San, M. F. Crook and E. G. Nabel (2008). "KIS protects against adverse vascular remodeling by opposing stathmin-mediated VSMC migration in mice." J Clin Invest **118**(12): 3848-3859.

Larsson, N., B. Segerman, H. M. Gradin, E. Wandzioch, L. Cassimeris and M. Gullberg (1999). "Mutations of oncoprotein 18/stathmin identify tubulin-directed regulatory activities distinct from tubulin association." Mol Cell Biol **19**(3): 2242-2250.

Liu, F., Y. L. Sun, Y. Xu, F. Liu, L. S. Wang and X. H. Zhao (2013). "Expression and phosphorylation of stathmin correlate with cell migration in esophageal squamous cell carcinoma." Oncol Rep **29**(2): 419-424.

Loi, M., D. Di Paolo, M. Soster, C. Brignole, A. Bartolini, L. Emionite, J. Sun, P. Becherini, F. Curnis, A. Petretto, M. Sani, A. Gori, M. Milanese, C. Gambini, R. Longhi, M. Cilli, T. M. Allen, F. Bussolino, W. Arap, R. Pasqualini, A. Corti, M. Ponzoni, S. Marchio and F. Pastorino (2013). "Novel phage display-derived neuroblastoma-targeting peptides potentiate the effect of drug nanocarriers in preclinical settings." J Control Release **170**(2): 233-241.

Lu, Y., C. Liu, H. Cheng, Y. Xu, J. Jiang, J. Xu, J. Long, L. Liu and X. Yu (2014). "Stathmin, interacting with Nf-kappaB, promotes tumor growth and predicts poor prognosis of pancreatic cancer." Curr Mol Med **14**(3): 328-339.

Ludueno, R. F. (2013). "A hypothesis on the origin and evolution of tubulin." International review of cell and molecular biology **302**: 41-185.

Machacek, M., L. Hodgson, C. Welch, H. Elliott, O. Pertz, P. Nalbant, A. Abell, G. L. Johnson, K. M. Hahn and G. Danuser (2009). "Coordination of Rho GTPase activities during cell protrusion." Nature **461**(7260): 99-103.

Maekawa, M., T. Ishizaki, S. Boku, N. Watanabe, A. Fujita, A. Iwamatsu, T. Obinata, K. Ohashi, K. Mizuno and S. Narumiya (1999). "Signaling from Rho to the actin cytoskeleton through protein kinases ROCK and LIM-kinase." Science **285**(5429): 895-898.

Manceau, V., O. Gavet, P. Curmi and A. Sobel (1999). "Stathmin interaction with HSC70 family proteins." Electrophoresis **20**(2): 409-417.

Maris, J. M. (2010). "Recent advances in neuroblastoma." N Engl J Med **362**(23): 2202-2211.

Maris, J. M., M. D. Hogarty, R. Bagatell and S. L. Cohn (2007). "Neuroblastoma." Lancet **369**(9579): 2106-2120.

Marklund, U., O. Osterman, H. Melander, A. Bergh and M. Gullberg (1994). "The phenotype of a "Cdc2 kinase target site-deficient" mutant of oncoprotein 18 reveals a role of this protein in cell cycle control." J Biol Chem **269**(48): 30626-30635.

Martin-Padura, I., S. Lostaglio, M. Schneemann, L. Williams, M. Romano, P. Fruscella, C. Panzeri, A. Stoppacciaro, L. Ruco, A. Villa, D. Simmons and E. Dejana (1998). "Junctional adhesion molecule, a novel member of the immunoglobulin superfamily that distributes at intercellular junctions and modulates monocyte transmigration." J Cell Biol **142**(1): 117-127.

- Martoglio, A. M., B. D. Tom, M. Starkey, A. N. Corps, D. S. Charnock-Jones and S. K. Smith (2000). "Changes in tumorigenesis- and angiogenesis-related gene transcript abundance profiles in ovarian cancer detected by tailored high density cDNA arrays." Mol Med **6**(9): 750-765.
- Matthay, K. K., J. G. Villablanca, R. C. Seeger, D. O. Stram, R. E. Harris, N. K. Ramsay, P. Swift, H. Shimada, C. T. Black, G. M. Brodeur, R. B. Gerbing and C. P. Reynolds (1999). "Treatment of high-risk neuroblastoma with intensive chemotherapy, radiotherapy, autologous bone marrow transplantation, and 13-cis-retinoic acid. Children's Cancer Group." N Engl J Med **341**(16): 1165-1173.
- Maucuer, A., J. H. Camonis and A. Sobel (1995). "Stathmin interaction with a putative kinase and coiled-coil-forming protein domains." Proc Natl Acad Sci U S A **92**(8): 3100-3104.
- Melhem, R. F., J. R. Strahler, N. Hailat, X. X. Zhu and S. M. Hanash (1991). "Involvement of OP18 in cell proliferation." Biochem Biophys Res Commun **179**(3): 1649-1655.
- Mierke, C. T., D. Rosel, B. Fabry and J. Brabek (2008). "Contractile forces in tumor cell migration." Eur J Cell Biol **87**(8-9): 669-676.
- Misek, D. E., C. L. Chang, R. Kuick, R. Hinderer, T. J. Giordano, D. G. Beer and S. M. Hanash (2002). "Transforming properties of a Q18-->E mutation of the microtubule regulator Op18." Cancer Cell **2**(3): 217-228.
- Mistry, S. J. and G. F. Atweh (2006). "Therapeutic interactions between stathmin inhibition and chemotherapeutic agents in prostate cancer." Mol Cancer Ther **5**(12): 3248-3257.
- Mistry, S. J., A. Bank and G. F. Atweh (2005). "Targeting stathmin in prostate cancer." Mol Cancer Ther **4**(12): 1821-1829.
- Mistry, S. J., A. Bank and G. F. Atweh (2007). "Synergistic antiangiogenic effects of stathmin inhibition and taxol exposure." Mol Cancer Res **5**(8): 773-782.
- Mistry, S. J., H. C. Li and G. F. Atweh (1998). "Role for protein phosphatases in the cell-cycle-regulated phosphorylation of stathmin." Biochem J **334** (Pt 1): 23-29.
- Mitra, M., M. Kandalam, C. S. Sundaram, R. S. Verma, U. K. Maheswari, S. Swaminathan and S. Krishnakumar (2011). "Reversal of stathmin-mediated microtubule destabilization sensitizes retinoblastoma cells to a low dose of antimicrotubule agents: a novel synergistic therapeutic intervention." Invest Ophthalmol Vis Sci **52**(8): 5441-5448.
- Modak, S. and N. K. Cheung (2007). "Disialoganglioside directed immunotherapy of neuroblastoma." Cancer Invest **25**(1): 67-77.
- Molina, A., L. Velot, L. Ghouinem, M. Abdelkarim, B. P. Bouchet, A. C. Luissint, I. Bouhlel, M. Morel, E. Sapharikas, A. Di Tommaso, S. Honore, D. Braguer, N. Gruel, A. Vincent-Salomon, O. Delattre, B. Sigal-Zafrani, F. Andre, B. Terris, A. Akhmanova, M. Di Benedetto, C. Nahmias and S. Rodrigues-Ferreira (2013). "ATIP3, a novel prognostic marker

of breast cancer patient survival, limits cancer cell migration and slows metastatic progression by regulating microtubule dynamics." *Cancer Res* **73**(9): 2905-2915.

Monclair, T., G. M. Brodeur, P. F. Ambros, H. J. Brisse, G. Cecchetto, K. Holmes, M. Kaneko, W. B. London, K. K. Matthay, J. G. Nuchtern, D. von Schweinitz, T. Simon, S. L. Cohn, A. D. Pearson and I. T. Force (2009). "The International Neuroblastoma Risk Group (INRG) staging system: an INRG Task Force report." *J Clin Oncol* **27**(2): 298-303.

Morowitz, M., S. Shusterman, Y. Mosse, G. Hii, C. L. Winter, D. Khazi, Q. Wang, R. King and J. M. Maris (2003). "Detection of single-copy chromosome 17q gain in human neuroblastomas using real-time quantitative polymerase chain reaction." *Mod Pathol* **16**(12): 1248-1256.

Morrison, E. E., B. N. Wardleworth, J. M. Askham, A. F. Markham and D. M. Meredith (1998). "EB1, a protein which interacts with the APC tumour suppressor, is associated with the microtubule cytoskeleton throughout the cell cycle." *Oncogene* **17**(26): 3471-3477.

Mouneimne, G., V. DesMarais, M. Sidani, E. Scemes, W. Wang, X. Song, R. Eddy and J. Condeelis (2006). "Spatial and temporal control of cofilin activity is required for directional sensing during chemotaxis." *Curr Biol* **16**(22): 2193-2205.

Mouneimne, G., L. Soon, V. DesMarais, M. Sidani, X. Song, S. C. Yip, M. Ghosh, R. Eddy, J. M. Backer and J. Condeelis (2004). "Phospholipase C and cofilin are required for carcinoma cell directionality in response to EGF stimulation." *J Cell Biol* **166**(5): 697-708.

Mujoo, K., D. A. Cheresch, H. M. Yang and R. A. Reisfeld (1987). "Disialoganglioside GD2 on human neuroblastoma cells: target antigen for monoclonal antibody-mediated cytolysis and suppression of tumor growth." *Cancer Res* **47**(4): 1098-1104.

Musarella, M. A., H. S. Chan, G. DeBoer and B. L. Gallie (1984). "Ocular involvement in neuroblastoma: prognostic implications." *Ophthalmology* **91**(8): 936-940.

Nalbant, P., L. Hodgson, V. Kraynov, A. Touthkine and K. M. Hahn (2004). "Activation of endogenous Cdc42 visualized in living cells." *Science* **305**(5690): 1615-1619.

Ng, D. C., B. H. Lin, C. P. Lim, G. Huang, T. Zhang, V. Poli and X. Cao (2006). "Stat3 regulates microtubules by antagonizing the depolymerization activity of stathmin." *J Cell Biol* **172**(2): 245-257.

Niethammer, P., P. Bastiaens and E. Karsenti (2004). "Stathmin-tubulin interaction gradients in motile and mitotic cells." *Science* **303**(5665): 1862-1866.

Nobes, C. D. and A. Hall (1995). "Rho, rac, and cdc42 GTPases regulate the assembly of multimolecular focal complexes associated with actin stress fibers, lamellipodia, and filopodia." *Cell* **81**(1): 53-62.

Nogales, E. (2000). "Structural insights into microtubule function." *Annu Rev Biochem* **69**: 277-302.

- Oberthuer, A., J. Theissen, F. Westermann, B. Hero and M. Fischer (2009). "Molecular characterization and classification of neuroblastoma." *Future Oncol* **5**(5): 625-639.
- Ozon, S., A. Guichet, O. Gavet, S. Roth and A. Sobel (2002). "Drosophila stathmin: a microtubule-destabilizing factor involved in nervous system formation." *Mol Biol Cell* **13**(2): 698-710.
- Pacuszka, T., R. O. Duffard, R. N. Nishimura, R. O. Brady and P. H. Fishman (1978). "Biosynthesis of bovine thyroid gangliosides." *J Biol Chem* **253**(16): 5839-5846.
- Pan, Y., R. Jing, A. Pitre, B. J. Williams and O. Skalli (2008). "Intermediate filament protein synemin contributes to the migratory properties of astrocytoma cells by influencing the dynamics of the actin cytoskeleton." *FASEB J* **22**(9): 3196-3206.
- Pancook, J. D., J. C. Becker, S. D. Gillies and R. A. Reisfeld (1996). "Eradication of established hepatic human neuroblastoma metastases in mice with severe combined immunodeficiency by antibody-targeted interleukin-2." *Cancer Immunol Immunother* **42**(2): 88-92.
- Park, J. R., J. R. Scott, C. F. Stewart, W. B. London, A. Naranjo, V. M. Santana, P. J. Shaw, S. L. Cohn and K. K. Matthay (2011). "Pilot induction regimen incorporating pharmacokinetically guided topotecan for treatment of newly diagnosed high-risk neuroblastoma: a Children's Oncology Group study." *J Clin Oncol* **29**(33): 4351-4357.
- Pasmantier, R., A. Danoff, N. Fleischer and U. K. Schubart (1986). "P19, a hormonally regulated phosphoprotein of peptide hormone-producing cells: secretagogue-induced phosphorylation in AtT-20 mouse pituitary tumor cells and in rat and hamster insulinoma cells." *Endocrinology* **119**(3): 1229-1238.
- Pearson, A. D., C. R. Pinkerton, I. J. Lewis, J. Imeson, C. Ellershaw and D. Machin (2008). "High-dose rapid and standard induction chemotherapy for patients aged over 1 year with stage 4 neuroblastoma: a randomised trial." *Lancet Oncol* **9**(3): 247-256.
- Pertz, O., L. Hodgson, R. L. Klemke and K. M. Hahn (2006). "Spatiotemporal dynamics of RhoA activity in migrating cells." *Nature* **440**(7087): 1069-1072.
- Phadke, A. P., C. M. Jay, Z. Wang, S. Chen, S. Liu, C. Haddock, P. Kumar, B. O. Pappen, D. D. Rao, N. S. Templeton, E. Q. Daniels, C. Webb, D. Monsma, S. Scott, D. Dylewski, H. B. Frieboes, F. C. Brunicardi, N. Senzer, P. B. Maples, J. Nemunaitis and A. W. Tong (2011). "In vivo safety and antitumor efficacy of bifunctional small hairpin RNAs specific for the human Stathmin 1 oncoprotein." *DNA Cell Biol* **30**(9): 715-726.
- Piskounova, E., C. Polytarchou, J. E. Thornton, R. J. LaPierre, C. Pothoulakis, J. P. Hagan, D. Iliopoulos and R. I. Gregory (2011). "Lin28A and Lin28B inhibit let-7 microRNA biogenesis by distinct mechanisms." *Cell* **147**(5): 1066-1079.
- Plantaz, D., H. Rubie, J. Michon, F. Mechinaud, C. Coze, P. Chastagner, D. Frappaz, M. Gigaud, J. G. Passagia and O. Hartmann (1996). "The treatment of neuroblastoma with intraspinal extension with chemotherapy followed by surgical removal of residual disease. A

prospective study of 42 patients--results of the NBL 90 Study of the French Society of Pediatric Oncology." Cancer **78**(2): 311-319.

Pollard, T. D. and G. G. Borisy (2003). "Cellular motility driven by assembly and disassembly of actin filaments." Cell **112**(4): 453-465.

Puthalakath, H., D. C. Huang, L. A. O'Reilly, S. M. King and A. Strasser (1999). "The proapoptotic activity of the Bcl-2 family member Bim is regulated by interaction with the dynein motor complex." Mol Cell **3**(3): 287-296.

Raftopoulou, M. and A. Hall (2004). "Cell migration: Rho GTPases lead the way." Dev Biol **265**(1): 23-32.

Rana, S., P. B. Maples, N. Senzer and J. Nemunaitis (2008). "Stathmin 1: a novel therapeutic target for anticancer activity." Expert Rev Anticancer Ther **8**(9): 1461-1470.

Ridley, A. J., H. F. Paterson, C. L. Johnston, D. Diekmann and A. Hall (1992). "The small GTP-binding protein rac regulates growth factor-induced membrane ruffling." Cell **70**(3): 401-410.

Ridley, A. J., M. A. Schwartz, K. Burridge, R. A. Firtel, M. H. Ginsberg, G. Borisy, J. T. Parsons and A. R. Horwitz (2003). "Cell migration: integrating signals from front to back." Science **302**(5651): 1704-1709.

Rodrigues-Ferreira, S., A. Di Tommaso, A. Dimitrov, S. Cazaubon, N. Gruel, H. Colasson, A. Nicolas, N. Chaverot, V. Molinie, F. Reyat, B. Sigal-Zafrani, B. Terris, O. Delattre, F. Radvanyi, F. Perez, A. Vincent-Salomon and C. Nahmias (2009). "8p22 MTUS1 gene product ATIP3 is a novel anti-mitotic protein underexpressed in invasive breast carcinoma of poor prognosis." PLoS One **4**(10): e7239.

Rodriguez, O. C., A. W. Schaefer, C. A. Mandato, P. Forscher, W. M. Bement and C. M. Waterman-Storer (2003). "Conserved microtubule-actin interactions in cell movement and morphogenesis." Nat Cell Biol **5**(7): 599-609.

Ross, R. A., J. L. Biedler and B. A. Spengler (2003). "A role for distinct cell types in determining malignancy in human neuroblastoma cell lines and tumors." Cancer Lett **197**(1-2): 35-39.

Ross-Macdonald, P., H. de Silva, Q. Guo, H. Xiao, C. Y. Hung, B. Penhallow, J. Markwalder, L. He, R. M. Attar, T. A. Lin, S. Seitz, C. Tilford, J. Wardwell-Swanson and D. Jackson (2008). "Identification of a nonkinase target mediating cytotoxicity of novel kinase inhibitors." Mol Cancer Ther **7**(11): 3490-3498.

Rossman, K. L., C. J. Der and J. Sondek (2005). "GEF means go: turning on RHO GTPases with guanine nucleotide-exchange factors." Nat Rev Mol Cell Biol **6**(2): 167-180.

Rubin, C. I. and G. F. Atweh (2004). "The role of stathmin in the regulation of the cell cycle." J Cell Biochem **93**(2): 242-250.

Sahai, E. and C. J. Marshall (2002). "RHO-GTPases and cancer." Nat Rev Cancer **2**(2): 133-142.

Sahai, E. and C. J. Marshall (2003). "Differing modes of tumour cell invasion have distinct requirements for Rho/ROCK signalling and extracellular proteolysis." Nat Cell Biol **5**(8): 711-719.

Sander, E. E., J. P. ten Klooster, S. van Delft, R. A. van der Kammen and J. G. Collard (1999). "Rac downregulates Rho activity: reciprocal balance between both GTPases determines cellular morphology and migratory behavior." J Cell Biol **147**(5): 1009-1022.

Satelli, A. and S. Li (2011). "Vimentin in cancer and its potential as a molecular target for cancer therapy." Cell Mol Life Sci **68**(18): 3033-3046.

Schiffelers, R. M., A. Ansari, J. Xu, Q. Zhou, Q. Tang, G. Storm, G. Molema, P. Y. Lu, P. V. Scaria and M. C. Woodle (2004). "Cancer siRNA therapy by tumor selective delivery with ligand-targeted sterically stabilized nanoparticle." Nucleic Acids Res **32**(19): e149.

Schroeder, A., D. A. Heller, M. M. Winslow, J. E. Dahlman, G. W. Pratt, R. Langer, T. Jacks and D. G. Anderson (2012). "Treating metastatic cancer with nanotechnology." Nat Rev Cancer **12**(1): 39-50.

Schubart, U. K., J. Xu, W. Fan, G. Cheng, H. Goldstein, G. Alpini, D. A. Shafritz, J. A. Amat, M. Farooq, W. T. Norton and et al. (1992). "Widespread differentiation stage-specific expression of the gene encoding phosphoprotein p19 (metablastin) in mammalian cells." Differentiation **51**(1): 21-32.

Scott, R. W., S. Hooper, D. Crighton, A. Li, I. Konig, J. Munro, E. Trivier, G. Wickman, P. Morin, D. R. Croft, J. Dawson, L. Machesky, K. I. Anderson, E. A. Sahai and M. F. Olson (2010). "LIM kinases are required for invasive path generation by tumor and tumor-associated stromal cells." J Cell Biol **191**(1): 169-185.

Seeger, R. C., G. M. Brodeur, H. Sather, A. Dalton, S. E. Siegel, K. Y. Wong and D. Hammond (1985). "Association of multiple copies of the N-myc oncogene with rapid progression of neuroblastomas." N Engl J Med **313**(18): 1111-1116.

Shen, M., F. Gong, P. Pang, K. Zhu, X. Meng, C. Wu, J. Wang, H. Shan and X. Shuai (2012). "An MRI-visible non-viral vector for targeted Bcl-2 siRNA delivery to neuroblastoma." Int J Nanomedicine **7**: 3319-3332.

Sherr, C. J. and J. M. Roberts (1999). "CDK inhibitors: positive and negative regulators of G1-phase progression." Genes Dev **13**(12): 1501-1512.

Shimada, H., I. M. Ambros, L. P. Dehner, J. Hata, V. V. Joshi, B. Roald, D. O. Stram, R. B. Gerbing, J. N. Lukens, K. K. Matthyay and R. P. Castleberry (1999). "The International Neuroblastoma Pathology Classification (the Shimada system)." Cancer **86**(2): 364-372.

Sihag, R. K., M. Inagaki, T. Yamaguchi, T. B. Shea and H. C. Pant (2007). "Role of phosphorylation on the structural dynamics and function of types III and IV intermediate filaments." Exp Cell Res **313**(10): 2098-2109.

- Singer, S., V. Ehemann, A. Brauckhoff, M. Keith, S. Vreden, P. Schirmacher and K. Breuhahn (2007). "Protumorigenic overexpression of stathmin/Op18 by gain-of-function mutation in p53 in human hepatocarcinogenesis." *Hepatology* **46**(3): 759-768.
- Singer, S., M. Malz, E. Herpel, A. Warth, M. Bissinger, M. Keith, T. Muley, M. Meister, H. Hoffmann, R. Penzel, G. Gdynia, V. Ehemann, P. A. Schnabel, R. Kuner, P. Huber, P. Schirmacher and K. Breuhahn (2009). "Coordinated expression of stathmin family members by far upstream sequence element-binding protein-1 increases motility in non-small cell lung cancer." *Cancer Res* **69**(6): 2234-2243.
- Sinha, P., G. Hutter, E. Kottgen, M. Dietel, D. Schadendorf and H. Lage (1999). "Increased expression of epidermal fatty acid binding protein, cofilin, and 14-3-3-sigma (stratifin) detected by two-dimensional gel electrophoresis, mass spectrometry and microsequencing of drug-resistant human adenocarcinoma of the pancreas." *Electrophoresis* **20**(14): 2952-2960.
- Small, J. V., T. Stradal, E. Vignal and K. Rottner (2002). "The lamellipodium: where motility begins." *Trends Cell Biol* **12**(3): 112-120.
- Sobel, A., M. C. Bouterin, L. Beretta, H. Chneiweiss, V. Doye and H. Peyro-Saint-Paul (1989). "Intracellular substrates for extracellular signaling. Characterization of a ubiquitous, neuron-enriched phosphoprotein (stathmin)." *J Biol Chem* **264**(7): 3765-3772.
- Sobel, A. and A. H. Tashjian, Jr. (1983). "Distinct patterns of cytoplasmic protein phosphorylation related to regulation of synthesis and release of prolactin by GH cells." *J Biol Chem* **258**(17): 10312-10324.
- Steeg, P. S. (2006). "Tumor metastasis: mechanistic insights and clinical challenges." *Nature Medicine* **12**(8): 895-904.
- Steinmetz, M. O. (2007). "Structure and thermodynamics of the tubulin-stathmin interaction." *J Struct Biol* **158**(2): 137-147.
- Stevens, P. L., D. B. Johnson, M. A. Thompson, V. L. Keedy, H. A. Frangoul and K. M. Snyder (2014). "Adult neuroblastoma complicated by increased intracranial pressure: a case report and review of the literature." *Case Rep Oncol Med* **2014**: 341980.
- Strasser, A., H. Puthalakath, P. Bouillet, D. C. Huang, L. O'Connor, L. A. O'Reilly, L. Cullen, S. Cory and J. M. Adams (2000). "The role of bim, a proapoptotic BH3-only member of the Bcl-2 family in cell-death control." *Ann N Y Acad Sci* **917**: 541-548.
- Sun, J., S. O. Marx, H. J. Chen, M. Poon, A. R. Marks and L. E. Rabbani (2001). "Role for p27(Kip1) in Vascular Smooth Muscle Cell Migration." *Circulation* **103**(24): 2967-2972.
- Svennerholm, L., K. Bostrom, P. Fredman, B. Jungbjer, A. Lekman, J. E. Mansson and B. M. Rynmark (1994). "Gangliosides and allied glycosphingolipids in human peripheral nerve and spinal cord." *Biochim Biophys Acta* **1214**(2): 115-123.
- Taberero, J., G. I. Shapiro, P. M. LoRusso, A. Cervantes, G. K. Schwartz, G. J. Weiss, L. Paz-Ares, D. C. Cho, J. R. Infante, M. Alsina, M. M. Gounder, R. Falzone, J. Harrop, A. C. White, I. Toudjarska, D. Bumcrot, R. E. Meyers, G. Hinkle, N. Svrzikapa, R. M. Hutabarat,

V. A. Clausen, J. Cehelsky, S. V. Nochur, C. Gamba-Vitalo, A. K. Vaishnav, D. W. Sah, J. A. Gollob and H. A. Burris, 3rd (2013). "First-in-humans trial of an RNA interference therapeutic targeting VEGF and KSP in cancer patients with liver involvement." Cancer Discov **3**(4): 406-417.

Tania, N., E. Prosk, J. Condeelis and L. Edelstein-Keshet (2011). "A temporal model of cofilin regulation and the early peak of actin barbed ends in invasive tumor cells." Biophys J **100**(8): 1883-1892.

Thiery, J. P., H. Acloque, R. Y. Huang and M. A. Nieto (2009). "Epithelial-mesenchymal transitions in development and disease." Cell **139**(5): 871-890.

Tian, X., Y. Tian, N. Sarich, T. Wu and A. A. Birukova (2012). "Novel role of stathmin in microtubule-dependent control of endothelial permeability." FASEB J **26**(9): 3862-3874.

Tivnan, A., W. S. Orr, V. Gubala, R. Nooney, D. E. Williams, C. McDonagh, S. Prenter, H. Harvey, R. Domingo-Fernandez, I. M. Bray, O. Piskareva, C. Y. Ng, H. N. Lode, A. M. Davidoff and R. L. Stallings (2012). "Inhibition of neuroblastoma tumor growth by targeted delivery of microRNA-34a using anti-disialoganglioside GD2 coated nanoparticles." PLoS One **7**(5): e38129.

Trovik, J., E. Wik, I. M. Stefansson, J. Marcickiewicz, S. Tingulstad, A. C. Staff, T. S. Njolstad, I. Vandenput, F. Amant, L. A. Akslen and H. B. Salvesen (2011). "Stathmin overexpression identifies high-risk patients and lymph node metastasis in endometrial cancer." Clin Cancer Res **17**(10): 3368-3377.

Turhani, D., K. Krapfenbauer, D. Thurnher, H. Langen and M. Fountoulakis (2006). "Identification of differentially expressed, tumor-associated proteins in oral squamous cell carcinoma by proteomic analysis." Electrophoresis **27**(7): 1417-1423.

Tweddle, D. A., A. J. Malcolm, N. Bown, A. D. Pearson and J. Lunec (2001). "Evidence for the development of p53 mutations after cytotoxic therapy in a neuroblastoma cell line." Cancer Res **61**(1): 8-13.

Tweddle, D. A., A. D. Pearson, M. Haber, M. D. Norris, C. Xue, C. Flemming and J. Lunec (2003). "The p53 pathway and its inactivation in neuroblastoma." Cancer Lett **197**(1-2): 93-98.

Umaphathy, G., A. El Wakil, B. Witek, L. Chesler, L. Danielson, X. Deng, N. S. Gray, M. Johansson, S. Kvarnbrink, K. Ruuth, C. Schonherr, R. H. Palmer and B. Hallberg (2014). "The kinase ALK stimulates the kinase ERK5 to promote the expression of the oncogene MYCN in neuroblastoma." Sci Signal **7**(349): ra102.

Valster, A., N. L. Tran, M. Nakada, M. E. Berens, A. Y. Chan and M. Symons (2005). "Cell migration and invasion assays." Methods **37**(2): 208-215.

van Golen, C. M., T. S. Schwab, B. Kim, M. E. Soules, S. Su Oh, K. Fung, K. L. van Golen and E. L. Feldman (2006). "Insulin-like growth factor-I receptor expression regulates neuroblastoma metastasis to bone." Cancer Res **66**(13): 6570-6578.

van Horck, F. P., M. R. Ahmadian, L. C. Haeusler, W. H. Moolenaar and O. Kranenburg (2001). "Characterization of p190RhoGEF, a RhoA-specific guanine nucleotide exchange factor that interacts with microtubules." *J Biol Chem* **276**(7): 4948-4956.

Van Sluis, G. L., T. M. Niers, C. T. Esmon, W. Tigchelaar, D. J. Richel, H. R. Buller, C. J. Van Noorden and C. A. Spek (2009). "Endogenous activated protein C limits cancer cell extravasation through sphingosine-1-phosphate receptor 1-mediated vascular endothelial barrier enhancement." *Blood* **114**(9): 1968-1973.

Vega, F. M. and A. J. Ridley (2008). "Rho GTPases in cancer cell biology." *FEBS Lett* **582**(14): 2093-2101.

Verhey, K. J. and J. Gaertig (2007). "The tubulin code." *Cell Cycle* **6**(17): 2152-2160.

Verma, N. K., J. Dourlat, A. M. Davies, A. Long, W. Q. Liu, C. Garbay, D. Kelleher and Y. Volkov (2009). "STAT3-stathmin interactions control microtubule dynamics in migrating T-cells." *J Biol Chem* **284**(18): 12349-12362.

Vermeulen, J., K. De Preter, P. Mestdagh, G. Laureys, F. Speleman and J. Vandesompele (2010). "Predicting outcomes for children with neuroblastoma." *Discov Med* **10**(50): 29-36.

Vežina, A., E. Vaillancourt-Jean, S. Albarao and B. Annabi (2014). "Mesenchymal stromal cell ciliogenesis is abrogated in response to tumor necrosis factor-alpha and requires NF-kappaB signaling." *Cancer Lett* **345**(1): 100-105.

Vicente-Manzanares, M. and F. Sanchez-Madrid (2004). "Role of the cytoskeleton during leukocyte responses." *Nat Rev Immunol* **4**(2): 110-122.

Vinci, M., S. Gowan, F. Boxall, L. Patterson, M. Zimmermann, W. Court, C. Lomas, M. Mendiola, D. Hardisson and S. A. Eccles (2012). "Advances in establishment and analysis of three-dimensional tumor spheroid-based functional assays for target validation and drug evaluation." *BMC Biol* **10**: 29.

Vogl, T., S. Ludwig, M. Goebeler, A. Strey, I. S. Thorey, R. Reichelt, D. Foell, V. Gerke, M. P. Manitz, W. Nacken, S. Werner, C. Sorg and J. Roth (2004). "MRP8 and MRP14 control microtubule reorganization during transendothelial migration of phagocytes." *Blood* **104**(13): 4260-4268.

Wade, R. H. (2009). "On and around microtubules: an overview." *Mol Biotechnol* **43**(2): 177-191.

Wang, R., K. Dong, F. Lin, X. Wang, P. Gao, S. H. Wei, S. Y. Cheng and H. Z. Zhang (2007). "Inhibiting proliferation and enhancing chemosensitivity to taxanes in osteosarcoma cells by RNA interference-mediated downregulation of stathmin expression." *Mol Med* **13**(11-12): 567-575.

Wang, W., R. Eddy and J. Condeelis (2007). "The cofilin pathway in breast cancer invasion and metastasis." *Nat Rev Cancer* **7**(6): 429-440.

Wang, W., S. Goswami, K. Lapidus, A. L. Wells, J. B. Wyckoff, E. Sahai, R. H. Singer, J. E. Segall and J. S. Condeelis (2004). "Identification and testing of a gene expression signature of invasive carcinoma cells within primary mammary tumors." Cancer Res **64**(23): 8585-8594.

Wang, W., G. Mouneimne, M. Sidani, J. Wyckoff, X. Chen, A. Makris, S. Goswami, A. R. Bresnick and J. S. Condeelis (2006). "The activity status of cofilin is directly related to invasion, intravasation, and metastasis of mammary tumors." J Cell Biol **173**(3): 395-404.

Williford, J. M., J. Wu, Y. Ren, M. M. Archang, K. W. Leong and H. Q. Mao (2014). "Recent advances in nanoparticle-mediated siRNA delivery." Annu Rev Biomed Eng **16**: 347-370.

Wilson, R. C. and J. A. Doudna (2013). "Molecular mechanisms of RNA interference." Annu Rev Biophys **42**: 217-239.

Wittmann, T., G. M. Bokoch and C. M. Waterman-Storer (2004). "Regulation of microtubule destabilizing activity of Op18/stathmin downstream of Rac1." J Biol Chem **279**(7): 6196-6203.

Wu, Z. L., E. Schwartz, R. Seeger and S. Ladisch (1986). "Expression of GD2 ganglioside by untreated primary human neuroblastomas." Cancer Res **46**(1): 440-443.

Wyckoff, J. B., S. E. Pinner, S. Gschmeissner, J. S. Condeelis and E. Sahai (2006). "ROCK- and myosin-dependent matrix deformation enables protease-independent tumor-cell invasion in vivo." Curr Biol **16**(15): 1515-1523.

Xi, W., W. Rui, L. Fang, D. Ke, G. Ping and Z. Hui-Zhong (2009). "Expression of stathmin/op18 as a significant prognostic factor for cervical carcinoma patients." J Cancer Res Clin Oncol **135**(6): 837-846.

Yamaguchi, H. and J. Condeelis (2007). "Regulation of the actin cytoskeleton in cancer cell migration and invasion." Biochim Biophys Acta **1773**(5): 642-652.

Yee, H. F., Jr., A. C. Melton and B. N. Tran (2001). "RhoA/rho-associated kinase mediates fibroblast contractile force generation." Biochem Biophys Res Commun **280**(5): 1340-1345.

Yoshizaki, H., Y. Ohba, K. Kurokawa, R. E. Itoh, T. Nakamura, N. Mochizuki, K. Nagashima and M. Matsuda (2003). "Activity of Rho-family GTPases during cell division as visualized with FRET-based probes." J Cell Biol **162**(2): 223-232.

Yu, A. L., A. L. Gilman, M. F. Ozkaynak, W. B. London, S. G. Kreissman, H. X. Chen, M. Smith, B. Anderson, J. G. Villablanca, K. K. Matthay, H. Shimada, S. A. Grupp, R. Seeger, C. P. Reynolds, A. Buxton, R. A. Reisfeld, S. D. Gillies, S. L. Cohn, J. M. Maris, P. M. Sondel and G. Children's Oncology (2010). "Anti-GD2 antibody with GM-CSF, interleukin-2, and isotretinoin for neuroblastoma." N Engl J Med **363**(14): 1324-1334.

Yu, H., D. Pardoll and R. Jove (2009). "STATs in cancer inflammation and immunity: a leading role for STAT3." Nat Rev Cancer **9**(11): 798-809.

Zhang, B., J. Chernoff and Y. Zheng (1998). "Interaction of Rac1 with GTPase-activating proteins and putative effectors. A comparison with Cdc42 and RhoA." J Biol Chem **273**(15): 8776-8782.

Zhang, H. Z., Y. Wang, P. Gao, F. Lin, L. Liu, B. Yu, J. H. Ren, H. Zhao and R. Wang (2006). "Silencing stathmin gene expression by survivin promoter-driven siRNA vector to reverse malignant phenotype of tumor cells." Cancer Biol Ther **5**(11): 1457-1461.

Zhang, T., K. J. Zaal, J. Sheridan, A. Mehta, G. G. Gundersen and E. Ralston (2009). "Microtubule plus-end binding protein EB1 is necessary for muscle cell differentiation, elongation and fusion." J Cell Sci **122**(Pt 9): 1401-1409.

Zhang, X., X. Xie, B. L. Heckmann, A. M. Saarinen, T. A. Czyzyk and J. Liu (2014). "Targeted disruption of G0/G1 switch gene 2 enhances adipose lipolysis, alters hepatic energy balance, and alleviates high-fat diet-induced liver steatosis." Diabetes **63**(3): 934-946.